Response to Comments of Reviewer #2

(comments in *italics*)

Manuscript number: acp-2018-1346

Title: MICS-Asia III: Multi-model comparison and evaluation of aerosol over East Asia

General comments:

Chemical transport models play important roles in advancing understanding of aerosol pollution and aerosol climate effects. This manuscript evaluates multiple model applications in Asia using observations from multiple platforms. The manuscript needs major revisions before publication.

Response:

Thanks to the reviewer for the helpful comments and suggestions. We have revised the manuscript carefully according to the reviewer's comments and suggestions. The point–to–point responses to the comments are listed as follows.

Major Comments:

1. *Improvements in language are needed. I would suggest that the authors ask native speakers for help.*

Response:

Thank you for your suggestion. The language in the entire revised manuscript has been carefully corrected.

2. *The authors fail to gain insights out of the evaluation and model inter-comparisons. As the result, the abstract and summary parts are a little weak. More efforts are needed to understand the details of model inputs, reactions, and etc.*

Response:

Thank you for your suggestion. According to the reviewer's comments, a major revision has been made in the entire manuscript, including the model configurations (Section 2.1), model inputs (Section 2.2), model evaluation (Section 3.1) and inter−model comparisons (Section 3.3). The parts of abstract and conclusion are also carefully revised.

In Section 2.1, more detailed descriptions about the model parameterizations, including gas phase chemistry **(Section 2.1.2.1 in Page 5−6)**, aerosol chemistry **(Section 2.1.2.2 in Page 6−7)**, dust scheme **(Section 2.1.3 in Page 8)** and sea-salt scheme **(Section 2.1.4 in Page 9)**, are added. Different mechanisms used in participant models can result in different simulation results (Gao et al., 2018). Understanding the details of model schemes can help to explain the biases between observations and simulations, and the diversities between simulation results.

In Section 2.2, descriptions about the "standard" model inputs, including meteorological fields **(Section 2.2.1 in Page 9−10)**, emission inventories **(Section 2.2.2 in Page 10−11)** and boundary

conditions **(Section 2.2.3 in Page 11)**, provided by MICS−Asia (Model Inter−Comparison Study for Asia) organizers are also added. Due to two sets of the boundary conditions (BCs) (CHASER and GEOS−Chem) can be selected by the fourteen participant models, detailed information about these two inputs are necessary, which may be helpful to explain the differences between simulation results when different BCs are used. Meanwhile, a discussion about the impacts of the model inputs (e.g. boundary conditions) is also added in the revised manuscript **(Section 4 in Page 22, Line 28−34)**.

According to the objective of MICS−Asia Phase III Topic 1, model evaluations against the extensive measurements are presented in Section 3.1. Detailed reasons are added in this revised section to explain the strengths and weaknesses of current air quality models in simulating aerosols **(Section 3.1.1−3.1.3 in Page 12−18)**. For example,

(1) The underestimated black carbon (BC) concentrations at polluted sites may be due to the high uncertainty of BC in current emission inventory;

(2) The absence of sulfate formation mechanisms (e.g. heterogeneous chemistry) in air quality models may cause the underestimation in SO_4^{2-};

(3) H_2SO_4 and HNO_3 can be neutralized by NH_3 to form $(NH_4)_2SO_4$ and NH_4NO_3, respectively. As H_2SO_4 is nonvolatile, and the equilibrium surface concentration is set to be zero in the model. So $(NH_4)_2SO_4$ is the preferential species in the completion when H_2SO_4 and HNO_3 are both present, and NH_4NO_3 is formed only if excess NH_3 is available beyond the sulfate requirement. If SO_4^{2-} is underestimated, then more NO_3^- will be predicted;

(4) NH_4^+ concentrations are influenced by the partitioning between gaseous NH_3 and aerosol NH_4^+, and are also associated with the concentrations of SO_4^{2-} and NO_3^-;

(5) Many precursors and formation pathways of organic aerosols are not considered in current air quality models, which may lead to the underestimation of $PM_{2.5}$ in Region_1;

(6) The inaccurate emission inventories, especially the natural emissions, including dust aerosols and sea salts, will result in the underestimation of PM_{10} in each defined sub−region.

A major revision has also been made in the section of model inter−comparisons **(Section 3.3 in Page 19−21)**. We mainly focus on the similarities and differences between simulated secondary inorganic aerosols (e.g. sulfate, nitrate and ammonium) and coarse particles from participant models. Major results from the inter−model comparisons can be summarized as follows:

(1) High $PM_{2.5}$ concentrations (> 40 μg m^{-3}) can be reproduced by all participant models, and the calculated CV (coefficient of variation) averaged over these regions are low (< 0.3), indicating similar performance of the air quality models in simulating the air pollutants over haze−polluted areas;

(2) Even though similar magnitude of $PM_{2.5}$ are simulated, the ratio of SNA (sulfate, nitrate and ammonium) to $PM_{2.5}$ varies a lot (about a factor of 2) among participant models, which means different gas−phase and aerosol chemistry mechanisms used in these models cause this inconsistency;

(3) CMAQ models show higher SOR (sulfur oxidation ratio) than other participant models, so more intense secondary formation of SO_4^{2-} may be simulated by CMAQ;

(4) Similar NOR (nitric oxidation ratio) is predicted by participant models, but the value is larger than the observed one, meaning more NO_3^- is produced by secondary formation in current models;

2

(5) NH₃−deficient air condition can be successfully simulated by all models, and a small reduction in ammonia may improve the air quality significantly, due to fewer H_2SO_4 and HNO_3 are neutralized to form SNA;

(6) For coarse particles (subtract $PM_{2.5}$ from PM_{10}), large CV is calculated, which means low consistency is among the simulation results, and the low consistency of simulated coarse particles in each region is mainly caused by the dust aerosols, indicating current air quality models have difficulty in producing similar dust emissions by using different dust schemes.

Following the reviewer's suggestion, we have revised the abstract part as follows: "Fourteen chemical transport models (CTMs) participate in the first topic of the Model Inter−Comparison Study for Asia (MICS–Asia) Phase III. These model results are compared with each other and an extensive set of measurements, aiming to evaluate the current CTMs' ability in simulating aerosol concentrations, to document the similarities and differences among model performances, and to reveal the characteristics of aerosol components in large cities over East Asia. In general, these CTMs can well reproduce the spatial–temporal distributions of aerosols in East Asia during the year 2010. The multi–model ensemble mean (MMEM) shows better performance than most single–model predictions, with correlation coefficients (between MMEM and measurements) ranging from 0.65 (nitrate, NO_3^-) to 0.83 ($PM_{2.5}$). The concentrations of black carbon (BC), sulfate (SO_4^{2-}), and PM_{10} are underestimated by MMEM, with normalized mean biases (NMBs) of −17.0%, −19.1%, and −32.6%, respectively. Positive biases are simulated for NO_3^- (NMB=4.9%), ammonium (NH_4^+) (NMB=14.0%), and $PM_{2.5}$ (NMB=4.4%). In comparison with the statistics calculated from MICS–Asia Phase II, frequent updates of chemical mechanisms in CTMs during recent years make the inter–model variability of simulated aerosol concentrations smaller, and better performance can be found in reproducing the temporal variations of observations. However, a large variation (about a factor of 2) in the ratios of SNA (sulfate, nitrate and ammonium) to $PM_{2.5}$ is calculated among participant models. A more intense secondary formation of SO_4^{2-} is simulated by CMAQ models, because of the higher SOR (sulfur oxidation ration) than other models (0.51 vs. 0.39). The NOR (nitric oxidation ratio) calculated by all CTMs has larger values (~0.20) than the observations, indicating that overmuch NO_3^- is simulated by current models. NH₃–limited condition (the mole ratio of ammonium to sulfate and nitrate is smaller than 1) can be successfully reproduced by all participant models, which indicates that a small reduction in ammonia may improve the air quality. A large coefficient of variation (CV>1.0) is calculated for simulated coarse particles, especially over arid and semi–arid regions, which means that current CTMs have difficulty in producing similar dust emissions by using different dust schemes. According to the simulation results of MMEM in six large Asian cities, different air–pollution control plans should be taken owing to their different major air pollutants in different seasons. MICS–Asia project gives an opportunity to discuss the similarities and differences of simulation results among CTMs in East Asia applications. In order to acquire a better understanding of aerosol properties and their impacts, more experiments should be designed to reduce the diversities among air quality models." **(Page 1−2)**

Following the reviewer's suggestion, we have revised the conclusion and discussion part as follows: "This manuscript mainly focuses on the first topic of the MICS−Asia Phase III, and intends to analyze the following objectives: (1) provide a comprehensive evaluation of current air quality models against observations, (2) analyze the diversity of simulated aerosols among participant

3

models, and (3) reveal the characteristics of aerosol components in large cities over East Asia."

"Comparisons against monthly observations from EANET and CNEMC demonstrate that all participant models can well reproduce the spatial–temporal distributions of aerosols. The multi–model ensemble mean (MMEM) shows better performance than most single–model predictions, with correlation coefficients (Rs, between MMEN and measurements) ranging from 0.65 (nitrate, NO_3^-) to 0.83 ($PM_{2.5}$). Differences between predictions and observations are also simulated, such as sulfate (SO_4^{2-}) is underestimated by participant models (except M12 and M14), with NMBs ranging from −67.7% (M7) to −1.6% (M8). The concentrations of nitrate (NO_3^-) and ammonium (NH_4^+) are overestimated by most models, with NMBs of 4.9% for NO_3^- and 14.0% for NH_4^+ in MMEM. The absence of sulfate formation mechanisms (e.g. heterogeneous chemistry) in chemical transport models (CTMs) can be used to explain the underestimation of SO_4^{2-}, and the underestimated SO_4^{2-} will result in the overestimation of NO_3^-. However, significant underestimations of NO_3^- and NH_4^+ are shown in M7 and M8. This is because extremely low values of NH_3 are simulated by these models. The inter–model spread of simulated $PM_{2.5}$ is large, with NMBs ranging from −26.5% (M13) to 46.0% (M14), and nearly all models underestimate the $PM_{2.5}$ concentrations in Region_1. The underestimation may be the insufficient precursors and formation pathways of organic aerosols in current CTMs. Underestimations of PM_{10} are also simulated in each sub–region, and the NMB is −32.6% in MMEM. This may due to the inaccurate emission inventories (e.g. anthropogenic emissions, biomass burning emissions, and natural emissions) considered in CMTs."

"In order to reveal the improvements of the simulation ability in current CTMs, statistics for observed and simulated SO_4^{2-}, NO_3^- and NH_4^+ from MICS–Asia Phase II and Phase III are compared. Results obviously show that the spread of root–mean squared errors (RMSEs) for each species in Phase III is smaller, meaning similar concentrations can be simulated by current CTMs. Meanwhile, the medians of the correlations, including the upper and lower quartiles, are larger, which means current CTMs show better performance in reproducing the temporal variations of observations."

"Analyzing the ratio of SNA (sulfate, nitrate and ammonium) to $PM_{2.5}$, large variations are simulated by participant models, with values ranging from 31.1% (M7) to 75.1% (M5). Different gas phase and aerosol schemes used in CTMs can explain this inconsistency. Higher SOR (sulfur oxidation ratio) is calculated by CMAQ models, indicating that CMAQ has a more intense secondary formation of SO_4^{2-} than other participant models. Similar NOR (nitric oxidation ration) is predicted by CTMs, but the value (~0.20) is larger than the observed one (~0.15), which means overmuch NO_3^- is simulated by current CTMs. According to the mole ratio of ammonium to sulfate and nitrate, NH_3–limited condition can be successfully simulated by all participant models, which indicates that a small reduction in ammonia may improve the air quality significantly."

"The coefficient of variation (CV) can be used to quantify the inter–model deviation, and a large CV is shown in simulated coarse particles (subtract $PM_{2.5}$ from PM_{10}). The poor consistency, especially over the arid and semi–arid regions, is mainly caused by the dust aerosols, which means current CTMs have difficulty in reproducing similar dust emissions by using different dust schemes. But the simulated fine particles are in good agreement, especially over the haze–polluted areas."

"According to the MMEM simulation results, the highest $PM_{2.5}$ concentrations in Beijing, Shanghai, Guangzhou and Delhi are shown in winter, mainly due to the high emissions and unfavorable weather conditions. But the highest value in Tokyo appears in summer. $PM_{2.5}$ concentrations are comparable in the four seasons in Seoul. Analyzing the ratios of each

composition to PM$_{2.5}$, NO$_3^-$ is the major component in Beijing and Delhi, SO$_4^{2-}$ is the major one in Guangzhou, similar contributions of SO$_4^{2-}$ and NO$_3^-$ are calculated in Shanghai, Seoul and Tokyo. All these suggest that different air−pollution control plans should be taken in different cities."

"MICS−Asia project gives an opportunity to understand the performance of CTMs in East Asia applications, including the similarities and differences among air quality models. In order to quantify the impacts of different model inputs and model configurations, and to reduce the diversities among simulation results, more detailed sensitivity experiments should be discussed. For example, simulation results from M1 and M2 can be used to assess the impacts of boundary conditions (BCs), since the configurations in these two models are similar except the BCs. M1 adopts the downscale results from GEOS−Chem, while M2 uses the default values from CMAQ. From Fig. S9 we can find that positive biases are simulated ($(M1 − M2)/M2 * 100\% > 0$), especially around the edges of the simulation domain, and the maximum deviation can be over 100%. This is because the boundary conditions from GEOS−Chem consider the impacts of aerosols outside the domain. All these demonstrate that the impacts of BCs should not be neglected when analyzing the spatial distribution characteristic of simulated aerosols around the edge of the domain. But in most inland regions, differences between M1 and M2 are smaller ($< \pm 10\%$). Meanwhile, process analysis techniques (i.e. integrated process rate (IPR) analysis) should be developed and implemented in air quality models. This is because IPR can be used to calculate the contributions of each physical/chemical process to variations in aerosol concentrations (Chen et al., 2019), then it will be easier to draw conclusions about the fundamental problems that cause the differences between model predictions (Carmichael et al., 2008). Fully understanding of the source−receptor relationship in each process for a given aerosol species can also be helpful to revise parameterization schemes for better simulation capability. What's more, extensive observations should be collected and used in the next MICS−Asia project." **(Section 4 in Page 21−23)**

Specific Comments:

1. *Page 4 line 23: to present and summary the: summary should be summarize; please improve the language carefully through the entire manuscript.*

Response:

Following the reviewer's suggestion, we have revised the sentence: "This manuscript focuses on the first topic of the MICS−Asia Phase III, and intends to present and summarize the following three objectives." **(Page 4, Line 21−22)**

2. *Page 7 line 3: weird expression "incredible" here.*

Response:

Thank you for your suggestion. We have revised the sentences: "Simulation results of BC, OC, SO$_4^{2-}$, NO$_3^-$, NH$_4^+$, PM$_{2.5}$, PM$_{10}$ and AOD are requested to submit for the project, but no data can be acquired from M10, and extremely large values are predicted by M3." **(Page 12, Line 25−27)**

3. *Page 11 line 7: "incorrect treatments of the NH3 emission inputs": this statement is not supported by any evidence in the manuscript. How about plotting NH3 emissions from these*

two models? From Fig. 15, predicted sulfate from M7 and M8 look consistent with others. If NH3 emissions are not treated well, it should affect sulfate significantly. My sense is that nitrate from M7 and M8 are problematic. Please figure out the real reason.

Response:

Thank you for your suggestion.

Generally, there are two pathways about the NO_3^- formation in air quality models. The dominant pathway is the homogeneous gas−phase reactions between HNO_3 and NH_3 under ammonia−rich conditions, and the second pathway is the heterogeneous hydrolysis of N_2O_5 on aerosol surface at night in ammonia−poor environment. As H_2SO_4 is nonvolatile, and the equilibrium surface concentration in the model is set to be zero. So $(NH4)_2SO_4$ is the preferential species in the completion when H_2SO_4 and HNO_3 are both present, and NH_4NO_3 is formed only if excess NH_3 is available beyond the sulfate requirement.

However, the mole ratio of nNH_4^+/nSO_4^{2-} (n refers to the molar concentration) calculated by M7 and M8 are relative small (0.42 for M7 and 1.1 for M8), which means acidic sulfate cannot be fully neutralized by ammonia to form $(NH_4)_2SO_4$ or even NH_4HSO_4, especially in M7. This is because extremely low concentrations of NH_3 are simulated by M7 and M8 (Fig. S4). So fewer NH_4NO_3 and/or NO_3^- can be formed. Meanwhile, the hydrolysis of N_2O_5 is not considered in M7 and M8. All these result in the lower concentrations of NO_3^-.
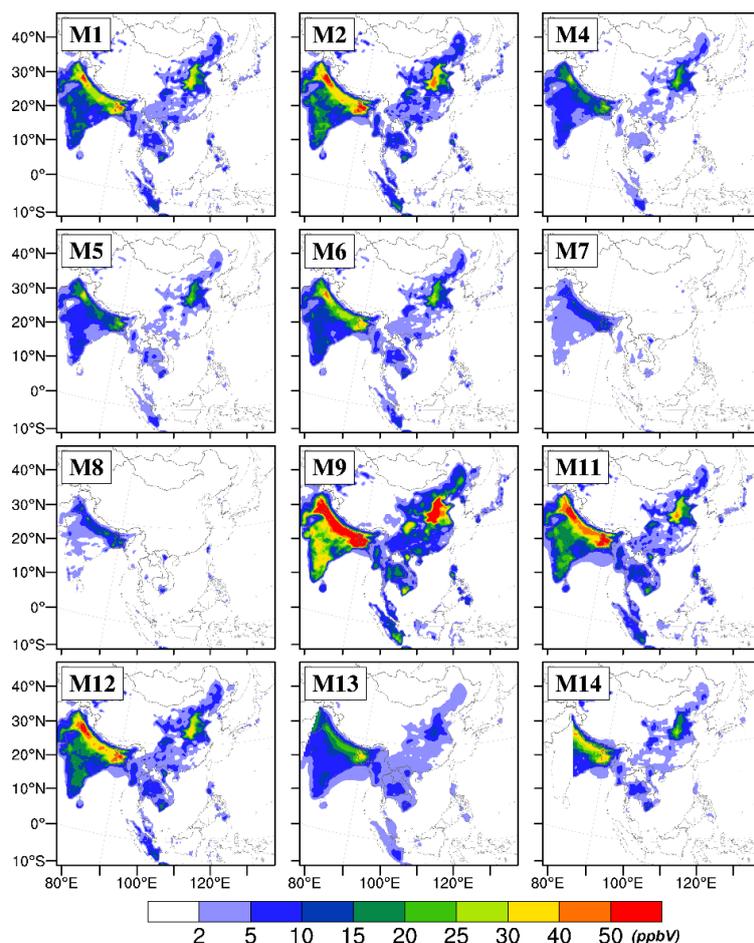

Figure S4. Spatial distributions of simulated NH₃ concentrations from each participant model.

Simulated NH_4^+ concentrations are influenced by the partitioning between gaseous NH_3 and aerosol NH_4^+, and are also associated with the SO_4^{2-} and NO_3^- concentrations. Even though the same NH_3 emissions are employed by all participant models (Fig. S2(c)), extremely low values are simulated by M7 and M8, especially over the mainland of China, which means fewer gaseous NH_3 can be converted to aerosol NH_4^+. Analyzing the mole ratios of nNH_4^+/nSO_4^{2-} from M7 (0.42) and M8 (1.1), lower concentrations of NH_4^+ will be simulated by M7.
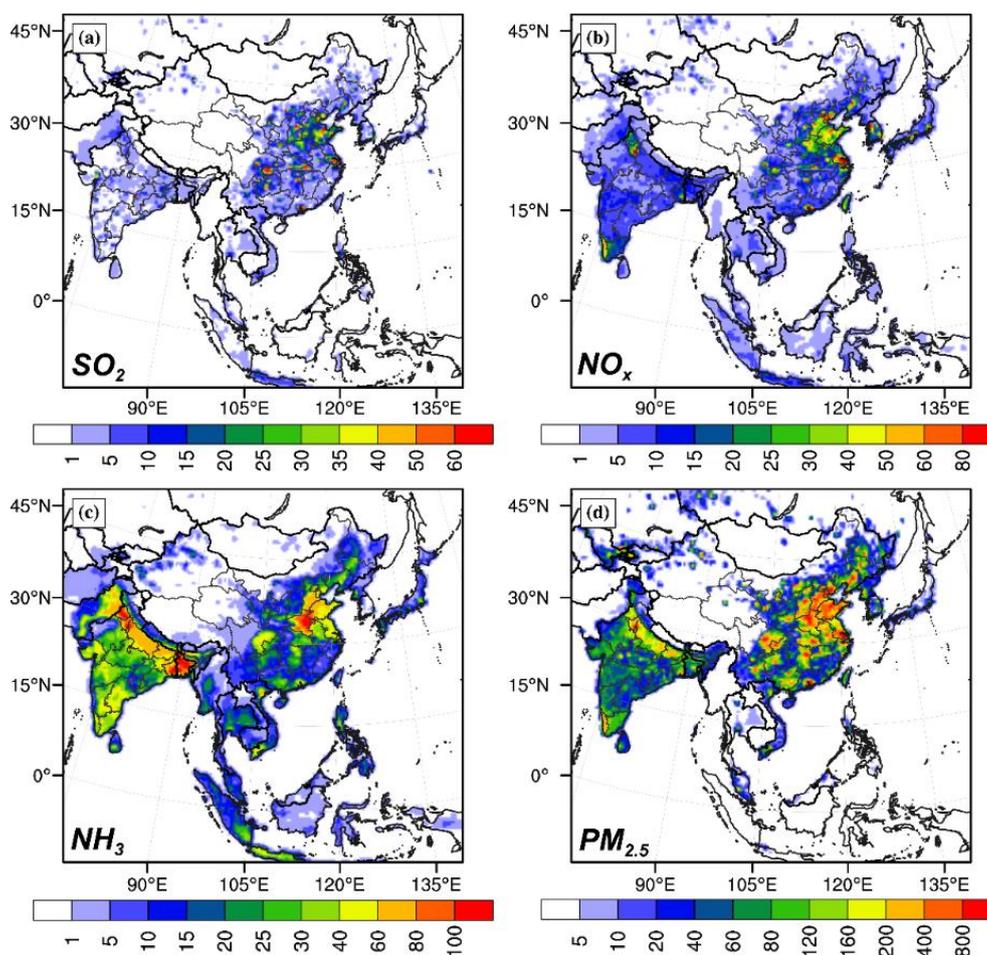
**Figure S2.** The merged emissions of (a) SO₂, (b) NOₓ, (c) NH₃ and (d) PM₂.₅ in 2010 from MIX (anthropogenic emission), MEGAN (biogenic emission), GFED (biomass burning emission), air and ship emission, and volcanic emission. The unit for gas is Mmol/month/grid, and the unit for particulate is Mg/month/grid.

Following the reviewer's suggestion, we have revised the sentences as "For NO_3^-, low concentrations are observed in Region_1 (1.5 μg m⁻³), Region_3 (0.6 μg m⁻³) and Region_4 (1.8 μg m⁻³), but high values are presented in Region_2 (13.4 μg m⁻³), showing the similar spatial distribution characteristics as the observed SO_4^{2-}. In CTMs, there are two pathways about the nitrate formation. The dominant pathway is the homogeneous gas−phase reaction between HNO_3 (NO_2 oxidation by OH during the daytime) and NH_3 under ammonia−rich conditions, and the second pathway is the heterogeneous hydrolysis of N_2O_5 on aerosol surface at night in ammonia−poor environment (Seinfeld and Pandis, 2006; Archer−Nicholls et al., 2014). As NH_4NO_3 is semi−volatile species, and the equilibrium surface concentration of H_2SO_4 is set to be zero in CTMs, so $(NH_4)_2SO_4$ is the preferential species in the completion when H2SO4 and HNO3 are both present. Only if NH_3

is excess, then NH_4NO_3 will been formed. Analyzing the performance of each participant model, NO_3^- concentration is overpredicted by most models, and the underestimation of SO_4^{2-} can be used to explain this overestimation (Chen et al., 2017). Meanwhile, the biases of model calculated gas−phase oxidation (e.g. $NO_2 + OH \rightarrow HNO_3$) and/or gas−aerosol phase partitioning (e.g. $HNO_{3(g)} + NH_{3(g)} \leftrightarrow NH_4NO_{3(s,\ aq)}$) may also result in the overestimation (Brunner et al., 2014; Gao et al., 2014). However, M7 and M8 significantly underestimate the observed NO_3^- concentrations (NMB~−93.4%). One reason for the extremely low values may result from the incorrect concentrations of NH_3 simulated by M7 and M8 (Fig. S4). As Chen et al. (2016) pointed out that the amount of NH_3 is a key factor in determining the NO_3^- concentration. Another reason for this underestimation is M7 and M8 did not consider the impacts of N_2O_5 heterogeneous reaction ($N_2O_{5(g)} + H_2O_{(aq)} \rightarrow 2HNO_{3(aq)}$). Su et al. (2017) pointed out that the hydrolysis of N_2O_5 can led up to 21.0% enhancement of NO_3^-, especially over polluted regions. Although the NMB calculated in Region_All for MMEM is only −1.1%, MMEM systematically overpredicts observations in Region_1 (NMB=45.2%) and Region_3 (NMB=38.2%), but underpredicts in Region_2 (NMB=−0.7%) and Region_4 (NMB=−44.9%)" and "Simulated NH_4^+ concentrations are influenced by the partitioning between gaseous NH_3 and aerosol NH_4^+, and are also associated with the SO_4^{2-} and NO_3^- concentrations (Gao et al., 2018). Model predictions (except M7, M8 and M14) can reproduce the measurements relatively well in each defined sub−region. But significant overestimation is shown by M14, while significant underestimation is simulated by M7 and M8, especially in Region_2 with NMBs of 72.2% for M14, −94.9% for M7, and −81.0% for M8, respectively. For M14, overestimated SO_4^{2-} and NO_3^- make the concentrations of NH_4^+ higher, since more ammonium is required to neutralize particle−phase acid. For M7 and M8, extremely low concentrations of NH_3 are simulated, which means fewer gaseous NH_3 can be converted to aerosol NH_4^+. In general, the calculated NMB in Region_All for MMEM is 4.0%." **(Section 3.1.1 in Page 13−14)**

4. *Many statements in the manuscript were presented without showing any evidence. Another example is in page 10 line 27: I doubt M7 and M9 include heterogeneous uptake of SO2 on aerosols. Please make sure the descriptions of model cover the inclusion of important chemical reactions, which will help understand the reasons for differences.*

Response:

Thank you for your suggestion. We have revised the sentence: "As Zheng et al. (2015) and Shao et al. (2019) pointed out that missing sulfate formation mechanisms (e.g. heterogeneous sulfate chemistry) on aerosol in current air quality models may result in this underestimation, especially in China where significant increase of secondary aerosols (such as sulfate) can be observed during polluted periods (Liu et al. 2015)." **(Page 13, Line 16−19)**

According to the reviewer's comments, detailed descriptions about the model parameterizations, including gas phase chemistry **(Section 2.1.2.1 in Page 5−6)**, aerosol chemistry **(Section 2.1.2.2 in Page 6−7)**, dust scheme **(Section 2.1.3 in Page 8)** and sea−salt scheme **(Section 2.1.4 in Page 9)**, have been added in the revised manuscript.

5. *What can we learn from the evaluation and comparison? The authors need to add more discussions on this.*

Response:

Thank you for your suggestion. MICS−Asia project gives an opportunity to understand the performance of CTMs in East Asia applications, including the similarities and differences between simulation results from participant models.

From the revised model evaluation section **(Section 3.1, Page 12−18)**, we can conclude that:

(1) Air quality models can well reproduce the spatial and temporal variability patterns of aerosols in East Asia in 2010;

(2) Multi–model ensemble mean (MMEM) shows better performance than most single−model predictions, which means analyzing the simulation results from MMEM can have a relative common understanding of the properties of atmospheric aerosols and their impacts;

(3) The higher uncertainties in emission inventory, the larger biases will be simulated by air quality models;

(4) Nearly all participant models underpredict the concentrations of SO_4^{2-}, which means sulfate formation mechanisms should be updated in current CTMs.

From the revised model inter–comparison **(Section 3.3, Page 19−21)**, we can conclude that:

(1) High $PM_{2.5}$ concentrations (> 40 µg m^{-3}) can be reproduced by all participant models, and the calculated CV (coefficient of variation) averaged over these regions are low (< 0.3), indicating similar performance of the air quality models in simulating the air pollutants over haze–polluted areas;

(2) Even though similar magnitude of $PM_{2.5}$ are simulated, the ratio of SNA (sulfate, nitrate and ammonium) to $PM_{2.5}$ varies a lot (about a factor of 2) among participant models, which means different gas–phase and aerosol chemistry mechanisms used in these models cause this inconsistency;

(3) CMAQ models show higher SOR (sulfur oxidation ratio) than other participant models, so more intense secondary formation of SO_4^{2-} is simulated by CMAQ;

(4) Similar NOR (nitric oxidation ratio) is predicted by participant models, but the value (~0.20) is larger than the observed one (~0.15), meaning more NO_3^- is simulated by secondary formation in current air quality models;

(5) NH_3–deficient atmospheric condition can be successfully simulated by all participant models. A small reduction in ammonia will make the neutralizing effect weaker, and fewer SNA can be formed, which may improve the air quality significantly.

(6) For coarse particles (subtract $PM_{2.5}$ from PM_{10}), large CV is calculated, which means low consistency can be found in the simulation results. The low consistency of simulated coarse particles in each region is mainly caused by the dust aerosols, indicating current air quality models have difficulty in producing similar dust emissions by using different dust schemes.

Meanwhile, following the reviewer's suggestion, we also add the following discussion about the impacts of BCs in the revised manuscript: "MICS–Asia project gives an opportunity to understand the performance of CTMs in East Asia applications, including the similarities and differences among air quality models. In order to quantify the impacts of different model inputs and model configurations, and to reduce the diversities among simulation results, more detailed

sensitivity experiments should be discussed. For example, simulation results from M1 and M2 can be used to assess the impacts of boundary conditions (BCs), since the configurations in these two models are similar except the BCs. M1 adopts the downscale results from GEOS–Chem, while M2 uses the default values from CMAQ. From Fig. S9 we can find that positive biases are simulated $((M1 - M2)/M2 * 100\% > 0)$, especially around the edges of the simulation domain, and the maximum deviation can be over 100%. This is because the boundary conditions from GEOS-Chem consider the impacts of aerosols outside the domain. All these demonstrate that the impacts of BCs should not be neglected when analyzing the spatial distribution characteristic of simulated aerosols around the edge of the domain. But in most inland regions, differences between M1 and M2 are smaller ($< \pm 10\%$)." **(Section 4 in Page 22, Line 25−34)**

References:

Gao, M., Han, Z., Liu, Z., Li, M., Xin, J., Tao, Z., Li, J., Kang, E., Huang, K., Dong, X., Zhuang, B., Li, S., Ge, B., Wu, Q., Cheng, Y., Wang, Y., Lee, H. J., Kim, C. H., Fu, J. S., Wang, T., Chin, M., Woo, J. H., Zhang, Q., Wang, Z., and Carmichael, G. R.: Air Quality and Climate Change, Topic 3 of the Model Inter Comparison Study for Asia Phase III (MICS Asia III), Part I: overview and model evaluation, Atmospheric Chemistry and Physics, 18, 4859 4884, 10.5194/acp 18 4859 2018, 2018.

Thank you very much for your comments and suggestions.

Marked-up Manuscript:

MICS-Asia III: Multi-model comparison and evaluation of aerosol over East Asia

Lei Chen[1,2,6], Yi Gao[1], Meigen Zhang[1,3,4], Joshua S. Fu[5], Jia Zhu[62,6,7], Hong Liao[2,67], Jialin Li[1], Kan Huang[5], Baozhu Ge[1], Xuemei Wang[8], Yun Fat LAM[9], Chuan Yao Lin[10], Syuichi Itahashi[11,12], Tatsuya Nagashima[13], Mizuo Kajino[14,15], Kazuyo Yamaji[16], Zifa Wang[1,3], and Jun-ichi Kurokawa[17]

[1]State Key Laboratory of Atmospheric Boundary Layer Physics and Atmospheric Chemistry, Institute of Atmospheric Physics, Chinese Academy of Sciences, Beijing, China
[2]School of Environmental Science and Engineering, Nanjing University of Information Science & Technology, Nanjing 210044, China
[3]University of Chinese Academy of Sciences, Beijing, China
[4]Center for Excellence in Regional Atmospheric Environment, Institute of Urban Environment, Chinese Academy of Sciences, Xiamen, China
[5]Department of Civil and Environmental Engineering, University of Tennessee, Knoxville, TN 37996, USA
[6]Research Institute of Climatic and Environmental Governance, Nanjing University of Information Science & Technology, Nanjing 210044, China
[6]Jiangsu Key Laboratory of Atmospheric Environment Monitoring and Pollution Control, Jiangsu Collaborative Innovation Center of Atmospheric Environment and Equipment Technology, Nanjing University of Information Science & Technology, Nanjing 210044, China
[7]International Joint Laboratory on Climate and Environmental Change, Nanjing University of Information Science & Technology, Nanjing 210044, China
[7]Research Institute of Climatic and Environmental Governance, Nanjing University of Information Science & Technology, Nanjing 210044, China
[8]Institute for Environment and Climate Research, Jinan University, Guangzhou, China
[9]School of Energy and Environment, City University of Hong Kong, Hong Kong
[10]Research Center for Environmental Changes, Academia Sinica, Taiwan
[11]Central Research Institute of Electric Power Industry, Abiko, Chiba 270-1194, Japan;
[12]Department of Marine, Earth, and Atmospheric Sciences, North Carolina State University, Raleigh, NC 27607, USA
[13]National Institute for Environmental Studies, Tsukuba, Japan
[14]Meteorological Research Institute, Japan Meteorological Agency, Tsukuba, 305-0052, Japan
[15]Faculty of Life and Environmental Sciences, University of Tsukuba, Tsukuba, 305-8577, Japan
[16]School of Science and Engineering, Meisei University, Hino, Tokyo 191-8506, Japan
[17]Asia Center for Air Pollution Research, 1182 Sowa, Nishi-ku, Niigata, Niigata, 950-2144, Japan

Correspondence to: M.G. Zhang (mgzhang@mail.iap.ac.cn)

带格式的：行距：多倍行距 1.15 字行

带格式的：字体：9.5 磅

Abstract. Fourteen chemical transport models (CTMs) participate in the topic 1 of the the Model Inter−Comparison Study

1

for Asia (MICS–Asia) Phase III. ~~MICS–Asia Phase III Topic 1. Their simulation~~These model results are compared with each other and ~~with~~ an extensive set of measurements, aiming to evaluate the current ~~multi–scale air quality models~~CTMs' ability in simulating aerosol ~~species~~ concentrations, ~~and~~ to document the similarities and differences among model performances, ~~also~~ to reveal the characteristics of aerosol ~~chemical~~ components ~~over big cities~~in large cities in East Asia. In general, ~~all participant models~~CTMs can well reproduce the spatial distribution and ~~seasonal~~ temporal variability of aerosol ~~concentrations~~s in ~~the year 2010~~East Asia during the year 2010, and multi–model ensemble mean (MMEM) shows better performance than most ~~individual~~ participant models, with ~~correlation coefficients Rs~~ ranging from 0.65 (NO_3^-) to 0.83 ($PM_{2.5}$). But the concentrations of black carbon, SO_4^{2-} and PM_{10} are underestimated by MMEM, with normalized mean biases (NMBs) of −17.0%, −19.1% and −32.6%, respectively. Positive biases are simulated in NO_3^- (NMB=4.9%), NH_4^+ (NMB=14.0%) and $PM_{2.5}$ (NMB=4.4%). In comparison with the statistics calculated from MICS–Asia Phase II, frequent updates of chemical mechanisms in CTMs during recent years make the inter–model variability of simulated aerosol concentrations smaller, and better performance can be found in reproducing the variation tendency of observations. However, a large variation (about a factor of 2) of the ratios of SNA (sulfate, nitrate and ammonium) to $PM_{2.5}$ is calculated among participant models, and a relative more intense secondary formation of SO_4^{2-} is simulated by CMAQ models due to the higher SOR (sulfur oxidation ration) than other models (0.51 vs. 0.39). Similar NOR (nitric oxidation ratio) is predicted by CTMs, but the value is large (~0.20), indicating overmuch NO_3^- is produced by current models. NH_3–limited condition can be reproduced by all participant models (the mole ratio of ammonium to sulfate and nitrate is smaller than 1), and a small reduction in ammonia may improve the current air quality. ~~Underestimations of BC (NMB=−17.0%), SO_4^{2-} (NMB=−19.1%) and PM_{10} (NMB=−32.6%) are simulated by EM, but positive biases are shown in NO_3^- (NMB=4.9%), NH_4^+ (NMB=14.0%) and $PM_{2.5}$ (NMB=4.4%). Simulation results of BC, OC, SO_4^{2-}, NO_3^- and NH_4^+ among CTMs are in good agreements, especially over polluted areas, such as the eastern China and the northern part of India. But large coefficients of variations (CV > 1.5) are also calculated over arid and semi–arid regions. This poor consistency among CTMs may attribute to their different processing capacities for dust aerosols.~~ A large coefficient of variation (CV>1.0) is shown in simulated coarse particles, especially over arid and semi–arid regions, which means current CTMs have difficulty in estimating similar dust emissions by using different dust schemes. According to the simulation results in the six Asian cities from MMEM, different air–pollution control plans should be made due to their different major air pollutants in different seasons. MICS–Asia project gives an opportunity to understand the performance of air quality models in East Asia. In order to acquire a mature comprehension of the properties of atmospheric aerosols and their impacts, and to reduce the diversities of simulated aerosols among CTMs, more detailed sensitivity experiments about parameterizations and model inputs should be carried out in future.

~~Although a more considerable capacity for reproducing the concentrations of aerosol chemical compositions and their variation tendencies is shown in current CTMs by comparing statistics (e.g. RMSE and R) between MICS–Asia Phase II and Phase III, detailed process analysis and a fully understanding of the source–receptor relationship in each process may be helpful to explain and to reduce large diversities of simulated aerosol concentrations among CTMs, and these may be the~~

带格式的：下标

带格式的：下标

带格式的：下标

potential development directions for future modeling studies in East Asia.

1 Introduction

~~Rapid u~~Urbanization and industrialization have stimulated economic growth and population expansion during the last several decades in East Asia (Spence et al., 2008; Yan et al., 2016; Chen et al., 2016), but also ~~brought about the~~bring about noticeable degradation of ecological environment at the same time (Hall 2002; Han et al., 2014; Yue et al., 2017). Significant increase in atmospheric aerosol loading, especially from anthropogenic emissions, can exert ~~much influence~~adverse effects on weather (Cowan et al., 2013~~; Gao et al., 2015a~~), climate (Wang et al., 2016a), air quality (Gao et al., 2016a), and even human health (Carmichael et al., 2009). For example, aerosols can ~~enhance the absorption and scattering of solar radiation to~~ modify the thermodynamic structure of the atmospheric boundary layer by absorbing and scattering solar radiation (Ding et al., 2016; Petaja et al., 2016), ~~can act as cloud condensation nuclei and ice nuclei to~~ alter cloud properties and precipitation by acting as cloud condensation nuclei and ice nuclei (Lohmann and Diehl, 2006; Wang, 2013a), ~~can trigger~~deteriorate visibility ~~deterioration and result in~~and cause haze events (Singh and Dey, 2012; Li et al., 2014). In addition, fine particulate matter with aerodynamic diameters smaller than 2.5 μm ($PM_{2.5}$) ~~can also~~may enter into the alveoli ~~to~~ and cause severe cardiovascular diseases, respiratory diseases and even lung cancer (Pope and Dockery, 2006; Gao et al., 2015a). ~~All these~~The impacts have attracted considerable attention~~s~~ ~~among~~from the public and policy makers in East Asia, and therefore the research on aerosols has become a hot topic ~~, which is frequently reported and deeply studied~~ during recent years.

In order to better understand the properties of atmospheric aerosols and their impacts, chemical transport models (CTMs) can be a critical tool, and they have been ~~drawn up and~~ applied to study various air pollution issues all over the world. For example, a fully coupled online Weather Research and Forecasting/Chemistry (WRF/Chem) model was developed by Grell et al. (2005), and ~~it has been widely~~was used to study the aerosol–radiation–cloud feedbacks on meteorology and air quality (Gao et al., 2014; Zhang et al., 2015a; Qiu et al., 2017); a Models–3 Community Multi–scale Air Quality (CMAQ) modeling system was designed by the US Environmental Protection Agency (Byun and Ching, 1999), and ~~was carried out~~it has been applied to address acid deposition, visibility and haze pollution issues (Zhang et al., 2006; Han et al., 2014; Fan et al., 2015); a nested air quality prediction model system (NAQPMS) was developed by the Institute of Atmospheric Physics, Chinese Academy of Science (IAP/CAS) (Wang et al., 2001) ~~for targeting at reproducing~~to reproduce the mechanism of transport and evolution of atmospheric pollutants in Asia (Li et al., 2012a; Wang et al., 2013c; Li et al., 2017a); a global three–dimensional chemical transport model (GEOS–~~CHEM~~Chem) was first presented by Bey et al. (2001), and ~~was applied~~researchers use the GEOS–Chem model to study the source sector contribution, long–range transport and the prediction of future change in ozone and aerosol concentrations (Liao et al., 2006; Li et al., 2016b; Zhu et al., 2017).

Although significant ~~advances have taken place~~advantages can be found in CTMs~~ in these CTMs~~, how to accurately reproduce ~~and/or~~or predict the concentrations and the distributions of atmospheric pollutants is still a challenge, with the problems of inaccurate emission inventories, poorly represented initial and boundary conditions, and imperfect physical, dynamical and chemical parameterizations (Carmichael et al., 2008). Meanwhile, most CTMs are designed to focus on the air quality over developed countries, such as Europe and America, rather than ~~in~~Asia, and the assumptions or look–up tables

4

used in ~~models~~ CTMs may not be suitable ~~to simulate the Asian environment~~for the simulation of the East Asian environment (Gao et al., 2018). Therefore, before providing ~~scientifically~~ meaningful ~~information~~ results and answering "what–if" questions for policy makers, model performances must be carefully ~~first~~ evaluated. Hayami et al. (2008) and Mann et al. (2014) pointed out that different parameterizations used in CTMs can cause large variations in simulation results, and multi–model ensemble mean (~~M~~MEM) tends to show better performance than most participant models when comparing with observations~~, and large variation in simulation results can be found among participant models, which may be caused by using different parameters and calculation methods in each CTM~~ (Carmichael et al., 2002; Hayami et al., 2008; Wang et al., 2008; Holloway et al., 2008). In order to develop a better common understanding of the performance and uncertainties of CTMs in East Asia applications, and to acquire a more mature comprehension of the properties of atmospheric aerosols and their impacts ~~in East Asia~~, a model inter–comparison study should be initiated, and Model Inter–Comparison Study for Asia (MICS–Asia) gives an opportunity to investigate these questions. Meanwhile, model inter–comparison study in East Asia is very limited (Phadnis et al., 1998; Kiley et al., 2003; Han et al., 2008), and far more efforts are needed in future.

The MICS–Asia project was initiated in 1998. In the first phase of MICS–Asia (MICS–Asia Phase I), the primary target was~~is~~ to study the long–range transport and deposition of SO_4^{2-} in East Asia by analyzing the submitted simulation results from eight CTMs. Source–receptor relationships, contributions ~~of wet/dry pathways for remove~~from removal processes, and the influences of model structures and ~~parameters~~ parameterizations on simulation ~~capability~~ results ~~are~~ were also estimated. More details can be found in Carmichael et al. (2002). As an extension of Phase I, MICS–Asia Phase II ~~includes~~ included more chemical species of concern, such as sulfur, nitrogen and ozone. This broader collaborative study examined four different periods, encompassing two different years and three different seasons (March, July, and December in 2001, and March in 2002). Simulation results ~~are~~ from nine different regional modeling groups were analyzed. Detailed information about this project can be found on the overview paper of Carmichael et al. (2008). In 2010, the MICS–Asia III project was launched. As a part of EANET additional research activity and a continuing research of MICS–Asia series, three topics ~~are~~ were discussed, including comparison and evaluation of current multi–scale air quality models (Topic 1), development of reliable emission inventories for CTMs in Asia (Topic 2), and interactions between air quality and climate changes (Topic 3).

This manuscript focuses on the first topic of the MICS–Asia Phase III~~,~~ and ~~tries~~ intends to ~~present and summary~~analyze the following three objectives, ~~which mainly specialize~~specializing in the ~~analysis~~topic of aerosol~~ species~~. Firstly, ~~a~~ comprehensive evaluations of the strengths and weaknesses of current ~~multi–scale air quality models~~CTMs for simulating particulate matter (PM) ~~is~~ are provided against extensive measurements from in–situ and satellites, aiming to show the capability of participant models. Secondly, ~~the~~ diversit~~y~~ies of simulated aerosol concentrations among participant models ~~is~~ are analyzed, including possible reasons for the bias. ~~suggestions about how to reduce uncertainties in simulation results, which can be used as a reference for future development and improvement of models.~~ Thirdly, characteristics of aerosol chemical ~~components~~ compositions in the six high–profile cities ~~over analyzed regions~~ in East Asia ~~are revealed~~analyzed, which may be helpful to provide confidence for future investigation of aerosol impacts on local and regional climate in East Asia.

The descriptions of model configurations, model inputs, ~~, analyzing area~~ and observation ~~data~~s are presented in Section 2. The evaluation for model performance and the inter–comparison between participant models are shown in Section 3. The conclusions and discussions are presented in Sections 4.

2 Inter–comparison framework

2.1 Model description

Fourteen regional models~~modeling groups~~ (M1–M14) participated in MICS–Asia phase III Topic 1. All models were required to run for the whole year of 2010 and to provide gridded monthly simulation results of aerosols in the first model layer. These CTMs include the Weather Research and Forecasting model coupled with Community Multiscale Air Quality (WRF–CMAQ), the Weather Research and Forecasting Model coupled with Chemistry (WRF–Chem), the nested air quality prediction model system (NAQPMS), the non–hydrostatic mesoscale model coupled with chemistry transport model (NHM–Chem), the global three–dimensional chemical transport model (GEOS–Chem), and the Regional Atmospheric Modeling System coupled with Community Multiscale Air Quality (RAMS–CMAQ). Among these models, there are three different versions of WRF–CMAQ (v5.0.2 is used by M1 and M2, v5.0.1 is used by M3, and v4.7.1 is used by M4, M5 and M6), four different versions of WRF–Chem (v3.7.1 is used by M7, v3.6.1 is used by M8, v3.6 is used by M9, and v3.5.1 is used by M10), one version of NAQPMS (M11), NHM–Chem (M12), GEOS–Chem (v9.1.3 is used by M13) and RAMS–CMAQ (v4.6 is used by M14). Basic information about the configurations of each model ~~is summarized~~is summarized in **Table 1**.

2.1 Model ~~description~~configurations

2.1.1 Simulation domain

A unified simulation domain was designed by MICS–Asia organizers, which covers the region of (15.4°S–58.3°N, 48.5°E–160.2°E) with 180×170 grid points at 45 km horizontal resolution, but participant models employed different modeling domains (as shown in **Fig. 1**) with different grid resolutions (e.g. 0.5° of latitude×0.667° of longitude for M13, 64 km×64 km for M14, others are 45 km×45 km). In order to minimize the influence from lateral boundary conditions and to cover most high–profile areas of East Asia, an analyzed region was chosen in this manuscript (the red box in **Fig. 1**). For M13 and M14, missing values were used to fill the grids outside their simulation domains. Meanwhile, the analyzed region was divided into five different areas (Region_1 to Region_5). Region_1 contains Korean Peninsula and Japan (filled with blue in **Fig. 1**). Region_2 only contains China (filled with cyan in **Fig. 1**). Region_3 contains Mongolia and parts of Russia (filled with chartreuse in **Fig. 1**). Region_4 covers most countries in Southeast Asia (filled with orange in **Fig. 1**). Region_5 contains most countries in South Asia (filled with purple in **Fig. 1**). Therefore, simulation results in each sub–region can be analyzed and compared to show the performance of current CTMs.

2.1.2 Gas and aerosol modules

Among these models, five different kinds of chemistry modules are applied, including CMAQ (Community Multiscale Air Quality), WRF–Chem (Weather Research and Forecasting Model coupled with Chemistry), NAQPMS (nested air quality prediction model system), NHM–Chem (non–hydrostatic mesoscale model coupled with chemistry transport model), and GEOS–Chem (global three–dimensional chemical transport model). For CMAQ, there are four different versions: CMAQ5.0.2 (M1 and M2), CMAQ5.0.1 (M3), CMAQ4.7.1 (M4, M5 and M6), and CMAQ4.6 (M14). For WRF–Chem, there are also four different versions: WRF–Chem3.7.1 (M7), WRF–Chem3.6.1 (M8), WRF–Chem3.6 (M9), and WRF–Chem3.5.1 (M10). Only one version is used for NAQPMS (M11), NHM–Chem (M12) and GEOS–Chem (version 9.1.3, M13).

The settings of gGas phase chemistry and aerosol chemistry are key componentsimportant parameterizations inof chemical transport modelsCTMs., Luecken et al. (2008) and Balzarini et al. (2015) pointed out that different settings of chemical mechanisms could influence the simulation results significantly.

2.1.2.1 Gas phase chemistry

(1) and can influence the simulation results significantly (Cuchiara et al., 2014). TThe gas chemistry of SAPRC–99 (Statewide Air Pollution Research Center 99the 1999 Statewide Air Pollution Research Center) was used in M1, M2, M4, M5, M6, M12 and M14. It is a detailed mechanism for the gas–phase atmospheric reactions of volatile organic compounds (VOCs) and oxides of nitrogen (NO_x) in urban and regional atmosphere (Carter, 2000)s. The SAPRC99 mechanism has already been incorporated into CMAQ v4.6 with about 72 species and 214 reactions. Meanwhile, another three heterogeneous chemistry reactions of N_2O_5, HO_2 and NO_2 are also considered in the SAPRC99 gas phase chemistry in M12 (Kajino et al., 2018).

(2) The Carbon Bond mechanism (CB05)It includes 76 species reacting in 214 reactions (Carter, 2000). CB05 (2005 Carbon Bond) chemical mechanism was used in M3. It describes tropospheric oxidant chemistry and provides a basis for computer modeling studies of ozone, particulate matter, visibility, acid deposition and air toxics issues, is a condensed mechanism of atmospheric oxidant chemistry that provides a basis for computer modeling studies of ozone, particulate matter (PM), visibility, acid deposition and air toxics issues, with 51 species and 156 reactions (Yarwood et al., 2005).

(3) The second generation Regional Acid Deposition Model (RADM2) gas phase chemical mechanism was used in M9 and M10. The inorganic species considered in RADM2 include M9 and M10 used RADM2 (Regional Acid Deposition Model, version 2) gas chemistry mechanism. The inorganic species 14 stable species, 4 reactive intermediates and 3 abundant stable species. The organic chemistry is included in the RADM2 are 14 stable species, 4 reactive intermediates, and 3 abundant stable species. Atmospheric organic chemistry is represented by 26 stable species and 16 peroxy radicals (Stockwell et al., 1990). This module can simulate the concentrations of PAN, HNO_3 and H_2O_2 under different environmental conditions (Stockwell et al., 1990).

(4) Based on RADM2, the Regional Atmospheric Chemistry Mechanism (RACM) was developed with updated reaction rate constants and product yields according to more recent laboratory measurements. It is capable of simulating the troposphere from the Earth's surface through the upper troposphere and to be valid for simulating remote to polluted urban conditions (Stockwell et al., 1997). M7 and M8 selected the RACM module, and the rate coefficients were further updated in M7 (Kim et al., 2009).

(5) The gas chemistry of Carbon–Bond Mechanism version Z (CBMZ) was used in M11. This lumped–structure mechanism ~~It has been extensively used in atmospheric models to predict concentrations of oxidants and other air pollutants. Based on RADM2, Regional Atmospheric Chemistry Mechanism (RACM) created by Stockwell et al. (1997) is capable of modeling a wide variety of complex and practical situations, from the Earth's surface to the troposphere and from remote to polluted urban conditions. This mechanism was used in M7 and M8, including 17 stable inorganic species, 4 inorganic intermediates, 32 stable organic species, and 24 organic intermediates, with up to 237 reactions. M11 used CBMZ (Carbon–Bond Mechanism version Z) and this mechanism~~ extends the original framework of CBM–IV to function properly at larger spatial and longer timescales, with revised inorganic chemistry, isoprene chemistry, and many other related parameterizations~~67 species and 164 reactions~~ (Zaveri and Peters, 1999).

(6) In M13, the NOx–Ox–HC–Br tropospheric gas chemistry mechanism was used. It includes about 80 species and 300 chemical reactions (Bey et al., 2001; Zhu et al., 2017).

Jimenez et al. (2003), Luecken et al. (2008) and Yang et al. (2018) summarized that different gas–phase chemistry mechanisms could predict large variations in reactive species, such as HO_2 and NO_3, making the production of OH and H_2O_2 different. In addition to the different number of species and reactions considered in each gas module, the reaction rates of the oxidation of SO_2, NO_x and some VOCs to condensable SO_4^{2-}, NO_3^- and organic species are also largely different (Pan and Zhang, 2008). All these would affect the concentration of particulate matter (PM), especially under the urban condition.

2.1.2.2 Aerosol chemistry

(1) AERO with ISORROPIA: Aerosol modules (AERO5 and AERO6) with thermodynamic equilibrium models (ISORROPIA v1.7 and v2) were used in M1, M2, M3, M4, M5, M6, M11, M12 and M14. Aerosols in AERO were divided into three modes: Aitken, accumulation and coarse modes. Gas–liquid–solid equilibrium in inorganic aerosol was predicted by the ISORROPIA model. The AERO5 ISORROPIA (v1.7) was mainly used in CMAQ v4, and the updated AERO6 ISORROPIA (v2) has been implemented since CMAQ v5. Nine new PM species (e.g. Ca^{2+}, K^+ and Mg^{2+}) were added in the new aerosol module of AERO6. In order to support the additional crustal ion emissions introduced in AERO6, ISORROPIA (v1.7) was replaced by ISORROPIA (v2) (Nenes et al, 1998; Fountoukis and Nenes, 2007), and the corresponding modifications could affect the gas–particle partitioning of NO_3^- and NH_4^+. The rate constants for the S (IV) to S (VI) conversion through in–cloud oxidation pathways were also modified, including the catalysis effects through aqueous chemistry from Fe and Mn (Appel et al., 2013). In order to solve the over–predictions of the unspeciated $PM_{2.5}$ (also called PM_{other}) in CMAQ v4, detailed speciation profiles derived from Reff et al. (2009) were adopted in CMAQ v5 to

subdivide the emissions of PM_{other} into primary NO_4^+, Na^+, Cl^- and other selected trace elements. Comparing with CMAQ v4.6, a new parameterization of heterogeneous N_2O_5 hydrolysis was included in CMAQ v4.7 to improve the simulation results of NO_3^-. Comparing with CMAQ v5.0.1, a mass balance correction of NO_3^- aerosol under cold conditions was adopted in CMAQ v5.0.2, and this adjustment would reduce the concentration of NO_3 and HNO_3 at the surface level.

(2) MADE/SORGAM and MADE/VBS: Detailed treatments of inorganic aerosol effects in M7, M8 and M9 were simulated by Modal Aerosol Dynamics Model for Europe (MADE). Three log–normal modes (Aitken, accumulation and coarse modes) were used in this module to present the particle size distribution of submicrometer aerosol, such as SO_4^{2-}, NO_3^-, NH_4^+, BC, OC and aerosol water (Ackermann et al., 1998). Aerosols were assumed to be internally mixed in the same mode but externally mixed among different modes (Zhao et al., 2010). The organic chemistry used in M7 and M9 was based on SORGAM (Secondary Organic Aerosol Model). This model was capable of simulating SOA formation including the production of low–volatility products and their subsequent gas–particle partitioning (Schell et al., 2001), but all activity coefficients were assumed to be 1 due to insufficient information. However, when it was coupled with MADE, the biogenic precursors and their resulting particle concentrations were set to be zero. The organic chemistry used in M8 was based on the Volatility Basis Set (VBS) approach (Ahmadov et al., 2012). This module used the volatility basis set framework to simulate primary organic aerosol partitioning between the gas and particulate phases and the gas–phase oxidation of the corresponding vapors (Murphy and Pandis, 2009).

(3) GOCART In order to have a comprehensive understanding of factors controlling tropospheric ozone, one major theme of the gas chemistry mechanism used in M13 (GEOS–Chem) is the simulation of ozone–NOₓ–hydrocarbon chemistry, which includes about 80 species and 300 chemical reactions (Bey et al., 2001; Zhu et al., 2017).:

The Goddard Chemistry Aerosol Radiation and Transport (GOCART) model was used in M10 to simulate tropospheric aerosol components, such as SO_4^{2-}, dust, BC, OC and sea–salt aerosols (NO_3^- and NH_4^+ are not considered), and all these aerosol species were assumed to be log–normal size distributions (Chin et al., 2000). SO_4^{2-} was formed by the oxidation of SO_2 in the atmosphere, but the impacts from in–cloud oxidation pathways were not included (Chin et al., 2002). The source emission of BC and OC was mainly from biomass burning. Dust emission was following Ginoux et al. (2001). Sea-salt emission was highly dependent on wind speed. More details about the simulations of dust and sea–salt aerosols in GOCART will be described in Section 2.1.3 and 2.1.4.

Different chemical species are considered in numerous aerosol equilibrium models, resulting in different equilibrium partitioning and water uptake during their simulation processes, which can affect the predicted aerosol concentrations (Fountoukis and Nenes, 2007). As Moya et al. (2002) and Wang et al. (2012b) classified that the treatment of crustal material in aerosol chemistry could considerably improve model prediction in predicting the partitioning of NO_3^- and NH_4^+. Different heterogeneous reactions and their activity coefficients used in the thermodynamic equilibrium would also be a major source of uncertainty in simulated aerosol concentrations (Li et al., 2012a; Kim et al., 2011; Chen et al., 2016a).

2.1.3 Dust scheme

Natural emissions of windblown dust have been explicitly parameterized ~~The Aero5/Aero6 aerosol module with ISORROPIA aerosol thermodynamics v1.7/v2 were used in M1, M2, M3, M4, M5, M6, M11, M12 and M14. It is designed to simulate the thermodynamic equilibrium of inorganic species (e.g. NH_4^+, sodium, chloride, NO_3^-, SO_4^{2-} and water), and all the aerosol particles are assumed to be internally mixed (Nenes et al, 1998). Meanwhile, these modules use a weighted average approach to approximate the aerosol composition in mutual deliquescence regions, which can speed up the solution time. The Aero5 ISORROPIA (v1.7) was mainly used in CMAQ model version before 5.0, after which the second version (ISORROPIA (v2)) was implemented. The main change in ISORROPIA v2 is to introduce thermodynamics of crustal species such as Ca^{2+}, K^+ and Mg^{2+} (Fountoukis and Nenes, 2007), and the corresponding impacts are mainly on the gas-particle partitioning of NO_3^- and NH_4^+ in areas with high dust emissions. Wang et al. (2012b) pointed out that the updated treatment of crustal species in ISORROPIA v2 can reduce fine mode of particle matter over polluted areas. The aerosol module used in M7 and M9 is MADE (Modal Aerosol Dynamics Model for Europe) (Ackermann et al., 1998) for the inorganic fraction, and the Secondary Organic Aerosol Model (SORGAM) (Schell et al., 2001) for the carbonaceous secondary fraction. For MADE/SORGAM, the modal approach with three log-normally distributed modes (nuclei, accumulation and coarse mode) is implemented in the WRF-Chem model. Similar as the aerosol chemistry of MADE/SORGAM, secondary organic aerosols (SOA) was also simulated by the advanced Volatility Basis Set (VBS) approach in M8 (Tuccella et al., 2015). The bulk GOCART (Goddard Global Ozone Chemistry Aerosol Radiation and Transport) aerosol module (originally developed by NASA) used in M10 can output fourteen aerosol species, including hydrophobic and hydrophilic organic carbon (OC1 and OC2) and black carbon (BC1 and BC2), SO_4^{2-}, dust in five particle-size bins, and sea salt in four particle-size bins. This mechanism can provide an integrated sectional scheme for dust emission and aerosol advection, but indirect effects and wet scavenging/deposition schemes regarding cloud interactions are not supported (Chin et al., 2000). Aerosol species considered in GEOS-Chem (M13) include SO_4^{2-} (Park et al., 2004), NO_3^- (Pye et al., 2009), NH_4^+, OC and BC (Park et al., 2003), mineral dust (Fairlie et al., 2007), and sea salt (Alexander et al., 2005).~~since CMAQ v5 (Foroutan et al., 2017), but all the participated WRF–CMAQ models did not turn this option on, which means dust aerosols were not considered in M1–M6. Meanwhile, the dust scheme in M7 and M8 was also turned off.

Dust particles in M10 and M13 were simulated by the GOCART model (Ginoux et al., 2001). This model includes eight size groups of mineral dust ranging from 0.1 to 10 μm. The emission flux for a size group can be expressed as follows: $F = C \times S \times s_p \times u_{10}^2 \times (u_{10} - u_t), if\ u_{10} > u_t$, where C is a constant with the value of 1 μg $s^2\ m^{-5}$. S means the probability source function, representing the fraction of alluvium available for wind erosion. s_p is the fraction of each size group within the soil. u_{10} and u_t are the wind speed at 10 m and threshold velocity of wind erosion, respectively.

A simplified dust emission parameterization proposed by Shao (2001) was used in M9 (Shao, 2004). ~~The d~~Dust emission in Shao_2004 is proportional to streamwise saltation flux, and the proportionality depends on soil texture and soil plastic pressure. The size–resolved dust flux goes into four size bins, with diameters ranging from 1.95 to 20 μm (Kang et al.,

带格式的：上标
带格式的：上标

2011). More detail about the dust emission rate and the total dust flux can be found in Shao (2004).

A size–segregated dust deflation module proposed by Wang et al. (2000) was used in M11. It was developed based on three major predictors (friction velocity, surface humidity and dominant weather system), and has been successfully applied in many dust-related simulations (Wang et al., 2002; Yue et al., 2010). The dust flux F is calculated as follows:

$$F = C \times \frac{\rho_a}{g} \times E \times u^{*3} \times \left(1 + \frac{u_0^*}{u^*}\right) \times \left(1 - \frac{u_0^{*2}}{u^{*2}}\right) \times \left(1 - \frac{RH}{RH_0}\right),$$ where C equals to 10^{-5}, ρ_a means air density, g is gravitational acceleration. E is the weighting factor, representing the uplifting capability of land surface. u_0^* and u^* are the fraction and threshold friction velocities, respectively. RH and RH_0 are relative humidity and threshold relative humidity, respectively. According to soil categories and vegetation coverage, the dust emission intensity was further modified by Luo and Wang (2006). Four size bins of dust particles ranging from 0.43 to 10 μm were considered in this emission module. Meanwhile, several heterogeneous reactions on dust particles were also considered (Li et al., 2012a).

An empirical dust emission mechanism based on the approach of Gillette and Passi (1988) was used in M12 and M14 (Han et al., 2004). Dust flux can be calculated through the following formula: $F = C \times u_*^4 \times \left(1 - \frac{u_*}{u}\right) \times (1 - f \times R), if \, u > u_*$, where u and u_* are the friction and the threshold friction velocities, respectively. C is the correction coefficient (1.4×10^{-15}). f and R represent the fractional coverage of vegetation and the reduction factor in a model grid.

Dust particles with diameters ranging from 0.43 to 42 μm were grouped into 11 bins, with the first eight bins below 11 μm for aerosol sampler, and the additional three bins above 11 μm for larger particles (Han et al., 2004).

Different dust schemes will produce different dust emission fluxes over arid and semi-arid regions (Zhao et al., 2010; Su and Fung, 2015).

Several factors, such as potential source regions, threshold friction velocity, size distribution, and other surface and soil–related parameters used in equations can be the primary causes for the inconsistency, and the differences in simulated dust emissions will affect the characteristics of spatial–temporal variations of atmospheric aerosol particles.

2.1.4 Sea–salt scheme

As one of the major components of primary aerosols, sea–salt aerosols contributes to 20–40% of secondary inorganic aerosols (SIAs) over coastal regions (Liu et al., 2015; Yang et al., 2016). These particles can provide surface areas for condensation and reaction of nitrogen and sulfur, making the simulated concentrations of SIAs more accurate (Kelly et al., 2010; Im, 2013).

In M12, the method of Clarke et al. (2006) was used to simulate the sea–salt emissions as follows: $S_{100} = \frac{C_S \times k \times V_{wind} \times h}{A_{avg} \times L + 0.5 \times w_0}$. The sea–salt source function (S_{100}) is defined as the number of sea–salt aerosols generated per unit area of ocean surface completely covered by bubbles (100% coverage) per unit time. C_S is the differences of condensation nuclei concentrations collected at 5 m (impacted by breaking waves) and 20 m (background values). k is the multiplier for tower C_S compared to mean profile. V_{wind} means surf zone wind speed. h is the height of plume layer for beach profile. A_{avg}

represent mean bubble fractional coverage area between waves. L is the distance wave travels to shore, and w_0 is the initial width of breaking wave bubble front.

In other participating models (sea–salt emission is not considered in M7 and M8), sea–salt emissions were simulated online by using the algorithm proposed by Gong et al. (2003). The density function $\frac{dF}{dr}$ (m^{-2} s^{-2} μm^{-1}) is calculated as follows:

$$\frac{dF}{dr} = 1.373 \times u_{10m}^{3.41} \times r^{-A} \times (1 + 0.057 \times r^{3.45}) \times 10^{1.607e^{-B^2}}$$

, where u_{10m} is the 10 m wind speed, r is the particle radius at RH=80%. A represents an adjustment parameter, which control the shape of submicron size distribution. B = $(0.433 - log_{10}(r))/0.433$, meaning a parameter related to particle radius. In CMAQ model, the sea–salt scheme was updated by Kelly et al. (2010) to enhance the emission of sea–salt from coastal surf zone, and to allow dynamic transfer of HNO$_3$, H$_2$SO$_4$, HCl, and NH$_3$ between coarse particles and gas phase. In GEOS-Chem model, it was updated by Jaegle et al. (2011) to improve the simulation of sea–salt with dry radii smaller than 0.1 μm.

~~As is known to all that meteorological fields has a profound impact on air quality, and aerosol compositions can affect weather and climate directly by changing clouds, radiation, and precipitation (Forkel et al., 2015). In order to simulate the concentrations of air pollutants, meteorological models and chemistry transport models can be implemented either offline or online (Kong et al., 2015). Offline modeling implies that CTM is run after the meteorological simulation is completed, and the chemistry feedbacks on meteorology are not considered. Online modeling allows coupling and integration of some of the physical and chemical components (Baklanov et al., 2014). According to the extent of online coupling, there are two ways of coupling: online integrated coupling (meteorology and chemistry are simulated in one model using the same grid and using one main time step for integration) and online access coupling (meteorology and chemistry are independent, but information can be exchanged between meteorology and chemistry on a regular basis) (Baklanov et al., 2014). Among these participating models, M4, M5, M6, M12, M13 and M14 are offline models. M1, M2, M3, and M11 are online access models. M7, M8, M9 and M10 are online integrated models. Different coupling methods can cause different simulation results due to the interactions among aerosol, weather and climate. Even though using the same coupling way, different parameterizations can also cause uncertainties. More details about the model configurations are summarized in Table 1 and other MICS–Asia Phase III companion papers.~~

~~For aerosol species, modeling variables of BC, OC, SO$_4^{2-}$, NO$_3^-$, NH$_4^+$, PM$_{2.5}$, PM$_{10}$ and AOD from the fourteen participant models, as listed in Table 2, are requested to upload to a public server. But no data are acquired from M10, and all simulation results from M3 are incredible. Therefore, only twelve models are analyzed in this manuscript. Meanwhile, M5, M6 and M8 did not submit simulated AOD. M13 did not submit simulated PM$_{10}$. M7 did not submit OC. Neither BC nor OC was submitted from M9.~~

2.2 ~~Information about m~~Model inputs

Based on the experience ~~of~~ concluded from Phase I and Phase II, all the fourteen ~~participant~~ models in Phase III Topic 1, in principle, ~~are~~ were required to use ~~common~~ "standard" meteorological fields, emission inventories and boundary

conditions in order to reduce the potential diversity of inter-model variability that may be caused by input datasets. But different inputs were selected by participant models. In this section, some basic information about these inputs will be described.

2.2.1 Meteorological fields

The "standard" hourly meteorological fields were simulated by the Weather Research and Forecasting Model (WRF v3.4.1) with the initial and lateral boundary conditions taken from the National Center for Environmental Prediction (NCEP) Final Analysis (FNL) data. Four–dimensional data assimilation nudging toward the NCEP FNL data was also adopted to increase the accuracy of simulated meteorological variables. The reference meteorological fields were only used in M1–M6 and M11. For M7, M8 and M9, the standard meteorological simulation was run by the same model (WRF), but feedbacks between meteorological variables and pollutants were also considered in these WRF–Chem models. For M10, the Modern Era Retrospective–analysis for Research and Applications (MERRA) reanalysis were used to driven the WRF (v3.5.1) model. The outputs from the Japan Meteorological Agency (JMA) non–hydrostatic mesoscale model (NHM) were used to initialize M12 (Kajino et al., 2012). M13 was driven by assimilated meteorological data from the Goddard Earth Observing System (GEOS) of NASA's Global Modeling and Assimilation Office (Chen et al., 2009; Li et al., 2016c). Although the meteorological initial and lateral boundary conditions were taken from the same NCEP FNL data, three dimensional meteorological fields used in M14 were simulated by Regional Atmospheric Modeling System (RAMS) (Zhang et al., 2002, 2007; Han et al., 2009, 2013). Consequently, different meteorological fields used in the fourteen participant models will show different meteorological characteristics (Gao et al., 2018ACP), which can further influence the spatial–temporal variation of air pollutants.

2.2.2 Emission inventories

All participant models utilized the "standard" emission inventory, including anthropogenic, biogenic, biomass burning, air and ship, and volcano emissions, which was prepared by the emission group in MICS–Asia phase III. The anthropogenic emission dataset over Asia, named MIX, was developed by harmonizing five regional and national emission inventories with a mosaic approach. These five inventories are REAS2 (REAS inventory version 2.1 for the whole of Asia, Kurokawa et al., 2013), MEIC (the Multi-resolution Emission Inventory for China developed by Tsinghua University), PKU–NH_3 (a high–resolution NH_3 emission inventory by Peking University, Huang et al., 2012), ANL–India (an Indian emission inventory developed by Argonne National Laboratory, Lu et al., 2011), and CAPSS (the official Korean emission inventory form the Clean Air Policy Support System, Lee et al., 2011). The MIX inventory includes ten species (SO_2, NO_3, CO, CO_2, NMVOC (non–methane volatile organic compounds), NH_3 (ammonia), BC (black carbon), OC (organic carbon), $PM_{2.5}$ and PM_{10}) in each sector (power, industry, residential, transportation, and agriculture), and is developed for the year 2010 with monthly temporal resolution and 0.25 degree spatial resolution. More details can be found in Li et al. (2017b). Weekly and diurnal profiles of the anthropogenic emissions provided by the emission group were used in model simulations, including

the emission factors for the first seven vertical levels (Fig. S1). Biogenic emissions were calculated by the Model of Emissions of Gases and Aerosols from Nature (MEGAN) version 2.04 (Guenther et al., 2006). In MEGAN v2.04, meteorological variables (e.g. solar radiation, air temperature, soil moisture) and land cover information (e.g. leaf area index and plant functional types) were necessary inputs, and these data were obtained from the WRF v3.4.1 simulation results and MODIS (Moderate Resolution Imaging Spectroradiometer) products, respectively. Biomass burning emissions were processed by re-gridding the Global Fire Emissions Database (GFED) version 3 (van der Werf et al., 2010), and the diurnal profile was also provided. The aircraft and shipping emissions were based on the 2010 HTAPv2 (Hemispheric Transport of Air Pollution) emission inventory (0.1 by 0.1 degree) (Janssens-Maenhout et al., 2015). Daily volcanic SO_2 emissions were collected from the AEROCOM program (http://www-lscedods.cea.fr/aerocom/AEROCOM\HC/volc/, Diehl et al., 2012; Stuefer et al., 2013). The spatial distribution of the merged emissions of SO_2, NO_x, NH_3 and $PM_{2.5}$ from anthropogenic, biogenic, biomass burning, air and ship, and volcano emissions are shown in Fig. S2. Similar spatial patterns can be found among these species, with high values in eastern China and northern India.

2.2.3 Boundary conditions

The meteorological fields are outputted from the Weather Research and Forecasting Model (WRF v3.4.1) using the National Center for Environmental Prediction (NCEP) Final Analysis (FNL) data with 1°×1° spatial resolution and 6 h temporal interval, but M10, M12, M13 and M14 choose to use others. In M10, the initial and lateral boundary meteorological fields are run by WRF (v3.5.1) driven by Modern Era Retrospective-analysis for Research and Applications (MERRA) reanalysis dataset. The outputs from the Japan Meteorological Agency (JMA) non-hydrostatic mesoscale model (NHM) are initialized in M12 (Kajino et al., 2012). M13 is driven by assimilated meteorological data from the Goddard Earth Observing System (GEOS) of NASA's Global Modeling and Assimilation Office (Chen et al., 2009; Li et al., 2016c). Although initial and lateral boundary conditions are taken from the same NCEP FNL data, three dimensional meteorological fields used in M14 are simulated by Regional Atmospheric Modeling System (RAMS) (Zhang et al., 2002, 2007; Han et al., 2009, 2013). These different atmospheric forcing dataset may result in differences in simulated circulation fields and other meteorological variables, which can further influence the concentrations and the distributions of simulated air pollutants.

All models utilized a common emission inventory, which includes anthropogenic, biogenic, biomass burning, air and ship, and volcano emissions. The anthropogenic emission dataset over Asia, named MIX, is developed by harmonizing five regional and national emission inventories with a mosaic approach. These five inventories are REAS2 (REAS inventory version 2.1 for the whole of Asia, Kurokawa et al., 2013), MEIC (the Multi-resolution Emission Inventory for China developed by Tsinghua University), PKU-NH_3 (a high-resolution NH_3 emission inventory by Peking University, Huang et al., 2012), ANL-India (an Indian emission inventory developed by Argonne National Laboratory, Lu et al., 2011), and CAPSS (the official Korean emission inventory form the Clean Air Policy Support System, Lee et al., 2011). The MIX inventory includes ten species (SO_2, NO_x, CO, CO_2, NMVOC (non-methane volatile organic compounds), NH_3 (ammonia), BC (black carbon), OC (organic carbon), $PM_{2.5}$ and PM_{10}) in each sector (power, industry, residential, transportation, and

agriculture), and is developed for the year 2010 with monthly temporal resolution and 0.25 degree spatial resolution. More details can be found in Li et al. (2017b). Weekly and diurnal profiles of the anthropogenic emissions provided by the MICS–Asia organizers are used in model simulations, including the emission factors for the first seven vertical levels (Fig. S1). Hourly biogenic emissions quantified by the Model of Emissions of Gases and Aerosols from Nature (MEGAN) version 2.04 (Guenther et al., 2006) are provided for the whole MICS–Asia phase III simulation period. To drive MEGAN, meteorological variables (e.g. solar radiation, air temperature, soil moisture) and land cover information (e.g. leaf area index (LAI), plant functional types (PFTs)) are necessary inputs, and these data are obtained from WRF simulations and MODIS (Moderate Resolution Imaging Spectroradiometer) products, respectively. Biomass burning emissions are processed by re–gridding the Global Fire Emissions Database (GFED) version 3 (van der Werf et al., 2010). Hourly fraction of biomass burning emission for each day during the entire year is also provided. The aircraft and shipping emissions are based on the 2010 HTAPv2 (Hemispheric Transport of Air Pollution) emission inventory (0.1 by 0.1 degree) (Janssens–Maenhout et al., 2015). Daily volcanic SO_2 emissions can be collected from the AEROCOM program (http://www-lscedods.cea.fr/aerocom/AEROCOM\HC/volc/, Diehl et al., 2012; Stuefer et al., 2013). The spatial distribution of the merged emissions of SO_2, NO_x and $PM_{2.5}$ from anthropogenic, biogenic, biomass burning, air and ship, and volcano emissions are shown in Fig. 1. Similar spatial patterns can be found among these species, with high values in eastern China and northern India.

Two sets of the chemical initial and boundary conditions (CHASER and GEOS–Chem) were provided by MICS–Asia phase III. The 3–hourly global CTM outputs of CHASER (prepared by Nagoya University, Sudo et al., 2002a; Sudo et at., 2002b) was run with 2.8 °×2.8 °horizontal resolution and 32 vertical layers. The hourly outputs from GEOS–Chem (prepared by University of Tennessee, http://acmg.seas.harvard.edu/geos/) was run with 2.5 °×2 °horizontal resolution and 47 vertical layers. All participant models, except M2, M7 and M10, chose between them. For M2 and M7, the default chemical boundary condition provided by CMAQ and WRF–Chem were used, respectively. For M10, the global GOCART simulations were used for atmospheric aerosols. Chemical concentrations at the top and lateral boundary conditions from 3 hourly global CTM outputs of CHASER (run by Nagoya University, Sudo et al., 2002a; Sudo et at., 2002b) and GEOS–Chem (run by University of Tennessee, http://acmg.seas.harvard.edu/geos/) are provided by MICS–Asia III. CHASER model is run with 2.8 °×2.8 °horizontal resolution and 32 vertical layers, and GEOS–Chem is run with 2.5 °×2 °horizontal resolution and 47 vertical layers.

A reference model computational domain recommended by MICS–Asia organizers covers the region of (15.4 °S–58.3 °N, 48.5 °E–160.2 °E) using 180×170 grid points at 45 km horizontal resolution, but most participant models employ different extents of the region as shown in Fig. 2. In order to minimize the influence from lateral boundary conditions and to cover most high–profile areas of East Asia, a common domain is designed in this manuscript as shown in Fig. 2 with the red solid line. For M13 and M14, missing value is used to fill the grids beyond their simulation domains. In this common domain, five different regions are assigned with different colors (Fig. 3): Region_1, filled with blue, contains Korean Peninsula and Japan; Region_2, filled with cyan, contains China only; Region_3, filled with chartreuse, contains Mongolia and parts of Russia;

域代码已更改

域代码已更改

15

Region 4, filled with orange, contains most countries in Southeast Asia; Region 5, filled with purple, contains most countries in South Asia. Therefore, modeling results in different geographical sub regions of East Asia can be analyzed and compared with each other to show the simulation performance of current CTMs.

The whole year 2010 is chosen as the study period for MICS–Asia Phase III Topic 1. During 2010, many important weather events have been documented, such as extreme summer heat waves and widespread monsoon precipitation which affected many Asian countries (Chen et al., 2015; Jongman et al., 2015); a super dust storm originated from Gobi Desert in March 2010 and swept across vast areas of East Asia (Li et al., 2011); a winter severe haze episode occurred in the North China Plain (NCP) in January 2010 (Gao et al., 2016b). All these provide good opportunities to analyze the characteristics of the spatial and temporal distribution of aerosol concentrations over East Asia.

2.3 Coupled meteorology and chemistry modelling methods

As is known to all that meteorological fields have significant influences on air quality. Meanwhile, atmospheric compositions can also affect weather and climate. As Gao et al. (2018ACP) pointed out that different coupling methods between aerosols and meteorological variables can cause different simulation results.

In order to simulate the concentrations of air pollutants, meteorological models and chemistry transport models should be implemented either offline or online (Kong et al., 2015). Offline modeling implies that CTM is run after the meteorological simulation is completed, which means the chemical impacts on meteorology are not considered. Online modeling allows coupling and integration of some of the physical and chemical components (Baklanov et al., 2014). According to the extent of online coupling, there are two ways of coupling: (1) online integrated coupling (meteorology and chemistry are simulated simultaneously in the same grid) and (2) online access coupling (meteorology and chemistry are independent, but information can be exchanged between meteorology and chemistry) (Baklanov et al., 2014). Among these participating models, M4, M5, M6, M12, M13 and M14 are offline models. M1, M2, M3 and M11 are online access models. M7, M8, M9 and M10 are online integrated models.

More details about the model configurations can be found in Table 1 and other MICS–Asia Phase III companion papers (Itahashi et al., 2019ACPD; Kong et al., 2019; Li et al., 2019).

2.3 4 Observation data

Monthly In order to make an international common understanding and improve air pollution modeling in East Asia, observation dataobservations (e.g. of SO$_4^{2-}$, NO$_3^-$, NH$_4^+$, PM$_{2.5}$ and PM$_{10}$) collected at from 39 sites stations of the Acid Deposition Monitoring Network in East Asia (EANET) are were used used to evaluate the model performancethe simulations, as did in MICS–Asia Phase II. Common quality assurance and quality control standards promoted by the ADORC (Acid Deposition and Oxidant Research Center) are were adopted among these EANET stations to guarantee high quality dataset. More information about the EANET dataset can be found at http://www.eanet.asia/index.html. In addition to the EANET data, monthly measurements mean concentrations of air pollutants (e.g. SO$_2$, NO$_2$, PM$_{2.5}$ and PM$_{10}$) over the

Beijing ~~--~~ Tianjin ~~--~~ Hebei (BTH) region (19 sites) and the Pearl River Delta (PRD) region (13 sites) provided by the China National Environmental Monitoring Center (CNEMC) ~~are~~ were also used to compare with the simulation results from participating models.

As is known to all, China has been experiencing heavy air pollution~~s~~ with high concentrations of fine particles, and recent studies highlight~~ed~~ the importance of secondary aerosols in the formation of haze episodes (Liu et al., 2013; Sun et al., 2016a; Chen et al., 2018). However, ~~observed aerosol components~~observations (e.g. SO_4^{2-}, NO_3^- and NH_4^+) in ~~inland~~ China ~~are~~ were only available at one EANET site (the Hongwen site). In order to make the ~~evaluation of the model performance~~model evaluation more credible, observed monthly/seasonal/yearly concentrations of BC, SO_4^{2-}, NO_3^-, NH_4^+ and $PM_{2.5}$ in China were also collected from published literatures. ~~BC, SO_4^{2-}, NO_3^-, NH_4^+ and $PM_{2.5}$ concentrations at several Chinese stations (five stations for BC, thirteen stations for SO_4^{2-}, NO_3^- and NH_4^+ and twenty two stations for $PM_{2.5}$) are collected from published documents (Chen et al., 2012; Li, 2012b; Liu, 2012; Meng et al., 2012; Shao, 2012; Wang et al., 2012a; Xu, 2012; Xie et al., 2013; Yu, 2013; Zhao et al., 2013; Tao et al., 2014; Wang, 2014a; Li, 2015; Sun et al., 2015; Wang et al., 2015; Zhang, 2015b; Lai et al., 2016; Li et al., 2016a; Wang et al., 2016b; Deng et al., 2016; Yao et al., 2016).~~

~~The~~ Aerosol Robotic Network (AERONET), a ground–based remote–sensing aerosol network consisting of worldwide automatic sun– and sky–scanning spectral radiometers (Holben et al., 1998), provides the aerosol optical depth (AOD) products at 440 nm and 675 nm, which can ~~are~~ be used to calculate the AOD at 550 nm ~~with~~ according to the Angström exponent. The AERONET Level 2.0 monthly AOD data (cloud–screened and quality–assured data) at ~~thirty–three~~33 sites ~~are~~ were utilized in this study. Meanwhile, satellite–retrieved 550 nm AOD products from the Moderate Resolution Imaging Spectroradiometer (MODIS) ~~and Multi–angle Imaging Spectroradiometer (MISR) are~~were also used to compare with ~~the~~ simulations.

Figure ~~3~~2 and Figure S3 show~~s~~ the geographical locations of all the ~~observational~~ observation sites. ~~(marked with black dots) for each measured species.~~ Most SO_4^{2-}, NO_3^- and NH_4^+ monitoring sites are located in China, Japan and the Southeast Asia, only two in Mongolia and four in Russia. ~~Except t~~Three PM_{10} sites are located in the Southeast Asia, while~~s~~ other~~s PM observational stations~~ are in China and Japan. Detailed information about ~~all these ground–level~~these stations ~~can be found~~is listed in Table S1 and Table S2.

In general, the wide variety of measurements from in–situ and satellites used in this manuscript can allow for a rigorous and comprehensive evaluation of model performance~~s~~.

3 Results and discussions

3.1 Model evaluation

~~Following~~ According to the objective of MICS–Asia Phase III Topic 1, comparisons of aerosol concentrations ~~(BC, SO_4^{2-}, NO_3^-, NH_4^+, $PM_{2.5}$ and PM_{10}), including aerosol optical depth (AOD),~~ between observations and simulations ~~(results~~

from individual models and EM) are presented to evaluate the performance of current multi–scale air quality models in East Asia simulation, as well as toincluding analyzinge the similarities and differences between participant models.

Simulation results of BC, OC, SO_4^{2-}, NO_3^-, NH_4^+, PM2.5, PM10 and AOD (Table S3) are requested to upload, but no data can be acquired from M10, all simulation results from M3 are incredible. Therefore, only twelve models are considered in this manuscript. Meanwhile, M5, M6 and M8 did not submit simulated AOD. M13 did not submit simulated PM10. M7 did not submit OC. Neither BC nor OC was submitted from M9.

3.1.1 Evaluation for aerosol particlescompositions

Figure 4 3 illustrates the observed and simulated ground level annual mean concentrations of BC, SO_4^{2-}, NO_3^-, NH_4^+, PM2.5 and PM10. EMsMulti–model ensemble mean (MMEM), derived from averaging all the available participating models (except M3 and M10), are is also presented to exhibit a composite of model performances. Monitoring sites are categorized into five regions (Region_1, Region_2, Region_3, Region_4 and Region_5) by their geographic locations as listed in Table S1, and are separated by vertical dashed lines in Fig. 4. Normalized mean biases (NMBs) between observations and EMs MMEM in each defined sub–regionregion (Region_1 to Region_5) and the whole analyzed domain region (Region_All) are calculated.

Analyzing Fig. 43(a), we can find that most models show good skills in simulating the BC concentrations and their spatial distribution characteristics, its spatial distribution, with relative high values over large emission areas (e.g. North China) (Li et al., 2016c). North China Plain (NCP) and Yangtze River Delta (YRD) regions, and low values over Central West of China. But the NMB for EM MMEM is −15.8%. This underestimation may be be attributeded to the large negative bias from all participant models at site 24 (the Gucheng site (site 24) (NMB for MMEM is −38.3%). This station is locatedlocates in the Hebei industrial province of Hebei, which is an industrial city, where air pollution is serious and BC emission is large (Wang et al., 2016c). Due to the low reactivity of BC in the atmosphere, the high uncertainty of BC in current emission inputs (Hong et al., 2017; Li et al., 2017b) may explain cause this underestimation.

For SO_4^{2-}, observations are relative low in Region_1 (mean value is 3.8 μg m^{-3}), Region_3 (mean value is 2.5 μg m^{-3}) and Region_4 (mean value is 3.5 μg m^{-3}), and most models (except M7, M9 and M14) perform well over these regionsareas (NMBs range from −26.3% to 30.0%). In Region_2, all But nearly the observed concentrations of SO_4^{2-} all observed annual mean SO_4^{2-} concentrations in Region_2 areare larger than 10 μg m^{-3} (mean value is 16.9 μg m^{-3}), and but most models fail to reproduce the high magnitude. As Zheng et al. (2015) and Shao et al. (2019) pointed out that missing sulfate formation mechanisms (e.g. heterogeneous sulfate chemistry) on aerosol in current air quality models may result in this underestimation, especially in China where significant increase of secondary aerosols (such as sulfate) can be observed during polluted periods (Liu et al. 2015). Huang et al. (2014) and Zheng et al. (2015) pointed out that heterogeneous chemistry on the surface of aerosol can enhance the production of SO_4^{2-}, especially under polluted conditions (Li et al., 2018). But the mechanism of the heterogeneous uptake of SO2 on deliquesced aerosols may have not been updated in M7 and M9.A large variance can be foundis also simulated among models, e.g. M14 obviously overpredicts the ground–level

SO_4^{2-} concentrations, especially in Region_1 (NMB=118.6%). ~This significant overestimation in coastal stations may be caused by its high concentrations of sea salt aerosols (Fig. 10), which makes the sea−salt sulfate higher. whereas Meanwhile, M7 and M9 obviously consistently underpredict SO_4^{2-} at nearly all sites (NMB=−73.5% and −71.7%, respectively.). Huang et al. (2014) and Zheng et al. (2015) pointed out that heterogeneous chemistry on the surface of aerosol can enhance the

5 production of SO_4^{2-}, especially under polluted conditions (Li et al., 2018). But the mechanism of the heterogeneous uptake of SO_2 on deliquesced aerosols may have not been updated in M7 and M9. Generally, The model EM better agrees with measurements of SO_4^{2-} concentration than most participating models, and EM MMEM can well reproduce the spatial variation of SO_4^{2-}, but the predicted concentration is underestimated, spatial distribution of SO_4^{2-}. However, underestimation is found in each defined region, especially in Region_2 (NMB=−43.5%) and Region_3 (NMB=−35.3%).

10 For NO_3^-, low concentrations are observed Similar spatial distribution of observed NO_3^- concentrations can also be in Region_1 (1.5 μg m⁻³), Region_3 (0.6 μg m⁻³) and Region_4 (1.8 μg m⁻³), but high values are presented in Region_2 (13.4 μg m⁻³), showing the similar spatial distribution characteristics as the observed SO_4^{2-}. In CTMs, there are two pathways about the nitrate formation. The dominant pathway is the homogeneous gas−phase reaction between HNO_3 (NO_2 oxidation by OH during the daytime) and NH_3 under ammonia−rich conditions, and the second pathway is the heterogeneous hydrolysis of

15 N_2O_5 on aerosol surface at night in ammonia−poor environment (Seinfeld and Pandis, 2006; Archer-Nicholls et al., 2014). As NH_4NO_3 is semi−volatile species, and the equilibrium surface concentration of H_2SO_4 is set to be zero in CTMs, so $(NH_4)_2SO_4$ is the preferential species in the completion when H2SO4 and HNO_3 are both present. Only if NH_3 is excess, then NH_4NO_3 will been formed. found in Fig. 4(c). The mean values of observed NO_3^- concentrations in each region are 1.5 μg m⁻³ (Region_1), 13.4 μg m⁻³ (Region_2), 0.6 μg m⁻³ (Region_3) and 1.8 μg m⁻³ (Region_4), respectively. Analyzing the

20 performance of each participant model, NO_3^- concentration is overpredicted by most models, and the underestimation of SO_4^{2-} can be used to explain this overestimation (Chen et al., 2017). Meanwhile, the biases of model calculated gas−phase odixation (e.g. $NO_2 + OH \rightarrow HNO_3$) and/or gas−aerosol phase partitioning (e.g. $HNO_{3(g)} + NH_{3(g)} \leftrightarrow NH_4NO_{3(s,\ aq)}$) may also result in the overestimation (Brunner et al., 2014; Gao et al., 2014). However, M7 and M8 significantly underestimate the observed NO_3^- concentrations (NMB~−93.4%). One reason for the extremely low values may result from

25 the incorrect concentrations of NH_3 simulated by M7 and M8 (**Fig. S4**). As Chen et al. (2016) pointed out that the amount of NH_3 is a key factor in determining the NO_3^- concentration. Another reason for this underestimation is M7 and M8 did not consider the impacts of N_2O_5 heterogeneous reaction ($N_2O_{5(g)} + H_2O_{(aq)} \rightarrow 2HNO_{3(aq)}$). a significant overestimation (underestimation) is simulated by M9 (M7 and M8), especially in Region_2. This may result from the biases of model calculation of heterogeneous reactions (Kim et al., 2014), gas aerosol phase partitioning (Brunner et al., 2014), and deposition (Shimadera et al., 2014). For example, N_2O_5 hydrolysis is considered in M9, but not in M7 and M8. Su et al.

30 (2016 2017) pointed out that the hydrolysis of N_2O_5 can led up to 21.0% enhancement of NO_3^-, especially over polluted regions. This may partly explain the differences of simulated NO_3^- concentrations between M7, M8 and M9. Another major possible reason to explain this extreme underestimation of NO_3^- in M7 and M8 is their incorrect treatments of the

19

带格式的：字体颜色：红色
带格式的：下标
带格式的：下标
带格式的：下标
带格式的：下标
带格式的：下标
带格式的：下标
带格式的：下标
带格式的：下标
带格式的：下标
带格式的：下标
带格式的：下标
带格式的：下标
带格式的：非突出显示
带格式的：非突出显示
带格式的：非突出显示
带格式的：非突出显示
带格式的：非突出显示
带格式的：下标
带格式的：字体：加粗，字体颜色：红色
带格式的：下标
带格式的：下标
带格式的：下标
带格式的：非突出显示
带格式的：非突出显示

Although the NMB calculated in Region_All ~~(Region_All means the whole analyzed region)~~ for ~~EM~~ MMEM is only −1.1%, ~~EM~~ MMEM systematically overpredicts observations in Region_1 (NMB=45.2%) and Region_3 (NMB=38.2%), but underpredicts in Region_2 (NMB=−0.7%) and Region_4 (NMB=−44.9%).

Simulated NH_4^+ concentrations are influenced by the partitioning between gaseous NH_3 and aerosol NH_4^+, and are also ~~are~~ associated with the amounts of SO_4^{2-} and NO_3^- (Gao et al., 2018). ~~, but~~ Mmodel predictions (except M7, M8 and M14) can reproduce the measurements relatively well in each defined sub−region. ~~with NMBs ranging from~~ But significant overestimation is shown by M14, while significant underestimation is simulated by M7 and M8, especially in Region_2 with NMBs of 72.2% for M14, −94.9% for M7, and −81.0% for M8, respectively. For M14, overestimated SO_4^{2-} and NO_3^- make the concentrations of NH_4^+ higher, since more ammonium is required to neutralize particle−phase acid. For M7 and M8, extremely low concentrations of NH_3 are simulated, which means fewer gaseous NH_3 can be converted to aerosol NH_4^+. ~~−7.8% to 32.0%.~~ In general, the calculated NMB in Region_All for MMEM is 4.0%.

~~However, obviously overestimation (underestimation) is also simulated by M14 (M7 and M8), especially in Region_2.~~

On average, the observed PM₂.₅ concentration in Region_2 is larger than 50 μg m⁻³, ~~while~~ but the mean value in Region_1 is only about 10 μg m⁻³ ~~in Region_1~~. All participating models can generally capture this spatial distribution pattern. However, significant underestimation is ~~found~~ simulated at the three remote stations (site 1, 2 and 7) in Region_1 with the NMB of −39.0% for ~~EM~~MMEM. Similar negative bias can also be found in Ikeda et al. (2013), who compared CMAQ (v4.7.1) simulation results against observations from the same remote monitoring stations (Rishiri and Oki) ~~throughout the same year~~in 2010. ~~And~~ Ikeda et al. (2013) pointed that the underestimation of organic aerosols may cause this bias. ~~caused the negative bias of simulated PM₂.₅ mass concentration.~~ In Region_2, the NMB for ~~EM~~ MMEM is −10.0%.

For PM₁₀, the mean observed concentrations in each region are 26.6 μg m⁻³ (Region_1), 114.4 μg m⁻³ (Region_2) and 38.1 μg m⁻³ (Region_4), respectively. But nearly all participant models underestimate the PM₁₀ concentrations, except 14, ~~Comparing with observations, an underprediction tendency can be found among almost all participating models except M14,~~ which predicts higher concentrations in Region_1, especially at coastal sites, such as site 1 (Rishiri), site 2 (Ochiishi), site 4 (Sadoseki), site 7 (Oki) and site 14 (Cheju). The high−value anomalies along coastal areas simulated by M14 can also be found in Fig. ~~19~~10, and the positive bias may be caused by the emission and gravitational settling of sea salt. As Monahan and Muircheartaigh (1980) pointed out that sea salt emissions can be enhanced in the surf zone due to the increased number of wave breaking events, and the degree of the enhancement highly depends on the 10 m wind speed used in the whitecap coverage parameterization. According to the simulation results from published literatures, higher wind speed is simulated by M14 (RAMSCMAQ) when comparing with observations, especially at coastal stations (Han et al., 2013; Han et al., 2018). ~~Meanwhile, higher wind speed at coastal stations was simulated by M14 (RAMSCMAQ) when comparing with observations~~

~~from previous related studies (Han et al., 2013; Han et al., 2018). In addition~~Meanwhile, a gravitational settling mechanism of coarse aerosols from upper to lower layers ~~is~~ was added in M14, and the net effect of this update could ~~is~~ make an increase in the concentrations of PM_{10} ~~coarse particles~~~~concentrations~~, especially near coastal areas impacted by sea spray (Nolte et al., 2015). ~~In general~~Generally, the NMB for ~~EM~~ MMEM in Region_All is −31.0%.

5　~~Figure 5 and Figure 6 show t~~The seasonalit~~yy~~ of observed and simulated ~~aerosol particle mass concentrations~~aerosol compositions, including BC, SO_4^{2-}, NO_3^-, NH_4^+, PM2.5 and PM10, are shown in Fig. 4 and Fig. 5. ~~.~~According to the defined sub−regions as illustrated in Fig. 2, all simulations and observations are grouped into the five regions, ~~All simulations and observations are grouped into five defined regions as illustrated in Fig. 3,~~ with the modeling results sampled at the corresponding observation ~~sites~~ stations before averaging together. Individual models are ~~represented~~ shown by the thin grey lines, with the grey shaded areas indicating their spread. The thick black line ~~is~~ represent the MM~~EM,~~ ~~T~~the red solid line is the observational mean, and the dashed red lines ~~represent~~ represent one standard deviation ~~for each group of stations~~. In each panel, ~~T~~the correlation coefficients (Rs) for MM~~EMs~~ versus the monthly observations are calculated ~~in each panel, and~~ and the normalized mean biases (NMBs) in each season (spring: from March to May; summer: from June to August; autumn: from September to November; winter: January, February and December) ~~for EM~~ are also given.

15　The measured BC concentrations in Region_2 exhibit an obvious seasonal variation, with the minimum (~ 3.5 μg m^{-3}) ~~during~~in spring and summer, and the maximum (~ 8 μg m^{-3}) during late autumn and winter. ~~All participating~~ Participant models can capture this ~~observed~~ seasonality quite well, and nearly all ~~modeling~~simulation results are within the standard deviation of the observations, but a large inter−model variation is ~~found~~also simulated, especially in winter when BC concentration is high. Due to its low reactivity in the atmosphere, this variation may be caused by their simulated meteorological conditions, including the impacts of different coupling ways between meteorological and chemical modules (Gao et al., 2015b). ~~Different coupling ways between meteorological and chemical modules, as listed in Table 1, can be used to explain this variation.~~ As ~~Gao et al. (2015b),~~ Briant et al. (2017) and Huang et al. (2018) concluded that the online integrated models can simulate higher BC concentrations than offline models, especially during polluted periods. The correlation coefficient for ~~EM~~ MMEM is 0.73.

25　~~In each month~~For PM2.5, the ~~mean observed~~observed monthly ~~PM2.5~~concentration~~s~~ ~~over~~in Region_2 ~~is~~are ~~larger~~ higher than ~~that~~ those in Region_1. This is because the emissions of primary aerosols and their precursors in China are larger than that in Japan and Korean Peninsula (as shown in Fig. S12). But ~~N~~nearly all models tend to underpredict the ~~magnitude~~ concentrations of PM2.5 in Region_1 ~~during the whole simulation period,~~ with ~~the range of~~ NMBs ranging from −44.3% (in winter) to −22.7% (in summer) for MM~~EM~~. Comparing with the correlation coefficient (R=0.40) in Region_1, CTMs can better reproduce t~~T~~he seasonality of ~~modeling~~observed PM2.5 ~~concentration~~ in Region_2 ~~is better~~, with the R of 0.69 for MM~~EM~~. ~~, comparing with the correlation coefficient (R=0.40) in Region_1.~~ ~~In general~~Generally, the R for ~~EM~~ MMEM in Region_All is 0.83 and the NMB ranges from −2.2% (in autumn) to 13.9% (in winter) ~~among four seasons~~.

Similar temporal−variation characteristics of PM10 concentrations are observed in Region_1, Region_2 and Region_4, with the

maximum occurred in ~~The characteristics of the observed PM$_{10}$ concentrations in Region_1, Region_2 and Region_4 are similar, with the maximum in~~ March and November, and the minimum ~~during~~ occurred during summer. M14 consistently overestimates the PM$_{10}$ concentrations in Region_1 ~~for all periods~~, while others fall within the standard deviation of the observations. The simulated PM$_{10}$ concentrations in Region_2 show less diversity, but nearly all models peak 2 months later. A distinctive seasonality can be found in Region_4, with the ~~maximum~~ highest value (nearly 80 µg m^{-3}) observed in March, but most models cannot reproduce ~~the maximum~~this characteristic. This is because the GFED substantially underestimate~~d~~ the biomass burning emissions over Southeast Asia (Fu et al., 2012), especially during March–April when most intense biomass burning occurred in Myanmar, Thailand and other Southeast Asian countries (Huang et al., 2012), and the emission bias is mainly due to the lack of agricultural fires (Nam et al., 2010). Finally, a weak ~~PM$_{10}$~~ seasonality in PM$_{10}$ ~~was~~ is simulated by ~~EM~~ MMEM with R of 0.58 in Region_4. In Region_all, although consistent~~ly~~ underestimation is ~~found~~ simulated during the whole ~~simulation~~ period, with NMB ranging from –40.8% to –25.2% for MM~~EM~~, the seasonal cycle can be well ~~captured~~ reproduced by ~~EM~~ MMEM with R of 0.78.

~~For SO$_4^{2-}$, NO$_3^-$ and NH$_4^+$ in Region_1, T~~the seasonal variation characteristics of ~~observations~~ observed SO$_4^{2-}$, NO$_3^-$ and NH$_4^+$ in Region_1 are not obvious, with the annual mean ~~values~~ of ~ 4 µg m^{-3} for SO$_4^{2-}$, 1.5 µg m^{-3} for NO$_3^-$ and 1.0 µg m^{-3} for NH$_4^+$, respectively. A large inter–model spread of simulated SO$_4^{2-}$ is shown in Fig. 5~~6~~(a1), with the maximum variation range in June. ~~Double–peak curve is displayed in Fig. 6(b1) with the maximums in May and November, and M~~most models significantly overpredict the observed NO$_3^-$ concentrations, especially in summer with the NMB of 164.3% for MMEN. ~~Unlike SO$_4^{2-}$ and NO$_3^-$, the s~~Simulated monthly NH$_4^+$ concentrations from most models are within the standard deviation of observations, and the R for ~~multi–model mean~~MMEM is ~~highest with the value of~~as high as 0.74. In Region_2, the ~~observed monthly mean aerosol components~~ observations are only available at one EANET site (the Hongwen site, located in the eastern coastal area of China), and the seasonality of observed ~~observed~~ SO$_4^{2-}$, NO$_3^-$ and NH$_4^+$ from this station is obvious with the maximum in spring and winter, and the minimum in later summer and early autumn. Nearly all models tend to underpredict these concentrations, but the ~~EM~~ MMEM captures the seasonal cycle~~s~~ relative well with Rs of 0.57 for SO$_4^{2-}$, 0.85 for NO$_3^-$ and 0.86 for NH$_4^+$, respectively. In Region_3, the observed maximum concentrations of SO$_4^{2-}$ and NH$_4^+$ are in winter, but most models cannot reproduce the increasing tendency ~~during~~in the late autumn and the early winter, ~~and then~~which means participant models fail to capture the seasonality (Rs of 0.20 for SO$_4^{2-}$, 0.34 for NO$_3^-$ and 0.18 for NH$_4^+$, respectively). This may due to the low emission~~s~~ of primary aerosol~~s~~ and their precursors in Region_3. Meanwhile, ~~, as shown in Fig.1.~~ the Regional Emission Inventory in Asia (REAS v2.1) is used in Region_3, which is calculated based on the emissions from 2000 to 2008 (Li et al., 2017b), not extended to the simulation year of 2010. The updated emissions with localized data may increase the accuracy of simulation results. In Region_4, the simulated concentrations of SO$_4^{2-}$, NO$_3^-$ and NH$_4^+$ are fairly good when compared with the ~~measurements~~measurements. The Rs of ~~EM~~ MMEM are 0.73 for SO$_4^{2-}$, 0.63 for NO$_3^-$ and 0.73 for NH$_4^+$. Meanwhile, the model diversities are small. Generally, in Region_All, ~~EM~~ MMEM can well reproduce the magnitudes of observed SO$_4^{2-}$, NO$_3^-$ and NH$_4^+$ ~~fairly well~~during the

22

whole simulation period, as well as the seasonal variation characteristics.

As mentioned above, the ~~that~~ observed monthly mean concentrations of aerosol compositions in China are only available at one EANET station (site 17, the Hongwen station), with missing values in June and October. In order to make the evaluation ~~of simulated aerosol chemical components over China~~ more comprehensive, observed seasonal mean concentrations of SO_4^{2-}, NO_3^- and NH_4^+ collected from published ~~documents~~ literatures are also used to compare with simulation results (~~as shown in Fig. S5~~7). M2, M12 ~~and~~ M14 reasonably ~~show~~ reproduce the ~~reasonable~~ SO_4^{2-} concentrations in the four seasons, while others fail to ~~reproduce~~ simulate the high observed SO_4^{2-} concentrations. The NMBs of SO_4^{2-} range from ~~, with the NMBs ranging from~~ −79.4% (M7) to ~~−28.0~~12.8% (~~M12~~M14). On the contrary, nearly all participant models overestimate the concentrations of NO_3^- (except M4, M7 and M8), with NMBs ranging from 1.7% (M5) to 50.2% (M9). The underestimation of SO_4^{2-} and the overestimation of NO_3^- may be the ~~common phenomenon~~general performance in ~~most~~ current ~~air quality models~~CTMs (Wang et al., 2013b; Gao et al., 2014; Huang et al., 2014; Zheng et al., 2015), and some hypotheses should be deeply tested in future to reduce ~~the~~these deviations, such as (1) missing oxidation mechanisms of SO_2 may lead to low concentrations of SO_4^{2-}, which allows for excess NO_3^- in the presence of ammonia, (2) there is an issue with NO_x partitioning and/or missing NO_x sink. Meanwhile, Seinfeld and Pandis (2006) pointed out that the chemical productions of SO_4^{2-} and NO_3^- are mainly from the gas−phase and/or liquid−phase oxidation of SO_2 and NO_2. Therefore, further comparisons of observed and simulated SO_2 and NO_2 are shown in Fig. S6 and Fig. S7. From Fig. S~~2~~6, ~~participating~~participant models can generally reproduce the seasonality of the two gases, with Rs of 0.61 for SO_2 and 0.65 for NO_2, respectively. But overestimations (underestimations) of SO_2 (NO_2) are found ~~in~~during most simulation periods, not only in China, but also in other defined sub−regions (Fig. S~~3~~7), ~~and t~~. The overestimation (underestimation) of SO_2 (NO_2) can be used to explain the underestimation (overestimation) of simulated SO_4^{2-} (NO_3^-). However, significant underestimation of NO_3^- is also simulated by M7 and M8. As mentioned above, the extremely low concentrations of NH_3 in M7 and M8 may be the main reason for this negative bias. ~~Most models overestimate the concentrations of NO_3^- and NH_4^+ in China, but significant underestimation can be found in M7 and M8 (NMBs are larger than −70%). The underestimation may be due to their incorrect treatments of the NH_3 emission inputs, including missing aqueous−phase and heterogeneous chemistry reactions or the implementations of a different gas phase oxidation mechanism (RACM gas phase chemistry mechanism). In fact, the underestimation of SO_4^{2-} and the overestimation of NO_3^- may be the common phenomenon in most current air quality models (Wang et al., 2013b; Gao et al., 2014; Huang et al., 2014; Zheng et al., 2015), and some hypotheses should be deeply tested in future to reduce the deviation, such as (1) missing oxidation mechanism of SO_2 may lead to low concentration of SO_4^{2-}, which allows for excess NO_3^- in the presence of ammonia, (2) there is an issue with NO_x partitioning or missing NO_x sink.~~ Analyzing the results from ensemble mean, ~~MM~~EM shows better performance than participating models, with NMBs of −46.0% for SO_4^{2-}, 1.9% for NO_3^- and 13.1% for NH_4^+.

~~Seinfeld and Pandis (2016) pointed out that chemical productions of SO_4^{2-} and NO_3^- are mainly from the gas−phase or liquid−phase oxidation of SO_2 and NO_2. Therefore, further comparisons of observed and simulated seasonal cycle of SO_2~~

and NO₂ in Region_2 and annual mean concentrations of SO₂ and NO₂ at corresponding stations are shown in Fig. S2 and Fig. S3, respectively. From Fig. S2, participating models can generally reproduce the seasonality of the two gases, with Rs of 0.61 for SO₂ and 0.65 for NO₂, respectively. But overestimations (underestimations) of SO₂ (NO₂) are found in most simulation periods, not only in China, but also in other defined regions (Fig. S3), and the overestimation (underestimation) of SO₂ (NO₂) can be used to explain the underestimation (overestimation) of simulated SO_4^{2-} (NO_3^-).

3.1.2 Evaluation for aerosol optical depth

The seasonal cycle of simulated aerosol optical depth (AOD) at 550 nm is also compared with measurements at thirty-three AERONET stations. Simulated aerosol optical depth (AOD) at 550 nm from the nine participating models (M1, M2, M4, M7, M9, M11, M12, M13 and M14) are compared with the measurements averaged over the thirty–three AERONET stations. Only nine participating models (M1, M2, M4, M7, M9, M11, M12, M13 and M14) submitted their simulated AOD values, and the EM is calculated by these nine models. From Fig. 8 6 we can find that most models tend to overpredict AOD values during the whole simulation period in Region_1, Region_2 and Region_3 with NMBs of 74.0%, 38.8% and 107.0% for MMEM, respectively. In Region_4, an obvious seasonality is observed with the maximum in spring and the minimum in summer. Models can capture thise seasonality well, although underestimation is found in spring. The R for MMEM is 0.65 and the NMB is −−8.7% in Region_4. Smaller NMB (−4.2%) is calculated in Region_5 for MMEM, Model bias in Region_5 is smaller with the NMB of −4.2% for EM, but a quite weak seasonality is simulated shown with underestimation underestimated AOD in in spring and summer, and overestimation overestimated AOD in autumn and winter. Generally, simulated AOD values lie are within a standard deviation of the observations in Region_All with a slight overestimation in autumn and winter. The MMEM can reproduce the seasonal cycle with R of 0.68, and the NMB for MMEM is 18.7%.

Figure 9 7 presents the spatial distribution of 550 nm AOD retrieved fromby MODIS and simulated by the nine participant models. _ In this study, MODIS AOD is collected by from the Terra and Aqua satellites during the whole year of 2010. The observed AOD from AERONET are also shown. AOD observed from AERONET stations are also shown. In order to quantify the ability of each model in simulating the to reproduce the spatial distribution of aerosol particles, spatial correlation coefficients are also given in the bottom left corner of each panel. Analyzing the observations from MODIS, we can conclude that AOD values are higher in central and eastern China, including the Sichuan province, with the maximum over 1.0. High values can also be found observed in the north India. Due to dust events happened in arid and semi–arid regionsspring, , AOD values over the Taklimakan area are also large (~0.5). Comparing with MODIS AOD, almost all models can reproduce the spatial distribution feature characteristics, with high values in China and India, and low values in other countries. The Rs range from 0.78– to 0.86. But most models tend to underestimate the AOD in the eastern coastal regions of China and the north regions of India where anthropogenic emissions are large, including the areas where dust particles are frequently observed (Fig. S8). Generally, The model MMEM captures the AOD spatial variability variation better with R of 0.87, and the mean bias is −0.08..

24

Figure 10 shows the differences between model results and MODIS AOD to further discuss the performance of participant models. We can conclude that most models tend to underestimate the AOD values in the eastern coastal regions of China and the north regions of India where the emissions are large, in addition to the Taklimakan area in China where dust particles can be lifted up frequently. Meanwhile, overestimation is simulated by M2 and M14, especially in the Sichuan province of China. Generally, mean biases averaged over the whole analyzed region for the nine models ranges from −0.16 to 0.05, and the mean bias for EM is −0.08.

Figure 11 shows the annual mean 550 nm AOD from each available model averaged over the five defined regions (Region_1 to Region_5) and the whole analyzed domain (Region_All), together with the measured AOD retrieved from MODIS and MISR. AOD averaged over the corresponding AEROENT stations in each region are also shown. Analyzing the observations, MODIS AOD is the highest and AERONET value is the lowest. This difference can be explained by the systematic biases in MODIS retrievals due to the impacts of aerosol model assumptions and cloud contamination (Hauser et al., 2005; Toth et al., 2013), in addition to the difference in number of days used to calculate the average (Li et al., 2009). Meanwhile, observations from AERONET sites only represent special samples in each region. Similar results can also be found in other researches (Alpert et al., 2012; Li et al., 2014; Liu et al., 2014). Analyzing the simulations, multi-model mean can generally reproduce the magnitude of observations within a factor from 0.5 to 1.6, especially comparing with AOD values retrieved from MISR, and the EMs in the five defined regions are 0.29±0.12 for Region_1, 0.34±0.26 for Region_2, 0.21±0.09 for Region_3, 0.18±0.17 for Region_4 and 0.23±0.13 for Region_5, respectively. But the inter-model spread is large by a factor of 2–5 in magnitude, and in most regions, AOD values simulated by M4 are lowest, M2 and M11 show the highest.

3.1.3 Statistics for aerosol particles and aerosol optical depth

Table 3 2 shows the statistics of correlation coefficient (R), normalized mean bias (NMB) and root−mean squared error (RMSE) for BC, SO_4^{2-}, NO_3^-, NH_4^+, $PM_{2.5}$, PM_{10} and AOD. Simulation Rresults from twelve participant models and MMEM are compared with available observations. Best results are set to be bold with underline.

It can be found that all participant models are able to generally capture the variability of BC in China, with Rs ranging from 0.65 (of M5) to 0.80 (of M8), but nearly all models tend to underestimate the BC concentration, except M1 and M2. The maximum negative deviation is simulated by M5 (with NMB= of −54.9%), while the maximum positive deviation is from M2 with NMB of 12.7%. All the RMSEs are less than the mean observed BC mean concentrationobservation of BC (5.0 μg m^{-3}). Comparing to the observed SO_4^{2-}, most models fail to reproduce the magnitude of concentrationshigh values, and . tNMBs range from −67.7% of M7 to 69.3% of M14, and the NMB for MMEM is −19.1%, meaning the underprediction underestimation of the simulated SO_4^{2-} concentration is a general phenomenon in current CMTs. Implementing more detailed sulfate aerosol formation mechanisms (e.g. heterogeneous reaction and catalytic oxidation) into air quality models will improve the accuracy of simulation results (Huang et al., 2014, Zheng et al., 2015; Fu et al., 2016). is found in most

~~participating models. This may be caused by the imperfect mechanism of gas–phase and liquid–phase oxidation of SO₂, in addition to the missing heterogeneous reactions on the surface of aerosol particles in most current multi–scale air quality models (Huang et al., 2014, Zheng et al., 2015; Fu et al., 2016).~~ But most models can capture the variation of SO_4^{2-} with Rs ranging from 0.46 (~~of~~ M14) to 0.76 (~~of~~ M13). For NO_3^-, Rs vary from 0.29 (~~of~~ M8) to as high as 0.65 (MM~~of~~ EM). M5 ~~exhibits~~ <u>shows</u> the largest correlation (0.65) and the smallest NMB (–1.7%) ~~along all~~ <u>among</u> models. Although a high ~~R~~ <u>value of R</u> (0.64) is calculated by M9, the NMB is the largest (125.7%). All RMSEs are larger than the measured NO_3^- (1.7 µg m⁻³), meaning a relative poor performance for current ~~air quality models~~ <u>CTMs</u> to simulate the NO_3^- concentration<u>s</u> in East Asia. For NH_4^+, underestimation can be found in M4, M7 and M8, while the others tend to overestimate the NH_4^+ concentration. Although all RMSEs are larger than the observed NH_4^+ <u>(mean value is</u> ~~concentration of~~ 1.1 µg m⁻³<u>,</u>~~)~~. most models can capture the variability, with Rs ranging from 0.34 (~~of~~ M8) to 0.75 (~~of~~ M9). Generally, <u>MMEM</u> ~~the multi–model mean~~ matches the ~~observed values~~ <u>observations</u> with R of 0.71, NMB of 14.0% and RMSE of 1.11 µg m⁻³, respectively. Although significant underprediction~~s~~ ~~are~~ <u>is</u> found in PM_{10} (NMBs range from –55.7% of M5 to ~~–~~<u>–</u>16.9% of M9, except M14)~~,~~ and the inter–model spread ~~of $PM_{2.5}$~~ is large <u>in $PM_{2.5}$</u> (NMBs range from ~~–~~<u>–</u>26.5% of M13 to 46.0% of M14), <u>the variations of</u> simulated $PM_{2.5}$ and PM_{10} ~~variations~~ are well correlated with measurements (Rs > 0.60)~~,~~ and the RMSEs are all smaller than the averaged ~~measurements~~ <u>concentrations</u> (51.4 µg m⁻³ for $PM_{2.5}$~~,~~ <u>and</u> 80.7 µg m⁻³ for PM_{10}~~, respectively~~). For AOD, large positive deviation~~s~~ ~~can be found in~~ <u>are simulated by</u> M2, M9, M11, M13 and M14, ~~although~~ <u>but these models can reproduce the spatial–temporal variation characteristics relative well with Rs larger than 0.5.</u> ~~their Rs are all larger than 0.5.~~ M4 and M7 show the large negative deviation with NMBs of –28.5% and –21.8%, respectively. But their RMSEs are relative small (0.16 for M4 and 0.18 for M7). Generally, the R, NMB and RMSE for <u>MM</u>EM are 0.68, 18.7% and 0.14, respectively.

3.2 Inter–comparison between MICS–Asia Phase II and Phase III

The main purpose of MICS–Asia Phase III Topic 1 is to assess the ability of current multi–scale air quality models to reproduce <u>the</u> air pollutant concentrations <u>in East Asia</u>. In order to reflect how well the performance of air quality model~~s~~ <u>improves, especially</u> ~~in East Asia simulation after~~ undergoing substantial development during last several years, statistics (e.g. RMSE and R) ~~for~~ <u>between</u> observed and simulated SO_4^{2-}, NO_3^- and NH_4^+ from MICS–Asia Phase II and Phase III are compared in <u>Fig.</u> ~~12~~<u>8</u>.

The statistics of MICS–Asia Phase II are taken from Hayami et al. (2008), ~~in which~~ <u>and the</u> observed monthly mean ~~aerosol composition~~ concentrations ~~were~~ <u>are</u> monitored with high completeness at <u>the</u> fourteen EANET stations in March, July and December 2001 and March 2002, while model–predicted monthly surface concentrations are from eight regional CTMs. Notably, NO_3^- and NH_4^+ used in Hayami et al. (2008) are total NO_3^- (= gaseous HNO_3 + particulate NO_3^-) and total NH_4^+ (= gaseous NH_3 + particulate NH_4^+), respectively. More detailed information can be found in Hayami et al. (2008).

Analyzing the RMSEs in Fig. ~~12~~8, we can conclude that the medians (interquartile ranges) for SO_4^{2-}, NO_3^- and NH_4^+ are 3.60 μg m^{-3} (3.24 ~~,~~ and –4.01 μg m^{-3} for 25th and ~~/~~75th percentiles), 2.76 μg m^{-3} (2.49 ~~,~~ and –2.96 μg m^{-3} for 25th and ~~/~~75th percentiles) and 1.28 μg m^{-3} (1.21 ~~,~~ and –1.47 μg m^{-3} for 25th and ~~/~~75th percentiles) in Phase III, respectively. Although the medians (except NH_4^+) are a little ~~bit~~ larger than that in Phase II, the interquartile ranges are quite smaller, ~~meaning~~ indicating the inter–model variability of simulated aerosol concentrations among current CTMs is becoming smaller. ~~similar aerosol concentrations can be simulated by current multi-scale models.~~ Meanwhile, the medians of the correlations of SO_4^{2-}, NO_3^-, and NH_4^+ in Phase III, including the upper and lower quartiles, are all ~~significantly~~ larger than that in Phase II, which means current CTMs show better performance in ~~meaning the better performance of current air quality models in~~ reproducing the spatial–temporal variation tendency of observations.

~~the variation tendency of observations.~~

Although the participating models (8 verses 12 CTMs), ~~evaluation~~ observation sites (14 verses 31 EANET stations) and simulation periods (4 months verses 1 year) are different between Phase II and Phase III, more reasonable statistics are calculated by current CTMs, reflecting better performance in simulating the concentrations of aerosol particles and their variation tendency.

~~the compared results of statistics calculated from observations and simulations can still generally show that better performance is found in current multi-scale air quality models than those participating in MICS-Asia Phase II when reproducing the concentrations of aerosol particles and their variety characteristics.~~

3.3 Inter–comparison between participant models

Figure ~~13~~9 ~~to Figure 19~~ shows the spatial distribution of simulated $PM_{2.5}$ concentrations from each participating model and the MMEM. The coefficient of variation (hereinafter, CV), defined as the standard deviation of the models divided by their mean, is also calculated. The larger the value of CV, the lower the consistency among the participating models (Han et al., 2008; Gao et al., 2018). All simulation results can reproduce the high $PM_{2.5}$ in the northern India and the eastern China, including the Sichuan province in China. The areas with high $PM_{2.5}$ concentrations (> 40 μg m^{-3}) are consistent with the regions where CV are low (< 0.3), indicating similar performance of the CTMs in simulating the air pollutants over haze–polluted areas.

Previous studies have revealed that sulfate, nitrate and ammonium (denoted as SNA) are the predominant inorganic aerosols in PM, and SNA can contribute to nearly half of the total $PM_{2.5}$ mass (about 20%–60%) (Wang et al., 2014c; Sun et al., 2016b; Lin et al., 2018). All these show the necessity to exactly simulate the concentrations of SNA. Analyzing the mean ratio of SNA to $PM_{2.5}$ averaged over the five defined sub–regions (Fig. 9), large variations are simulated by participant models, with values ranging from 31.1% (M7) to 75.1% (M5). Different gas–phase and aerosol chemistry mechanisms used in these CTMs can explain this inconsistency. The calculated SOR (sulfur oxidation ratio, $SOR = nSO_4^{2-}/(nSO_4^{2-} + nSO_2)$), NOR (nitric oxidation ratio, $NOR = nNO_3^-/(nNO_3^- + nNO_2)$) and PNR (particle neutralization ratio, $PNR = nNH_4^+/(2 \times nSO_4^{2-} + nNO_3^-)$) are also obviously different.

SOR and NOR can be used to estimate the degree of secondary formation of SO_4^{2-} and NO_3^- (Sun et al., 2006; Zhao et al., 2013). When SOR and NOR are less than 0.1, SO_4^{2-} and NO_3^- mainly come from the primary source emissions; otherwise, high oxidation rates of SOR and NOR can result in large fractions of SO_4^{2-} and NO_3^- in $PM_{2.5}$ (Fu et al., 2008b). Generally, CMAQ models (M1, M2, M4, M5, M6 and M14) produce 30.7% higher SOR than others (except M8), which means more intense secondary formation of SO_4^{2-} is simulated by CMAQ. Similar NOR is predicted by participant models (~0.24), except M7 and M8. The extremely low value of NOR (~0.02) from M7 and M8 is due to the unreasonable low NO_3^- concentrations. Previous measurements show that the mean value of NOR is about 0.15 (Du et al., 2011; Zhang et al., 2018), which is lower than the predicted one from MMEM (0.20) in this study, indicating more NO_3^- is produced by secondary formation in current CTMs.

PNR is defined as the mole ratio of ammonium to sulfate and nitrate. When PNR is larger than unity, sufficient ammonia can be used to neutralize the acidic sulfate and nitrate; otherwise, there is an incomplete neutralization of acidic species. Analyzing the calculated PNRs from participant models, all values are smaller than 1, which means air conditions are considered to be ammonia deficient. But the mole ratios of $nNH_4^+/(2 \times nSO_4^{2-})$ are all larger than 1 (~1.6, except M7 and M8). All these indicate that acidic sulfate is fully neutralized to form $(NH_4)_2SO_4$ or NH_4HSO_4, and parts of acidic nitrate is changed to NH_4NO_3. Meanwhile, under NH_3–limited conditions, small reductions in ammonia may cause significant reductions in particulate matter (Makar et al., 2009).

However, large CV (> 1.0) is calculated over arid and semi–arid regions (Fig. 9), such as the Taklimakan Desert and the Gobi Desert, where dust events are often observed, which means current CTMs have difficulty in processing dust aerosols, especially in producing a similar amount of dust emissions and in identifying the same potential dust source regions, by using different dust schemes. Larger CV can also be found in simulated coarse particles (subtract $PM_{2.5}$ from PM_{10}) in Fig. 10. High concentrations of coarse particles simulated by M9 over arid and semi–arid regions may be caused by the inaccurate physicochemical parameters (e.g. plastic pressure of the soil surface) used in the Shao dust scheme (Kang et al., 2011). Large values (> 20 µg m⁻³) over coastal regions from M14 may result from the inadequate simulation results of sea salt aerosols.

From Table 3 we can further conclude that the low consistency (or the large CV) of simulated coarse particles in each defined sub–region is mainly caused by the dust particles. Without the impacts of dust aerosols and sea salts (only simulation results from M7 and M8 are considered), the calculated CVs for Region_1 to Reiong_5 are 0.29, 0.30, 0.33, 0.19 and 0.10, respectively. Without the impacts of dust aerosols (only simulation results from M1, M2, M4, M5 and M6 are considered), similar spatial distribution patterns are found in Fig. 10, and the CVs averaged over each sub–region are 0.37 (Region_1), 0.65 (Region_2), 0.48 (Region_3), 0.59 (Region_4), and 0.65 (Region_5), respectively. But when the influences of dust aerosols and sea salts are both considered (simulation results from M9, M11, M12 and M14 are used), larger CVs are obtained with values of 0.97 for Region_1, 1.04 for Region_2, 1.27 for Region_3, 0.95 for Region_4, and 0.88 for Region_5.

Aerosol chemical compositions simulated by each participating model and the MMEM in the six high–profile cities (Beijing, Shanghai, Guangzhou, Delhi, Seoul and Tokyo) are shown in Fig. 11. BC, OC, SO_4^{2-}, NO_3^-, NH_4^+, $PM_{2.5}$ and PM_{10}

带格式的：下标

带格式的：非突出显示

带格式的：下标
带格式的：下标
带格式的：下标
带格式的：下标
带格式的：下标
带格式的：下标
带格式的：下标
带格式的：下标
带格式的：字体颜色：红色
带格式的：字体颜色：红色

带格式的：字体颜色：红色

带格式的：字体颜色：红色
带格式的：非突出显示

带格式的：字体颜色：红色

concentrations from each participating model and the multi-model EM. The coefficient of variation (hereinafter, CV), defined as the standard deviation of the models divided by their mean, is also calculated. The larger CV, the lower the consistency is among participating models.

For BC, high values (> 5 µg m^{-3}) can be successfully simulated by all models (except M5) over the eastern China including the Sichuan province, and the northeast part of India. Meanwhile, areas with high concentrations (> 5 µg m^{-3}) are nearly consistent with the regions where CV values are relative low (< 0.5). However, large CV (> 1.0) is shown over the Himalayas and the Indian Ocean. This is probably due to the different vertical resolutions in addition to the different transmission mechanisms. Generally, the CVs in the five defined regions are all smaller than 0.6. All participant models show similar spatial distribution and magnitude of OC, except M5 and M8 with obvious low values over China and India. Analyzing the results from EM, the highest concentrations are simulated over the Eastern China, Sichuan Province and the northern part of India with values larger than 10 µg m^{-3}. CVs are lower than 0.7 in these relative high-concentration areas, while high CV values (> 1.5) are shown over the Tibetan Plateau and low-latitude oceans. For SO_4^{2-}, NO_3^- and NH_4^+, high concentrations are centered in the eastern China and the north India, including the Sichuan province of China. However, apparent low SO_4^{2-} (NO_3^- and NH_4^+) concentrations are simulated by M7 and M9 (M7 and M8). Meanwhile, noticeable high concentrations of SO_4^{2-} are simulated by M14, especially along coastal regions. CVs of SO_4^{2-} and NH_4^+ averaged over the five defined regions are all lower than 0.7, and maximum CVs are all smaller than 1.5, indicating simulation results are in good agreement. But a poor consistency is shown among simulated NO_3^- concentrations with CVs larger than 0.6 over each defined region. For PM$_{2.5}$ and PM$_{10}$, high values are simulated by M9, M12 and M14 over arid and semi-arid regions, such as the Taklimakan Desert and the Gobi Desert, where dust events were observed in spring. The CVs in these regions are quite large (over 1.5), which means different processing capacities for dust aerosols and different dust emission mechanisms used among these models. M14 also shows higher values of PM$_{10}$ over coastal regions than other models. This may be caused by the inadequate simulation results of sea salt.

3.4 **Characteristics of chemical compositions of particulate matter**

Figure 20 shows the chemical compositions of simulated particulate matter (PM) averaged over the whole analyzed area in 2010 from each participating model and the multi-model EM. PM$_{2.5}$ is composed of SNA (SO_4^{2-} + NO_3^- + NH_4^+) and OTHER1 (BC + OC + OTHER2), while PM$_{10}$ includes PM$_{2.5}$ and PM$_{coarse}$. PM$_{10}$ includes PM$_{2.5}$ and OTHER2, while PM$_{2.5}$ is composed of BC, OC, SO_4^{2-}, NO_3^-, NH_4^+ and OTHER1. Notably, PM$_{coarse}$ OTHER2 cannot be calculated in from M13 because PM$_{10}$ has not been is not submitted.

High values of PM$_{2.5}$ and PM$_{10}$ in Beijing, Shanghai, Guangzhou and Delhi can be simulated by nearly all models, and the annual mean concentrations of PM$_{2.5}$ and PM$_{10}$ from MMEM are all larger than the IT-1 (Interim target-1, 35 µg m^{-3} for PM$_{2.5}$, 70 µg m^{-3} for PM$_{10}$) proposed by WHO. But relative small concentrations are presented in Tokyo (15.5 and 21.3 µg m^{-3} for PM$_{2.5}$ and PM$_{10}$, respectively) and Seoul (21.7 and 27.6 µg m^{-3} for PM$_{2.5}$ and PM$_{10}$, respectively). For each city, a large spread of concentrations of aerosol compositions can be found among participant models (a factor of ~10 for SNA, a

带格式的：删除线

带格式的：下标

factor of ~2 for $PM_{2.5}$ and PM_{10}). This is partly caused by the differences in gas–aerosol partitioning and dust emissios, including the removal processes (e.g. dry and wet depositions).

~~OC is not available in M7, so we leave it into OTHER1. BC and OC are not available in M9 and these concentrations are grouped into OTHER1.~~

~~From Fig. 20 we can find that the simulated concentrations of PM_{10} vary a lot by about a factor of 4 among models, with the highest in M9 (46.5 µg m^{-3}) and the lowest in M5 (11.5 µg m^{-3}). This large spread can be explained by the differences in simulated concentrations of OTHER2, which is mainly composed of dust aerosol and sea salt aerosol. Generally, the mean PM_{10} concentration from EM is 24.1 µg m^{-3}, including 0.9 µg m^{-3} (3.5%) for BC, 2.5 µg m^{-3} (10.3%) for OC, 3.1 µg m^{-3} (12.9%) for SO_4^{2-}, 2.7 µg m^{-3} (11.3%) for NO_3^-, 1.7 µg m^{-3} (7.1%) for NH_4^+, 6.4 µg m^{-3} (26.7%) for OTHER1 and 6.8 µg m^{-3} (28.2%) for OTHER2. For $PM_{2.5}$, the regional mean concentration from EM is 17.3 µg m^{-3}, with an inter-model range from 9.7 µg m^{-3} of M5 to 28.1 µg m^{-3} of M14. Except OTHER1, the major compositions in $PM_{2.5}$ in East Asia are SO_4^{2-} (18.0%), NO_3^- (15.7%) and OC (14.4%).~~

~~Aerosol chemical compositions in six high–profile cities in East Asia (Beijing, Shanghai, Guangzhou, Delhi, Seoul and Tokyo) simulated by each participating model and the multi–model EM are shown in Fig. 21. High values of $PM_{2.5}$ and PM_{10} in Beijing, Shanghai, Guangzhou and Delhi can be simulated by nearly all models, while relative small concentrations are presented in Seoul and Tokyo. For each city, a large spread of PM concentrations can be found among models, this is mainly caused by the differences of the simulated concentrations of OTHER1 and OTHER2. In other words, although common emissions are used, different physical–chemical parameterizations can cause large uncertainties in transmission and remove processes of aerosols, including the emission processes of dust and sea salt.~~ Analyzing the ratio~~s~~s of aerosol compositions to ~~PM (PM_{10} and~~ $PM_{2.5}$) from simulation results of $\underline{MM}$~~EM~~ in ~~Fig. 22~~$\underline{11(B1–B6)}$, the sums of the contributions of BC, OC, SO_4^{2-}, NO_3^- and NH_4^+ in Beijing $\underline{(63.8\%)}$, Shanghai $\underline{(60.4\%)}$, Guangzhou $\underline{(63.1\%)}$ and Delhi $\underline{(65.1\%)}$ are all less than those in $\underline{Tokyo (87.2\%)}$ and $\underline{Seoul (75.2\%)}$. ~~and Tokyo. A~~$\underline{A}$mong these components ~~in $PM_{2.5}$ (Fig. 22(b1–b6)), except OTHER1~~, NO_3^- is the major ~~component~~ $\underline{species}$ in Beijing (20.7%) and Delhi (23.6%), while SO_4^{2-} is the major ~~one~~ $\underline{species}$ in Guangzhou (22.2%). Similar contributions of SO_4^{2-} and NO_3^- can be found in Shanghai, Seoul and Tokyo. All these suggest that different air–pollution control plans should be made in different metropolitans.

For seasonal variations of $PM_{2.5}$ concentrations ($\underline{Fig. 11}$~~22~~$\underline{(C}$~~c~~$\underline{1–C}$~~c~~$\underline{6)}$), the highest values in Beijing (107.6 µg m^{-3}), Shanghai (87.5 µg m^{-3}), Guangzhou (59.9 µg m^{-3}) and Delhi (108.7 µg m^{-3}) are all simulated in winter. This can be explained by their high emissions $\underline{during this season}$~~in winter~~. However, in Tokyo, the highest $PM_{2.5}$ concentration ~~appears~~ $\underline{is}$ in summer (21.8 µg m^{-3}) and the lowest $\underline{value}$ is in winter (10.3 µg m^{-3}). In Seoul, $PM_{2.5}$ concentrations are comparable during the four seasons.

4 Conclusion and Discussion

$\underline{This\ manuscript\ mainly\ focuses\ on\ the\ first\ topic\ of\ the\ MICS–Asia\ Phase\ III,\ and\ intends\ to}$ ~~As part of the research of~~

30

the first topic in MICS–Asia Phase III, this manuscript mainly focuses on the analysis topic of aerosol species, and tries to present and summaryanalyze the following three objectives: (1) provide a comprehensive evaluation of the strengths and weaknesses of current multi–scale air quality models against extensive measurements from in–situ and satellitesobservations, (2) analyze the diversity of simulated aerosols concentrations among participant models, and (3) reveal the characteristics of key aerosol chemical components components over in the high–profile cities in East Asia.

Fourteen regional modeling groups participating in Topic 1 are required to simulate aerosol species using common meteorological fields, emission inventories and boundary conditions during the entire year of 2010 in East Asia. Model predictions are compared with each other, and with measurements of BC, OC, SO_4^{2-}, NO_3^- NH_4^+, $PM_{2.5}$ and PM_{10}. Aerosol optical depth is also rigorously evaluated against observations from AERONET, MODIS and MISR. Note that all simulation results from M3 are incredible, and no data is gained from M10. Meanwhile, M5, M6 and M8 did not submit simulated AOD. M13 did not submit simulated PM_{10}. M7 did not submit OC. Neither BC nor OC was submitted from M9.

Comparisonss against monthly observations from EANET and CNEMC demonstrate that all participant models can well reproduce the spatial and temporal variability patterns in aerosols, evolution of the concentrations of aerosol species, and multi–model ensemble mean (MMEM) shows better performance than most models, with Rs ranging from 0.65 (NO_3^-) to 0.83 ($PM_{2.5}$) for EM. Significant biases Differences between simulations predictions and observations can also becan also be found found during the analyzing period, such as SO_4^{2-} is underestimated by participant models (except M12 and M14) with NMBs ranging from −67.7% to −1.6%, while most models overestimate the concentrations of NO_3^- and NH_4^+, and the NMBs are 4.9% and 14.0% for MMEM, respectively. The absence of sulfate formation mechanisms (e.g. heterogeneous chemistry) in CTMs can explain the underestimation of SO_4^{2-}, and the underestimated SO_4^{2-} will result in the overestimation of NO_3^-. However, significant underestimations of NO_3^- and NH_4^+ are shown in M7 and M8. This is because extremely low values of NH_3 are simulated by these models. These biases may be caused by the imperfect mechanisms of gas–phase or liquid–phase oxidation of SO_2 and NO_2, including the missing heterogeneous chemistry reactions in most current multi–scale air quality models. Notably, significant underestimations of NO_3^- and NH_4^+ in M7 and M8 may be due to their incorrect treatments of the NH_3 emission inputs. The inter–model spread of simulated $PM_{2.5}$ is large, with NMBs ranging from −26.5% of M13 to 46.0% of M14, and nearly all models underestimate the $PM_{2.5}$ concentrations in Region_1. This is because the precursors and the formation pathways of organic aerosols are insufficient in current CTMs, which may cause this negative bias. Inaccurate aerosol long–range transport from high–concentration source regions (e.g. Region_2) to low–concentration downstream areas (e.g. Region_1) may explain this bias. Underestimations of PM_{10} are also simulated in each sub–over the whole analyzed regions, and the NMB of MMEM in Region_All is −32.6% for PM_{10}. This may due to the inaccurate emission inventories (e.g. anthropogenic emissions, biomass burning emissions, and natural emissions) considered in CMTs.

For AOD, participating models can reasonably reproduce the spatial variability and the seasonal cycle when comparing with observations from AERONET and MODIS. But underestimations are found along the eastern coastal regions of China and the northern regions of India, where anthropogenic emissions are large, in addition to the Taklimakan area where dust

~~particles can be frequently lifted up. Different capacities to process dust particles and different dust schemes used in participating models may cause the bias.~~

In order to reveal <u>the improvements of the simulation ability in current CTMs,</u> ~~how well the CTMs can reproduce the characteristics of aerosol species in East Asia after undergoing substantial development during recent years,~~ statistics for observed and simulated SO_4^{2-}, NO_3^- and NH_4^+ from MICS–Asia Phase II and Phase III are compared. <u>R</u>~~R~~esults obviously show that ~~the~~ <u>the spread of RMSEs for each species</u> ~~variation ranges of RMSEs for each species among participating models~~ in Phase III ~~become~~ <u>is</u> smaller, meaning similar concentrations ~~are~~ <u>can be</u> simulated <u>by current CTMs</u>. Meanwhile, ~~–~~the median<u>s</u> of the correlations, including the upper and lower quartiles, ~~is~~ <u>are</u> larger, <u>which means current CTMs show better performance in reproducing the spatial–temporal variation tendency of observations.</u>

带格式的：字体颜色：文字 1

~~indicating the evolution characteristics of observations are better simulated. All these demonstrate a more considerable capacity for reproducing aerosol concentrations and their variation tendencies in current air quality models.~~<u>Analyzing the ratio of SNA (sulfate, nitrate and ammonium) to $PM_{2.5}$, large variations are simulated by participant models, with values ranging from 31.1% (M7) to 75.1% (M5). Different gas phase and aerosol schemes used in CTMs can explain this inconsistency. Meanwhile, higher SOR (sulfur oxidation ratio) is calculated by CMAQ models, indicating more intense secondary formation of SO_4^{2-} in CMAQ than other participant models. Similar NOR (nitric oxidation ration) is predicted by CTMs, but the value (~0.20) is larger than the observed one (~0.15), which means overmuch NO_3^- is produced by current CTMs. According to the mole ratio of ammonium to sulfate and nitrate, NH_3–limited conditions are simulated by all participant models. So a small reduction in ammonia may improve the air quality significantly.</u>

带格式的：下标

带格式的：下标

The coefficient of variation <u>(CV) is frequently</u>~~can be~~ used to quantify the inter–model deviation, and a large CV is ~~calculated~~ <u>shown</u> in simulated coarse particles (subtract $PM_{2.5}$ from PM_{10}). <u>The poor consistency, especially over the arid and semi–arid regions, is mainly caused by the dust aerosols, which means current CTMs have difficulty in estimating similar dust emissions by using different dust schemes. But the simulated fine particles</u> ~~over the arid and semi–arid regions, where dust events were observed in the spring of 2010. The poor consistency may be associated with the different dust emission mechanisms used in participating models. But in general, simulation results of BC, OC, SO_4^{2-}, NO_3^- and NH_4^+~~ are ~~all~~ in good agreement, especially over the ~~relative highly polluted areas~~<u>haze–polluted areas.</u>~~, such as the eastern and northeast China, and the northeast part of India.~~

带格式的：下标
带格式的：下标

According to the simulation results from ~~EM~~<u>MMEM</u>, the highest $PM_{2.5}$ concentrations ~~of~~ <u>in</u> Beijing ~~(107.6 μg m⁻³)~~, Shanghai ~~(87.5 μg m⁻³)~~, Guangzhou ~~(59.9 μg m⁻³)~~ and Delhi ~~(108.7 μg m⁻³)~~ are shown in winter, mainly due to the high emissions and unfavorable weather conditions ~~in winter~~. But the highest <u>value</u> in Tokyo appears in summer ~~(21.8 μg m⁻³)~~. $PM_{2.5}$ concentrations are comparable during the four seasons in Seoul. Analyzing the ratios of <u>each composition</u>~~chemical compositions~~ to $PM_{2.5}$ ~~in these cities~~, NO_3^- is the major component in Beijing ~~(20.7%)~~ and Delhi ~~(23.6%)~~, SO_4^{2-} is the major one in Guangzhou ~~(22.2%)~~, similar contributions of SO_4^{2-} and NO_3^- are calculated in Shanghai, Seoul ~~–~~and Tokyo. <u>All these suggest that different air–pollution control plans should be made</u>~~All these suggest that different air–pollution control plans should be made according to the main contaminants~~ in different cities.

MICS–Asia project gives an opportunity to understand the performance of air quality models in East Asia applications. Analyzing the results concluded above, in order to reduce the diversities of simulated aerosol concentrations among participant models, detailed sensitivity experiments about parameterizations, model inputs and even grid resolutions should be further quantitatively discussed. For example, simulation results from M1 and M2 can be used to assess the impacts of boundary conditions (BCs), since the configurations in these two models are similar except the BCs. M1 adopts the downscale results from GEOS–Chem, while M2 uses the default values from CMAQ. From Fig. S9 we can find that positive biases are simulated, especially around the edges of the simulation domain, and the maximum deviation can be over 100%. This is because the boundary conditions from GEOS-Chem consider the impacts of aerosols outside the analyzed domain. But in most inland regions, differences between M1 and M2 are small (< ±10%).

Meanwhile, process analysis techniques (i.e. integrated process rate (IPR) analysis) should be developed and implemented in air quality models. This is because IPR can be used to calculate the contributions of each physical/chemical process to variations in aerosol concentrations (Chen et al., 2019), and it will become easier to draw conclusions about the fundamental problems that cause the differences between model predictions (Carmichael et al., 2008). Fully understanding of the source–receptor relationship in each process for a given aerosol species can also be helpful to revise parameterization schemes for better simulation capability. What's more, extensive observations should be collected and used in the next MICS–Asia project.

MICS–Asia project gives an opportunity to understand the performance of air quality models in East Asia applications. Analyzing the results concluded above, in order to reduce the diversities of simulated aerosol concentrations among participant models, more efforts are needed for future modeling studies. For example, process analysis scheme should be developed and implemented in air quality models, and individual process, such as advection, diffusion, emission, dry deposition, wet scavenging, gas-phase chemistry and cloud chemistry should be isolated to make a quantitative attribution for the cause of the differences between model predictions. Fully understanding of the source–receptor relationship in each process for a given aerosol species can be helpful to revise parameterization schemes for better simulation capability. Meanwhile, more observations should be collected and used in the next MICS–Asia project.

_____

Author contribution

LC, YG and MZ conducted the study design. LC, JZ, HL, JL, KH, BG, XW, YL, CL, SI, TN, MK and KY contributed to modeling data. JF, ZW and JK provided the emission data and observation data. YG and JZ helped with data processing. MZ, JF and JZ were involved in the scientific interpretation and discussion. LC prepared the manuscript with contributions from all co-authors.

Competing interests

The authors declare that they have no conflict of interest.

References

Ackermann, I. J., Hass, H., Memmesheimer, M., Ebel, A., Binkowski, F. S., and Shankar, U. M. A.: Modal aerosol dynamics model for Europe: Development and first applications. Atmospheric environment, 32(17), 2981-2999, 10.1016/S1352-2310(98)00006-5, 1998.

5 ~~Alexander, B.: Sulfate formation in sea-salt aerosols: Constraints from oxygen isotopes, Journal of Geophysical Research, 110, 10.1029/2004jd005659, 2005.~~

Ahmadov, R., McKeen, S. A., Robinson, A., Bahreini, R., Mid-dlebrook, A., de Gouw, J., Meagher, J., Hsie, E., Edgerton,E., Shaw, S., and Trainer, M.: A volatility basis set modelfor summertime secondary organic aerosols over the east-ern United States in 2006, J. Geophys. Res., 117, D06301,doi:10.1029/2011JD016831, 2012.

10 Appel, K. W., Pouliot, G. A., Simon, H., Sarwar, G., Pye, H. O. T., Napelenok, S. L., Akhtar, F., and Roselle, S. J.: Evaluation of dust and trace metal estimates from the Community Multiscale Air Quality (CMAQ) model version 5.0, Geoscientific Model Development, 6, 883-899, 10.5194/gmd-6-883-2013, 2013.

Archer-Nicholls, S., Lowe, D., Utembe, S., Allan, J., Zaveri, R. A., Fast, J. D., Hodnebrog, Ø., Denier van der Gon, H., and Mc-Figgans, G.: Gaseous chemistry and aerosol mechanism developments for version 3.5.1 of the online regional
15 model, WRFChem, Geosci. Model Dev., 7, 2557–2579, doi:10.5194/gmd-7-2557-2014, 2014.

Baklanov, A., Schlünzen, K., Suppan, P., Baldasano, J., Brunner, D., Aksoyoglu, S., Carmichael, G., Douros, J., Flemming, J., Forkel, R., Galmarini, S., Gauss, M., Grell, G., Hirtl, M., Joffre, S., Jorba, O., Kaas, E., Kaasik, M., Kallos, G., Kong, X., Korsholm, U., Kurganskiy, A., Kushta, J., Lohmann, U., Mahura, A., Manders-Groot, A., Maurizi, A., Moussiopoulos, N., Rao, S. T., Savage, N., Seigneur, C., Sokhi, R. S., Solazzo, E., Solomos, S., Sørensen, B., Tsegas,
20 G., Vignati, E., Vogel, B., and Zhang, Y.: Online coupled regional meteorology chemistry models in Europe: current status and prospects, Atmos. Chem. Phys., 14, 317–398, https://doi.org/10.5194/acp-14-317-2014, 2014.

Balzarini, A., Pirovano, G., Honzak, L., Žabkar, R., Curci, G., Forkel, R., Hirtl, M., San José, R., Tuccella, P., and Grell, G. A.: WRF-Chem model sensitivity to chemical mechanisms choice in reconstructing aerosol optical properties, Atmos. Environ., 115, 604–619, 10.1016/j.atmosenv.2014.12.033, 2014.

25 Bey, I., Jacob, D. J., Yantosca, R. M., Logan, J. A., Field, B. D., Fiore, A. M., Li, Q., Liu, H. Y., Mickley, L. J., and Schultz, M. G.: Global modeling of tropospheric chemistry with assimilated meteorology: Model description and evaluation, Journal of Geophysical Research: Atmospheres, 106, 23073-23095, 10.1029/2001jd000807, 2001.

Briant, R., Tuccella, P., Deroubaix, A., Khvorostyanov, D., Menut, L., Mailler, S., and Turquety, S.: Aerosol–radiation interaction modelling using online coupling between the WRF 3.7.1 meteorological model and the CHIMERE 2016
30 chemistry-transport model, through the OASIS3-MCT coupler, Geoscientific Model Development, 10, 927-944, 10.5194/gmd-10-927-2017, 2017.

Brunner, D., Savage, N., Jorba, O., Eder, B., Giordano, L., Badia, A., Balzarini, A., Baró, R., Bianconi, R., Chemel, C., Curci, G., Forkel, R., Jiménez-Guerrero, P., Hirtl, M., Hodzic, A., Honzak, L., Im, U., Knote, C., Makar, P., Manders-Groot, A., van Meijgaard, E., Neal, L., Pérez, J. L., Pirovano, G., San Jose, R., Schröder, W., Sokhi, R. S., Syrakov, D., Torian, A.,
35 Tuccella, P., Werhahn, J., Wolke, R., Yahya, K., Zabkar, R., Zhang, Y., Hogrefe, C., and Galmarini, S.: Comparative analysis of meteorological performance of coupled chemistry-meteorology models in the context of AQMEII phase 2, Atmospheric Environment, 115, 470-498, 10.1016/j.atmosenv.2014.12.032, 2015.

Byun, D. W. and Ching, J. K. S.: Science algorithms of the EPA Models-3 Community Multiscale Air Quality (CMAQ) modeling system, US Environmental Protection Agency Report EPA/600/R-99/030, Research Triangle Park, NC, 1999.
40 Carmichael, G. R., Calori, G., Hayami, H., Uno, I., Cho, S. Y., Engardt, M., Kim, S., Ichikawa, Y., Ikeda, Y., Ueda, H., Amann, M.: The MICS-Asia study: model intercomparison of long-range transport and sulfur deposition in East Asia. Atmospheric Environment, 36(2), 175-199, 10.1023/A:1012291200633, 2002.

Carmichael, G., Sakurai, T., Streets, D., Hozumi, Y., Ueda, H., Park, S., Fung, C., Han, Z., Kajino, M., and Engardt, M.: MICS-Asia II: The model intercomparison study for Asia Phase II methodology and overview of findings, Atmospheric
45 Environment, 42, 3468-3490, 10.1016/j.atmosenv.2007.04.007, 2008.

Carmichael, G. R., Adhikary, B., Kulkarni, S., D'Allura, A., Tang, Y., Streets, D., Zhang, Q., Bond, T. C., Ramanathan, V., Jamroensan, A., and Marrapu, P.: Asian Aerosols: Current and Year 2030 Distributions and Implications to Human Health and Regional Climate Change, Environmental Science & Technology, 43, 5811-5817, 10.1021/es8036803, 2009.

Carter, W. P. L.: Documentation of the SAPRC-99 chemical mechanism for VOC reactivity assessment. Final Report to

California Air Resources Board Contract 92-329 and Contract 95-308, Air Pollution Research Center and College of Engineering Center for Environmental Research and Technology, University of California Riverside, California, 2000

Chen, D., Wang, Y., McElroy, M. B., He, K., Yantosca, R. M., and Sager, P. L.: Regional CO pollution and export in China simulated by the high-resolution nested-grid GEOS-Chem model. Atmospheric Chemistry and Physics, 9(11), 3825-3839, 10.5194/acp-9-3825-2009, 2009.

Chen, D., Liu, Z., Fast, J., and Ban, J.: Simulations of sulfate–nitrate–ammonium (SNA) aerosols during the extreme haze events over northern China in October 2014, Atmos. Chem. Phys., 16, 10707-10724, https://doi.org/10.5194/acp-16-10707-2016, 2016a.

Chen, K., Huang, L., Zhou, L., Ma, Z., Bi, J., and Li, T.: Spatial analysis of the effect of the 2010 heat wave on stroke mortality in Nanjing, China, Sci Rep, 5, 10816, 10.1038/srep10816, 2015.

Chen, L., Zhang, L., Zhang, L., Cao, X., Huang, J., Zhang, W., and Zhang, B.: Characteristics of black carbon aerosol and carbonaceous gases and their emission sources in semi-arid region, China Environmental Science, 32(8), 1345-1352, 2012.

Chen, L., Zhang, M., and Wang, Y.: Model analysis of urbanization impacts on boundary layer meteorology under hot weather conditions: a case study of Nanjing, China, Theoretical and Applied Climatology, 125, 713-728, 10.1007/s00704-015-1535-6, 2016b.

Chen, L., Zhang, M., Zhu, J., and Skorokhod, A.: Model analysis of soil dust impacts on the boundary layer meteorology and air quality over East Asia in April 2015, Atmospheric Research, 187, 42-56, 10.1016/j.atmosres.2016.12.008, 2017.

Chen, L., Zhang, M. G., Zhu, J., Wang, Y. W., Skorokhod, A.: Modeling impacts of urbanization and urban heat island mitigation on boundary layer meteorology and air quality in Beijing under different weather conditions, Journal of Geophysical Research: Atmospheres, 123, doi: 10.1002/2017JD027501, 2018.

Chen, L., Zhu, J., Liao, H., Gao, Y., Qiu, Y., Zhang, M., and Li, N.: Assessing the formation and evolution mechanisms of severe haze pollution in Beijing−Tianjin−Hebei region by using process analysis, Atmos. Chem. Phys. Discuss., 10.5194/acp-2019-245, in review, 2019.

Chin, M., Rood, R. B., Lin, S.-J., Müller, J.-F., and Thompson, A. M.: Atmospheric sulfur cycle simulated in the global model GOCART: Model description and global properties, Journal of Geophysical Research: Atmospheres, 105, 24671-24687, 10.1029/2000jd900384, 2000.

Chin, M., Ginoux, P., Kinne, S., Torres, O., Holben, B. N., Duncan, B. N., Martin, R. V., Logan, J. A., Higurashi, A., and Nakajima, T.: Tropospheric aerosol optical thickness from the GOCART model and comparisons with satellite and Sun photometer measurements, Journal of the Atmospheric Sciences, 59, 461-483, 2002.

Chin, M., Ginoux, P., Kinne, S., Torres, O., Holben, B. N., Duncan, B. N., Martin, R. V., Logan, J. A., Higurashi, A., and Nakajima, T.: Tropospheric aerosol optical thickness from the GOCART model and comparisons with satellite and Sun photometer measurements, J. Atmos. Sci., 59, 461-483, 10.1175/1520-0469(2002)059<0461:taotft>2.0.co;2, 2002.

Clarke, A. D., Owens, S. R., and Zhou, J. C.: An ultrafine sea-salt flux from breaking waves: Implications for cloud condensation nuclei in the remote marine atmosphere, J. Geophys. Res. Atmos, 111, 2006.

Cowan, T., Cai, W., Purich, A., Rotstayn, L., and England, M. H.: Forcing of anthropogenic aerosols on temperature trends of the sub-thermocline southern Indian Ocean, Sci Rep, 3, 2245, 10.1038/srep02245, 2013.

Cuchiara, G. C., Li, X., Carvalho, J., and Rappenglück, B.: Intercomparison of planetary boundary layer parameterization and its impacts on surface ozone concentration in the WRF/Chem model for a case study in Houston/Texas, Atmospheric Environment, 96, 175-185, 10.1016/j.atmosenv.2014.07.013, 2014.

Deng, X. L., Shi, C. E., Wu, B. W., Yang, Y. J., Jin, Q., Wang, H. L., Zhu, S., and Yu, C.: Characteristics of the water-soluble components of aerosol particles in Hefei, China, Journal of environmental sciences, 42, 32-40, 10.1016/j.jes.2015.07.010, 2016.

Diehl, T., Heil, A., Chin, M., Pan, X., Streets, D., Schultz, M., and Kinne, S.: Anthropogenic, biomass burning, and volcanic emissions of black carbon, organic carbon, and SO_2 from 1980 to 2010 for hindcast model experiments, Atmospheric Chemistry and Physics Discussions, 12, 24895-24954, 10.5194/acpd-12-24895-2012, 2012.

Ding, A. J., Huang, X., Nie, W., Sun, J. N., Kerminen, V. M., Petäjä, T., Su, H., Cheng, Y. F., Yang, X. Q., Wang, M. H., Chi, X. G., Wang, J. P., Virkkula, A., Guo, W. D., Yuan, J., Wang, S. Y., Zhang, R. J., Wu, Y. F., Song, Y., Zhu, T., Zilitinkevich, S., Kulmala, M., and Fu, C. B.: Enhanced haze pollution by black carbon in megacities in China, Geophysical Research Letters, 43, 2873-2879, 10.1002/2016gl067745, 2016.

带格式的：删除线

带格式的：删除线

Du, H., Kong, L., Cheng, T., Chen, J., Du, J., Li, L., Xia, X., Leng, C., Huang, G.: Insights into summertime haze pollution events over Shanghai based on online water-soluble ionic composition of aerosols. Atmos. Environ. 45, 5131–5137, 2011.

5 ~~Duncan Fairlie, T., Jacob, D. J., and Park, R. J.: The impact of transpacific transport of mineral dust in the United States, Atmospheric Environment, 41, 1251-1266, 10.1016/j.atmosenv.2006.09.048, 2007.~~

Easter, R. C.: MIRAGE: Model description and evaluation of aerosols and trace gases, Journal of Geophysical Research, 109, 10.1029/2004jd004571, 2004.

Fan, Q., Lan, J., Liu, Y., Wang, X., Chan, P., Hong, Y., Feng, Y., Liu, Y., Zeng, Y., and Liang, G.: Process analysis of regional aerosol pollution during spring in the Pearl River Delta region, China, Atmospheric Environment, 122, 829-838, 10 10.1016/j.atmosenv.2015.09.013, 2015.

Foroutan, H., Young, J., Napelenok, S., Ran, L., Appel, K. W., Gilliam, R. C., and Pleim, J. E.: Development and evaluation of a physics-based windblown dust emission scheme implemented in the CMAQ modeling system, Journal of Advances in Modeling Earth Systems, 9, 585-608, 10.1002/2016ms000823, 2017.

Fountoukis, C. and Nenes, A.: ISORROPIA II: a computationally efficient thermodynamic equilibrium model for 15 K^+–Ca^{2+}–Mg^{2+}– NH_4^+ –Na^+– SO_4^{2-} – NO_3^- –Cl^-–H_2O aerosols, Atmos. Chem. Physics, 7, 4639–4659, doi:10.5194/acp-7-4639-2007, http://www.atmos-chem-phys.net/7/4639/2007/, 2007.

~~Forkel, R., Balzarini, A., Baro, R., Curci, C., Jimenez Guerrero, P., Hirtl, J., Honzak, L., Im, U., Lorenz, C., Perez, J. L., Provano, G., San Jose, R., Tuccella, P., Werhahn, I., and Zabkar, R.: Analysis of the WRF Chem contributions to AQMEII phase 2 with respect to aerosol radiative feedbacks on meteorology and pollutant distribution, Atmospheric 20 Environment, 115, 630-645, doi: 10.1016/j.atmosenv.2014.10.056, 2015.~~

Fu, J., Jang, C., Streets, D., Li, Z., Kwok, R., Park, R., and Han, Z.: MICS-Asia II: Modeling gaseous pollutants and evaluating an advanced modeling system over East Asia, Atmospheric Environment, 42, 3571-3583, 10.1016/j.atmosenv.2007.07.058, 2008a.

Fu, Q., Zhuang, G., Wang, J., Xu, C., Huang, K., Li, J., Hou, B., Lu, T., Streets, D.G.: Mechanism of formation of the heaviest pollution episode ever recorded in the Yangtze River Delta, China. Atmos. Environ. 42, 2023–2036, 2008b.

25 Fu, J. S., Hsu, N. C., Gao, Y., Huang, K., Li, C., Lin, N. H., and Tsay, S. C.: Evaluating the influences of biomass burning during 2006 BASE-ASIA: a regional chemical transport modeling, Atmospheric Chemistry and Physics, 12, 3837-3855, 10.5194/acp-12-3837-2012, 2012.

Gao, M., Guttikunda, S. K., Carmichael, G. R., Wang, Y., Liu, Z., Stanier, C. O., Saide, P. E., and Yu, M.: Health impacts and 30 economic losses assessment of the 2013 severe haze event in Beijing area, Sci Total Environ, 511, 553-561, 10.1016/j.scitotenv.2015.01.005, 2015a.

Gao, M., Carmichael, G. R., Wang, Y., Saide, P. E., Yu, M., Xin, J., Liu, Z., and Wang, Z.: Modeling study of the 2010 regional haze event in the North China Plain, Atmospheric Chemistry and Physics, 16, 1673-1691, 10.5194/acp-16-1673-2016, 2016b.

35 Gao, M., Han, Z., Liu, Z., Li, M., Xin, J., Tao, Z., Li, J., Kang, J.-E., Huang, K., Dong, X., Zhuang, B., Li, S., Ge, B., Wu, Q., Cheng, Y., Wang, Y., Lee, H.-J., Kim, C.-H., Fu, J. S., Wang, T., Chin, M., Woo, J.-H., Zhang, Q., Wang, Z., and Carmichael, G. R.: Air Quality and Climate Change, Topic 3 of the Model Inter-Comparison Study for Asia Phase III (MICS-Asia III), Part I: overview and model evaluation, Atmospheric Chemistry and Physics, 18, 4859-4884, doi: 10.5194/acp-18-4859-2018, 2018.

40 Gao, Y., Zhao, C., Liu, X., Zhang, M., and Leung, L. R.: WRF-Chem simulations of aerosols and anthropogenic aerosol radiative forcing in East Asia, Atmospheric Environment, 92, 250-266, 10.1016/j.atmosenv.2014.04.038, 2014.

Gao, Y., Zhang, M., Liu, Z., Wang, L., Wang, P., Xia, X., Tao, M., and Zhu, L.: Modeling the feedback between aerosol and meteorological variables in the atmospheric boundary layer during a severe fog–haze event over the North China Plain, Atmospheric Chemistry and Physics, 15, 4279-4295, 10.5194/acp-15-4279-2015, 2015b.

45 Gao, Y., Zhang, M., Liu, X., and Wang, L.: Change in diurnal variations of meteorological variables induced by anthropogenic aerosols over the North China Plain in summer 2008, Theoretical and applied climatology, 124(1-2), 103-118, 10.1007/s00704-015-1403-4, 2016a.

Gillette, D. A., and Passi, R.: Modeling Dust Emission Caused by Wind Erosion, J Geophys Res-Atmos, 93, 14233-14242, 1988.

50 Grell, G. A., Peckham, S. E., Schmitz, R., McKeen, S. A., Frost, G., Skamarock, W. C., and Eder, B.: Fully coupled "online"

chemistry within the WRF model, Atmospheric Environment, 39, 6957-6975, 10.1016/j.atmosenv.2005.04.027, 2005.

Guenther, C. C.: Estimates of global terrestrial isoprene emissions using MEGAN (Model of Emissions of Gases and Aerosols from Nature). Atmospheric Chemistry and Physics, 6, www.atmos-chem-phys.net/6/3181/2006, 2006.

Gong, S. L.: A parameterization of sea-salt aerosol source function for sub- and super-micron particles, Global Biogeochem Cy, 17, 2003.

Hall, D.: Environmental change, protest, and havens of environmental degradation: Evidence from Asia. Global Environmental Politics, 2(2), 20-28, 10.1162/15263800260047808, 2002.

Han, X., Zhang, M., Liu, X., Steven, G., Xin, J., Wang, L.: Development of RAMS-CMAQ to simulate aerosol optical depth and aerosol direct radiative forcing and its application to East Asia. Atmospheric and Oceanic Science Letters, 2(6), 368-375, 10.1080/16742834.2009.11446831, 2009.

Han, X., Zhang, M., Tao, J., Wang, L., Gao, J., Wang, S., and Chai, F.: Modeling aerosol impacts on atmospheric visibility in Beijing with RAMS-CMAQ, Atmospheric Environment, 72, 177-191, 10.1016/j.atmosenv.2013.02.030, 2013.

Han, X., Zhang, M., Gao, J., Wang, S., and Chai, F.: Modeling analysis of the seasonal characteristics of haze formation in Beijing, Atmospheric Chemistry and Physics, 14, 10231-10248, 10.5194/acp-14-10231-2014, 2014.

Han, X., Zhu, L., Wang, S., Meng, X., Zhang, M., and Hu, J.: Modeling study of impacts on surface ozone of regional transport and emissions reductions over North China Plain in summer 2015, Atmospheric Chemistry and Physics, 18, 12207-12221, 10.5194/acp-18-12207-2018, 2018.

Han, Z. W., Ueda, H., Matsuda, K., Zhang, R. J., Arao, K., Kanai, Y., and Hasome, H.: Model study on particle size segregation and deposition during Asian dust events in March 2002, J Geophys Res-Atmos, 109, 2004.

Han, Z., Sakurai, T., Ueda, H., Carmichael, G., Streets, D., Hayami, H., Wang, Z., Holloway, T., Engardt, M., and Hozumi, Y.: MICS-Asia II: Model intercomparison and evaluation of ozone and relevant species, Atmospheric Environment, 42, 3491-3509, 10.1016/j.atmosenv.2007.07.031, 2008.

Hauser, A., Oesch, D., and Foppa, N.: Aerosol optical depth over land: Comparing AERONET, AVHRR and MODIS, Geophysical Research Letters, 32, 10.1029/2005gl023579, 2005.

Hayami, H., Sakurai, T., Han, Z., Ueda, H., Carmichael, G., Streets, D., Holloway, T., Wang, Z., Thongboonchoo, N., and Engardt, M.: MICS-Asia II: Model intercomparison and evaluation of particulate sulfate, nitrate and ammonium, Atmospheric Environment, 42, 3510-3527, 10.1016/j.atmosenv.2007.08.057, 2008.

Holben, B. N., Eck, T. F., Slutsker, I., Tanre, D., Buis, J. P., Setzer, A., Vermote, E., Reagan, J. A., Kaufman, Y. J., Nakajima, T., Lavenu, F., Jankowiak, I., Smirnov, A.: AERONET—A federated instrument network and data archive for aerosol characterization. Remote sensing of environment, 66(1), 1-16, 10.1016/S0034-4257(98)00031-5, 1998.

Holloway, T., Sakurai, T., Han, Z., Ehlers, S., Spak, S., Horowitz, L., Carmichael, G., Streets, D., Hozumi, Y., and Ueda, H.: MICS-Asia II: Impact of global emissions on regional air quality in Asia, Atmospheric Environment, 42, 3543-3561, 10.1016/j.atmosenv.2007.10.022, 2008.

Hong, C., Zhang, Q., He, K., Guan, D., Li, M., Liu, F., and Zheng, B.: Variations of China's emission estimates: response to uncertainties in energy statistics, Atmospheric Chemistry and Physics, 17, 1227-1239, 10.5194/acp-17-1227-2017, 2017.

Horowitz, L. W., Walters, S., Mauzerall, D. L., Emmons, L. K., Rasch, P. J., Granier, C., Tie, X. X., Lamarque, J. F., Schultz, M. G., Tyndall, G. S., Orlando, J. J., and Brasseur, G. P.: A global simulation of tropospheric ozone and related tracers: Description and evaluation of MOZART, version 2, J. Geophys. Res. Atmos., 108, 29, 10.1029/2002jd002853, 2003.

Huang, K., Fu, J. S., Hsu, N. C., Gao, Y., Dong, X., Tsay, S.-C., and Lam, Y. F.: Impact assessment of biomass burning on air quality in Southeast and East Asia during BASE-ASIA, Atmospheric Environment, 78, 291-302, 10.1016/j.atmosenv.2012.03.048, 2013.

Huang, X., Song, Y., Li, M., Li, J., Huo, Q., Cai, X., Zhu, T., Hu, M., and Zhang, H.: A high-resolution ammonia emission inventory in China, Global Biogeochem. Cy., 26, GB1030, doi:10.1029/2011GB004161, 2012.

Huang, X., Song, Y., Zhao, C., Li, M., Zhu, T., Zhang, Q., and Zhang, X.: Pathways of sulfate enhancement by natural and anthropogenic mineral aerosols in China, J. Geophys. Res.-Atmos., 119, https://doi.org/10.1002/2014JD022301, 2014.

Huang, X., Wang, Z., and Ding, A.: Impact of Aerosol-PBL Interaction on Haze Pollution: Multiyear Observational Evidences in North China, Geophysical Research Letters, 10.1029/2018gl079239, 2018.

Ikeda, K., Yamaji, K., Kanaya, Y., Taketani, F., Pan, X., Komazaki, Y., Kurokawa, J.-i., and Ohara, T.: Sensitivity analysis of source regions to PM2.5 concentration at Fukue Island, Japan, Journal of the Air & Waste Management Association, 64,

中 **域代码已更改**

带格式的： 删除线

带格式的： 删除线

445-452, 10.1080/10962247.2013.845618, 2013.

Itahashi, S., Uno, I., Irie, H., Kurokawa, J. I., and Ohara, T.: Regional modeling of tropospheric NO_2 vertical column density over East Asia during the period 2000–2010: comparison with multisatellite observations, Atmospheric Chemistry and Physics, 14, 3623-3635, 10.5194/acp-14-3623-2014, 2014.

5   Im, U.: Impact of sea-salt emissions on the model performance and aerosol chemical composition and deposition in the East Mediterranean coastal regions, Atmospheric Environment, 75, 329-340, 2013.

Jaeglé L., Quinn, P. K., Bates, T. S., Alexander, B., and Lin, J.-T.: Global distribution of sea salt aerosols: new constraints from in situ and remote sensing observations, Atmos. Chem. Phys., 11, 3137-3157, https://doi.org/10.5194/acp-11-3137-2011, 2011.

10   Janssens-Maenhout, G., Crippa, M., Guizzardi, D., Dentener, F., Muntean, M., Pouliot, G., Keating, T., Zhang, Q., Kurokawa, J., Wankmüller, R., Denier van der Gon, H., Kuenen, J. J. P., Klimont, Z., Frost, G., Darras, S., Koffi, B., and Li, M.: HTAP_v2.2: a mosaic of regional and global emission grid maps for 2008 and 2010 to study hemispheric transport of air pollution, Atmospheric Chemistry and Physics, 15, 11411-11432, 10.5194/acp-15-11411-2015, 2015.

Jimenez, P., Baldasano, J. M., and Dabdub, D.: Comparison of photochemical mechanisms for air quality modeling, Atmos.
15   Environ., 37, 4179–4194, 10.1016/S1352-2310(03)00567-3, 2003.

Jongman, B., Winsemius, H. C., Aerts, J. C., Coughlan de Perez, E., van Aalst, M. K., Kron, W., and Ward, P. J.: Declining vulnerability to river floods and the global benefits of adaptation, Proc Natl Acad Sci U S A, 112, E2271-2280, 10.1073/pnas.1414439112, 2015.

20   Kajino, M., Inomata, Y., Sato, K., Ueda, H., Han, Z., An, J., Katata, G., Deushi, M., Maki, T., Oshima, N., Kurokawa, J., Ohara, T., Takami, A., and Hatakeyama, S.: Development of the RAQM2 aerosol chemical transport model and predictions of the Northeast Asian aerosol mass, size, chemistry, and mixing type. Atmospheric Chemistry and Physics, 12(24), 11833, 10.5194/acp-12-11833-2012, 2012.

Kajino, M., Deushi, M., Sekiyama, T. T., Oshima, N., Yumimoto, K., Tanaka, T. Y., Ching, J., Hashimoto, A., Yamamoto, T.,
25   Ikegami, M., Kamada, A., Miyashita, M., Inomata, Y., Shima, S.-I., Adachi, K., Zaizen, Y., Igarashi, Y., Ueda, H., Maki, T., and Mikami, M.: NHM-Chem, the Japan Meteorological Agency's regional meteorology – chemistry model (v1.0): model description and aerosol representations, Geosci. Model Dev. Discuss., 10.5194/gmd-2018-128, 2018.

Kang, J.Y., Yoon, S.C., Shao, Y., and Kim, S.W.: Comparison of vertical dust flux by implementing three dust emission schemes in WRF/Chem, J. Geophys. Res., 116, D09202, doi:10.1029/2010JD014649, 2011.

30   Kelly, J. T., Bhave, P. V., Nolte, C. G., Shankar, U., and Foley, K. M.: Simulating emission and chemical evolution of coarse sea-salt particles in the Community Multiscale Air Quality (CMAQ) model, Geoscientific Model Development, 3, 257-273, 2010.

Kurokawa, J., Ohara, T., Morikawa, T., Hanayama, S., Janssens-Maenhout, G., Fukui, T., Kawashima, K., and Akimoto, H.: Emissions of air pollutants and greenhouse gases over Asian regions during 2000–2008: Regional Emission inventory
35   in Asia (REAS) version 2, Atmos. Chem. Phys., 13, 11019–11058, doi:10.5194/acp-13-11019-2013, 2013.

Kiley, C. M., Fuelberg, H. E., Palmer, P. I., Allen, D. J., Carmichael, G. R., Jacob, D. J., Mari, C., Pierce, R. B., Pickering, K. E., Tang, Y., Wild, O., Fairlie, T. D., Logan, J. A., Sachse, G. W., Shaack, T. K., and Streets, D. G.: An intercomparison and evaluation of aircraft-derived and simulated CO from seven chemical transport models during the TRACE-P experiment, Journal of Geophysical Research: Atmospheres, 108, 10.1029/2002jd003089, 2003.

40   Kim, Y. J., Spak, S. N., Carmichael, G. R., Riemer, N., and Stanier, C. O.: Modeled aerosol nitrate formation pathways during wintertime in the Great Lakes region of North America, J. Geophys. Res. Atmos., 119, 12420-12445, 2014.

Kim, S. W., Heckel, A., Frost, G. J., Richter, A., Gleason, J., Burrows, J. P., McKeen, S., Hsie, E. Y., Granier, C., and Trainer, M.: NO2 columns in the western United States observed from space and simulated by a regional chemistry model and their implications for NOx emissions, J. Geophys. Res.-Atmos., 114, D11301, 10.1029/2008JD011343, 2009.

45   Kim, Y., Couvidat, F., Sartelet, K., and Seigneur, C.: Comparison of different gas-phase mechanisms and aerosol modules for simulating particulate matter formation, J. Air Waste Manage. Assoc, 61, 1218–1226, 10.1080/10473289.2011.603999, 2011

Kong, X., Forkel, R., Sokhi, R. S., Suppan, P., Baklanov, A., Gauss, M., Brunner, D., Baro, R., Balzarini, A., Chemel, C.,
50   Curci, G., Jimenez-Guerrero, P., Hirtl, M., Honzak, L., Im, U., Perez, J. L., Pirovano, G., Jose, R. S., Schlunzen, K. H.,

Tsegas, G., Tuccella, P., Werhahn, J., Zabkar, R., and Galmarini, S.: Analysis of meteorology-chemistry interactions during air pollution episodes using online coupled models within AQMEII phase-2, 115, 527-540, doi: 10.1016/j.atmosenv.2014.09.020, 2015.

5   Kong, L., Tang, X., Zhu, J., Wang, Z., Fu, J. S., Wang, X., Itahashi, S., Yamaji, K., Nagashima, T., Lee, H.-J., Kim, C.-H., Lin, C.-Y., Chen, L., Zhang, M., Tao, Z., Li, J., Kajino, M., Liao, H., Sudo, K., Wang, Y., Pan, Y., Tang, G., Li, M., Wu, Q., Ge, B., and Carmichael, G. R.: Evaluation and uncertainty investigation of the NO2, CO and NH3 modeling over China under the framework of MICS-Asia III, Atmos. Chem. Phys. Discuss., 10.5194/acp-2018-1158, in review, 2019.

Kurokawa, J., Ohara, T., Morikawa, T., Hanayama, S., Janssens-Maenhout, G., Fukui, T., Kawashima, K., and Akimoto, H.: Emissions of air pollutants and greenhouse gases over Asian regions during 2000–2008: Regional Emission inventory in Asia (REAS) version 2, Atmos. Chem. Phys., 13, 11019–11058, doi:10.5194/acp-13-11019-2013, 2013.

Lai, S., Zhao, Y., Ding, A., Zhang, Y., Song, T., Zheng, J., Ho, K. F., Lee, S.-c., and Zhong, L.: Characterization of PM 2.5 and the major chemical components during a 1-year campaign in rural Guangzhou, Southern China, Atmospheric Research, 167, 208-215, 10.1016/j.atmosres.2015.08.007, 2016.

15   Lam, Y. F., Fu, J. S., Wu, S., and Mickley, L. J.: Impacts of future climate change and effects of biogenic emissions on surface ozone and particulate matter concentrations in the United States, Atmospheric Chemistry and Physics, 11, 4789-4806, 10.5194/acp-11-4789-2011, 2011.

Lee, D. G., Lee, Y. M., Jang, K. W., Yoo, C., Kang, K. H., Lee,J. H., Jung, S. W., Park, J. M., Lee, S. B., Han, J. S., Hong, J. H., and Lee, S. J.: Korean national emissions inventory system and 2007 air pollutant emissions, Asian J. Atmos. Environ., 5, 278–291, 2011.

Lee, H.-J., Jo, H.-Y., Nam, K.-P., Lee, K.-H., Kim, C.-H.: Measurement, simulation, and meteorological interpretation of medium-range transport of radionuclides to Korea during the Fukushima Dai-ichi nuclear accident, Annals of Nuclear Energy, 103, 412-423, doi: 10.1016/j.anucene.2017.01.037, 2017.

25 ~~Li, B., Yuan, H., Feng, N., and Tao, S.: Comparing MODIS and AERONET aerosol optical depth over China, International Journal of Remote Sensing, 30, 6519-6529, 10.1080/01431160903111069, 2009.~~

~~Li, J., Han, Z., and Zhang, R.: Model study of atmospheric particulates during dust storm period in March 2010 over East Asia, Atmospheric Environment, 45, 3954-3964, 10.1016/j.atmosenv.2011.04.068, 2011.~~

Li, J., Wang, Z., Zhuang, G., Luo, G., Sun, Y., and Wang, Q.: Mixing of Asian mineral dust with anthropogenic pollutants over East Asia: a model case study of a super-duststorm in March 2010, Atmospheric Chemistry and Physics, 12, 7591-7607, 10.5194/acp-12-7591-2012, 2012a.

Li, J.: Research on pollution characteristics of PM10 in Jinan and inversion of aerosol optical thickness, M.S. thesis, Shandong Normal University, China, 64 pp., 2012b.

Li, J.: Seasonal characteristics of air pollution and weekend effect in Shanghai, M.S. thesis, the University of Chinese Academy of Sciences, China, 77 pp., 2015.

35   Li, J., Du, H., Wang, Z., Sun, Y., Yang, W., Li, J., Tang, X., and Fu, P.: Rapid formation of a severe regional winter haze episode over a mega-city cluster on the North China Plain, Environ Pollut, 223, 605-615, 10.1016/j.envpol.2017.01.063, 2017a.

Li, J., Nagashima, T., Kong, L., Ge, B., Yamaji, K., Fu, J. S., Wang, X., Fan, Q., Itahashi, S., Lee, H.-J., Kim, C.-H., Lin, C.-Y., Zhang, M., Tao, Z., Kajino, M., Liao, H., Li, M., Woo, J.-H., Kurokawa, J.-I., Wu, Q., Akimoto, H., Carmichael, G. R., and Wang, Z.: Model evaluation and inter-comparison of surface-level ozone and relevant species in East Asia in the context of MICS-Asia phase III Part I: overview, Atmos. Chem. Phys. Discuss., 10.5194/acp-2018-1283, in review, 2019.

45 ~~Li, J., Chen, X., Wang, Z., Du, H., Yang, W., Sun, Y., Hu, B., Li, J., Wang, W., Wang, T., Fu, P., and Huang, H.: Radiative and heterogeneous chemical effects of aerosols on ozone and inorganic aerosols over East Asia, The Science of the total environment, 622-623, 1327-1342, 10.1016/j.scitotenv.2017.12.041, 2018.~~

~~Li, Y., An, J., and Gultepe, I.: Effects of additional HONO sources on visibility over the North China Plain, Advances in Atmospheric Sciences, 31, 1221-1232, 10.1007/s00376-014-4019-1, 2014.~~

50 ~~Li, Y., Tao, J., Zhang, L., Jia, X., and Wu, Y.: High Contributions of Secondary Inorganic Aerosols to PM$_{2.5}$ under Polluted Levels at a Regional Station in Northern China, International journal of environmental research and public health, 13,~~

~~10.3390/ijerph13121202, 2016a.~~

Li, K., Liao, H., Zhu, J., and Moch, J. M.: Implications of RCP emissions on future PM$_{2.5}$ air quality and direct radiative forcing over China, Journal of Geophysical Research: Atmospheres, 121, 12,985-913,008, 10.1002/2016jd025623, 2016b.

5   Li, K., Liao, H., Mao, Y., and Ridley, D. A.: Source sector and region contributions to concentration and direct radiative forcing of black carbon in China, Atmospheric Environment, 124, 351-366, 10.1016/j.atmosenv.2015.06.014, 2016c.

~~Li, J., Du, H., Wang, Z., Sun, Y., Yang, W., Li, J., Tang, X., and Fu, P.: Rapid formation of a severe regional winter haze episode over a mega-city cluster on the North China Plain, Environ Pollut, 223, 605-615, 10.1016/j.envpol.2017.01.063, 2017a.~~

10   Li, M., Zhang, Q., Kurokawa, J.-i., Woo, J.-H., He, K., Lu, Z., Ohara, T., Song, Y., Streets, D. G., Carmichael, G. R., Cheng, Y., Hong, C., Huo, H., Jiang, X., Kang, S., Liu, F., Su, H., and Zheng, B.: MIX: a mosaic Asian anthropogenic emission inventory under the international collaboration framework of the MICS-Asia and HTAP, Atmospheric Chemistry and Physics, 17, 935-963, 10.5194/acp-17-935-2017, 2017b.

Li, Y., An, J., and Gultepe, I.: Effects of additional HONO sources on visibility over the North China Plain, Advances in Atmospheric Sciences, 31, 1221-1232, 10.1007/s00376-014-4019-1, 2014.

15   Li, Y., Tao, J., Zhang, L., Jia, X., and Wu, Y.: High Contributions of Secondary Inorganic Aerosols to PM$_{2.5}$ under Polluted Levels at a Regional Station in Northern China, International journal of environmental research and public health, 13, 10.3390/ijerph13121202, 2016a.

20   Liao, H., Chen, W.-T., and Seinfeld, J. H.: Role of climate change in global predictions of future tropospheric ozone and aerosols, Journal of Geophysical Research, 111, 10.1029/2005jd006852, 2006.

Lin, C. Y., Zhao, C., Liu, X., Lin, N. H., and Chen, W. N.: Modelling of long-range transport of Southeast Asia biomass-burning aerosols to Taiwan and their radiative forcings over East Asia. Tellus B: Chemical and Physical Meteorology, 66(1), 23733, 10.3402/tellusb.v66.23733, 2014.

25   Lin, Y., Zou, J., Yang, W., and Li, C.Q: A review of recent advances in research on PM2. 5 in China. International journal of environmental research and public health, 15(3), 438, 10.3390/ijerph15030438, 2018.

Liu, H., Jacob, D. J., Bey, I., and Yantosca, R. M.: Constraints from210Pb and7Be on wet deposition and transport in a global three-dimensional chemical tracer model driven by assimilated meteorological fields, Journal of Geophysical Research: Atmospheres, 106, 12109-12128, 10.1029/2000jd900839, 2001.

30   Liu, S.: Research of observations of haze and precursors in Tangshan industrial zone, M.S. thesis, Nanjing University of Information Science & Technology, China, 71 pp., 2012.

Liu, X. G., Li, J., Qu, Y., Han, T., Hou, L., Gu, J., Chen, C., Yang, Y., Liu, X., Yang, T., Zhang, Y., Tian, H., and Hu, M.: Formation and evolution mechanism of regional haze: a case study in the megacity Beijing, China, Atmos. Chem. Phys., 13, 4501–4514, doi:10.5194/acp-13-4501-2013, 2013.

35   Liu, Y. M., Zhang, S. T., Fan, Q., Wu, D., Chan, P. W., Wang, X. M., Fan, S. J., Feng, Y. R., and Hong, Y. Y.: Accessing the Impact of Sea-Salt Emissions on Aerosol Chemical Formation and Deposition over Pearl River Delta, China, Aerosol Air Qual Res, 15, 2232-2245, 2015.

Lohmann, U., and Diehl, K.: Sensitivity studies of the importance of dust ice nuclei for the indirect aerosol effect on stratiform mixed-phase clouds. Journal of the Atmospheric Sciences, 63(3), 968-982, 10.1175/JAS3662.1, 2006.

40   Lu, Z., Zhang, Q., and Streets, D. G.: Sulfur dioxide and primary carbonaceous aerosol emissions in China and India, 1996–2010, Atmos. Chem. Phys., 11, 9839–9864, doi:10.5194/acp-11-9839-2011, 2011.

Luecken, D. J., Phillips, S., Sarwar, G., and Jang, C.: Effects of using the CB05 vs. SAPRC99 vs. CB4 chemical mechanism on model predictions: ozone and gas-phase photochemical precursor concentrations, Atmos. Environ., 42, 5805–5820, 10.1016/j.atmosenv.2007.08.056, 2008.

45   Luo, G. andWang, Z. F.: A global environmental atmospheric transport model (GEATM): Model Description and validation (in Chinese), Chinese Journal of Atmospheric Sciences, 30, 504–518, doi:10.3878/j.issn.1006-9895.2006.03.13, 2006.

Makar, P. A., Moran, M. D., Zheng, Q., Cousineau, S., Sassi, M., Duhamel, A., Besner, M., Davignon, D., Crevier, L.-P., and Bouchet, V. S.: Modelling the impacts of ammonia emissions reductions on North American air quality, Atmos. Chem. Phys., 9, 7183-7212, https://doi.org/10.5194/acp-9-7183-2009, 2009.

50   Meng, Z., Jia, X., Zhang, R., Yu, X., and Ma, Q.: Characteristics of PM2.5 at Lin'an regional background station in the

Yangtze River Delta Region, Journal of Applied Meteorological Science, 23(4), 424-432, 2012.

Monahan, E. C. and Muircheartaigh, I. O.: Optimal Power-Law Description of Oceanic Whitecap Coverage Dependence on Wind Speed, J. Phys. Oceanogr., 10, 2094–2099, doi:10.1175/1520-0485(1980)010<2094:OPLDOO>2.0.CO;2, 1980.

Murphy, B. N., and Pandis, S. N.: Simulating the Formation of Semivolatile Primary and Secondary Organic Aerosol in a Regional Chemical Transport Model, Environmental science & technology, 43, 4722-4728, 2009.

Nagashima, T., Sudo, K., Akimoto, H., Kurokawa, J., and Ohara T.: Long-term change in the source contribution to surface ozone over Japan, Atmos. Chem. Phys., 17, 8231-8246, doi: 10.5194/acp-17-8231-2017, 2017.

Nenes, A., Pandis, S. N., and Pilinis, C.: ISORROPIA: A new thermodynamic equilibrium model for multiphase multicomponent inorganic aerosols. Aquatic geochemistry, 4(1), 123-152, 10.1023/A:1009604003981, 1998.

Nolte, C. G., Gilliland, A. B., Hogrefe, C., and Mickley, L. J.: Linking global to regional models to assess future climate impacts on surface ozone levels in the United States, Journal of Geophysical Research, 113, 10.1029/2007jd008497, 2008.

Pan, Y., Zhang, Y., and Sarwar, G.: Impact of gas-phase chemistry on WRF/CHEM predictions of O3 and PM2.5: Mechanism implementation and comparative evaluation, 7th annual CMAS conference, Chapel Hill, North Carolina, 2008.

Pan, Y., Tian, S., Liu, D., Fang, Y., Zhu, X., Zhang, Q., Zheng, B., Michalski, G., and Wang, Y.,: Fossil fuel combustion related emissions dominate atmospheric ammonia sources during severe haze episodes: evidence from ^{15}N Stable isotope in size resolved aerosol ammonium, Environ. Sci. Technol., 50(15), 8049-8056, 10.1021/acs.est.6b00634, 2016.

Park, R. J.: Sources of carbonaceous aerosols over the United States and implications for natural visibility, Journal of Geophysical Research, 108, 10.1029/2002jd003190, 2003.

Park, R. J.: Natural and transboundary pollution influences on sulfate-nitrate-ammonium aerosols in the United States: Implications for policy, Journal of Geophysical Research, 109, 10.1029/2003jd004473, 2004.

Petaja, T., Jarvi, L., Kerminen, V. M., Ding, A. J., Sun, J. N., Nie, W., Kujansuu, J., Virkkula, A., Yang, X. Q., Fu, C. B., Zilitinkevich, S., and Kulmala, M.: Enhanced air pollution via aerosol-boundary layer feedback in China, Sci Rep, 6, 18998, 10.1038/srep18998, 2016.

Phadnis, M. J., Carmichael, G. R., Ichikawa, Y., and Hayami, H.: Evaluation of long-range transport models for acidic deposition in East Asia. Journal of Applied Meteorology, 37(10), 1127-1142, 10.1175/1520-0450(1998)037<1127:EOLRTM>2.0.CO;2, 1998.

Pleim, J. E., and Chang, J. S.: A non-local closure model for vertical mixing in the convective boundary layer. Atmospheric Environment. Part A. General Topics, 26(6), 965-981, 10.1016/0960-1686(92)90028-J, 1992.

Pleim, J. E., Xiu, A., Finkelstein, P. L., and Otte, T. L.: A coupled land-surface and dry deposition model and comparison to field measurements of surface heat, moisture, and ozone fluxes. Water, Air, & Soil Pollution: Focus, 1(5), 243-252, 10.1023/A:1013123725860, 2001.

Pope, C. A., and Dockery, D. W.: Health Effects of Fine Particulate Air Pollution: Lines that Connect, Journal of the Air & Waste Management Association, 56, 709-742, 10.1080/10473289.2006.10464485, 2006.

Pye, H. O. T., Liao, H., Wu, S., Mickley, L. J., Jacob, D. J., Henze, D. K., and Seinfeld, J. H.: Effect of changes in climate and emissions on future sulfate-nitrate-ammonium aerosol levels in the United States, Journal of Geophysical Research, 114, 10.1029/2008jd010701, 2009.

Qiu, Y., Liao, H., Zhang, R., and Hu, J.: Simulated impacts of direct radiative effects of scattering and absorbing aerosols on surface layer aerosol concentrations in China during a heavily polluted event in February 2014, Journal of Geophysical Research: Atmospheres, 122, 5955-5975, 10.1002/2016jd026309, 2017.

Tao, J., Zhang, L., Ho, K., Zhang, R., Lin, Z., Zhang, Z., Lin, M., Cao, J., Liu, S., and Wang, G.: Impact of PM2.5 chemical compositions on aerosol light scattering in Guangzhou — the largest megacity in South China, Atmospheric Research, 135-136, 48-58, 10.1016/j.atmosres.2013.08.015, 2014.

Toth, T. D., Zhang, J., Campbell, J. R., Reid, J. S., Shi, Y., Johnson, R. S., Smirnov, A., Vaughan, M. A., and Winker, D. M.: Investigating enhanced Aqua MODIS aerosol optical depth retrievals over the mid to high latitude Southern Oceans through intercomparison with co-located CALIOP, MAN, and AERONET data sets, Journal of Geophysical Research: Atmospheres, 118, 4700-4714, 10.1002/jgrd.50311, 2013.

Reams, M. A., Lam, N. S., and Baker, A.: Measuring Capacity for Resilience among Coastal Counties of the US Northern

Gulf of Mexico Region, Am J Clim Change, 1, 194-204, 10.4236/ajcc.2012.14016, 2012.

Reff, A., Bhave, P. V., Simon, H., Pace, T. G., Pouliot, G. A., Mobley, J. D., and Houyoux, M.: Emissions inventory of PM2.5 trace elements across the United States, Environ. Sci. Technol., 43, 5790–5796, doi:10.1021/es802930x, 2009.

Schell, B., Ackermann, I. J., Hass, H., Binkowski, F. S., and Ebel, A.: Modeling the formation of secondary organic aerosol within a comprehensive air quality model system, Journal of Geophysical Research: Atmospheres, 106, 28275-28293, 10.1029/2001jd000384, 2001.

Seinfeld, J. H. and Pandis, S. N.: Atmospheric chemistry and physics: from air pollution to climate change, John Wiley & Sons, USA New Jersey John Wiley & Sons, INC, 2016.Seinfeld, J.H. and Pandis, S.N.: Atmospheric Chemistry and Physics: From Air Pollution to Climate Change, second ed. John Willey & Sons, Inc., New York, 2006.

Shao, Y.,: A model for mineral dust emission, J. Geophys. Res., 106(D17), 20,239–20,254, doi:10.1029/2001JD900171, 2001.

Shao, Y.,: Simplification of a dust emission scheme and comparison with data, J. Geophys. Res., 109, D10202, doi:10.1029/2003JD004372, 2004.

Shao, P.: The network observation and research on air pollution in Zhangjiakou, Beijing and Langfang, M.S. thesis, Nanjing University of Information Science & Technology, China, 66 pp., 2012.

Shao, J., Chen, Q., Wang, Y., Lu, X., He, P., Sun, Y., Shah, V., Martin, R. V., Philip, S., Song, S., Zhao, Y., Xie, Z., Zhang, L., and Alexander, B.: Heterogeneous sulfate aerosol formation mechanisms during wintertime Chinese haze events: air quality model assessment using observations of sulfate oxygen isotopes in Beijing, Atmos. Chem. Phys., 19, 6107-6123, https://doi.org/10.5194/acp-19-6107-2019, 2019.

Shimadera, H., Hayami, H., Chatani, S., Morino, Y., Mori, Y., Morikawa, T., Yamaji, K., and Ohara, T.: Sensitivity analyses of factors influencing CMAQ performance for fine particulate nitrate, Journal of the Air & Waste Management Association, 64, 374-387, 10.1080/10962247.2013.778919, 2013.

Singh, A., and Dey, S.: Influence of aerosol composition on visibility in megacity Delhi, Atmospheric Environment, 62, 367-373, 10.1016/j.atmosenv.2012.08.048, 2012.

Spence, M., Clarke, A., Buckley, R.M.: Urbanization and Growth; Commission on Growth and Development, World Bank Publications: Washington, DC, USA, 2008.

Stockwell, W. R., Middleton, P., Chang, J. S., and Tang, X.: The second generation regional acid deposition model chemical mechanism for regional air quality modeling. Journal of Geophysical Research: Atmospheres, 95(D10), 16343-16367, 10.1029/JD095iD10p16343, 1990.

Stockwell, W. R., Kirchner, F., Kuhn, M., and Seefeld, S.: A new mechanism for regional atmospheric chemistry modeling, Journal of Geophysical Research: Atmospheres, 102, 25847-25879, 10.1029/97jd00849, 1997.

Stuefer, M., Freitas, S. R., Grell, G., Webley, P., Peckham, S., McKeen, S. A., and Egan, S. D.: Inclusion of ash and SO 2 emissions from volcanic eruptions in WRF-Chem: development and some applications. Geoscientific Model Development, 6(2), 457-468, 10.5194/gmd-6-457-2013, 2013.

Su, L., and Fung, J.C.H.: Sensitivities of WRF-Chem to dust emission schemes and land surface properties in simulating dust cycles during springtime over East Asia, J. Geophys. Res. Atmos., 120, 11,215–11,230, doi:10.1002/2015JD023446, 2015.

Su, X., Tie, X., Li, G., Cao, J., Huang, R., Feng, T., Long, X., and Xu, R.: Effect of hydrolysis of N2O5 on nitrate and ammonium formation in Beijing China: WRF-Chem model simulation, The Science of the total environment, 579, 221-229, 10.1016/j.scitotenv.2016.11.125, 2017.

Sudo, K., Takahashi, M., Kurokawa, J., and Akimoto, H.: CHASER: A global chemical model of the troposphere-1. Model description, J. Geophys. Res.-Atmos., 107, 20, 10.1029/2001jd001113, 2002a.

Sudo, K., Takahashi, M., and Akimoto, H.: CHASER: A global chemical model of the troposphere-2. Model results and evaluation, J. Geophys. Res.-Atmos., 107, 39, 10.1029/2001jd001114, 2002b.

Sun, Y. L., Zhuang, G. S., Tang, A. H., Wang, Y., and An, Z. S.: Chemical characteristics of PM2:5 and PM10 in haze-fog episodes in Beijing, Environ. Sci. Technol., 40, 3148–3155, 10.1021/es051533g, 2006.

Sun, Y. L., Wang, Z. F., Du, W., Zhang, Q., Wang, Q. Q., Fu, P. Q., Pan, X. L., Li, J., Jayne, J., and Worsnop, D. R.: Long-term real-time measurements of aerosol particle composition in Beijing, China: seasonal variations, meteorological effects, and source analysis, Atmospheric Chemistry and Physics, 15, 10149-10165, 10.5194/acp-15-10149-2015, 2015.

带格式的： 删除线

Sun, Y. L., Du, W., Fu, P., Wang, Q., Li, J., Ge, X., Zhang, Q., Zhu, C., Ren, L., Xu, W., Zhao, J., Han, T., Worsnop, D. R., and Wang, Z.: Primary and secondary aerosols in Beijing in winter: sources, variations and process, Atmos. Chem. Phys., 16,8309-8329, doi: 10.5194/acp-16-8309-2016, 2016a.

Sun, Y. L., Wang, Z., Wild, O., Xu, W., Chen, C., Fu, P., Du, W., Zhou, L., Zhang, Q., Han, T., Wang, Q., Pan, X., Zheng, H., Li, J., Guo, X., Liu, J., and Worsnop, D. R.: "APEC Blue": Secondary Aerosol Reductions from Emission Controls in Beijing, Sci. Rep., 6, 20668, 10.1038/srep20668, 2016b.

Tuccella, P., Curci, G., Grell, G. A., Visconti, G., Crumeyrolle, S., Schwarzenboeck, A., and Mensah, A. A.: A new chemistry option in WRF-Chem v. 3.4 for the simulation of direct and indirect aerosol effects using VBS: evaluation against IMPACT EUCAARI data, Geoscientific Model Development, 8, 2749-2776, 10.5194/gmd-8-2749-2015, 2015.

van der Werf, G. R., Randerson, J. T., Giglo, L., Collatz, G. J., Mu, M., Kasibhatla, P. S., Morton, D. C., DeFries, R. S., Jin, Y., and van Leeuwen, T. T.: Global fire emissions and the contribution of deforestation, savanna, forest, agricultural, and peat fires (1997-2009). Atmos. Chem. Phys., 10, 11707-11753, 10.5194/acp-10-11707-2010, 2010.

Walcek, C. J., and Taylor, G. R.: A theoretical method for computing vertical distributions of acidity and sulfate production within cumulus clouds. Journal of the Atmospheric Sciences, 43(4), 339-355, 10.1175/1520-0469(1986)043<0339:ATMFCV>2.0.CO;2, 1986.

Wang, C.: Impact of anthropogenic absorbing aerosols on clouds and precipitation: A review of recent progresses, Atmospheric Research, 122, 237-249, 10.1016/j.atmosres.2012.11.005, 2013a.

Wang, H., He, Q., Chen, Y., and Kang, Y.: Analysis of Characteristics of Black Carbon Concentration in Shanghai from 2008 to 2012, Environmental Science, 35(4), 1215-1222, 2014a.

Wang, H., Xie, S.-P., and Liu, Q.: Comparison of Climate Response to Anthropogenic Aerosol versus Greenhouse Gas Forcing: Distinct Patterns, Journal of Climate, 29, 5175-5188, 10.1175/jcli-d-16-0106.1, 2016a.

Wang, H. L., Qiao, L. P., Lou, S. R., Zhou, M., Ding, A. J., Huang, H. Y., Chen, J. M., Wang, Q., Tao, S. K., Chen, C. H., Li, L., and Huang, C.: Chemical composition of PM2.5 and meteorological impact among three years in urban Shanghai, China, Journal of Cleaner Production, 112, 1302-1311, 10.1016/j.jclepro.2015.04.099, 2016b.

Wang, J., Wang, X., Zhang, H., Lu, F., and Hou, P.: Comparison of PM2.5 concentration and elemental compositions in two typical sites in Beijing urban area, Acta Scientiae Circumstantiae, 32(1), 74-80, 2012a.

Wang, K., Zhang, Y., Nenes, A., and Fountoukis, C.: Implementation of dust emission and chemistry into the Community Multiscale Air Quality modeling system and initial application to an Asian dust storm episode, Atmospheric Chemistry and Physics, 12, 10209-10237, 2012b.

Wang, P., Cao, J.-j., Shen, Z.-x., Han, Y.-m., Lee, S.-c., Huang, Y., Zhu, C.-s., Wang, Q.-y., Xu, H.-m., and Huang, R.-j.: Spatial and seasonal variations of PM 2.5 mass and species during 2010 in Xi'an, China, Science of The Total Environment, 508, 477-487, 10.1016/j.scitotenv.2014.11.007, 2015.

Wang, P., Wang, H., Wang, Y. Q., Zhang, X. Y., Gong, S. L., Xue, M., Zhou, C. H., Liu, H. L., An, X. Q., Niu, T., and Cheng, Y. L.: Inverse modeling of black carbon emissions over China using ensemble data assimilation, Atmospheric Chemistry and Physics, 16, 989-1002, 10.5194/acp-16-989-2016, 2016c.

Wang, X., Liao, J.B., Zhang, J., Shen, C., Chen, W.H., Xia, B.C. and Wang, T.J.: A Numeric Study of Regional Climate Change Induced by Urban Expansion in the Pearl River Delta, China, J. Appl. Meteor. Climatol., 53, 346-362, doi: 10.1175/JAMC-D-13-054.1, 2014b.

Wang, Y., Zhang, Q., He, K., Zhang, Q., and Chai, L.: Sulfate-nitrate-ammonium aerosols over China: response to 2000-2015 emission changes of sulfate dioxide, nitrogen oxides, and ammonia, Atmos. Chem. Phys., 13, 2635-2652, doi: 10.5194/acp-13-2635-2013, 2013b.

Wang, Y. S., Yao, L., Wang, L. L., Liu, Z. R., Ji, D. S., Tang, G. Q., Zhang, J. K., Sun, Y., Hu, B., and Xin, J. Y.: Mechanism for the formation of the January 2013 heavy haze pollution episode over central and eastern China, Sci. China Earth Sci., 57, 14–25, doi:10.1007/s11430-013-4773-4, 2014c.

Wang, Z. F., Ueda, H., and Huang, M. Y.: A deflation module for use in modeling long-range transport of yellow sand over East Asia, J. Geophys. Res.-Atmos., 105, 26947–26959, 2000.

Wang, Z., Maeda, T., Hayashi, M., Hsiao, L. F., and Liu, K. Y.: A nested air quality prediction modeling system for urban and regional scales: Application for high-ozone episode in Taiwan. Water, Air, & Soil Pollution, 130(1), 391-396, 10.1023/A:1013833217916, 2001.

带格式的：删除线

带格式的：删除线

Wang, Z. F., Akimoto, H., and Uno, I.: Neutralization of soil aerosol and its impact on the distribution of acid rain over east Asia: Observations and model results, J. Geophys. Res.-Atmos., 107, 4389, doi:10.1029/2001JD001040, 2002.

Wang, Z., Xie, F., Sakurai, T., Ueda, H., Han, Z., Carmichael, G., Streets, D., Engardt, M., Holloway, T., and Hayami, H.: MICS-Asia II: Model inter-comparison and evaluation of acid deposition, Atmospheric Environment, 42, 3528-3542, 10.1016/j.atmosenv.2007.12.071, 2008.

~~Wang, Z., Maeda, T., Hayashi, M., Hsiao, L. F., and Liu, K. Y.: A nested air quality prediction modeling system for urban and regional scales: Application for high-ozone episode in Taiwan. Water, Air, & Soil Pollution, 130(1), 391-396, 10.1023/A:1013833217916, 2001.~~

Wang, Z., Li, J., Wang, Z., Yang, W., Tang, X., Ge, B., Yan, P., Zhu, L., Chen, X., Chen, H., Wand, W., Li, J., Liu, B., Wang, X., Wand, W., Zhao, Y., Lu, N., and Su, D.: Modeling study of regional severe hazes over mid-eastern China in January 2013 and its implications on pollution prevention and control, Science China Earth Sciences, 57, 3-13, 10.1007/s11430-013-4793-0, 2013c.

Wesely, M. L.: Parameterization of surface resistances to gaseous dry deposition in regional-scale numerical models. Atmospheric Environment (1967), 23(6), 1293-1304, 10.1016/0004-6981(89)90153-4, 1989.

Xie, H., Wu, D., Zhang, G., Li, M., Fang, H., Chen, Q., Li, X., and Zhai, G.: Characteristic analysis of fine particles PM2.5 in the ambient air in Dongguan, Air Pollution Control, doi:10.13205/j.hjgc.201406016, 2013.

Xu, Y.: The level of haze and PM2.5 in Zhengzhou and heat power plants' atmospheric environmental impact assessment, M.S. thesis, Zhengzhou University, China, 77 pp., 2012.

Yamaji, K., Ohara, T., Uno, I., Kurokawa, J.-i., Pochanart, P., and Akimoto, H.: Future prediction of surface ozone over east Asia using Models-3 Community Multiscale Air Quality Modeling System and Regional Emission Inventory in Asia, Journal of Geophysical Research, 113, 10.1029/2007jd008663, 2008.

Yan, Z.-W., Wang, J., Xia, J.-J., and Feng, J.-M.: Review of recent studies of the climatic effects of urbanization in China, Advances in Climate Change Research, 7, 154-168, 10.1016/j.accre.2016.09.003, 2016.

Yang, J.H., Kang, S.C., Ji, Z.M., and Chen, D.L.: Modeling the origin of anthropogenic black carbon and its climatic effect over the Tibetan Plateau and surrounding regions, J. Geophys. Res.-Atmos., 123, 671-692, 10.4209/aaqr.2017.05.0156, 2018.

Yang, Y., Russell, L. M., Lou, S., Lamjiri, M. A., Liu, Y., Singh, B., and Ghan, S. J.: Changes in Sea Salt Emissions Enhance ENSO Variability, J. Climate, 29, 8575–8588, 10.1175/JCLI-D-16-0237.1, 2016.

Yao, L., Yang, L., Yuan, Q., Yan, C., Dong, C., Meng, C., Sui, X., Yang, F., Lu, Y., and Wang, W.: Sources apportionment of PM2.5 in a background site in the North China Plain, The Science of the total environment, 541, 590-598, 10.1016/j.scitotenv.2015.09.123, 2016.

Yarwood, G., Rao, S., Yocke, M., and Whitten, G. Z.: Updates to the Carbon Bond Chemical Mechanism: CB05. Final Report to the US EPA, RT-0400675, 2005.

Yu, Y., Hu, B., and Wang, Y.: Changing characteristics of the main air pollutants of the Dongling Mountain in Beijing, Environmental Science, 34(7), doi:,10.13227/j.hjkx.2013.07.021, 2013.

Yue, X., Wang, H. J., Liao, H., and Fan, K.: Simulation of dust aerosol radiative feedback using the GMOD: 2. Dust climate interactions, J. Geophys. Res.-Atmos., 115, D10202, doi:10.1029/2008JD010995, 2010.

Yue, X., Unger, N., Harper, K., Xia, X., Liao, H., Zhu, T., Xiao, J., Feng, Z., and Li, J.: Ozone and haze pollution weakens net primary productivity in China, Atmospheric Chemistry and Physics, 17, 6073-6089, 10.5194/acp-17-6073-2017, 2017.

Zaveri, R. A., and Peters, L. K.: A new lumped structure photochemical mechanism for large-scale applications, Journal of Geophysical Research: Atmospheres, 104, 30387-30415, 10.1029/1999jd900876, 1999.

Zhang, B., Wang, Y., and Hao, J.: Simulating aerosol–radiation–cloud feedbacks on meteorology and air quality over eastern China under severe haze condition in winter, Atmospheric Chemistry and Physics, 15, 2387-2404, 10.5194/acp-15-2387-2015, 2015a.

Zhang, L., Gong, S., Padro, J., and Barrie, L.:. A size-segregated particle dry deposition scheme for an atmospheric aerosol module. Atmospheric Environment, 35(3), 549-560, 10.1016/S1352-2310(00)00326-5, 2001.

~~Zhang, L., Chen, Y., Zhao Y., Henze, D., Zhu, L., Song, Y., Paulot, F., Liu, X., Pan, Y., Lin, Y., and Huang B.,: Agricultural ammonia emissions in China: Reconciling bottom-up and top-down estimates, Atmospheric Chemistry and Physics, 18,~~

339-355, 10.5194/acp-18-339-2018, 2018.

Zhang, M.: Numerical study of boundary layer ozone transport and photochemical production in east Asia in the wintertime, Geophysical Research Letters, 29, 10.1029/2001gl014368, 2002.

Zhang, M., Uno, I., Zhang, R., Han, Z., Wang, Z., and Pu, Y.: Evaluation of the Models-3 Community Multi-scale Air Quality (CMAQ) modeling system with observations obtained during the TRACE-P experiment: Comparison of ozone and its related species, Atmospheric Environment, 40, 4874-4882, 10.1016/j.atmosenv.2005.06.063, 2006.

Zhang, M., Han, Z., and Zhu, L.: Simulation of atmospheric aerosols in East Asia using modeling system RAMS-CMAQ: Model evaluation, China Particuology, 5, 321-327, 10.1016/j.cpart.2007.07.002, 2007.

Zhang, R., Sun, X. S., Shi, A. J., Huang, Y. H., Yan, J., Nie, T., Yan, X., and Li, X.: Secondary inorganic aerosols formation during haze episodes at an urban site in Beijing, China, Atmos. Environ., 177, 275–282, 10.1016/j.atmosenv.2017.12.031, 2018.

Zhang, X.: Study on long-term variation of Black Carbon aerosol over Peking and Hebei province during 2006-2012, M.S. thesis, Yunnan University, China, 116 pp., 2015b.

Zhao, C., Liu, X., Leung, L. R., Johnson, B., McFarlane, S. A., Gustafson Jr., W. I., Fast, J. D., and Easter, R.: The spatial distribution of mineral dust and its shortwave radiative forcing over North Africa: modeling sensitivities to dust emissions and aerosol size treatments, Atmos. Chem. Phys., 10, 8821-8838, https://doi.org/10.5194/acp-10-8821-2010, 2010.

Zhao, P. S., Dong, F., He, D., Zhao, X. J., Zhang, X. L., Zhang, W. Z., Yao, Q., and Liu, H. Y.: Characteristics of concentrations and chemical compositions for $PM_{3.5}$ in the region of Beijing, Tianjin, and Hebei, China, Atmospheric Chemistry and Physics, 13, 4631-4644, 10.5194/acp-13-4631-2012, 2013.

Zhao, X. J., Zhao, P. S., Xu, J., Meng,, W., Pu, W. W., Dong, F., He, D., and Shi, Q. F.: Analysis of a winter regional haze event and its formation mechanism in the North China Plain, Atmos. Chem. Phys., 13, 5685-5696, https://doi.org/10.5194/acp-13-5685-2013, 2013.

Zheng, B., Zhang, Q., Zhang, Y., He, K. B., Wang, K., Zheng, G. J., Duan, F. K., Ma, Y. L., and Kimoto, T.: Heterogeneous chemistry: a mechanism missing in current models to explain secondary inorganic aerosol formation during the January 2013 haze episode in North China, Atmos. Chem. Phys., 15, 2031–2049, https://doi.org/10.5194/acp-15-2031-2015, 2015.

Zhu, J., Liao, H., Mao, Y., Yang, Y., and Jiang, H.: Interannual variation, decadal trend, and future change in ozone outflow from East Asia, Atmospheric Chemistry and Physics, 17, 3729-3747, 10.5194/acp-17-3729-2017, 2017.

带格式的：删除线

Table 1. Basic configurations of participant models in MICS−Asia Phase III

Model Index	Model Version	Vertical Layers (1st height)	Horizontal advection	Vertical diffusion	Gas phase chemistry	Aerosol chemistry	Dry deposition	Wet scavenging	Dust scheme	Sea-salt scheme	Meteorology	Boundary Condition	Online/Offline	References
M1	WRFCMAQ5.0.2	40 (57 m)	Yamo	ACM2	SAPRC99	Aero6 ISORROPIA(v2)	Wesely	Henry's law	NA	Gong, Kelly	Standard[a]	GEOS-Chem	Online access	Fu et al., (2008)
M2	WRFCMAQ5.0.2	40 (57 m)	Yamo	ACM2	SAPRC99	Aero6 ISORROPIA(v2)	Wesely	Henry's law	NA	Gong, Kelly	Standard[a]	Default	Online access	Wang et al., (2014b)
M3	WRFCMAQ5.0.1	40 (57 m)	Yamo	ACM2	CB05	Aero6 ISORROPIA(v2)	Wesely	Henry's law	NA	Gong, Kelly	Standard[a]	GEOS-Chem	Online access	Lam et al., (2011)
M4	WRFCMAQ4.7.1	40 (57 m)	Yamo	ACM2	SAPRC99	Aero5 ISORROPIA(v1.7)	Wesely	Henry's law	NA	Gong, Kelly	Standard[a]	CHASER	Offline	Itahashi et al., (2014)
M5	WRFCMAQ4.7.1	40 (57 m)	Yamo	ACM2	SAPRC99	Aero5 ISORROPIA(v1.7)	M3DRY	Henry's law	NA	Gong, Kelly	Standard[a]	CHASER	Offline	Yamaji et al., (2008)
M6	WRFCMAQ4.7.1	40 (57 m)	Yamo	ACM2	SAPRC99	Aero5 ISORROPIA(v1.7)	M3DRY	Henry's law	NA	Gong, Kelly	Standard[a]	CHASER	Offline	Nagashima et al., (2017)
M7	WRFChem3.7.1	40 (29 m)	5th order Monotonic	−	RACM−ESRL with KPP	MADE/SORGAM	Wesely	Henry's law	NA	NA	WRF/NCEP	Default	Online integrated	Park et al., (2018)
M8	WRFChem3.6.1	40 (57 m)	5th order Monotonic	MYJ	RACM with KPP	MADE/VBS	Wesely	Henry's law	NA	NA	WRF/NCEP	CHASER	Online integrated	Lin et al., (2014)
M9	WRFChem3.6	40 (16 m)	5th order Monotonic	YSU	RADM2	MADE/SORGAM	Wesely	Henry's law	Shao (2004)	Gong	WRF/NCEP	CHASER	Online integrated	Chen et al., (2017)
M10	NU-WRF v7lis7-3.5.1-p3	60 (44 m)	5th order Monotonic	YSU	RADM2	GOCART	Wesely	Grell	GOCART	Gong	WRF/MERRA2	MOZART+GOCART	Online integrated	Tao et al., (2013)
M11	NAQPMS	20 (50 m)	Walcek and Aleksic (1998)	K−theory	CBMZ	Aero5 ISORROPIA(v1.7)	Wesely	Henry's law	Wang (2000)	Gong	Standard[a]	CHASER	Online access	Wang et al., (2008)
M12	NHMChem	40 (54 m)	Walcek and Aleksic (1998)	FTCS	SAPRC99	ISORROPIA(v2)	Kajino	Kajino	Han (2004)	Clarke	JMA NHM	CHASER	Offline	Kajino et al., (2012)
M13	GEOS-Chem9.1.3	47 (60 m)	ppm	Lin and McElroy (2010)	Nox-Ox-HC-Br mechanism	ISORROPIA(v2)	Wesely	Liu	GOCART	Gong, Jaegle	Geos-5	NA	Offline	Zhu et al., (2017)
M14	RAMSCMAQ4.6	15 (100 m)	Yamo	ACM2	SAPRC99	Aero5 ISORROPIA(v1.7)	Wesely	Henry's law	Han (2004)	Gong	RAMS/NCEP	CHASER	Offline	Zhang et al., (2002)

[a]'Standard meteorology' represents the reference meteorological field provided by MICS−Asia III project.

带格式的: 删除线

M8	WRFChem3.6.1	RACM	MADE/VBS	Wesely	Henry's law	Standard[a]	CHASER	Online integrated	Lin et al., (2014)
M9	WRFChem3.6	RADM2	MADE/SORGAM	Wesely	Easter	Standard[a]	GEOS-Chem	Online integrated	Chen et al., (2017)
M10	WRFChem3.5.1	RADM2	GOCART	Wesely	Henry's law	WRF/MERRA2	MOZART/GOCART[b]	Online integrated	—
M11	NAQPMS	CBMZ	Aero5 ISORROPIA(v1.7)	Wesely	Henry's law	Standard[a]	CHASER	Online access	Wang et al., (2008)
M12	NHMChem	SAPRC99	ISORROPIA(v2)/MADMS	Kajino, Zhang	Kajino, Pleim and Chang	JMA NHM	CHASER	Offline	Kajino et al., (2012)
M13	GEOS-Chem9.1.3	Bey	Park, Pye	Wesely	Liu	Geos-5	GEOS-Chem	Offline	Zhu et al., (2017)
M14	RAMSCMAQ4.6	SAPRC99	Aero5 ISORROPIA(v1.7)	Wesely	Henry's law	RAMS/NCEP	GEOS-Chem	Offline	Zhang et al., (2002)

[a]'Standard' represents the reference meteorological field provided by MICS-Asia III project.

[b]Boundary conditions used in M10 are taken from MOZART and GOCART (Chin et al., 2002; Horowitz et al.,2003), which provides results for gaseous pollutants and aerosols, respectively.

SAPRC99: Carter (2000). CB05: Yarwood (2005). Bey: Bey et al., (2001). CBMZ: Zaveri and Peters (1999). RACM: Stockwell et al., (1997). RADM2: Stockwell et al., (1990). Aero5 ISORROPIA (v1.7): Nenes et al., (1998). Aero6 ISORROPIA (v2): Fountoukis and Nenes (2007). Park: Park et al., (2004). Pye: Pye et al., (2009). MADE-VBS: Tuccella et al., (2015). MADE: Ackermann et al., (1998). M3DRY: Pleim et al., (2001). Wesely: Wesely (1989). Kajino: Kajino et al., (2012). Zhang: Zhang et al., (2001). Liu: Liu et al., (2001). Pleim and Chang: Pleim and Chang (1992). Easter: Easter et al., (2004). Walcek and Taylor: Walcek and Taylor (1986).

5

Table 2. Statistics of BC, SO_4^{2-}, NO_3^-, NH_4^+, PM2.5, PM10, and AOD. Best results are set to be bold with underline. Monthly mean observations and the number of stations (nstd) are listed with italic. In this table, monthly measurements except BC are taken from EANET, CNEMC, and AERONET; the monthly BC concentrations are collected from published literatures.

Species	Statistics	M1	M2	M4	M5	M6	M7	M8	M9	M11	M12	M13	M14	EM
BC	R	0.70	0.73	0.71	0.65	0.70	0.73	**0.80**	−	0.69	0.68	0.75	0.72	0.73
(5.0 µg m⁻³)	NMB(%)	**1.0**	12.7	−24.7	−54.9	−17.8	−11.7	−34.2	−	−17.5	−2.2	−26.8	−11.6	−17.0
(nstd=5)	RMSE	4.10	4.30	2.95	4.06	2.99	2.69	2.84	−	2.91	3.52	2.80	**2.64**	2.77
SO_4^{2-}	R	0.69	0.71	0.64	0.58	0.66	0.48	0.53	0.65	0.55	0.50	**0.76**	0.46	0.69
(3.8 µg m⁻³)	NMB(%)	−23.1	−13.0	−31.0	−26.4	−26.9	−67.7	**−1.6**	−67.0	−34.5	23.2	−31.9	69.3	−19.1
(nstd=31)	RMSE	3.21	**3.00**	3.46	3.57	3.35	4.64	3.62	4.45	3.78	4.01	3.24	5.51	3.22
NO_3^-	R	0.55	0.51	0.62	**0.65**	0.58	0.45	0.29	0.64	0.59	0.60	0.43	0.58	**0.65**
(1.7 µg m⁻³)	NMB(%)	9.0	−7.2	−42.7	**−1.7**	−11.8	−81.2	−80.6	125.7	46.5	54.0	22.7	35.4	4.9
(nstd=31)	RMSE	2.70	2.71	2.48	2.29	2.46	3.37	3.18	4.37	2.89	2.80	2.96	2.62	**2.27**
NH_4^+	R	0.67	0.64	0.68	0.66	0.69	0.55	0.34	**0.75**	0.66	0.62	0.64	0.68	0.71
(1.1 µg m⁻³)	NMB(%)	23.2	33.7	−10.6	**7.4**	14.6	−93.5	−34.2	45.3	35.0	49.9	34.9	56.3	14.0
(nstd=31)	RMSE	1.24	1.42	1.15	1.21	1.16	1.83	1.53	1.26	1.27	1.54	1.29	1.47	**1.11**
PM2.5	R	0.80	0.78	0.80	0.71	0.80	0.80	0.77	0.82	0.80	0.78	0.75	0.81	**0.83**
(51.4µg m⁻³)	NMB(%)	10.0	13.6	**−1.3**	−25.3	−5.8	−5.7	−15.3	26.2	5.2	31.4	−26.5	46.0	4.4
(nstd=14)	RMSE	27.56	34.88	23.03	28.00	21.80	23.54	24.83	28.52	22.06	34.87	27.10	35.85	**21.23**
PM10	R	0.75	0.74	0.74	0.65	0.75	0.70	0.70	0.66	0.78	**0.82**	−	0.63	0.78
(80.7µg m⁻³)	NMB(%)	−40.7	−38.7	−35.7	−55.7	−46.6	−43.7	−43.4	−16.9	−25.4	−18.8	−	**7.1**	−32.6
(nstd=51)	RMSE	51.31	50.88	49.10	64.55	55.31	55.07	55.11	50.67	42.91	**37.28**	−	47.26	45.81
AOD	R	0.64	0.55	0.56	−	−	0.54	−	0.60	0.69	0.66	**0.71**	0.57	0.68
(0.2)	NMB(%)	**−2.0**	63.7	−28.5	−	−	−21.8	−	11.1	73.1	−6.2	47.1	36.7	18.7
(nstd=38)	RMSE	0.15	0.22	0.16	−	−	0.18	−	0.19	0.22	**0.13**	0.25	0.22	0.14

5

Table 3. The coefficient of variation (CV, standard deviation divided by the mean) of simulated coarse particles (subtract PM$_{2.5}$ from PM$_{10}$) in each defined sub-region.

CV	Normal[a]	Without_SS_Dust[b]	Without_Dust[c]	With_SS_Dust[d]
Region_1	1.3	0.29	0.37	0.97
Region_2	1.39	0.3	0.65	1.04
Region_3	1.43	0.33	0.48	1.27
Region_4	1.21	0.19	0.59	0.95
Region_5	0.85	0.09	0.65	0.88

[a]"Normal" means that simulation results from all participant models are considered.
[b]"Without_SS_Dust" means that the impacts of sea salt and dust aerosols are not considered, i.e., only simulation results from M7 and M8 are used to calculate the CV.
[c]"Without_Dust" means that the impacts of dust aerosols are not considered, i.e., only simulation results from M1, M2, M4, M5, and M6 are used to calculate the CV.
[d]"With_SS_Dust" means that both the impacts of sea salt and dust aerosols are considered, i.e., simulation results from M9, M11, M12, and M14 are used to calculate the CV.

Table 2. Aerosol species simulated by each participating model

Model Index	BC	OC	SO$_4^{2-}$	NO$_3^-$	NH$_4^+$	PM$_{2.5}$	PM$_{10}$	AOD
M1	Y	Y	Y	Y	Y	Y	Y	Y
M2	Y	Y	Y	Y	Y	Y	Y	Y
M3	Y	Y	Y	Y	Y	Y	Y	Y
M4	Y	Y	Y	Y	Y	Y	Y	Y
M5	Y	Y	Y	Y	Y	Y	Y	—
M6	Y	Y	Y	Y	Y	Y	Y	—
M7	Y	—	Y	Y	Y	Y	Y	Y
M8	Y	Y	Y	Y	Y	Y	Y	—
M9	—	—	Y	Y	Y	Y	Y	Y
M10	—	—	—	—	—	—	—	—
M11	Y	Y	Y	Y	Y	Y	Y	Y
M12	Y	Y	Y	Y	Y	Y	Y	Y
M13	Y	Y	Y	Y	Y	Y	—	Y
M14	Y	Y	Y	Y	Y	Y	Y	Y

"Y" means aerosol species is analyzed in this manuscript.

Table 3. Performance statistics of BC, SO_4^{2-}, NO_3^-, NH_4^+, $PM_{2.5}$, PM_{10} and AOD. Best results are set to be bold with underline. The mean observation of each species and the number of observations are also given with italic. In this table, observed monthly mean values from EANET, CNEMC and AERONET are used (except BC, the monthly BC concentrations are collected from published documents).

Species	Statistics	M1	M2	M4	M5	M6	M7	M8	M9	M11	M12	M13	M14	EM
BC *(5.0 μg m⁻³)* *(nstd=5)*	R	0.70	0.73	0.71	0.65	0.70	0.73	**0.80**	–	0.69	0.68	0.75	0.72	0.73
	NMB(%)	**1.0**	12.7	−24.7	−54.9	−17.8	−11.7	−34.2	–	−17.5	−2.2	−26.8	−11.6	−17.0
	RMSE	4.10	4.30	2.95	4.06	2.99	2.69	2.84	–	2.91	3.52	2.80	**2.64**	2.77
SO_4^{2-} *(3.8 μg m⁻³)* *(nstd=31)*	R	0.69	0.71	0.64	0.58	0.66	0.48	0.53	0.65	0.55	0.50	**0.76**	0.46	0.69
	NMB(%)	−23.1	−13.0	−31.0	−26.4	−26.9	−67.7	**−1.6**	−67.0	−34.5	23.2	−31.9	69.3	−19.1
	RMSE	3.21	**3.00**	3.46	3.57	3.35	4.64	3.62	4.45	3.78	4.01	3.24	5.51	3.22
NO_3^- *(1.7 μg m⁻³)* *(nstd=31)*	R	0.55	0.51	0.62	**0.65**	0.58	0.45	0.29	0.64	0.59	0.60	0.43	0.58	**0.65**
	NMB(%)	9.0	−7.2	−42.7	**−1.7**	−11.8	−81.2	−80.6	125.7	46.5	54.0	22.7	35.4	4.9
	RMSE	2.70	2.71	2.48	2.29	2.46	3.37	3.18	4.37	2.89	2.80	2.96	2.62	**2.27**
NH_4^+ *(1.1 μg m⁻³)* *(nstd=31)*	R	0.67	0.64	0.68	0.66	0.69	0.55	0.34	**0.75**	0.66	0.62	0.64	0.68	0.71
	NMB(%)	23.2	33.7	−10.6	**7.4**	14.6	−93.5	−34.2	45.3	35.0	49.9	34.9	56.3	14.0
	RMSE	1.24	1.42	1.15	1.21	1.16	1.83	1.53	1.26	1.27	1.54	1.29	1.47	**1.11**
$PM_{2.5}$ *(51.4 μg m⁻³)* *(nstd=14)*	R	0.80	0.78	0.80	0.71	0.80	0.80	0.77	0.82	0.80	0.78	0.75	0.81	**0.83**
	NMB(%)	10.0	13.6	**−1.3**	−25.3	−5.8	−5.7	−15.3	26.2	5.2	31.4	−26.5	46.0	4.4
	RMSE	27.56	34.88	23.03	28.00	21.80	23.54	24.83	28.52	22.06	34.87	27.10	35.85	**21.23**
PM_{10} *(80.7 μg m⁻³)* *(nstd=51)*	R	0.75	0.74	0.74	0.65	0.75	0.70	0.70	0.66	0.78	**0.82**	–	0.63	0.78
	NMB(%)	−40.7	−38.7	−35.7	−55.7	−46.6	−43.7	−43.4	−16.9	−25.4	−18.8	–	**7.1**	−32.6
	RMSE	51.31	50.88	49.10	64.55	55.31	55.07	55.11	50.67	42.91	**37.28**	–	47.26	45.81
AOD *(0.2)* *(nstd=38)*	R	0.64	0.55	0.56	–	–	0.54	–	0.60	0.69	0.66	**0.71**	0.57	0.68
	NMB(%)	**−2.0**	63.7	−28.5	–	–	−21.8	–	11.1	73.1	−6.2	47.1	36.7	18.7
	RMSE	0.15	0.22	0.16	–	–	0.18	–	0.19	0.22	**0.13**	0.25	0.22	0.14

5

Figure 1. Simulation domain for each participant model. The final analyzed region is also shown.

Figure 1: The merged emission inventories of MIX emission, MEGAN biogenic emission, GFED biomass burning emission, air and ship emission, and volcanic emission for SO_2, NO_x and $PM_{2.5}$ in 2010. The unit for gas is Mmol/month/grid, and the unit for aerosol is Mg/month/grid.
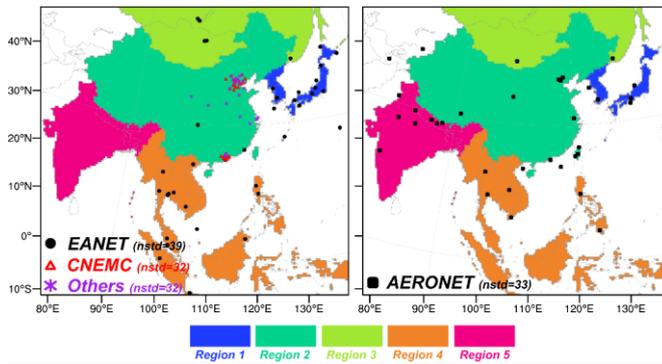
Figure 2. The geographical locations of observation stations: EANET (shown in black circles, the number of stations is 39), CNEMC (shown in red triangles, the number of stations is 32), Others (observations collected from published literatures, shown in purple stars, the number of stations is 32), and AERONET (shown in black boxs, the number of stations is 33). Five defined sub-regions (Region_1 to Region_5) are also shown.
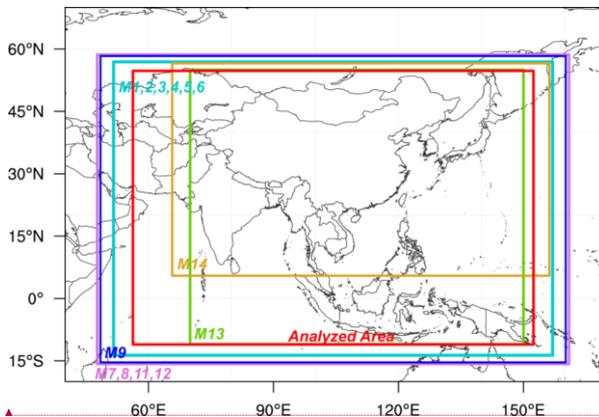
~~Figure 2: Simulation domain for each participating model and the final analyzed area used in this manuscript.~~
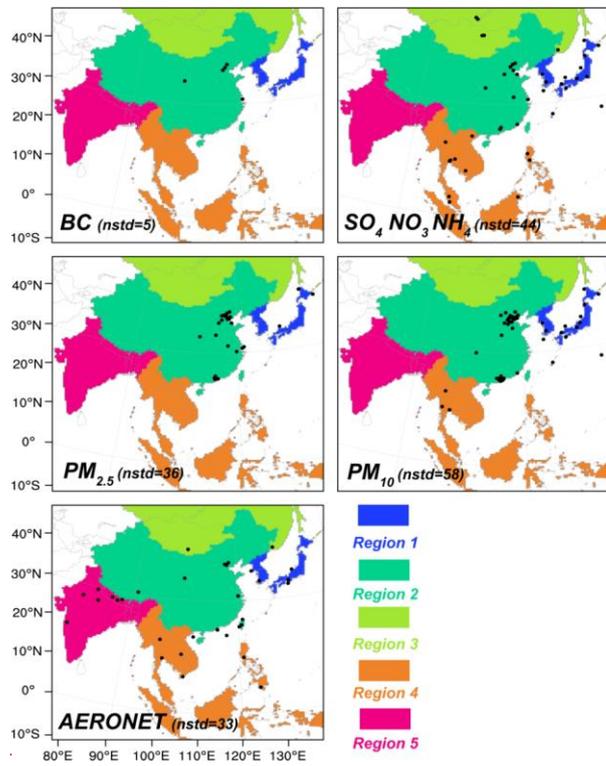
Figure 3: Spatial distribution of observation sites for each species. Five designed regions are also shown in each panel.

5

Figure 3. Comparison of observed and simulated concentrations of (a) BC, (b) SO_4^{2-}, (c) NO_3^-, (d) NH_4^+, (e) PM2.5, and (f) PM10. In each panel, the grey bars represent observations, the colored dots represent simulations, and the black solid lines represent the MMEM (multi–model ensemble mean). The x axis presents the monitoring sites (the information of these sites is listed in Table S1). Normalized mean biases (NMBs) between observations and MMEM in each defined sub-region (shown in black) and the entire analyzed region (shown in red) are also shown. In this figure, the annual mean observations are taken from EANET, CNEMC, and published literatures.

Figure 4: Comparison of observed and simulated concentrations of (a) BC, (b) SO_4^{2-}, (c) NO_3^-, (d) NH_4^+, (e) PM2.5 and (f) PM10. In each panel, the gray bars show observation data, the colored dots represent simulation results from participating models, and the black solid line is the ensemble mean. The numbers on x-axis represent the monitoring sites, and the information of these sites is listed in Table S1. Normalized mean biases (NMBs) between observations and ensemble means in each defined region (with black color) and the entire analyzed area (with red color) are also shown. In this picture, observed annual mean values from EANET, CNEMC and published documents are used.
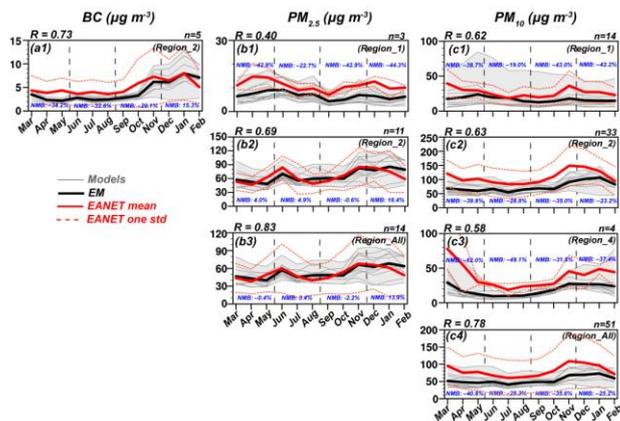
Figure 4. Time series of the monthly observed and simulated aerosol compositions: (a1) BC, (b1)-(b3) PM$_{2.5}$, (c1)-(c4) PM$_{10}$. The thin grey lines represent simulation results, and the grey shaded areas indicate the spread. The thick black lines are the ensemble mean. The red solid lines the mean observations, and the dashed red lines represent one standard deviation. Correlation coefficients (Rs, shown in black) for the the whole year and normalized mean biases (NMBs, shown in blue) for each season between observations and MMEM are shown in each panel. The number of monitoring sites used to calculate the statistics in each sub-region is also listed above each panel. In this figure, the monthly observations except BC are taken from EANET and CNEMC; the monthly BC concentrations are collected from published literatures.

Figure 5: Observed and simulated seasonal cycle of aerosol species. (a1) BC, (b1)-(b3) PM$_{2.5}$, (c1)-(c4) PM$_{10}$. Simulations and observations are grouped into five defined regions as illustrated in Figure 3, with each model sampled at the corresponding monitoring sites in each region before averaging together. Individual models are represented by the thin grey lines, with the grey shaded area indicating their spread. The thick black line is the ensemble mean. The red solid line is the observational mean and the dashed red lines mean one standard deviation for each group of stations. The correlations (Rs, with black color) and normalized mean biases (NMBs, with blue color) for ensemble-means versus observations during each season (spring: from March to May; summer: from June to August; autumn: from September to November; winter: January, February and December) and the entire year are shown in each panel. Also shown is the number of monitoring sites participating in calculating statistics in each region. In this picture, observed monthly mean values from EANET and CNEMC are used (except BC, the monthly BC concentrations are collected from published documents).
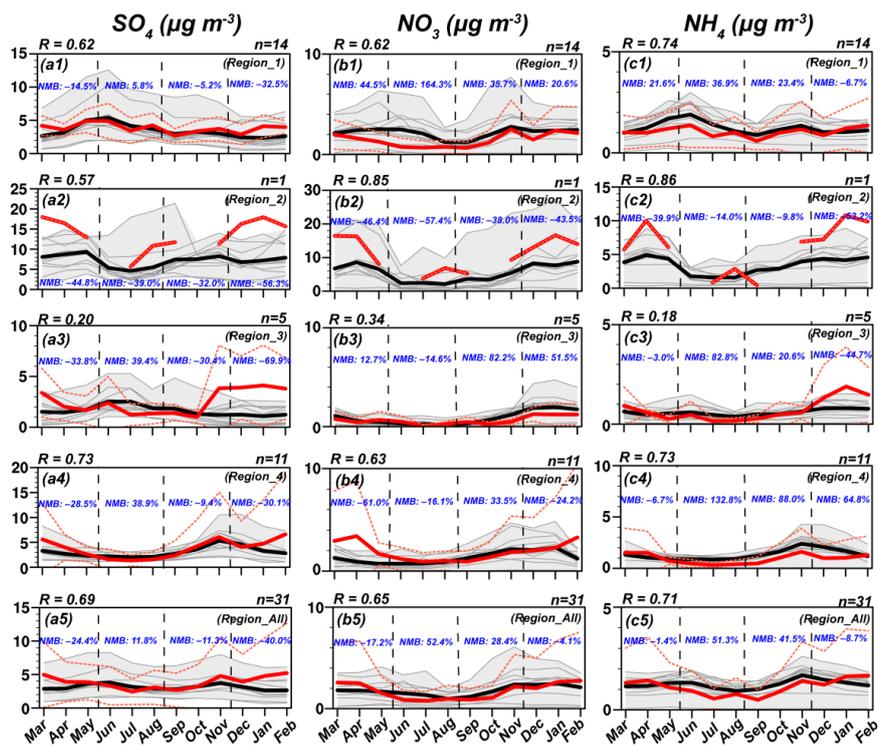
Figure 5. The same as Figure 4, but for SO_4^{2-} **(a1-a5),** NO_3^- **(b1-b5), and** NH_4^+ **(c1-c5). In this figure, the monthly measurements are taken from EANET.**

Figure 6: Same as Figure 5, but for SO_4^{2-} (a1-a5), NO_3^- (b1-b5) and NH_4^+ (c1-c5). In this picture, only monthly EANET observations are used.
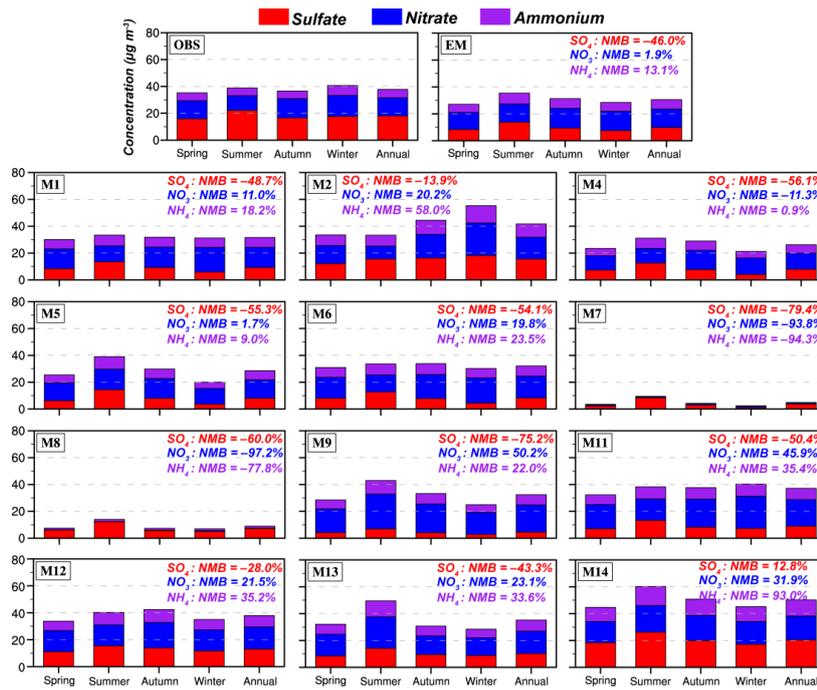
Figure 7: Observed and simulated seasonal mean concentrations of SO_4^{2-}, NO_3^- and NH_4^+ in Region_2. Normalized mean biases (NMBs) of SO_4^{2-} (with red color), NO_3^- (with blue color) and NH_4^+ (with purple color) for each participating model and the ensemble model are also shown. In this picture, seasonal observations are collected from published documents.
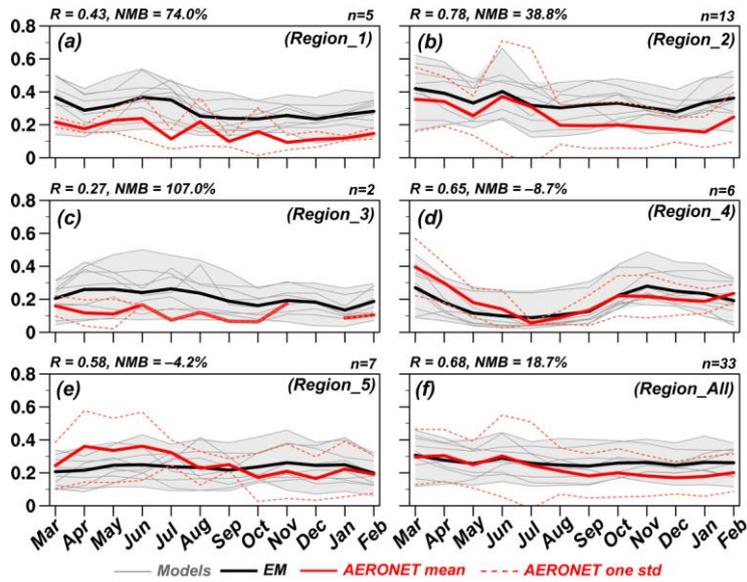
Figure 6. Similar as Figure 4, but for seasonal cycles of aerosol optical depth (AOD) at 550 nm. In this figure, the monthly measurements are taken from AERONET.

Figure 8: Similar as Figure 5, but for comparison of seasonal cycle of aerosol optical depth (AOD) at 550 nm between simulations and AERONET observations in each defined region. (a) Region_1, (b) Region_2, (c) Region_3, (d) Region_4, (e) Region_5, and (f) Region_All.
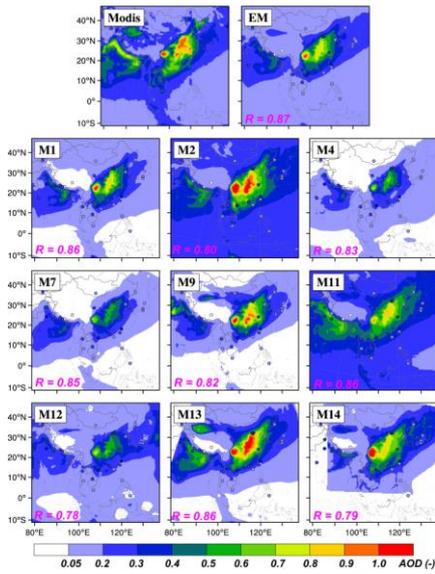
Figure 7. Spatial distributions of observed and simulated aerosol optical depth (AOD) at 550 nm. The observed AOD values are retrieved from MODIS. Spatial correlation coefficients are given in the bottom left corner of each panel. Observed AOD from AERONET are also shown in circles.

Figure 9: Spatial distribution of aerosol optical depth (AOD) at 550 nm retrieved by MODIS and simulated by participating models. The spatial correlation coefficients are given in the bottom left corner of each panel. Observed AOD from AERONET stations are also shown.
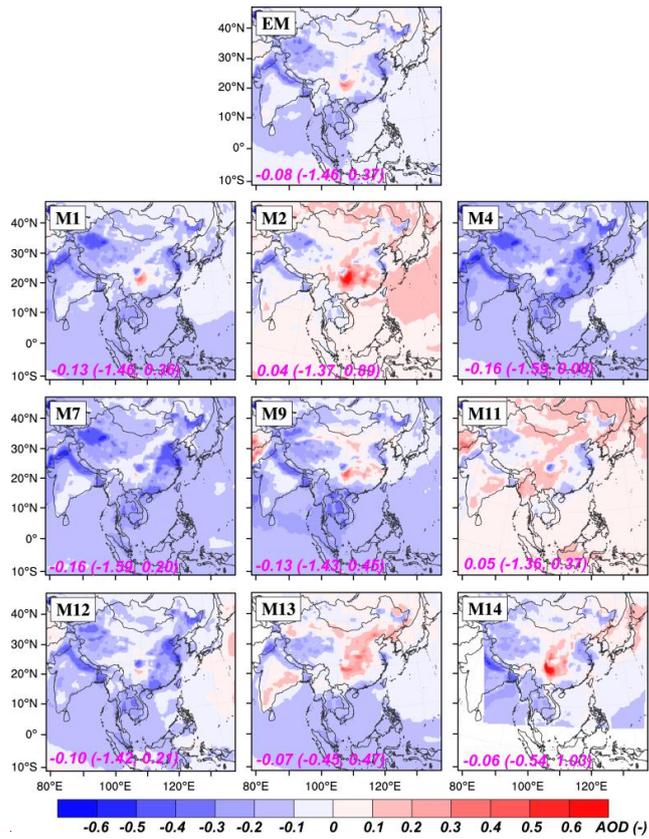
62
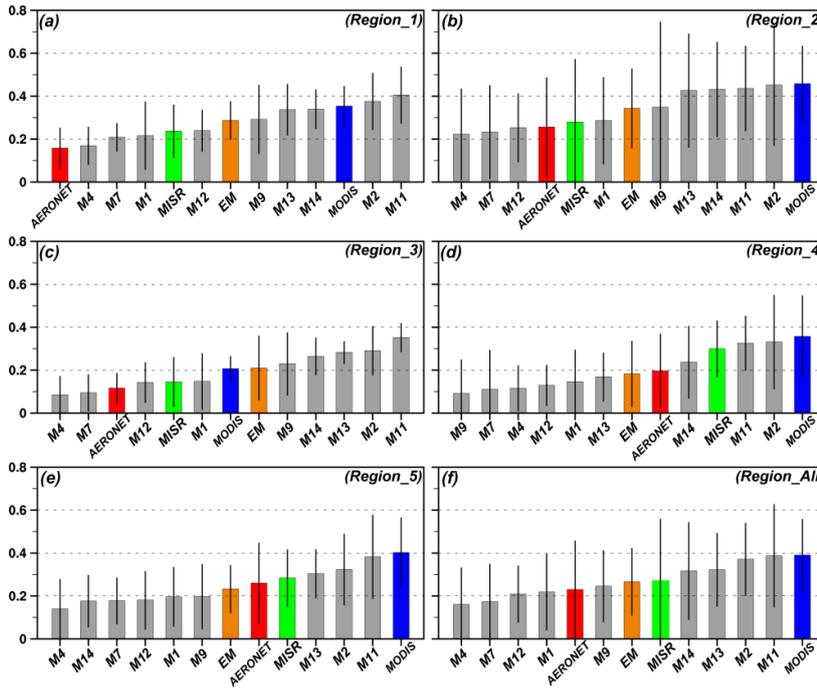
Figure 11: Multi-model AOD (grey bars) averaged over the five defined regions (Region_1 to Region_5) and the whole analyzed domain (Region_All), together with the ensemble mean predictions (orange bar), measured values retrieved from MODIS (blue bar) and MISR (green bar). AOD averaged over the corresponding AEROENT stations (red bar) in each region are also shown. The error bars represent one standard deviation. (a) Region_1, (b) Region_2, (c) Region_3, (d) Region_4, (e) Region_5, and (f) Regioin_All.
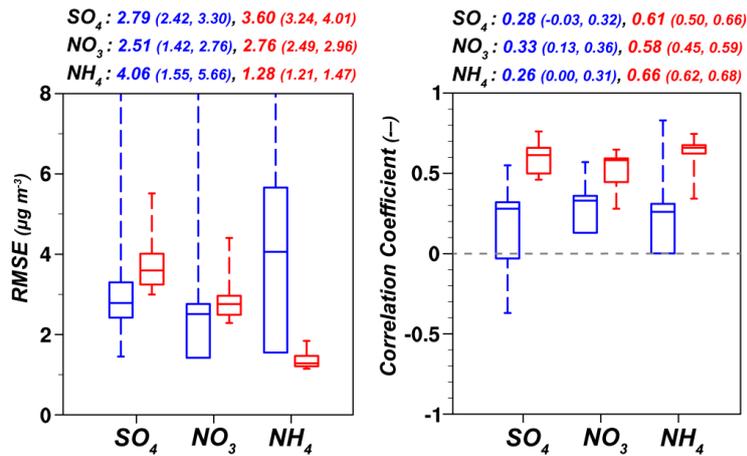
带格式的：删除线

SO$_4$: **2.79** *(2.42, 3.30)*, **3.60** *(3.24, 4.01)*
NO$_3$: **2.51** *(1.42, 2.76)*, **2.76** *(2.49, 2.96)*
NH$_4$: **4.06** *(1.55, 5.66)*, **1.28** *(1.21, 1.47)*

SO$_4$: **0.28** *(-0.03, 0.32)*, **0.61** *(0.50, 0.66)*
NO$_3$: **0.33** *(0.13, 0.36)*, **0.58** *(0.45, 0.59)*
NH$_4$: **0.26** *(0.00, 0.31)*, **0.66** *(0.62, 0.68)*

Figure 8. Inter-comparison of model performance between MICS-Asia Phase II (blue) and Phase III (red) for SO$_4^{2-}$, NO$_3^-$, and NH$_4^+$. Detailed information about the observations and simulations used in Phase II can be obtained from Hayami et al. (2008). Each boxplot exhibits the full range, the interquartile, and the median for RMSE and correlation coefficient. Detailed values of the median (the 25th percentile, the 75th percentile) are also listed above each panel.

Figure 12: Intercomparison of model performance in MICS-Asia II (blue) and MICS-Asia III (red) for SO$_4^{2-}$, NO$_3^-$ and NH$_4^+$. Eight models participated in MICS-Asia Phase II. Detailed information can be found in Hayami et al. (2008). Twelve models are analyzed in MICS-Asia Phase III. Statistics (e.g. RMSE and R) are calculated from all the available models against monthly observations provided by EANET. Each boxplot summarizes the statistical information including the interquartile range, the full range and the median. Detailed values of medians (interquartile ranges) for SO$_4^{2-}$, NO$_3^-$ and NH$_4^+$ are also listed at the top of each panel.
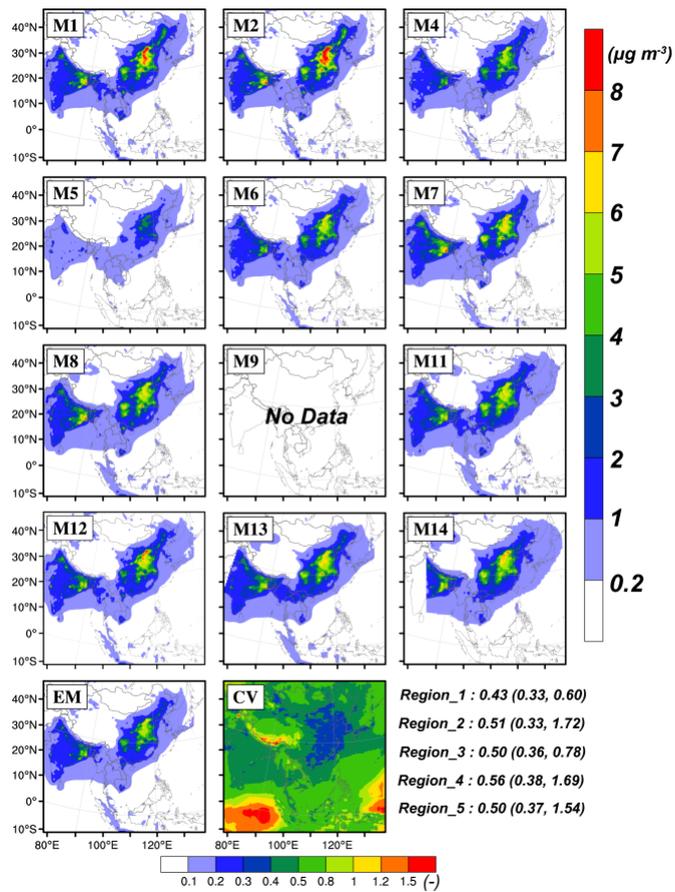
Figure 13: Spatial distribution of simulated BC concentrations from each participating model and the multi-model ensemble mean. The coefficient of variation (CV), defining as the standard deviation of these models divided by their mean, is also calculated. The values listed in the bottom right corner represent the averaged CV (the minimum CV, the maximum CV) in each defined region.
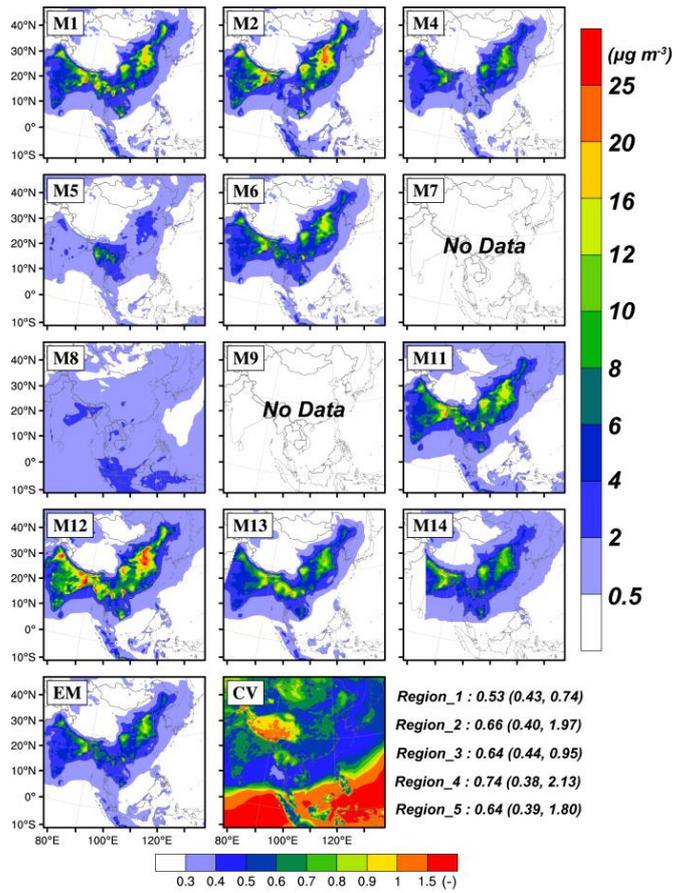
**Figure 14: Similar as Figure 13, but for OC.**
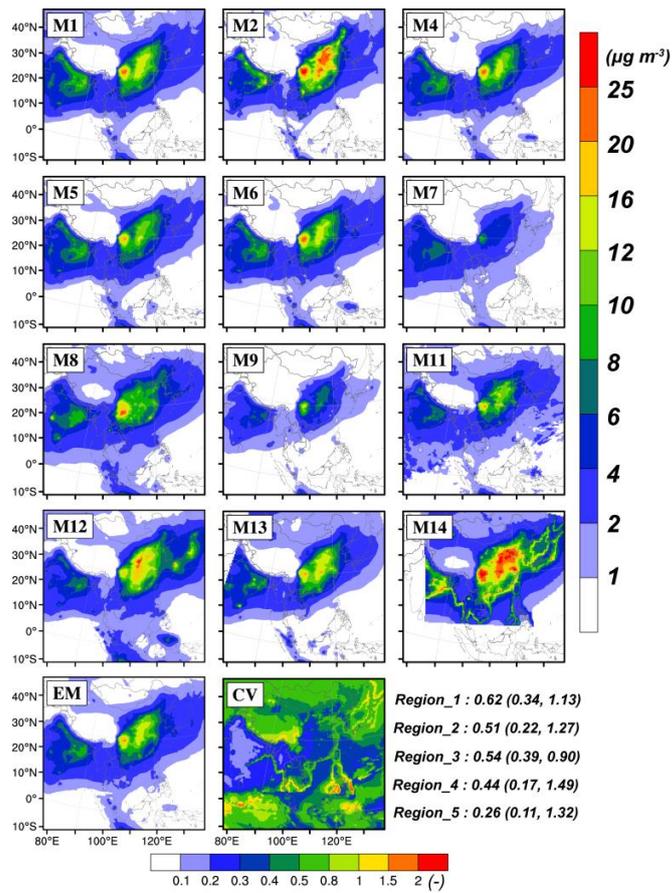
Figure 15: Similar as Figure 13, but for SO_4^{2-}.

5
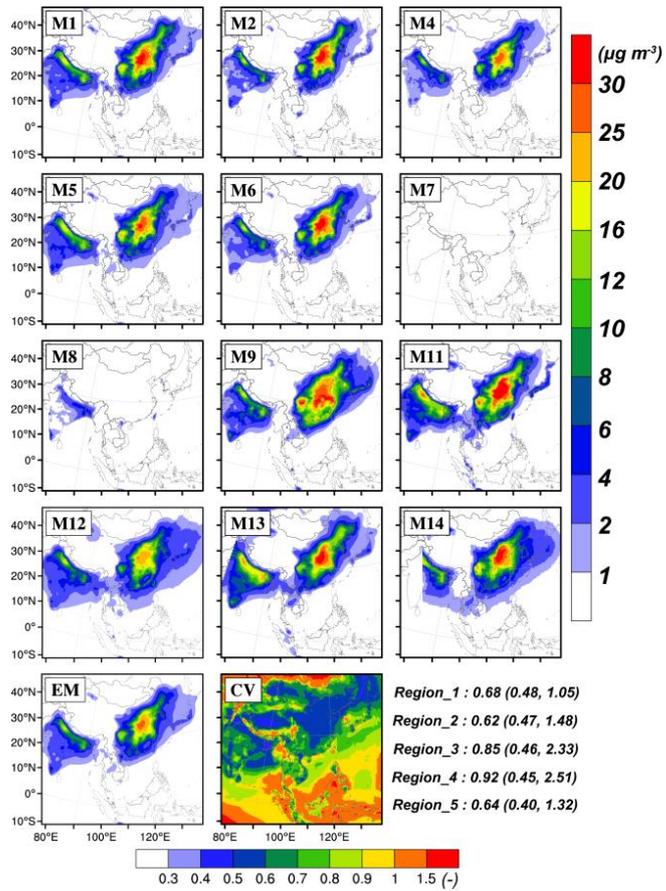
Figure 16: Similar as Figure 13, but for NO_3^-.

5
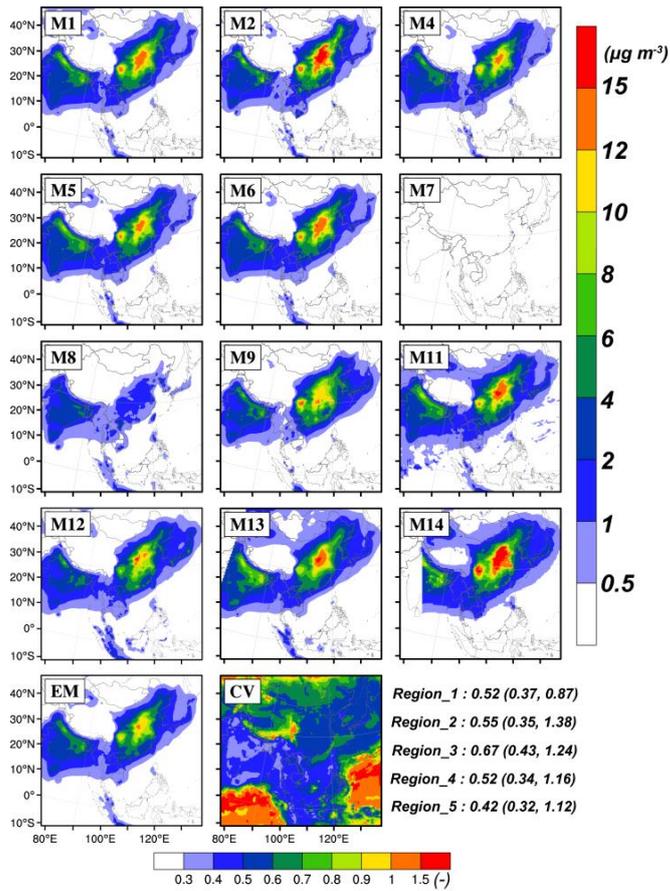
Figure 17: Similar as Figure 13, but for NH$_4^+$.
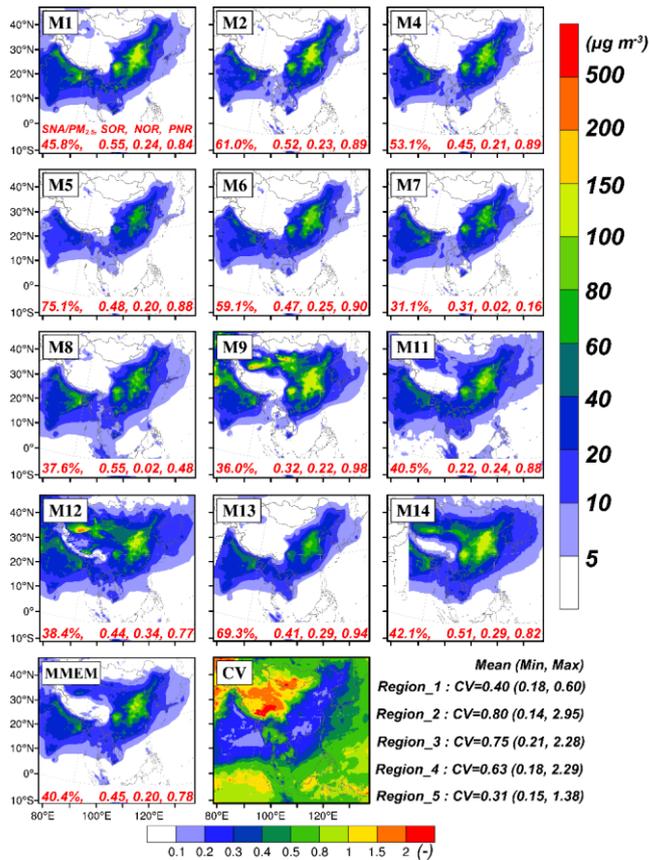
5

Figure 9. Spatial distributions of simulated PM₂.₅ concentrations from each participant model and the MMEM. The calculated coefficient of variation (CV, standard deviation divided by the mean) is also shown. The values listed in the bottom right corner of the figure represent the averaged CV (the minimum CV, the maximum CV) in each defined sub-region. The ratio of SNA (sulfate, nitrate, and ammonium) to PM₂.₅, the SOR (sulfur oxidation ratio), the NOR (nitric oxidation ratio), and the PNR (particle neutralization ratio) are also given at the bottom of each panel.
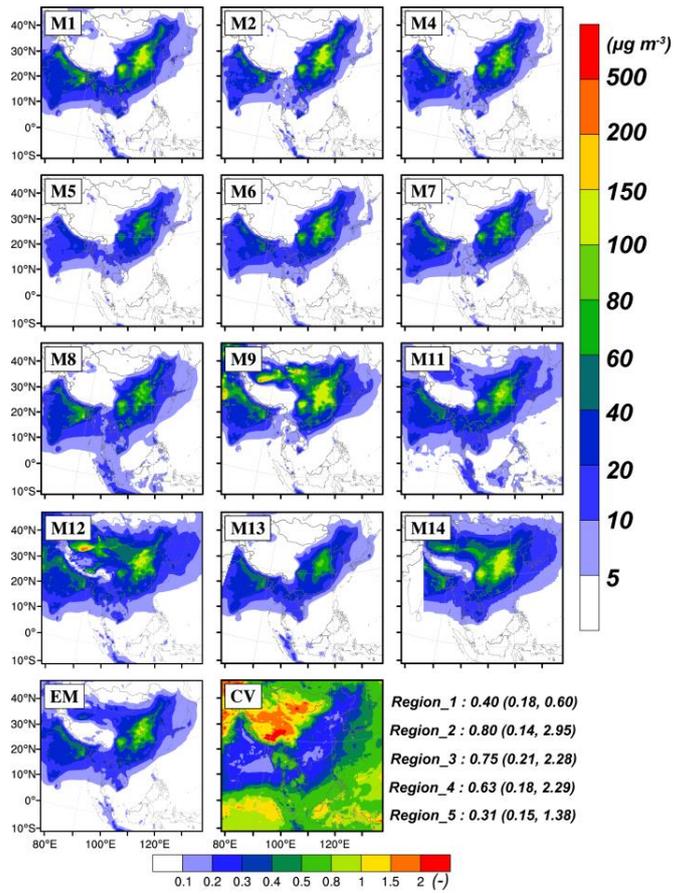
5
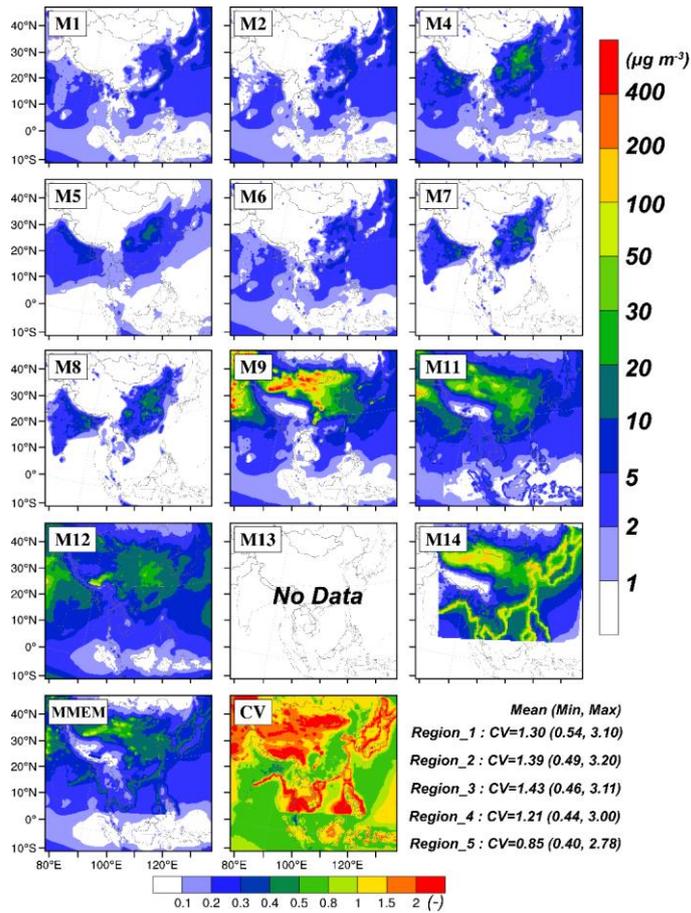
Figure 10. The same as Figure 9, but for PM_{coarse} (coarse particles, subtract PM_{2.5} from PM₁₀).
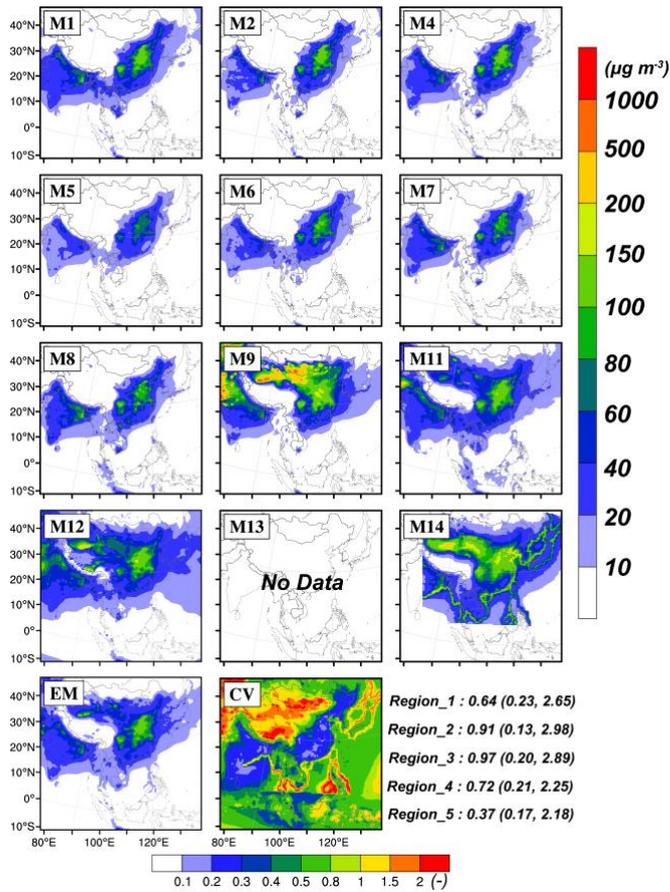
Figure 19: Similar as Figure 13, but for PM₁₀.

5

73
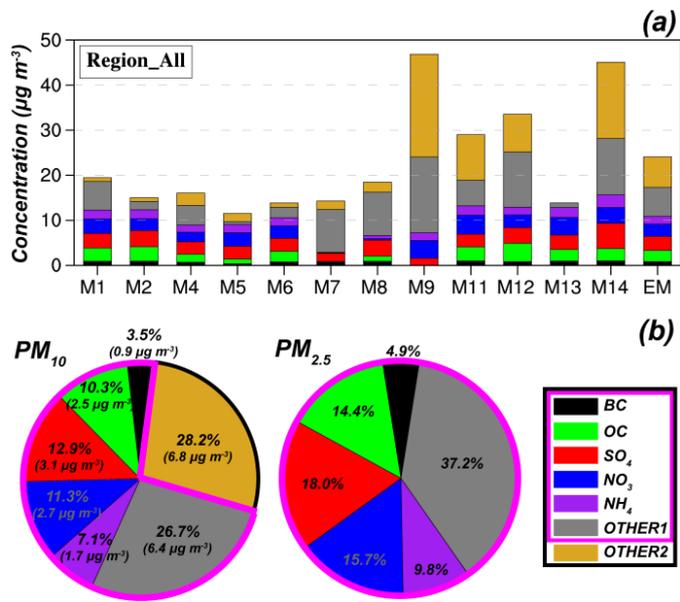
Figure 20: (a) Chemical compositions of simulated particle matter (PM) from all participating models and the ensemble mean. (b) The ratio of each composition to PM_{10} and $PM_{2.5}$ from multi-model ensemble mean. PM_{10} includes $PM_{2.5}$ and OTHER2, while $PM_{2.5}$ is composed of BC, OC, SO_4^{2-}, NO_3^-, NH_4^+ and OTHER1. Notably, OTHER2 cannot be calculated in M13 because PM_{10} concentration has not been submitted. OC is not available in M7, so we leave it into OTHER1. BC and OC are not available in M9 and these concentrations are grouped into OTHER1.
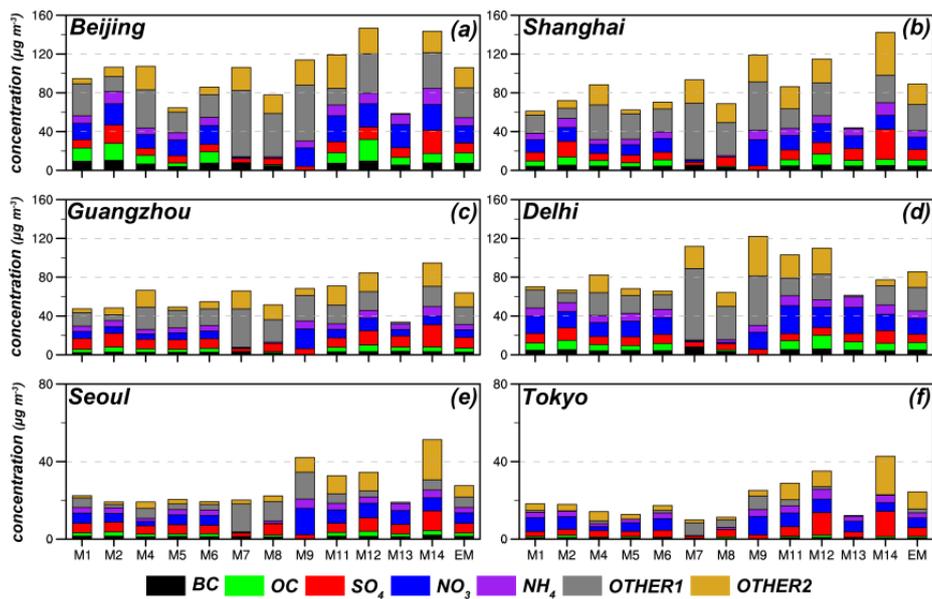
Figure 21: Chemical compositions of simulated particle matter in six metropolitans. (a) Beijing, (b) Shanghai, (c) Guangzhou, (d) Delhi, (e) Seoul and (d) Tokyo.
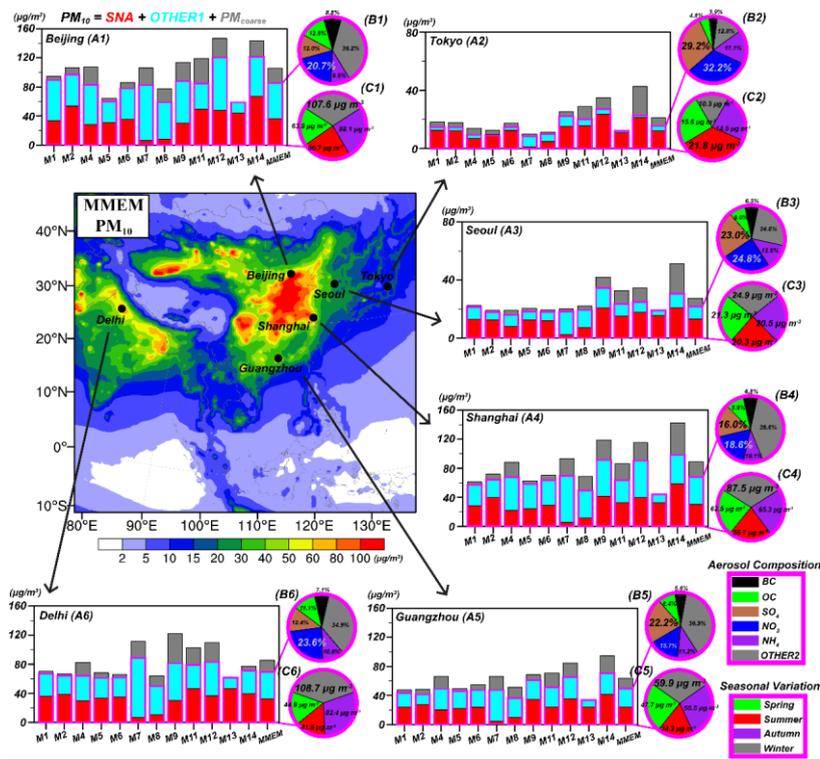
5

Figure 11. (A) The spatial distributions of PM$_{10}$ concentrations for MMEM. (A1-A6) Simulated aerosol chemical compositions for participant models and the MMEM in the six metropolitans (Beijing, Tokyo, Seoul, Shanghai, Guangzhou, and Delhi). (B1-B6) The ratios of each composition to PM$_{2.5}$ for MMEM. (C1-C6) The seasonal PM$_{2.5}$ concentrations for MMEM. It is noted that PM$_{10}$=SNA+OTHER1+PM$_{coarse}$, SNA=SO$_4^{2-}$+NO$_3^-$+NH$_4^+$, and OTHER1=BC+OC+OTHER2.
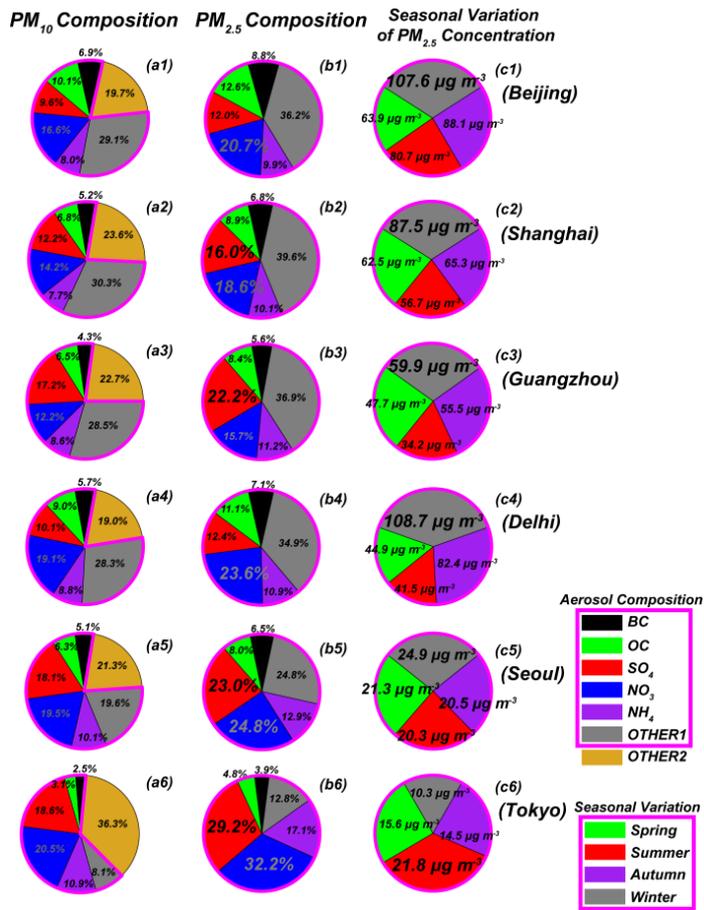
Figure 22: Ratios of chemical compositions to PM₁₀ (a1-a6) and PM₂.₅ (b1-b6) from multi-model ensemble mean in six cities. Seasonal variations of PM₂.₅ concentrations are also shown (c1-c6).

5

Final revised manuscript:

MICS-Asia III: Multi-model comparison and evaluation of aerosol over East Asia

Lei Chen[1,2,6], Yi Gao[1], Meigen Zhang[1,3,4], Joshua S. Fu[5], Jia Zhu[2,6,7], Hong Liao[2,6], Jialin Li[1], Kan Huang[5], Baozhu Ge[1], Xuemei Wang[8], Yun Fat LAM[9], Chuan-Yao Lin[10], Syuichi Itahashi[11,12], Tatsuya Nagashima[13], Mizuo Kajino[14,15], Kazuyo Yamaji[16], Zifa Wang[1,3], and Jun-ichi Kurokawa[17]

[1]State Key Laboratory of Atmospheric Boundary Layer Physics and Atmospheric Chemistry, Institute of Atmospheric Physics, Chinese Academy of Sciences, Beijing, China
[2]School of Environmental Science and Engineering, Nanjing University of Information Science & Technology, Nanjing 210044, China
[3]University of Chinese Academy of Sciences, Beijing, China
[4]Center for Excellence in Regional Atmospheric Environment, Institute of Urban Environment, Chinese Academy of Sciences, Xiamen, China
[5]Department of Civil and Environmental Engineering, University of Tennessee, Knoxville, TN 37996, USA
[6]Jiangsu Key Laboratory of Atmospheric Environment Monitoring and Pollution Control, Jiangsu Collaborative Innovation Center of Atmospheric Environment and Equipment Technology, Nanjing University of Information Science & Technology, Nanjing 210044, China
[7]Research Institute of Climatic and Environmental Governance, Nanjing University of Information Science & Technology, Nanjing 210044, China
[8]Institute for Environment and Climate Research, Jinan University, Guangzhou, China
[9]School of Energy and Environment, City University of Hong Kong, Hong Kong
[10]Research Center for Environmental Changes, Academia Sinica, Taiwan
[11]Central Research Institute of Electric Power Industry, Abiko, Chiba 270-1194, Japan;
[12]Department of Marine, Earth, and Atmospheric Sciences, North Carolina State University, Raleigh, NC 27607, USA
[13]National Institute for Environmental Studies, Tsukuba, Japan
[14]Meteorological Research Institute, Japan Meteorological Agency, Tsukuba, 305-0052, Japan
[15]Faculty of Life and Environmental Sciences, University of Tsukuba, Tsukuba, 305-8577, Japan
[16]School of Science and Engineering, Meisei University, Hino, Tokyo 191-8506, Japan
[17]Asia Center for Air Pollution Research, 1182 Sowa, Nishi-ku, Niigata, Niigata, 950-2144, Japan

Correspondence to: M.G. Zhang (mgzhang@mail.iap.ac.cn)

Abstract. Fourteen chemical transport models (CTMs) participate in the first topic of the Model Inter−Comparison Study for Asia (MICS−Asia) Phase III. These model results are compared with each other and an extensive set of measurements, aiming to evaluate the current CTMs' ability in simulating aerosol concentrations, to document the similarities and differences among model performances, and to reveal the characteristics of aerosol components in large cities over East Asia. In general, these CTMs can well reproduce the spatial–temporal distributions of aerosols in East Asia during the year 2010.

The multi–model ensemble mean (MMEM) shows better performance than most single–model predictions, with correlation coefficients (between MMEM and measurements) ranging from 0.65 (nitrate, NO_3^-) to 0.83 ($PM_{2.5}$). The concentrations of black carbon (BC), sulfate (SO_4^{2-}), and PM_{10} are underestimated by MMEM, with normalized mean biases (NMBs) of −17.0%, −19.1%, and −32.6%, respectively. Positive biases are simulated for NO_3^- (NMB=4.9%), ammonium (NH_4^+) (NMB=14.0%), and $PM_{2.5}$ (NMB=4.4%). In comparison with the statistics calculated from MICS–Asia Phase II, frequent updates of chemical mechanisms in CTMs during recent years make the inter–model variability of simulated aerosol concentrations smaller, and better performance can be found in reproducing the temporal variations of observations. However, a large variation (about a factor of 2) in the ratios of SNA (sulfate, nitrate and ammonium) to $PM_{2.5}$ is calculated among participant models. A more intense secondary formation of SO_4^{2-} is simulated by CMAQ models, because of the higher SOR (sulfur oxidation ration) than other models (0.51 vs. 0.39). The NOR (nitric oxidation ratio) calculated by all CTMs has larger values (~0.20) than the observations, indicating that overmuch NO_3^- is simulated by current models. NH_3–limited condition (the mole ratio of ammonium to sulfate and nitrate is smaller than 1) can be successfully reproduced by all participant models, which indicates that a small reduction in ammonia may improve the air quality. A large coefficient of variation (CV>1.0) is calculated for simulated coarse particles, especially over arid and semi–arid regions, which means that current CTMs have difficulty in producing similar dust emissions by using different dust schemes. According to the simulation results of MMEM in six large Asian cities, different air–pollution control plans should be taken owing to their different major air pollutants in different seasons. MICS–Asia project gives an opportunity to discuss the similarities and differences of simulation results among CTMs in East Asia applications. In order to acquire a better understanding of aerosol properties and their impacts, more experiments should be designed to reduce the diversities among air quality models.

1 Introduction

Urbanization and industrialization have stimulated economic growth and population expansion during the last several decades in East Asia (Spence et al., 2008; Yan et al., 2016; Chen et al., 2016), but also bring about noticeable degradation of ecological environment at the same time (Hall 2002; Han et al., 2014; Yue et al., 2017). Significant increase in atmospheric aerosol loading, especially from anthropogenic emissions, can exert adverse effects on weather (Cowan et al., 2013), climate (Wang et al., 2016a), air quality (Gao et al., 2016a), and human health (Carmichael et al., 2009). For example, aerosols can modify the thermodynamic structure of the atmospheric boundary layer by absorbing and scattering solar radiation (Ding et al., 2016; Petaja et al., 2016), alter cloud properties and precipitation by acting as cloud condensation nuclei and ice nuclei (Lohmann and Diehl, 2006; Wang, 2013a), deteriorate visibility and cause haze events (Singh and Dey, 2012; Li et al., 2014). In addition, fine particulate matter with aerodynamic diameters smaller than 2.5 μm ($PM_{2.5}$) may enter into the alveoli and cause severe cardiovascular diseases, respiratory diseases, and even lung cancer (Pope and Dockery, 2006; Gao et al., 2015a). The impacts have attracted considerable attentions from the public and policy makers in East Asia, and therefore the research on aerosol has become a hot topic during recent years.

In order to better understand the properties of atmospheric aerosols and their impacts, chemical transport models (CTMs) can be a critical tool, and they have been applied to study various air pollution issues all over the world. For example, a fully coupled online Weather Research and Forecasting/Chemistry (WRF/Chem) model was developed by Grell et al. (2005), and it has been widely used to study the aerosol–radiation–cloud feedbacks on meteorology and air quality (Gao et al., 2014; Zhang et al., 2015a; Qiu et al., 2017); a Models–3 Community Multi–scale Air Quality (CMAQ) modeling system was designed by the US Environmental Protection Agency (Byun and Ching, 1999), and it has been applied to address acid deposition, visibility and haze pollution issues (Zhang et al., 2006; Han et al., 2014; Fan et al., 2015); a nested air quality prediction model system (NAQPMS) was developed by the Institute of Atmospheric Physics, Chinese Academy of Science (IAP/CAS) (Wang et al., 2001) to reproduce the mechanism of transport and evolution of atmospheric pollutants in Asia (Li et al., 2012a; Wang et al., 2013c; Li et al., 2017a); a global three–dimensional chemical transport model (GEOS–Chem) was first presented by Bey et al. (2001), and researchers use the GEOS–Chem model to study the source sector contribution, long–range transport and the prediction of future change in ozone and aerosol concentrations (Liao et al., 2006; Li et al., 2016b; Zhu et al., 2017).

Although significant advantages can be found in CTMs, how to accurately reproduce or predict the concentrations and the distributions of atmospheric pollutants is still a challenge, with the problems of inaccurate emission inventories, poorly represented initial and boundary conditions, and imperfect physical, dynamical and chemical parameterizations (Carmichael et al., 2008). Meanwhile, most CTMs are designed to focus on the air quality over developed countries, such as Europe and America, rather than Asia. The assumptions or look–up tables used in CTMs may not be suitable for the simulations of the East Asian environment (Gao et al., 2018). Therefore, before providing meaningful results and answering "what–if" questions for policy makers, model performances must be carefully evaluated. Hayami et al. (2008) and Mann et al. (2014)

pointed out that different parameterizations used in CTMs can cause large variations in simulation results, and multi–model ensemble mean (MMEM) tends to show better performance than most single–model predictions when comparing with observations (Carmichael et al., 2002; Hayami et al., 2008; Wang et al., 2008; Holloway et al., 2008). In order to develop a better common understanding of the performance and uncertainties of CTMs in East Asia applications, and to acquire a more mature comprehension of the properties of atmospheric aerosols and their impacts, a model inter–comparison study should be initiated, and Model Inter–Comparison Study for Asia (MICS–Asia) gives an opportunity to investigate these questions. Meanwhile, model inter–comparison study in East Asia is very limited (Phadnis et al., 1998; Kiley et al., 2003; Han et al., 2008), and far more efforts are needed in future.

The MICS–Asia project was initiated in 1998. In the first phase of MICS–Asia (MICS–Asia Phase I), the primary target was to study the long–range transport and deposition of SO_4^{2-} in East Asia by analyzing the submitted simulation results from eight CTMs. Source–receptor relationships, contributions from removal processes, and the influences of model structures and parameterizations on simulation results were also estimated. More details can be found in Carmichael et al. (2002). As an extension of Phase I, MICS–Asia Phase II included more chemical species of concern, such as sulfur, nitrogen and ozone. This broader collaborative study examined four different periods, encompassing two different years and three different seasons (March, July, and December in 2001, and March in 2002). Simulation results from nine different regional modeling groups were analyzed. Detailed information about this project can be found in the overview paper of Carmichael et al. (2008). In 2010, the MICS–Asia III project was launched. As a part of EANET additional research activity and a continuing research of MICS–Asia series, three topics were discussed, including comparison and evaluation of current multi–scale air quality models (Topic 1), development of reliable emission inventories for CTMs in Asia (Topic 2), and interactions between air quality and climate changes (Topic 3).

This manuscript focuses on the first topic of the MICS–Asia Phase III, and intends to present and summarize the following three objectives, specializing in the topic of aerosols. Firstly, comprehensive evaluations of the strengths and weaknesses of current CTMs for simulating particulate matter (PM) are provided against extensive measurements from in–situ and satellites, aiming to show the capability of participant models. Secondly, diversities of simulated aerosol concentrations among participant models are analyzed, including possible reasons for the inconsistency. Thirdly, characteristics of aerosol compositions in six metropolitans in East Asia are analyzed, which may be helpful to take measures to prevent and control air pollutions in future.

The description of model configurations, model inputs and observations are presented in Section 2. The evaluation for model performance and the inter–comparison between participant models are shown in Section 3. The conclusions and discussions are presented in Section 4.

2 Inter–comparison framework

Fourteen regional models (M1–M14) participated in MICS–Asia phase III Topic 1. All models were required to run for

the whole year of 2010, and provide gridded monthly simulation results of aerosols in the first model layer. These CTMs include the Weather Research and Forecasting model coupled with Community Multiscale Air Quality (WRF–CMAQ), the Weather Research and Forecasting Model coupled with Chemistry (WRF–Chem), the nested air quality prediction model system (NAQPMS), the non–hydrostatic mesoscale model coupled with chemistry transport model (NHM–Chem), the global three–dimensional chemical transport model (GEOS–Chem), and the Regional Atmospheric Modeling System coupled with Community Multiscale Air Quality (RAMS–CMAQ). Among these models, there are three different versions of WRF–CMAQ (v5.0.2 is used by M1 and M2, v5.0.1 is used by M3, and v4.7.1 is used by M4, M5 and M6), four different versions of WRF–Chem (v3.7.1 is used by M7, v3.6.1 is used by M8, v3.6 is used by M9, and v3.5.1 is used by M10), one version of NAQPMS (M11), NHM–Chem (M12), GEOS–Chem (v9.1.3 is used by M13) and RAMS–CMAQ (v4.6 is used by M14). Basic information about the configurations of each model is summarized in Table 1.

2.1 Model configurations

2.1.1 Simulation domain

A unified simulation domain was designed by MICS–Asia organizers, which covers the region of (15.4°S–58.3°N, 48.5°E–160.2°E) with 180×170 grid points at 45 km horizontal resolution, but participant models employed different modeling domains (Fig. 1) with different grid resolutions (e.g. 0.5° of latitude×0.667° of longitude in M13, 64 km×64 km in M14, others are 45 km×45 km). In order to minimize the influence from lateral boundary conditions and to cover most areas of interest in East Asia, an analyzed region was chosen in this manuscript (Fig. 1). For M13 and M14, missing values were used to fill the grids outside their simulation domains. Meanwhile, the analyzed region was divided into five different areas (Region_1 to Region_5). Region_1 contains Korean Peninsula and Japan. Region_2 only contains China. Region_3 contains Mongolia and parts of Russia. Region_4 covers most countries in Southeast Asia. Region_5 contains most countries in South Asia. Therefore, simulation results in each sub–region can be analyzed and compared to show the performance of current CTMs.

2.1.2 Gas and aerosol modules

Gas phase chemistry and aerosol chemistry are important parameterizations in CTMs. Luecken et al. (2008) and Balzarini et al. (2015) pointed out that different settings of chemical mechanisms could influence the simulation results significantly.

2.1.2.1 Gas phase chemistry

(1) The gas chemistry of SAPRC99 (Statewide Air Pollution Research Center 99) was used in M1, M2, M4, M5, M6, M12 and M14. It is a detailed mechanism for the gas–phase atmospheric reactions of VOCs and NO_x in urban and regional atmosphere (Carter, 2000). The SAPRC99 mechanism has already been incorporated into CMAQ v4.6 with about 72 species

and 214 reactions. Meanwhile, another three heterogeneous chemistry reactions of N_2O_5, HO_2 and NO_2 are also considered in the SAPRC99 gas phase chemistry in M12 (Kajino et al., 2018).

(2) The Carbon Bond mechanism (CB05) was used in M3. It describes tropospheric oxidant chemistry and provides a basis for computer modeling studies of ozone, particulate matter, visibility, acid deposition and air toxics issues, with 51 species and 156 reactions (Yarwood et al., 2005).

(3) The second generation Regional Acid Deposition Model (RADM2) gas phase chemical mechanism was used in M9 and M10. The inorganic species considered in RADM2 include 14 stable species, 4 reactive intermediates and 3 abundant stable species. The organic chemistry is represented by 26 stable species and 16 peroxy radicals (Stockwell et al., 1990). This module can simulate the concentrations of PAN, HNO_3 and H_2O_2 under different environmental conditions (Stockwell et al., 1990).

(4) Based on RADM2, the Regional Atmospheric Chemistry Mechanism (RACM) was developed with updated reaction rate constants and product yields according to more recent laboratory measurements. It is capable of simulating the troposphere from the Earth's surface through the upper troposphere, and is valid for simulating remote to polluted urban conditions (Stockwell et al., 1997). M7 and M8 selected the RACM module. The rate coefficients were further updated in M7 (Kim et al., 2009). However, heterogeneous hydrolysis of N_2O_5 is not considered in M7 and M8.

(5) The gas chemistry of Carbon–Bond Mechanism version Z (CBMZ) was used in M11. This lumped–structure mechanism extends the original framework of CBM–IV to function properly at larger spatial and longer timescales, with revised inorganic chemistry, isoprene chemistry, and many other related parameterizations (Zaveri and Peters, 1999).

(6) In M13, the NOx–Ox–HC–Br tropospheric gas chemistry mechanism was used. It includes about 80 species and 300 chemical reactions (Bey et al., 2001; Zhu et al., 2017).

Jimenez et al. (2003), Luecken et al. (2008) and Yang et al. (2018) summarized that different gas–phase chemistry mechanisms could predict large variations in reactive species, such as HO_2 and NO_3, making the production of OH and H_2O_2 different. In addition to the different number of species and reactions considered in each gas module, the reaction rates of the oxidation of SO_2, NO_x and some VOCs to condensable SO_4^{2-}, NO_3^- and organic species are also largely different (Pan and Zhang, 2008). All these would affect the simulated aerosol concentrations, especially under the urban condition.

2.1.2.2 Aerosol chemistry

(1) AERO with ISORROPIA: Aerosol modules (AERO5 and AERO6) with thermodynamic equilibrium models (ISORROPIA v1.7 and v2) were used in M1, M2, M3, M4, M5, M6, M11, M12 and M14. Aerosols in AERO were divided into three modes: Aitken, accumulation and coarse modes. Gas–liquid–solid equilibrium in inorganic aerosol was predicted by the ISORROPIA model. The AERO5 ISORROPIA (v1.7) was mainly used in CMAQ v4, and the updated AERO6 ISORROPIA (v2) has been implemented since CMAQ v5. Nine new PM species (e.g. Ca^{2+}, K^+ and Mg^{2+}) were added in the new aerosol module of AERO6. In order to support the additional crustal ion emissions introduced in AERO6, ISORROPIA (v1.7) was replaced by ISORROPIA (v2) (Nenes et al, 1998; Fountoukis and Nenes, 2007), and the

corresponding modifications could affect the gas–particle partitioning of NO_3^- and NH_4^+. The rate constants for the S (IV) to S (VI) conversion through in–cloud oxidation pathways were also modified, including the catalysis effects through aqueous chemistry from Fe and Mn (Appel et al., 2013). In order to solve the over–predictions of the unspeciated PM$_{2.5}$ (also called PM$_{other}$) in CMAQ v4, detailed speciation profiles derived from Reff et al. (2009) were adopted in CMAQ v5 to subdivide the emissions of PM$_{other}$ into primary NO_4^+, Na^+, Cl^- and other selected trace elements. Comparing with CMAQ v4.6, a new parameterization of heterogeneous N_2O_5 hydrolysis was included in CMAQ v4.7 to improve the simulation results of NO_3^-. Comparing with CMAQ v5.0.1, a mass balance correction of NO_3^- aerosol under cold conditions was adopted in CMAQ v5.0.2. This adjustment would reduce the concentration of NO_3 and HNO_3 at the surface level.

(2) MADE/SORGAM and MADE/VBS: Detailed treatments of inorganic aerosol effects in M7, M8 and M9 were simulated by Modal Aerosol Dynamics Model for Europe (MADE). Three log–normal modes (Aitken, accumulation and coarse modes) were used in this module to present the particle size distribution of submicrometer aerosol, such as SO_4^{2-}, NO_3^-, NH_4^+, BC, OC and aerosol water (Ackermann et al., 1998). Aerosols were assumed to be internally mixed in the same mode but externally mixed among different modes (Zhao et al., 2010). The organic chemistry used in M7 and M9 was based on SORGAM (Secondary Organic Aerosol Model). This model was capable of simulating SOA formation including the production of low–volatility products and their subsequent gas–particle partitioning (Schell et al., 2001), but all activity coefficients were assumed to be 1 due to insufficient information. However, when it was coupled with MADE, the biogenic precursors and their resulting particle concentrations were set to be zero. The organic chemistry used in M8 was based on the Volatility Basis Set (VBS) approach (Ahmadov et al., 2012). This module used the volatility basis set framework to simulate primary organic aerosol partitioning between the gas and particulate phases and the gas–phase oxidation of the corresponding vapors (Murphy and Pandis, 2009).

(3) GOCART: The Goddard Chemistry Aerosol Radiation and Transport (GOCART) model was used in M10 to simulate tropospheric aerosol components, such as SO_4^{2-}, dust, BC, OC and sea–salt aerosols (NO_3^- and NH_4^+ are not considered), and all these aerosol species were assumed to be log–normal size distributions (Chin et al., 2000). SO_4^{2-} was formed by the oxidation of SO_2 in the atmosphere, but the impacts from in–cloud oxidation pathways were not included (Chin et al., 2002). The source emission of BC and OC was mainly from biomass burning. Dust emission was following Ginoux et al. (2001). Sea-salt emission was highly dependent on wind speed. More details about the simulations of dust and sea–salt aerosols in GOCART will be described in Section 2.1.3 and 2.1.4.

Different chemical species are considered in numerous aerosol equilibrium models, resulting in different equilibrium partitioning and water uptake during the simulation processes, which can affect the predicted aerosol concentrations (Fountoukis and Nenes, 2007). As Moya et al. (2002) and Wang et al. (2012b) classified that the treatment of crustal material in aerosol chemistry could considerably improve model results in predicting the partitioning of NO_3^- and NH_4^+. Different heterogeneous reactions and their activity coefficients used in the thermodynamic equilibrium would also be a major source of uncertainty in simulated aerosol concentrations (Li et al., 2012a; Kim et al., 2011; Chen et al., 2016a).

2.1.3 Dust scheme

Natural emissions of windblown dust have been explicitly parameterized since CMAQ v5 (Foroutan et al., 2017), but all the participated WRF–CMAQ models did not turn this option on, which means dust aerosols were not considered in M1–M6. Meanwhile, the dust scheme in M7 and M8 was also turned off.

Dust particles in M10 and M13 were simulated by the GOCART model (Ginoux et al., 2001). This model includes eight size groups of mineral dust ranging from 0.1 to 10 μm. The emission flux for a size group can be expressed as follows: $F = C \times S \times s_p \times u_{10}^2 \times (u_{10} - u_t), if\ u_{10} > u_t$, where C is a constant with the value of 1 μg s^2 m^{-5}. S means the probability source function, representing the fraction of alluvium available for wind erosion. s_p is the fraction of each size group within the soil. u_{10} and u_t are the wind speed at 10 m and threshold velocity of wind erosion, respectively.

A simplified dust emission parameterization proposed by Shao (2001) was used in M9 (Shao, 2004). Dust emission in Shao_2004 is proportional to streamwise saltation flux, and the proportionality depends on soil texture and soil plastic pressure. The size–resolved dust flux goes into four size bins, with diameters ranging from 1.95 to 20 μm (Kang et al., 2011). More detail about the dust emission rate and the total dust flux can be found in Shao (2004).

A size–segregated dust deflation module proposed by Wang et al. (2000) was used in M11. It was developed based on three major predictors (friction velocity, surface humidity and dominant weather system), and has been successfully applied in many dust-related simulations (Wang et al., 2002; Yue et al., 2010). The dust flux F is calculated as follows: $F = C \times \frac{\rho_a}{g} \times E \times u^{*3} \times \left(1 + \frac{u_0^*}{u^*}\right) \times \left(1 - \frac{u_0^{*2}}{u^{*2}}\right) \times \left(1 - \frac{RH}{RH_0}\right)$, where C equals to 10^{-5}, ρ_a means air density, g is gravitational acceleration. E is the weighting factor, representing the uplifting capability of land surface. u_0^* and u^* are the fraction and threshold friction velocities, respectively. RH and RH_0 are relative humidity and threshold relative humidity, respectively. According to soil categories and vegetation coverage, the dust emission intensity was further modified by Luo and Wang (2006). Four size bins of dust particles ranging from 0.43 to 10 μm were considered in this emission module. Meanwhile, several heterogeneous reactions on dust particles were also considered (Li et al., 2012a).

An empirical dust emission mechanism based on the approach of Gillette and Passi (1988) was used in M12 and M14 (Han et al., 2004). Dust flux can be calculated through the following formula: $F = C \times u_*^4 \times \left(1 - \frac{u_*}{u}\right) \times (1 - f \times R), if\ u > u_*$, where u and u_* are the friction and the threshold friction velocities, respectively. C is the correction coefficient (1.4×10^{-15}). f and R represent the fractional coverage of vegetation and the reduction factor in a model grid. Dust particles with diameters ranging from 0.43 to 42 μm were grouped into 11 bins, with the first eight bins below 11 μm for aerosol sampler, and the additional three bins above 11 μm for larger particles (Han et al., 2004).

Different dust schemes will produce different dust emission fluxes over arid and semi-arid regions (Zhao et al., 2010; Su and Fung, 2015). Several factors, such as potential source regions, threshold friction velocity, size distribution, and other surface and soil–related parameters used in equations can be the primary causes for the inconsistency, and the differences in simulated dust emissions will affect the characteristics of spatial–temporal variations of atmospheric aerosol particles.

2.1.4 Sea–salt scheme

As one of the major components of primary aerosols, sea–salt aerosols contributes to 20–40% of secondary inorganic aerosols (SIAs) over coastal regions (Liu et al., 2015; Yang et al., 2016). These particles can provide surface areas for condensation and reaction of nitrogen and sulfur, making the simulated concentrations of SIAs more accurate (Kelly et al., 2010; Im, 2013).

In M12, the method of Clarke et al. (2006) was used to simulate the sea–salt emissions as follows: $S_{100} = \frac{C_s \times k \times V_{wind} \times h}{A_{avg} \times L + 0.5 \times w_0}$. The sea–salt source function (S_{100}) is defined as the number of sea–salt aerosols generated per unit area of ocean surface completely covered by bubbles (100% coverage) per unit time. C_s is the differences of condensation nuclei concentrations collected at 5 m (impacted by breaking waves) and 20 m (background values). k is the multiplier for tower C_s compared to mean profile. V_{wind} means surf zone wind speed. h is the height of plume layer for beach profile. A_{avg} represent mean bubble fractional coverage area between waves. L is the distance wave travels to shore, and w_0 is the initial width of breaking wave bubble front.

In other participating models (sea–salt emission is not considered in M7 and M8), sea–salt emissions were simulated online by using the algorithm proposed by Gong et al. (2003). The density function $\frac{dF}{dr}$ (m^{-2} s^{-2} µm^{-1}) is calculated as follows: $\frac{dF}{dr} = 1.373 \times u_{10m}^{3.41} \times r^{-A} \times (1 + 0.057 \times r^{3.45}) \times 10^{1.607e^{-B^2}}$, where u_{10m} is the 10 m wind speed, r is the particle radius at RH=80%. A represents an adjustment parameter, which control the shape of submicron size distribution. B = $(0.433 - log_{10}(r))/0.433$, meaning a parameter related to particle radius. In CMAQ model, the sea–salt scheme was updated by Kelly et al. (2010) to enhance the emission of sea–salt from coastal surf zone, and to allow dynamic transfer of HNO$_3$, H$_2$SO$_4$, HCl, and NH$_3$ between coarse particles and gas phase. In GEOS-Chem model, it was updated by Jaegle et al. (2011) to improve the simulation of sea–salt with dry radii smaller than 0.1 µm.

2.2 Model inputs

Based on the experience concluded from Phase I and Phase II, all the fourteen models in Phase III Topic 1, in principle, were required to use the "standard" meteorological fields, emission inventories and boundary conditions in order to reduce the potential diversities caused by model inputs. But different data were selected by participant models. In this section, some basic information about the model inputs are described.

2.2.1 Meteorological fields

The "standard" hourly meteorological fields were simulated by the Weather Research and Forecasting Model (WRF v3.4.1) with the initial and lateral boundary conditions taken from the National Center for Environmental Prediction (NCEP) Final Analysis (FNL) data. Four–dimensional data assimilation nudging toward the NCEP FNL data was also adopted to increase the accuracy of simulated meteorological variables. The reference meteorological fields were only used in M1–M6

and M11. For M7, M8 and M9, the standard meteorological simulation was run by the same model (WRF), but feedbacks between meteorological variables and pollutants were also considered in these WRF–Chem models. For M10, the Modern Era Retrospective–analysis for Research and Applications (MERRA) reanalysis were used to driven the WRF (v3.5.1) model. The outputs from the Japan Meteorological Agency (JMA) non–hydrostatic mesoscale model (NHM) were used to initialize M12 (Kajino et al., 2012). M13 was driven by assimilated meteorological data from the Goddard Earth Observing System (GEOS) of NASA's Global Modeling and Assimilation Office (Chen et al., 2009; Li et al., 2016c). Although the meteorological initial and lateral boundary conditions were taken from the same NCEP FNL data, three dimensional meteorological fields used in M14 were simulated by Regional Atmospheric Modeling System (RAMS) (Zhang et al., 2002, 2007; Han et al., 2009, 2013). Consequently, different meteorological fields used in the fourteen participant models will cause different atmospheric circulation characteristics, which can further influence the spatial–temporal variation of air pollutants (Gao et al., 2018ACP).

2.2.2 Emission inventories

All participant models utilized the "standard" emission inventory, including anthropogenic, biogenic, biomass burning, air and ship, and volcano emissions, which was prepared by the emission group in MICS–Asia phase III. The anthropogenic emission dataset over Asia, named MIX, was developed by harmonizing five regional and national emission inventories with a mosaic approach. These five inventories are REAS2 (REAS inventory version 2.1 for the whole of Asia, Kurokawa et al., 2013), MEIC (the Multi-resolution Emission Inventory for China developed by Tsinghua University), PKU–NH_3 (a high–resolution NH_3 emission inventory by Peking University, Huang et al., 2012), ANL–India (an Indian emission inventory developed by Argonne National Laboratory, Lu et al., 2011), and CAPSS (the official Korean emission inventory form the Clean Air Policy Support System, Lee et al., 2011). The MIX inventory includes ten species (SO_2, NO_x, CO, CO_2, NMVOC (non–methane volatile organic compounds), NH_3 (ammonia), BC (black carbon), OC (organic carbon), $PM_{2.5}$ and PM_{10}) in each sector (power, industry, residential, transportation, and agriculture), and is developed for the year 2010 with monthly temporal resolution and 0.25 degree spatial resolution. More details can be found in Li et al. (2017b). Weekly and diurnal profiles of the anthropogenic emissions provided by the emission group were used in model simulations, including the emission factors for the first seven vertical levels (Fig. S1). Biogenic emissions were calculated by the Model of Emissions of Gases and Aerosols from Nature (MEGAN) version 2.04 (Guenther et al., 2006). In MEGAN v2.04, meteorological variables (e.g. solar radiation, air temperature, soil moisture) and land cover information (e.g. leaf area index and plant functional types) were necessary inputs, and these data were obtained from the WRF v3.4.1 simulation results and MODIS (Moderate Resolution Imaging Spectroradiometer) products, respectively. Biomass burning emissions were processed by re–gridding the Global Fire Emissions Database (GFED) version 3 (van der Werf et al., 2010), and the diurnal profile was also provided. The aircraft and shipping emissions were based on the 2010 HTAPv2 (Hemispheric Transport of Air Pollution) emission inventory (0.1 by 0.1 degree) (Janssens–Maenhout et al., 2015). Daily volcanic SO_2 emissions were collected from the AEROCOM program (http://www-lscedods.cea.fr/aerocom/AEROCOM\HC/volc/, Diehl et al., 2012;

Stuefer et al., 2013). The spatial distribution of the merged emissions of SO_2, NO_x, NH_3 and $PM_{2.5}$ from anthropogenic, biogenic, biomass burning, air and ship, and volcano emissions are shown in Fig. S2. Similar spatial patterns can be found among the four species, with high values in eastern China and northern India.

2.2.3 Boundary conditions

Two sets of the chemical initial and boundary conditions (CHASER and GEOS–Chem) were provided by MICS–Asia phase III. The 3–hourly global CTM outputs of CHASER (prepared by Nagoya University, Sudo et al., 2002a; Sudo et at., 2002b) was run with 2.8 °×2.8 °horizontal resolution and 32 vertical layers. The hourly outputs from GEOS–Chem (prepared by University of Tennessee, http://acmg.seas.harvard.edu/geos/) was run with 2.5 °×2 °horizontal resolution and 47 vertical layers. All participant models, except M2, M7 and M10, chose between them. For M2 and M7, the default chemical boundary condition provided by CMAQ and WRF–Chem were used, respectively. For M10, the global GOCART simulations were used for atmospheric aerosols.

2.3 Coupled meteorology and chemistry modelling methods

As is known to all that meteorological fields have significant influences on air quality. Meanwhile, atmospheric compositions can also affect weather and climate. As Gao et al. (2018ACP) pointed out that different coupling methods between aerosols and meteorological variables can cause different simulation results.

In order to simulate the concentrations of air pollutants, meteorological models and chemistry transport models should be implemented either offline or online (Kong et al., 2015). Offline modeling implies that CTM is run after the meteorological simulation is completed, which means the chemical impacts on meteorology are not considered. Online modeling allows coupling and integration of some of the physical and chemical components (Baklanov et al., 2014). According to the extent of online coupling, there are two ways of coupling: (1) online integrated coupling (meteorology and chemistry are simulated simultaneously in the same grid) and (2) online access coupling (meteorology and chemistry are independent, but information can be exchanged between meteorology and chemistry) (Baklanov et al., 2014). Among these participating models, M4, M5, M6, M12, M13 and M14 are offline models. M1, M2, M3 and M11 are online access models. M7, M8, M9 and M10 are online integrated models.

More details about the model configurations can be found in Table 1 and the other MICS–Asia Phase III companion papers (Kong et al., 2019; Li et al., 2019).

2.4 Observation data

Monthly observations of SO_4^{2-}, NO_3^-, NH_4^+, $PM_{2.5}$ and PM_{10} collected from 39 stations of the Acid Deposition Monitoring Network in East Asia (EANET) were used to evaluate the simulations. Common quality assurance and quality control standards promoted by the ADORC (Acid Deposition and Oxidant Research Center) were adopted among these EANET stations to guarantee high quality dataset. More information about the EANET dataset can be found at

. In addition to the EANET data, monthly mean concentrations of air pollutants (e.g. SO_2, NO_2, $PM_{2.5}$ and PM_{10}) over the Beijing–Tianjin–Hebei (BTH) region (19 sites) and the Pearl River Delta (PRD) region (13 sites) provided by the China National Environmental Monitoring Center (CNEMC) were also used to compare with the simulation results from participating models.

5   As is known to all, China has been experiencing heavy air pollution with high concentrations of fine particles. Recent studies highlighted the importance of secondary aerosols in the formation of haze episodes (Liu et al., 2013; Sun et al., 2016a; Chen et al., 2018). However, observations (e.g. SO_4^{2-}, NO_3^- and NH_4^+) in China were only available at one EANET site (the Hongwen site). In order to make the model evaluation more credible, observed monthly/seasonal/yearly concentrations of BC, SO_4^{2-}, NO_3^-, NH_4^+ and $PM_{2.5}$ in China were also collected from published literatures.

10   Aerosol Robotic Network (AERONET), a ground–based remote–sensing aerosol network consisting of worldwide automatic sun– and sky–scanning spectral radiometers (Holben et al., 1998), provides the aerosol optical depth (AOD) products at 440 nm and 675 nm, which can be used to calculate the AOD at 550 nm according to the Angström exponent. The AERONET Level 2.0 monthly AOD data (cloud–screened and quality–assured data) at 33 sites were utilized in this study. Meanwhile, satellite–retrieved 550 nm AOD products from the Moderate Resolution Imaging Spectroradiometer 15 (MODIS) were also used to compare with simulations.

     Figure 2 and Figure S3 show the geographical locations of all the observation sites. Most SO_4^{2-}, NO_3^- and NH_4^+ monitoring sites are located in China, Japan and the Southeast Asia. Three PM_{10} sites are located in the Southeast Asia, whiles others are in China and Japan. Detailed information about these stations is listed in Table S1 and Table S2.

     In general, the wide variety of measurements from in–situ and satellites used in this manuscript can allow for a rigorous 20 and comprehensive evaluation of model performance.

3 Results

3.1 Model evaluation

     According to the objective of MICS–Asia Phase III Topic 1, comparisons of aerosol concentrations between observations and simulations are presented to evaluate the performance of current multi–scale air quality models in East Asia, 25 including analyzing the similarities and differences between participant models. Simulation results of BC, OC, SO_4^{2-}, NO_3^-, NH_4^+, $PM_{2.5}$, PM_{10} and AOD are requested to submit for the project, but no data can be acquired from M10, and extremely large values are predicted by M3. Therefore, only twelve models are actually considered in this manuscript. Among the twelve models, AOD is missing in M5, M6 and M8, PM_{10} is missing in M13, OC is missing in M7, BC and OC are missing in M9 (Table S3).

3.1.1 Evaluation for aerosol compositions

Figure 3 illustrates the observed and simulated ground level annual mean concentrations of BC, SO_4^{2-}, NO_3^-, NH_4^+, $PM_{2.5}$ and PM_{10}. Multi–model ensemble mean (MMEM), defined as the average of all available participating models (except M3 and M10), is presented to exhibit a composite of model performance. Normalized mean biases (NMBs) between observations and MMEM in each defined sub–region (Region_1 to Region_5) and the whole analyzed region (Region_All) are also calculated.

Analyzing Fig. 3(a), we can find that most models show good skills in simulating the BC concentrations and their spatial distribution characteristics, with relative high values over large emission areas (e.g. North China) (Li et al., 2016c). But the NMB for MMEM is −15.8%. This underestimation may be attributed to the large negative bias at the Gucheng site (site 24) (NMB for MMEM is −38.3%). This station locates in the industrial province of Hebei, where air pollution is serious and BC emission is large (Wang et al., 2016c). Due to the low reactivity of BC in the atmosphere, the high uncertainty of BC in current emission inputs (Hong et al., 2017; Li et al., 2017b) may cause this underestimation.

For SO_4^{2-}, observations are relative low in Region_1 (mean value is 3.8 µg m^{-3}), Region_3 (mean value is 2.5 µg m^{-3}) and Region_4 (mean value is 3.5 µg m^{-3}), and most models (except M7, M9 and M14) perform well over these areas (NMBs range from −26.3% to 30.0%). In Region_2, all the observed concentrations of SO_4^{2-} are larger than 10 µg m^{-3} (mean value is 16.9 µg m^{-3}), but models fail to reproduce the high magnitude. As Zheng et al. (2015) and Shao et al. (2019) pointed out that missing sulfate formation mechanisms (e.g. heterogeneous sulfate chemistry) on aerosol in current air quality models may result in this underestimation, especially in China where significant increase of secondary aerosols (such as sulfate) can be observed during polluted periods (Liu et al. 2015). A large variance is also simulated among models, e.g. M14 overpredicts the ground–level SO_4^{2-} concentrations, especially in Region_1 (NMB=118.6%). This significant overestimation in coastal stations may be caused by its high concentrations of sea salt aerosols (Fig. 10), which makes the sea−salt sulfate higher. Meanwhile, M7 and M9 obviously underpredict SO_4^{2-} at nearly all sites (NMB=−73.5% and −71.7%, respectively.). Generally, MMEM can well reproduce the spatial variation of SO_4^{2-}, but the predicted concentration is underestimated, especially in Region_2 (NMB=−43.5%) and Region_3 (NMB=−35.3%).

For NO_3^-, low concentrations are observed in Region_1 (1.5 µg m^{-3}), Region_3 (0.6 µg m^{-3}) and Region_4 (1.8 µg m^{-3}), but high values are presented in Region_2 (13.4 µg m^{-3}), showing the similar spatial distribution characteristics as the observed SO_4^{2-}. In CTMs, there are two pathways about the nitrate formation. The dominant pathway is the homogeneous gas−phase reaction between HNO_3 (NO_2 oxidation by OH during the daytime) and NH_3 under ammonia−rich conditions, and the second pathway is the heterogeneous hydrolysis of N_2O_5 on aerosol surface at night in ammonia−poor environment (Seinfeld and Pandis, 2006; Archer-Nicholls et al., 2014). As NH_4NO_3 is semi−volatile species, and the equilibrium surface concentration of H_2SO_4 is set to be zero in CTMs, so $(NH_4)_2SO_4$ is the preferential species in the completion when H_2SO4 and HNO_3 are both present. Only if NH_3 is excess, then NH_4NO_3 will been formed. Analyzing the performance of each participant model, NO_3^- concentration is overpredicted by most models, and the underestimation of SO_4^{2-} can be used to

explain this overestimation (Chen et al., 2017). Meanwhile, the biases from model calculated gas−phase oxidation (e.g. $NO_2 + OH \rightarrow HNO_3$) and/or gas−aerosol phase partitioning (e.g. $HNO_{3(g)} + NH_{3(g)} \leftrightarrow NH_4NO_{3(s, aq)}$) may also result in the overestimation (Brunner et al., 2014; Gao et al., 2014). However, M7 and M8 significantly underestimate the observed NO_3^- concentrations (NMB~−93.4%). One reason for the extremely low values may result from the incorrect concentrations of NH_3 simulated by M7 and M8 (Fig. S4). As Chen et al. (2016) pointed out that the amount of NH_3 in the atmosphere is a key factor in determining the NO_3^- concentration. Another reason for this underestimation is that M7 and M8 did not consider the impacts of N_2O_5 heterogeneous reaction ($N_2O_{5(g)} + H_2O_{(aq)} \rightarrow 2HNO_{3(aq)}$). Su et al. (2017) pointed out that the hydrolysis of N_2O_5 can led up to 21.0% enhancement of NO_3^-, especially over polluted regions. Although the NMB calculated in Region_All for MMEM is only −1.1%, MMEM systematically overpredicts observations in Region_1 (NMB=45.2%) and Region_3 (NMB=38.2%), but underpredicts in Region_2 (NMB=−0.7%) and Region_4 (NMB=−44.9%).

Simulated NH_4^+ concentrations are influenced by the partitioning between gaseous NH_3 and aerosol NH_4^+, and are also associated with the SO_4^{2-} and NO_3^- concentrations (Gao et al., 2018). Model predictions (except M7, M8 and M14) can reproduce the measurements relatively well in each defined sub−region. But significant overestimation is shown by M14, while significant underestimation is simulated by M7 and M8, especially in Region_2 with NMBs of 72.2% for M14, −94.9% for M7, and −81.0% for M8, respectively. For M14, overestimated SO_4^{2-} and NO_3^- make the concentrations of NH_4^+ higher, since more ammonium is required to neutralize particle−phase acid. For M7 and M8, extremely low concentrations of NH_3 are simulated, which means fewer gaseous NH_3 can be converted to aerosol NH_4^+. In general, the calculated NMB in Region_All by MMEM is 4.0%.

On average, the observed PM$_{2.5}$ concentration in Region_2 is larger than 50 µg m^{-3}, but the mean value in Region_1 is only about 10 µg m^{-3}. All participating models can generally capture this spatial distribution pattern. However, significant underestimation is simulated at the three remote stations (site 1, 2 and 7) in Region_1 with the NMB of −39.0% for MMEM. Similar negative bias can also be found in Ikeda et al. (2013), who compared CMAQ (v4.7.1) simulation results against observations from the same remote monitoring stations (Rishiri and Oki) in 2010. Ikeda et al. (2013) pointed that the underestimated cocentrations of organic aerosols may cause this bias. In Region_2, the NMB for MMEM is −10.0%.

For PM$_{10}$, the mean observed concentrations in each region are 26.6 µg m^{-3} (Region_1), 114.4 µg m^{-3} (Region_2) and 38.1 µg m^{-3} (Region_4), respectively. But nearly all participant models (except M14) underestimate the PM$_{10}$ concentrations. M14 predicts higher concentrations in Region_1, especially at coastal sites, such as site 1 (Rishiri), site 2 (Ochiishi), site 4 (Sadoseki), site 7 (Oki) and site 14 (Cheju). The high−value anomalies in M14 at coastal stations can also be found in Fig. 10, and the positive bias may be caused by the emission and gravitational settling of sea salt. As Monahan and Muircheartaigh (1980) pointed out that sea salt emissions can be enhanced in the surf zone due to the increased number of wave breaking events, and the degree of the enhancement highly depends on the 10 m wind speed used in the whitecap coverage parameterization. According to the simulation results from published literatures, higher wind speed is simulated by M14

(RAMSCMAQ) when comparing with observations, especially at coastal stations (Han et al., 2013; Han et al., 2018). Meanwhile, a gravitational settling mechanism of coarse aerosols from upper to lower layers was added in M14, and the net effect of this update could make an increase in the concentrations of coarse particles, especially near coastal areas impacted by sea spray (Nolte et al., 2015). Generally, the NMB for MMEM in Region_All is −31.0%.

Time series of the monthly observed and simulated aerosol compositions, including BC, SO_4^{2-}, NO_3^-, NH_4^+, $PM_{2.5}$ and PM_{10}, are shown in Fig. 4 and Fig. 5. According to the pre−defined sub−regions as illustrated in Fig. 2, all simulations and observations are grouped into the five regions, with the modeling results sampled at the corresponding observation stations before averaging together.

The measured BC concentrations in Region_2 exhibit an obvious seasonal variation, with the minimum (~ 3.5 μg m^{-3}) in spring and summer, and the maximum (~ 8 μg m^{-3}) during late autumn and winter. Participant models can capture this seasonality quite well, and nearly all simulation results are within the standard deviation of the observations, but a large inter−model variation is also simulated, especially in winter when BC concentration is high. Due to its low reactivity in the atmosphere, this variation may be caused by their simulated meteorological conditions, including the impacts of different coupling ways between meteorological and chemical modules (Gao et al., 2015b). As Briant et al. (2017) and Huang et al. (2018) concluded that the online integrated models can simulate higher BC concentrations than offline models, especially during polluted periods. The correlation coefficient in MMEM is 0.73.

For $PM_{2.5}$, the observed monthly concentrations in Region_2 are higher than those in Region_1. This is because the emissions in China are larger than that in Japan and Korean Peninsula (Fig. S2). But nearly all models tend to underpredict the concentrations of $PM_{2.5}$ in Region_1, with NMBs ranging from −44.3% (in winter) to −22.7% (in summer) for MMEM. Comparing with the correlation coefficient (R=0.40) in Region_1, CTMs can better reproduce the seasonality of the observed $PM_{2.5}$ in Region_2, with the R of 0.69 for MMEM. Generally, the R for MMEM in Region_All is 0.83 and the NMB ranges from −2.2% (in autumn) to 13.9% (in winter).

Similar temporal−variation characteristics of PM_{10} concentrations are observed in Region_1, Region_2 and Region_4, with the maximum occurred in March and November, and the minimum occurred during summer. Most models fall within the standard deviation of the observations. The simulated PM_{10} concentrations in Region_2 show less diversity, but nearly all models peak 2 months later. A distinctive seasonality can be found in Region_4, with the highest value (nearly 80 μg m^{-3}) observed in March, but most models cannot reproduce this characteristic. This is because the GFED substantially underestimate the biomass burning emissions over Southeast Asia (Fu et al., 2012), especially during March−April when most intense biomass burning occurred in Myanmar, Thailand and other Southeast Asian countries (Huang et al., 2012), and the emission bias is mainly due to the lack of agricultural fires (Nam et al., 2010). Finally, a weak seasonality in PM_{10} is simulated by MMEM with R of 0.58 in Region_4. In Region_all, although consistent underestimation is simulated during the whole period, with NMB ranging from −40.8% to −25.2% for MMEM, the seasonal cycle can be well reproduced by MMEM with R of 0.78.

The seasonal variation characteristics of observed SO_4^{2-}, NO_3^- and NH_4^+ in Region_1 are not obvious, with the annual

mean of ~ 4 µg m^{-3} for SO_4^{2-}, 1.5 µg m^{-3} for NO_3^- and 1.0 µg m^{-3} for NH_4^+, respectively. A large inter–model spread of simulated SO_4^{2-} is shown in Fig. 5(a1), with the maximum variation range in June. Most models significantly overpredict the observed NO_3^- concentrations, especially in summer with the NMB of 164.3% for MMEN. Simulated monthly NH_4^+ concentrations from most models are within the standard deviation of observations, and the R for MMEM is as high as 0.74.

In Region_2, the observations are only available at one EANET site (the Hongwen site, located in the eastern coastal area of China), and the seasonality of observed SO_4^{2-}, NO_3^- and NH_4^+ from this station is obvious with the maximum in spring and winter, and the minimum in later summer and early autumn. Nearly all models tend to underpredict these concentrations, but the MMEM captures the seasonal cycle relative well with Rs of 0.57 for SO_4^{2-}, 0.85 for NO_3^- and 0.86 for NH_4^+, respectively. In Region_3, the observed maximum concentrations of SO_4^{2-} and NH_4^+ are in winter, but most models cannot reproduce the increasing tendency during the late autumn and the early winter, which means participant models fail to capture the seasonality (Rs of 0.20 for SO_4^{2-}, 0.34 for NO_3^- and 0.18 for NH_4^+, respectively). This may due to the low emission of primary aerosols and their precursors in Region_3. Meanwhile, the Regional Emission Inventory in Asia (REAS v2.1) is used in Region_3, which is calculated based on the emissions from 2000 to 2008 (Li et al., 2017b), not extended to the simulation year of 2010. The updated emissions with localized data may increase the accuracy of simulation results. In Region_4, the simulated concentrations of SO_4^{2-}, NO_3^- and NH_4^+ are fairly good when compared with the measurements. The Rs of MMEM are 0.73 for SO_4^{2-}, 0.63 for NO_3^- and 0.73 for NH_4^+. Meanwhile, the model diversities are small. Generally, in Region_All, MMEM can well reproduce the magnitudes of observed SO_4^{2-}, NO_3^- and NH_4^+ during the whole simulation period, as well as the seasonal variation characteristics.

As mentioned above, the observed monthly mean concentrations of aerosol compositions in China are only available at one EANET station (site 17, the Hongwen station), with missing values in June and October. In order to make the evaluation more comprehensive, observed seasonal mean concentrations of SO_4^{2-}, NO_3^- and NH_4^+ collected from published literatures are also used to compare with simulation results (Fig. S5). M2, M12 and M14 reasonably reproduce the SO_4^{2-} concentrations in the four seasons, while others fail to simulate the high observed SO_4^{2-} concentrations. The NMBs of SO_4^{2-} range from −79.4% (M7) to 12.8% (M14). On the contrary, nearly all participant models overestimate the concentrations of NO_3^- (except M4, M7 and M8), with NMBs ranging from 1.7% (M5) to 50.2% (M9). The underestimation of SO_4^{2-} and the overestimation of NO_3^- may be the general performance in current CTMs (Wang et al., 2013b; Gao et al., 2014; Huang et al., 2014; Zheng et al., 2015), and some hypotheses should be deeply tested in future to reduce these deviations, such as (1) missing oxidation mechanisms of SO₂ may lead to low concentrations of SO_4^{2-}, which allows for excess NO_3^- in the presence of ammonia, (2) there is an issue with NO$_x$ partitioning and/or missing NO$_x$ sink. Meanwhile, Seinfeld and Pandis (2006) pointed out that the chemical productions of SO_4^{2-} and NO_3^- are mainly from the gas−phase and/or liquid−phase oxidation of SO₂ and NO₂. Therefore, further comparisons of observed and simulated SO₂ and NO₂ are shown in Fig. S6 and Fig. S7. From Fig. S6, participant models can generally reproduce the seasonality of the two gases, with Rs of 0.61 for SO₂ and 0.65 for NO₂, respectively. But overestimations (underestimations) of SO₂ (NO₂) are found during most simulation

periods, not only in China, but also in other defined sub−regions (Fig. S7). The overestimated (underestimated) concentrations of SO_2 (NO_2) can be used to explain the underestimation (overestimation) of simulated SO_4^{2-} (NO_3^-). However, significant underestimation of NO_3^- is also simulated by M7 and M8. As mentioned above, the extremely low concentrations of NH_3 in M7 and M8 may be the main reason for this negative bias. Analyzing the results from ensemble mean, MMEM shows better performance than participating models, with NMBs of −46.0% for SO_4^{2-}, 1.9% for NO_3^- and 13.1% for NH_4^+, respectively.

3.1.2 Evaluation for aerosol optical depth

Simulated aerosol optical depth (AOD) at 550 nm from the nine participant models (M1, M2, M4, M7, M9, M11, M12, M13 and M14) are compared with the measurements from AERONET. From Fig. 6 we can find that most models tend to overpredict AOD values during the whole simulation period in Region_1, Region_2 and Region_3 with NMBs of 74.0%, 38.8% and 107.0% for MMEM, respectively. In Region_4, an obvious seasonality is observed with the maximum in spring and the minimum in summer. Models can capture this seasonality well, although underestimation is found in spring. The R for MMEM is 0.65 and the NMB is −8.7% in Region_4. Smaller NMB (–4.2%) is calculated in Region_5 by MMEM, but a quite weak seasonality is shown with underestimated AOD in spring and summer, and overestimated AOD in autumn and winter. Generally, simulated AOD values are within a standard deviation of the observations in Region_All with a slight overestimation in autumn and winter. The MMEM can reproduce the seasonal cycle with R of 0.68, and the NMB for MMEM is 18.7%.

Figure 7 presents the spatial distributions of the observed and simulated AOD at 550 nm. MODIS AOD is collected from the Terra and Aqua satellites during the year 2010. The observed AOD from AERONET are also shown. In order to quantify the ability of each model in simulating the spatial distribution of aerosol particles, spatial correlation coefficients are also given in the bottom left corner of each panel. Analyzing the observations from MODIS, we can conclude that AOD values are higher in central and eastern China, including the Sichuan province, with the maximum over 1.0. High values can also be observed in the north India. Due to dust events happened in arid and semi−arid regions, AOD values over the Taklimakan are also large (~0.5). Comparing with MODIS AOD, most models can reproduce the spatial distribution characteristics, with high values in China and India, and low values in other countries. The Rs range from 0.78 (M12) to 0.86 (M1, M11 and M13). But most models tend to underestimate the AOD in the eastern coastal regions of China and the north regions of India (Fig. S8), where anthropogenic emissions are large. Meanwhile and dust particles can be frequently observed. Generally, MMEM captures the AOD spatial variation better with R of 0.87, and the mean bias is −0.08.

3.1.3 Statistics for aerosol particles and aerosol optical depth

Table 2 shows the statistics of correlation coefficient (R), normalized mean bias (NMB) and root−mean squared error (RMSE) for BC, SO_4^{2-}, NO_3^-, NH_4^+, $PM_{2.5}$, PM_{10} and AOD. Simulation results from participant models and MMEM are compared with available observations. Best results are set to be bold with underline.

17

It can be found that participant models are able to capture the variability of BC in China, with Rs ranging from 0.65 (M5) to 0.80 (M8), but nearly all models tend to underestimate the BC concentration, except M1 and M2. The maximum negative deviation is simulated by M5 (NMB=−54.9%), while the maximum positive deviation is from M2 with NMB of 12.7%. All the RMSEs are less than the observed mean concentration of BC (5.0 μg m^{-3}). Comparing to the observed SO_4^{2-}, most models fail to reproduce the high values, and the NMB for MMEM is –19.1%, meaning the underestimation of the simulated SO_4^{2-} concentration is a general phenomenon in current CMTs. Implementing more detailed sulfate aerosol formation mechanisms (e.g. heterogeneous reaction and catalytic oxidation) into air quality models may improve the accuracy of simulation results (Huang et al., 2014, Zheng et al., 2015; Fu et al., 2016). But most models can capture the variation of SO_4^{2-} with Rs ranging from 0.46 (M14) to 0.76 (M13). For NO_3^-, Rs vary from 0.29 (M8) to as high as 0.65 (MMEM). M5 shows the largest correlation (0.65) and the smallest NMB (–1.7%) among models. Although a high value of R (0.64) is calculated by M9, the NMB is the largest (125.7%). All RMSEs are larger than the measured NO_3^- (1.7 μg m^{-3}), meaning a relative poor performance for current CTMs to simulate the NO_3^- concentrations in East Asia. For NH_4^+, underestimation can be found in M4, M7 and M8, while the others tend to overestimate the NH_4^+ concentration. Although all RMSEs are larger than the observed NH_4^+ (mean value is 1.1 μg m^{-3}), most models can capture the variability, with Rs ranging from 0.34 (M8) to 0.75 (M9). Generally, MMEM matches the observations with R of 0.71, NMB of 14.0% and RMSE of 1.11 μg m^{-3}, respectively. Although significant underprediction is found in PM$_{10}$ (NMBs range from –55.7% in M5 to –16.9% in M9, except M14) and the inter–model spread is large in PM$_{2.5}$ (NMBs range from –26.5% in M13 to 46.0% in M14), the variations of simulated PM$_{2.5}$ and PM$_{10}$ are well correlated with measurements (Rs > 0.60) and the RMSEs are all smaller than the averaged concentrations (51.4 μg m^{-3} for PM$_{2.5}$, 80.7 μg m^{-3} for PM$_{10}$). For AOD, large positive deviations are simulated by M2, M9, M11, M13 and M14, but these models can reproduce the spatial–temporal variation characteristics relative well with Rs larger than 0.5. M4 and M7 show the large negative deviation with NMBs of –28.5% and –21.8%, respectively. But their RMSEs are relative small (0.16 for M4 and 0.18 for M7). Generally, the R, NMB and RMSE for MMEM are 0.68, 18.7% and 0.14, respectively.

3.2 Inter–comparison between MICS–Asia Phase II and Phase III

The main purpose of MICS–Asia Phase III Topic 1 is to assess the ability of current multi–scale air quality models to reproduce the air pollutant concentrations in East Asia. In order to reveal the improvements of the simulation ability in current CTMs, statistics (e.g. RMSE and R) for observed and simulated SO_4^{2-}, NO_3^- and NH_4^+ from MICS–Asia Phase II and Phase III are compared in Fig. 8.

The statistics of MICS–Asia Phase II are taken from Hayami et al. (2008). The observed monthly mean concentrations are monitored with high completeness at the fourteen EANET stations in March, July and December 2001 and March 2002, and the model–predicted monthly surface concentrations are from eight regional CTMs. Notably, NO_3^- and NH_4^+ used in Hayami et al. (2008) are total NO_3^- (= gaseous HNO$_3$ + particulate NO_3^-) and total NH_4^+ (= gaseous NH$_3$ + particulate

NH_4^+), respectively. More detailed information can be found in Hayami et al. (2008).

Analyzing the RMSEs in Fig. 8, we can conclude that the medians (the 25th percentile, the 75th percentile) for SO_4^{2-}, NO_3^- and NH_4^+ are 3.60 µg m^{-3} (3.24 µg m^{-3}, 4.01 µg m^{-3}), 2.76 µg m^{-3} (2.49 µg m^{-3}, 2.96 µg m^{-3}) and 1.28 µg m^{-3} (1.21 µg m^{-3}, 1.47 µg m^{-3}) in Phase III, respectively. Although the medians (except NH_4^+) are a little larger than that in Phase II, the interquartile ranges are quite smaller, indicating similar concentrations can be simulated by current CTMs. Meanwhile, the medians of the correlations of SO_4^{2-}, NO_3^-, and NH_4^+ in Phase III, including the upper and lower quartiles, are all larger than that in Phase II, which means current CTMs show better performance in reproducing the spatial–temporal variations of observations.

Although the participating models (8 verses 12 CTMs), observation sites (14 verses 31 EANET stations), and simulation periods (4 months verses 1 year) are different between Phase II and Phase III, more reasonable statistics are calculated by current CTMs, reflecting better performance in simulating the concentrations of aerosols and their spatial–temporal variations.

3.3 Inter–comparison between participant models

Figure 9 shows the spatial distributions of simulated PM$_{2.5}$ concentrations from each participant model and the MMEM. The coefficient of variation (hereinafter, CV), defined as the standard deviation of the models divided by their mean, is also calculated. The larger the value of CV, the lower the consistency among the participating models (Han et al., 2008; Gao et al., 2018). All simulation results can reproduce the high PM$_{2.5}$ in the northern India and the eastern China, including the Sichuan province in China. The areas with high PM$_{2.5}$ concentrations (> 40 µg m^{-3}) are consistent with the regions where CV is low (< 0.3), indicating similar performance of the CTMs in simulating the air pollutants over haze–polluted areas.

Previous studies have revealed that sulfate, nitrate and ammonium (denoted as SNA) are the predominant inorganic aerosols in PM, and SNA can contribute to nearly half of the total PM$_{2.5}$ mass (about 20%–60%) (Wang et al., 2014c; Sun et al., 2016b; Lin et al., 2018). All these show the necessity to exactly simulate the concentrations of SNA. Analyzing the mean ratio of SNA to PM$_{2.5}$ averaged over the five defined sub–regions (Fig. 9), large variations are simulated by participant models, with values ranging from 31.1% (M7) to 75.1% (M5). Different gas–phase and aerosol chemistry mechanisms used in these CTMs can explain this inconsistency. The calculated SOR (sulfur oxidation ratio, $SOR = nSO_4^{2-}/(nSO_4^{2-} + nSO_2)$, n refers to the molar concentration), NOR (nitric oxidation ratio, $NOR = nNO_3^-/(nNO_3^- + nNO_2)$) and PNR (particle neutralization ratio, $PNR = nNH_4^+/(2 \times nSO_4^{2-} + nNO_3^-)$) are also obviously different.

SOR and NOR can be used to estimate the degree of secondary formation of SO_4^{2-} and NO_3^- (Sun et al., 2006; Zhao et al., 2013). When SOR and NOR are less than 0.1, SO_4^{2-} and NO_3^- mainly come from the primary source emissions; otherwise, high oxidation rates of SOR and NOR can result in large fractions of SO_4^{2-} and NO_3^- in PM$_{2.5}$ (Fu et al., 2008b). Generally, CMAQ models (M1, M2, M4, M5, M6 and M14) produce 30.7% higher SOR than others (except M8), which means more intense secondary formation of SO_4^{2-} is simulated by CMAQ. Similar NOR is predicted by participant models

(~0.24), except M7 and M8. The extremely low value of NOR (~0.02) from M7 and M8 is due to the unreasonable low NO_3^- concentrations. Previous measurements show that the mean value of NOR is about 0.15 (Du et al., 2011; Zhang et al., 2018), which is lower than the predicted one from MMEM (0.20) in this study, indicating more NO_3^- is produced by secondary formation in current CTMs.

PNR is defined as the mole ratio of ammonium to sulfate and nitrate. When PNR is larger than unity, sufficient ammonia can be used to neutralize the acidic sulfate and nitrate; otherwise, there is an incomplete neutralization of acidic species. Analyzing the calculated PNRs from participant models, all values are smaller than 1, which means atmospheric conditions are considered to be ammonia deficient. But the mole ratios of $nNH_4^+/(2 \times nSO_4^{2-})$ are all larger than 1 (~1.6, except M7 and M8). All these indicate that acidic sulfate is fully neutralized to form $(NH_4)_2SO_4$ or NH_4HSO_4, and parts of acidic nitrate is changed to NH_4NO_3. Meanwhile, under NH_3–limited conditions, small reductions in ammonia may cause significant reductions in particulate matter (Makar et al., 2009).

However, large CV (> 1.0) is simulated over arid and semi–arid regions (Fig. 9), such as the Taklimakan Desert and the Gobi Desert, where dust events are often observed, which means current CTMs have difficulty in processing dust aerosols, especially in producing a similar amount of dust emissions and in identifying the same potential dust source regions, by using different dust schemes. Large CV are also shown in simulated coarse particles (subtract $PM_{2.5}$ from PM_{10}) in Fig. 10. High concentrations of coarse particles simulated by M9 over arid and semi–arid regions may be caused by the inaccurate physicochemical parameters (e.g. plastic pressure of the soil surface) used in the Shao dust scheme (Kang et al., 2011). Large values (> 20 μg m^{-3}) over coastal regions from M14 may result from the inadequate simulation results of sea salt aerosols.

From Table 3 we can conclude that the low consistency (or the large CV) of simulated coarse particles in each defined sub–region is mainly caused by the dust particles. Without the impacts of dust aerosols and sea salts (only simulation results from M7 and M8 are considered), the calculated CVs for Region_1 to Reiong_5 are 0.29, 0.30, 0.33, 0.19 and 0.10, respectively. Without the impacts of dust aerosols (only simulation results from M1, M2, M4, M5 and M6 are considered), similar spatial distributions are found in Fig. 10, and the CVs averaged over each sub–region are 0.37 (Region_1), 0.65 (Region_2), 0.48 (Region_3), 0.59 (Region_4), and 0.65 (Region_5), respectively. But when the influences of dust aerosols and sea salts are both considered (simulation results from M9, M11, M12 and M14 are used), larger CVs are obtained with values of 0.97 for Region_1, 1.04 for Region_2, 1.27 for Region_3, 0.95 for Region_4, and 0.88 for Region_5.

Aerosol chemical compositions simulated by each participant model and the MMEM in the six metropolitans (Beijing, Shanghai, Guangzhou, Delhi, Seoul and Tokyo) are shown in Fig. 11. $PM_{2.5}$ is composed of SNA (SO_4^{2-} + NO_3^- + NH_4^+) and OTHER1 (BC + OC + OTHER2). PM_{10} includes $PM_{2.5}$ and PM_{coarse} (coarse particles). Notably, PM_{coarse} cannot be calculated by M13 because PM_{10} is missing in M13.

High values of $PM_{2.5}$ and PM_{10} in Beijing, Shanghai, Guangzhou and Delhi are simulated by nearly all models, and the annual mean concentrations of $PM_{2.5}$ and PM_{10} from MMEM are all larger than the IT-1 (Interim target-1, 35 μg m^{-3} for $PM_{2.5}$, 70 μg m^{-3} for PM_{10}) proposed by WHO. But relative small concentrations are presented in Tokyo (15.5 and 21.3 μg m^{-3} for $PM_{2.5}$ and PM_{10}, respectively) and Seoul (21.7 and 27.6 μg m^{-3} for $PM_{2.5}$ and PM_{10}, respectively). For each city, a

large spread of concentrations of aerosol compositions can be found among participant models (a factor of ~10 for SNA, a factor of ~2 for $PM_{2.5}$ and PM_{10}). This is partly caused by the differences in gas–aerosol partitioning and dust emissions, including the removal processes (e.g. dry and wet depositions).

Analyzing the ratios of aerosol compositions to $PM_{2.5}$ in MMEM (Fig. 11(b1–b6)), the sums of the contributions of BC, OC, SO_4^{2-}, NO_3^- and NH_4^+ in Beijing (63.8%), Shanghai (60.4%), Guangzhou (63.1%) and Delhi (65.1%) are all less than those in Tokyo (87.2%) and Seoul (75.2%). Among these components, NO_3^- is the major species in Beijing (20.7%) and Delhi (23.6%), while SO_4^{2-} is the major species in Guangzhou (22.2%). Similar contributions of SO_4^{2-} and NO_3^- can be found in Shanghai, Seoul and Tokyo. All these suggest that different air–pollution control plans should be taken in different metropolitans.

For seasonal variations of $PM_{2.5}$ concentrations (Fig. 11(c1–c6)), the highest values in Beijing (107.6 μg m^{-3}), Shanghai (87.5 μg m^{-3}), Guangzhou (59.9 μg m^{-3}) and Delhi (108.7 μg m^{-3}) are all simulated in winter. This can be explained by their high emissions during this season. However, in Tokyo, the highest $PM_{2.5}$ concentration is in summer (21.8 μg m^{-3}) and the lowest value is in winter (10.3 μg m^{-3}). In Seoul, $PM_{2.5}$ concentrations are comparable during the four seasons.

4 Conclusion and Discussion

This manuscript mainly focuses on the first topic of the MICS–Asia Phase III, and intends to analyze the following objectives: (1) provide a comprehensive evaluation of current air quality models against observations, (2) analyze the diversity of simulated aerosols among participant models, and (3) reveal the characteristics of aerosol components in large cities over East Asia.

Comparisons against monthly observations from EANET and CNEMC demonstrate that all participant models can well reproduce the spatial–temporal distributions of aerosols. The multi–model ensemble mean (MMEM) shows better performance than most single–model predictions, with correlation coefficients (Rs, between MMEN and measurements) ranging from 0.65 (nitrate, NO_3^-) to 0.83 ($PM_{2.5}$). Differences between predictions and observations are also simulated, such as sulfate (SO_4^{2-}) is underestimated by participant models (except M12 and M14), with NMBs ranging from −67.7% (M7) to −1.6% (M8). The concentrations of nitrate (NO_3^-) and ammonium (NH_4^+) are overestimated by most models, with NMBs of 4.9% for NO_3^- and 14.0% for NH_4^+ in MMEM. The absence of sulfate formation mechanisms (e.g. heterogeneous chemistry) in chemical transport models (CTMs) can be used to explain the underestimation of SO_4^{2-}, and the underestimated SO_4^{2-} will result in the overestimation of NO_3^-. However, significant underestimations of NO_3^- and NH_4^+ are shown in M7 and M8. This is because extremely low values of NH_3 are simulated by these models. The inter–model spread of simulated $PM_{2.5}$ is large, with NMBs ranging from –26.5% (M13) to 46.0% (M14), and nearly all models underestimate the $PM_{2.5}$ concentrations in Region_1. The underestimation may be the insufficient precursors and formation pathways of organic aerosols in current CTMs. Underestimations of PM_{10} are also simulated in each sub–region, and the NMB is −32.6% in MMEM. This may due to the inaccurate emission inventories (e.g. anthropogenic emissions, biomass

burning emissions, and natural emissions) considered in CMTs.

In order to reveal the improvements of the simulation ability in current CTMs, statistics for observed and simulated SO_4^{2-}, NO_3^- and NH_4^+ from MICS–Asia Phase II and Phase III are compared. Results obviously show that the spread of root–mean squared errors (RMSEs) for each species in Phase III is smaller, meaning similar concentrations can be simulated by current CTMs. Meanwhile, the medians of the correlations, including the upper and lower quartiles, are larger, which means current CTMs show better performance in reproducing the temporal variations of observations.

Analyzing the ratio of SNA (sulfate, nitrate and ammonium) to PM$_{2.5}$, large variations are simulated by participant models, with values ranging from 31.1% (M7) to 75.1% (M5). Different gas phase and aerosol schemes used in CTMs can explain this inconsistency. Higher SOR (sulfur oxidation ratio) is calculated by CMAQ models, indicating that CMAQ has a more intense secondary formation of SO_4^{2-} than other participant models. Similar NOR (nitric oxidation ration) is predicted by CTMs, but the value (~0.20) is larger than the observed one (~0.15), which means overmuch NO_3^- is simulated by current CTMs. According to the mole ratio of ammonium to sulfate and nitrate, NH$_3$–limited condition can be successfully simulated by all participant models, which indicates that a small reduction in ammonia may improve the air quality significantly.

The coefficient of variation (CV) can be used to quantify the inter–model deviation, and a large CV is shown in simulated coarse particles (subtract PM$_{2.5}$ from PM$_{10}$). The poor consistency, especially over the arid and semi–arid regions, is mainly caused by the dust aerosols, which means current CTMs have difficulty in reproducing similar dust emissions by using different dust schemes. But the simulated fine particles are in good agreement, especially over the haze–polluted areas.

According to the MMEM simulation results, the highest PM$_{2.5}$ concentrations in Beijing, Shanghai, Guangzhou and Delhi are shown in winter, mainly due to the high emissions and unfavorable weather conditions. But the highest value in Tokyo appears in summer. PM$_{2.5}$ concentrations are comparable in the four seasons in Seoul. Analyzing the ratios of each composition to PM$_{2.5}$, NO_3^- is the major component in Beijing and Delhi, SO_4^{2-} is the major one in Guangzhou, similar contributions of SO_4^{2-} and NO_3^- are calculated in Shanghai, Seoul and Tokyo. All these suggest that different air–pollution control plans should be taken in different cities.

MICS–Asia project gives an opportunity to understand the performance of CTMs in East Asia applications, including the similarities and differences among air quality models. In order to quantify the impacts of different model inputs and model configurations, and to reduce the diversities among simulation results, more detailed sensitivity experiments should be discussed. For example, simulation results from M1 and M2 can be used to assess the impacts of boundary conditions (BCs), since the configurations in these two models are similar except the BCs. M1 adopts the downscale results from GEOS–Chem, while M2 uses the default values from CMAQ. From Fig. S9 we can find that positive biases are simulated $((M1 - M2)/M2 * 100\% > 0)$, especially around the edges of the simulation domain, and the maximum deviation can be over 100%. This is because the boundary conditions from GEOS-Chem consider the impacts of aerosols outside the domain. All these demonstrate that the impacts of BCs should not be neglected when analyzing the spatial distribution characteristic of simulated aerosols around the edge of the domain. But in most inland regions, differences between M1 and M2 are

smaller (< ±10%). Meanwhile, process analysis techniques (i.e. integrated process rate (IPR) analysis) should be developed and implemented in air quality models. This is because IPR can be used to calculate the contributions of each physical/chemical process to variations in aerosol concentrations (Chen et al., 2019), then it will be easier to draw conclusions about the fundamental problems that cause the differences between model predictions (Carmichael et al., 2008).

5 Fully understanding of the source–receptor relationship in each process for a given aerosol species can also be helpful to revise parameterization schemes for better simulation capability. What's more, extensive observations should be collected and used in the next MICS–Asia project.

10

Author contribution

LC, YG and MZ conducted the study design. LC, JZ, HL, JL, KH, BG, XW, YL, CL, SI, TN, MK and KY contributed to modeling data. JF, ZW and JK provided the emission data and observation data. YG and JZ helped with data processing. MZ, JF and JZ were involved in the scientific interpretation and discussion. LC prepared the manuscript with contributions from all co-authors.

Competing interests

The authors declare that they have no conflict of interest.

Acknowledgements

References

Ackermann, I. J., Hass, H., Memmesheimer, M., Ebel, A., Binkowski, F. S., and Shankar, U. M. A.: Modal aerosol dynamics model for Europe: Development and first applications. Atmospheric environment, 32(17), 2981-2999, 10.1016/S1352-2310(98)00006-5, 1998.

Ahmadov, R., McKeen, S. A., Robinson, A., Bahreini, R., Mid-dlebrook, A., de Gouw, J., Meagher, J., Hsie, E., Edgerton,E., Shaw, S., and Trainer, M.: A volatility basis set modelfor summertime secondary organic aerosols over the east-ern United States in 2006, J. Geophys. Res., 117, D06301, 10.1029/2011JD016831, 2012.

Appel, K. W., Pouliot, G. A., Simon, H., Sarwar, G., Pye, H. O. T., Napelenok, S. L., Akhtar, F., and Roselle, S. J.: Evaluation of dust and trace metal estimates from the Community Multiscale Air Quality (CMAQ) model version 5.0, Geoscientific Model Development, 6, 883-899, 10.5194/gmd-6-883-2013, 2013.

Archer-Nicholls, S., Lowe, D., Utembe, S., Allan, J., Zaveri, R. A., Fast, J. D., Hodnebrog, Ø., Denier van der Gon, H., and Mc-Figgans, G.: Gaseous chemistry and aerosol mechanism developments for version 3.5.1 of the online regional model, WRFChem, Geosci. Model Dev., 7, 2557–2579, 10.5194/gmd-7-2557-2014, 2014.

Baklanov, A., Schlünzen, K., Suppan, P., Baldasano, J., Brunner, D., Aksoyoglu, S., Carmichael, G., Douros, J., Flemming, J., Forkel, R., Galmarini, S., Gauss, M., Grell, G., Hirtl, M., Joffre, S., Jorba, O., Kaas, E., Kaasik, M., Kallos, G., Kong, X., Korsholm, U., Kurganskiy, A., Kushta, J., Lohmann, U., Mahura, A., Manders-Groot, A., Maurizi, A., Moussiopoulos, N., Rao, S. T., Savage, N., Seigneur, C., Sokhi, R. S., Solazzo, E., Solomos, S., Sørensen, B., Tsegas, G., Vignati, E., Vogel, B., and Zhang, Y.: Online coupled regional meteorology chemistry models in Europe: current status and prospects, Atmos. Chem. Phys., 14, 317–398, 10.5194/acp-14-317-2014, 2014.

Balzarini, A., Pirovano, G., Honzak, L., Žabkar, R., Curci, G., Forkel, R., Hirtl, M., San José, R., Tuccella, P., and Grell, G. A.: WRF-Chem model sensitivity to chemical mechanisms choice in reconstructing aerosol optical properties, Atmos. Environ., 115, 604–619, 10.1016/j.atmosenv.2014.12.033, 2014.

Bey, I., Jacob, D. J., Yantosca, R. M., Logan, J. A., Field, B. D., Fiore, A. M., Li, Q., Liu, H. Y., Mickley, L. J., and Schultz, M. G.: Global modeling of tropospheric chemistry with assimilated meteorology: Model description and evaluation, Journal of Geophysical Research: Atmospheres, 106, 23073-23095, 10.1029/2001jd000807, 2001.

Briant, R., Tuccella, P., Deroubaix, A., Khvorostyanov, D., Menut, L., Mailler, S., and Turquety, S.: Aerosol–radiation interaction modelling using online coupling between the WRF 3.7.1 meteorological model and the CHIMERE 2016 chemistry-transport model, through the OASIS3-MCT coupler, Geoscientific Model Development, 10, 927-944, 10.5194/gmd-10-927-2017, 2017.

Brunner, D., Savage, N., Jorba, O., Eder, B., Giordano, L., Badia, A., Balzarini, A., Baró, R., Bianconi, R., Chemel, C., Curci, G., Forkel, R., Jiménez-Guerrero, P., Hirtl, M., Hodzic, A., Honzak, L., Im, U., Knote, C., Makar, P., Manders-Groot, A., van Meijgaard, E., Neal, L., Pérez, J. L., Pirovano, G., San Jose, R., Schröder, W., Sokhi, R. S., Syrakov, D., Torian, A., Tuccella, P., Werhahn, J., Wolke, R., Yahya, K., Zabkar, R., Zhang, Y., Hogrefe, C., and Galmarini, S.: Comparative analysis of meteorological performance of coupled chemistry-meteorology models in the context of AQMEII phase 2, Atmospheric Environment, 115, 470-498, 10.1016/j.atmosenv.2014.12.032, 2015.

Byun, D. W. and Ching, J. K. S.: Science algorithms of the EPA Models-3 Community Multiscale Air Quality (CMAQ) modeling system, US Environmental Protection Agency Report EPA/600/R-99/030, Research Triangle Park, NC, 1999.

Carmichael, G. R., Calori, G., Hayami, H., Uno, I., Cho, S. Y., Engardt, M., Kim, S., Ichikawa, Y., Ikeda, Y., Ueda, H., Amann, M.: The MICS-Asia study: model intercomparison of long-range transport and sulfur deposition in East Asia. Atmospheric Environment, 36(2), 175-199, 10.1023/A:1012291200633, 2002.

Carmichael, G., Sakurai, T., Streets, D., Hozumi, Y., Ueda, H., Park, S., Fung, C., Han, Z., Kajino, M., and Engardt, M.: MICS-Asia II: The model intercomparison study for Asia Phase II methodology and overview of findings, Atmospheric Environment, 42, 3468-3490, 10.1016/j.atmosenv.2007.04.007, 2008.

Carmichael, G. R., Adhikary, B., Kulkarni, S., D'Allura, A., Tang, Y., Streets, D., Zhang, Q., Bond, T. C., Ramanathan, V., Jamroensan, A., and Marrapu, P.: Asian Aerosols: Current and Year 2030 Distributions and Implications to Human Health and Regional Climate Change, Environmental Science & Technology, 43, 5811-5817, 10.1021/es8036803, 2009.

Carter, W. P. L.: Documentation of the SAPRC-99 chemical mechanism for VOC reactivity assessment. Final Report to California Air Resources Board Contract 92-329 and Contract 95-308, Air Pollution Research Center and College of Engineering Center for Environmental Research and Technology, University of California Riverside, California, 2000

Chen, D., Wang, Y., McElroy, M. B., He, K., Yantosca, R. M., and Sager, P. L.: Regional CO pollution and export in China simulated by the high-resolution nested-grid GEOS-Chem model. Atmospheric Chemistry and Physics, 9(11), 3825-3839, 10.5194/acp-9-3825-2009, 2009.

Chen, D., Liu, Z., Fast, J., and Ban, J.: Simulations of sulfate–nitrate–ammonium (SNA) aerosols during the extreme haze
5   events over northern China in October 2014, Atmos. Chem. Phys., 16, 10707-10724, https://doi.org/10.5194/acp-16-10707-2016, 2016a.

Chen, L., Zhang, L., Zhang, L., Cao, X., Huang, J., Zhang, W., and Zhang, B.: Characteristics of black carbon aerosol and carbonaceous gases and their emission sources in semi-arid region, China Environmental Science, 32(8), 1345-1352, 2012.

10   Chen, L., Zhang, M., and Wang, Y.: Model analysis of urbanization impacts on boundary layer meteorology under hot weather conditions: a case study of Nanjing, China, Theoretical and Applied Climatology, 125, 713-728, 10.1007/s00704-015-1535-6, 2016b.

Chen, L., Zhang, M., Zhu, J., and Skorokhod, A.: Model analysis of soil dust impacts on the boundary layer meteorology and air quality over East Asia in April 2015, Atmospheric Research, 187, 42-56, 10.1016/j.atmosres.2016.12.008, 2017.

15   Chen, L., Zhang, M. G., Zhu, J., Wang, Y. W., Skorokhod, A.: Modeling impacts of urbanization and urban heat island mitigation on boundary layer meteorology and air quality in Beijing under different weather conditions, Journal of Geophysical Research: Atmospheres, 123, doi: 10.1002/2017JD027501, 2018.

Chen, L., Zhu, J., Liao, H., Gao, Y., Qiu, Y., Zhang, M., and Li, N.: Assessing the formation and evolution mechanisms of severe haze pollution in Beijing−Tianjin−Hebei region by using process analysis, Atmos. Chem. Phys. Discuss.,
20   10.5194/acp-2019-245, in review, 2019.

Chin, M., Rood, R. B., Lin, S.-J., Müller, J.-F., and Thompson, A. M.: Atmospheric sulfur cycle simulated in the global model GOCART: Model description and global properties, Journal of Geophysical Research: Atmospheres, 105, 24671-24687, 10.1029/2000jd900384, 2000.

Chin, M., Ginoux, P., Kinne, S., Torres, O., Holben, B. N., Duncan, B. N., Martin, R. V., Logan, J. A., Higurashi, A., and
25   Nakajima, T.: Tropospheric aerosol optical thickness from the GOCART model and comparisons with satellite and Sun photometer measurements, Journal of the Atmospheric Sciences, 59, 461-483, 2002.

Clarke, A. D., Owens, S. R., and Zhou, J. C.: An ultrafine sea-salt flux from breaking waves: Implications for cloud condensation nuclei in the remote marine atmosphere, J. Geophys. Res. Atmos, 111, 2006.

Cowan, T., Cai, W., Purich, A., Rotstayn, L., and England, M. H.: Forcing of anthropogenic aerosols on temperature trends
30   of the sub-thermocline southern Indian Ocean, Sci Rep, 3, 2245, 10.1038/srep02245, 2013.

Deng, X. L., Shi, C. E., Wu, B. W., Yang, Y. J., Jin, Q., Wang, H. L., Zhu, S., and Yu, C.: Characteristics of the water-soluble components of aerosol particles in Hefei, China, Journal of environmental sciences, 42, 32-40, 10.1016/j.jes.2015.07.010, 2016.

Diehl, T., Heil, A., Chin, M., Pan, X., Streets, D., Schultz, M., and Kinne, S.: Anthropogenic, biomass burning, and volcanic
35   emissions of black carbon, organic carbon, and SO_2 from 1980 to 2010 for hindcast model experiments, Atmospheric Chemistry and Physics Discussions, 12, 24895-24954, 10.5194/acpd-12-24895-2012, 2012.

Ding, A. J., Huang, X., Nie, W., Sun, J. N., Kerminen, V. M., Petäjä, T., Su, H., Cheng, Y. F., Yang, X. Q., Wang, M. H., Chi, X. G., Wang, J. P., Virkkula, A., Guo, W. D., Yuan, J., Wang, S. Y., Zhang, R. J., Wu, Y. F., Song, Y., Zhu, T., Zilitinkevich, S., Kulmala, M., and Fu, C. B.: Enhanced haze pollution by black carbon in megacities in China,
40   Geophysical Research Letters, 43, 2873-2879, 10.1002/2016gl067745, 2016.

Du, H., Kong, L., Cheng, T., Chen, J., Du, J., Li, L., Xia, X., Leng, C., Huang, G.: Insights into summertime haze pollution events over Shanghai based on online water-soluble ionic composition of aerosols. Atmos. Environ. 45, 5131–5137, 2011.

Fan, Q., Lan, J., Liu, Y., Wang, X., Chan, P., Hong, Y., Feng, Y., Liu, Y., Zeng, Y., and Liang, G.: Process analysis of regional
45   aerosol pollution during spring in the Pearl River Delta region, China, Atmospheric Environment, 122, 829-838, 10.1016/j.atmosenv.2015.09.013, 2015.

Foroutan, H., Young, J., Napelenok, S., Ran, L., Appel, K. W., Gilliam, R. C., and Pleim, J. E.: Development and evaluation of a physics-based windblown dust emission scheme implemented in the CMAQ modeling system, Journal of Advances in Modeling Earth Systems, 9, 585-608, 10.1002/2016ms000823, 2017.

50   Fountoukis, C. and Nenes, A.: ISORROPIA II: a computationally efficient thermodynamic equilibrium model for

K$^+$–Ca^{2+}–Mg^{2+}– NH$_4^+$ –Na$^+$– SO$_4^{2-}$ – NO$_3^-$ –Cl$^-$–H$_2$O aerosols, Atmos. Chem. Physics, 7, 4639–4659, doi:10.5194/acp-7-4639-2007, http://www.atmos-chem-phys.net/7/4639/2007/, 2007.

Fu, J., Jang, C., Streets, D., Li, Z., Kwok, R., Park, R., and Han, Z.: MICS-Asia II: Modeling gaseous pollutants and evaluating an advanced modeling system over East Asia, Atmospheric Environment, 42, 3571-3583, 10.1016/j.atmosenv.2007.07.058, 2008a.

Fu, Q., Zhuang, G., Wang, J., Xu, C., Huang, K., Li, J., Hou, B., Lu, T., Streets, D.G.: Mechanism of formation of the heaviest pollution episode ever recorded in the Yangtze River Delta, China. Atmos. Environ. 42, 2023–2036, 2008b.

Fu, J. S., Hsu, N. C., Gao, Y., Huang, K., Li, C., Lin, N. H., and Tsay, S. C.: Evaluating the influences of biomass burning during 2006 BASE-ASIA: a regional chemical transport modeling, Atmospheric Chemistry and Physics, 12, 3837-3855, 10.5194/acp-12-3837-2012, 2012.

Gao, M., Guttikunda, S. K., Carmichael, G. R., Wang, Y., Liu, Z., Stanier, C. O., Saide, P. E., and Yu, M.: Health impacts and economic losses assessment of the 2013 severe haze event in Beijing area, Sci Total Environ, 511, 553-561, 10.1016/j.scitotenv.2015.01.005, 2015a.

Gao, M., Carmichael, G. R., Wang, Y., Saide, P. E., Yu, M., Xin, J., Liu, Z., and Wang, Z.: Modeling study of the 2010 regional haze event in the North China Plain, Atmospheric Chemistry and Physics, 16, 1673-1691, 10.5194/acp-16-1673-2016, 2016b.

Gao, M., Han, Z., Liu, Z., Li, M., Xin, J., Tao, Z., Li, J., Kang, J.-E., Huang, K., Dong, X., Zhuang, B., Li, S., Ge, B., Wu, Q., Cheng, Y., Wang, Y., Lee, H.-J., Kim, C.-H., Fu, J. S., Wang, T., Chin, M., Woo, J.-H., Zhang, Q., Wang, Z., and Carmichael, G. R.: Air Quality and Climate Change, Topic 3 of the Model Inter-Comparison Study for Asia Phase III (MICS-Asia III), Part I: overview and model evaluation, Atmospheric Chemistry and Physics, 18, 4859-4884, doi: 10.5194/acp-18-4859-2018, 2018.

Gao, Y., Zhao, C., Liu, X., Zhang, M., and Leung, L. R.: WRF-Chem simulations of aerosols and anthropogenic aerosol radiative forcing in East Asia, Atmospheric Environment, 92, 250-266, 10.1016/j.atmosenv.2014.04.038, 2014.

Gao, Y., Zhang, M., Liu, Z., Wang, L., Wang, P., Xia, X., Tao, M., and Zhu, L.: Modeling the feedback between aerosol and meteorological variables in the atmospheric boundary layer during a severe fog–haze event over the North China Plain, Atmospheric Chemistry and Physics, 15, 4279-4295, 10.5194/acp-15-4279-2015, 2015b.

Gao, Y., Zhang, M., Liu, X., and Wang, L.: Change in diurnal variations of meteorological variables induced by anthropogenic aerosols over the North China Plain in summer 2008, Theoretical and applied climatology, 124(1-2), 103-118, 10.1007/s00704-015-1403-4, 2016a.

Gillette, D. A., and Passi, R.: Modeling Dust Emission Caused by Wind Erosion, J Geophys Res-Atmos, 93, 14233-14242, 1988.

Ginoux, P., Chin, M., Tegen, I., Prospero, J. M., Holben, B., Dubovik, O., and Lin, S. J.: Sources and distributions of dust aerosols simulated with the GOCART model, J. Geophys. Res.-Atmos., 106, 20255–20273, 2001.

Grell, G. A., Peckham, S. E., Schmitz, R., McKeen, S. A., Frost, G., Skamarock, W. C., and Eder, B.: Fully coupled "online" chemistry within the WRF model, Atmospheric Environment, 39, 6957-6975, 10.1016/j.atmosenv.2005.04.027, 2005.

Guenther, C. C.: Estimates of global terrestrial isoprene emissions using MEGAN (Model of Emissions of Gases and Aerosols from Nature). Atmospheric Chemistry and Physics, 6, www.atmos-chem-phys.net/6/3181/2006, 2006.

Gong, S. L.: A parameterization of sea-salt aerosol source function for sub- and super-micron particles, Global Biogeochem Cy, 17, 2003.

Hall, D.: Environmental change, protest, and havens of environmental degradation: Evidence from Asia. Global Environmental Politics, 2(2), 20-28, 10.1162/15263800260047808, 2002.

Han, X., Zhang, M., Liu, X., Steven, G., Xin, J., Wang, L.: Development of RAMS-CMAQ to simulate aerosol optical depth and aerosol direct radiative forcing and its application to East Asia. Atmospheric and Oceanic Science Letters, 2(6), 368-375, 10.1080/16742834.2009.11446831, 2009.

Han, X., Zhang, M., Tao, J., Wang, L., Gao, J., Wang, S., and Chai, F.: Modeling aerosol impacts on atmospheric visibility in Beijing with RAMS-CMAQ, Atmospheric Environment, 72, 177-191, 10.1016/j.atmosenv.2013.02.030, 2013.

Han, X., Zhang, M., Gao, J., Wang, S., and Chai, F.: Modeling analysis of the seasonal characteristics of haze formation in Beijing, Atmospheric Chemistry and Physics, 14, 10231-10248, 10.5194/acp-14-10231-2014, 2014.

Han, X., Zhu, L., Wang, S., Meng, X., Zhang, M., and Hu, J.: Modeling study of impacts on surface ozone of regional transport and emissions reductions over North China Plain in summer 2015, Atmospheric Chemistry and Physics, 18,

12207-12221, 10.5194/acp-18-12207-2018, 2018.

Han, Z. W., Ueda, H., Matsuda, K., Zhang, R. J., Arao, K., Kanai, Y., and Hasome, H.: Model study on particle size segregation and deposition during Asian dust events in March 2002, J Geophys Res-Atmos, 109, 2004.

Han, Z., Sakurai, T., Ueda, H., Carmichael, G., Streets, D., Hayami, H., Wang, Z., Holloway, T., Engardt, M., and Hozumi, Y.: MICS-Asia II: Model intercomparison and evaluation of ozone and relevant species, Atmospheric Environment, 42, 3491-3509, 10.1016/j.atmosenv.2007.07.031, 2008.

Hayami, H., Sakurai, T., Han, Z., Ueda, H., Carmichael, G., Streets, D., Holloway, T., Wang, Z., Thongboonchoo, N., and Engardt, M.: MICS-Asia II: Model intercomparison and evaluation of particulate sulfate, nitrate and ammonium, Atmospheric Environment, 42, 3510-3527, 10.1016/j.atmosenv.2007.08.057, 2008.

Holben, B. N., Eck, T. F., Slutsker, I., Tanre, D., Buis, J. P., Setzer, A., Vermote, E., Reagan, J. A., Kaufman, Y. J., Nakajima, T., Lavenu, F., Jankowiak, I., Smirnov, A.: AERONET—A federated instrument network and data archive for aerosol characterization. Remote sensing of environment, 66(1), 1-16, 10.1016/S0034-4257(98)00031-5, 1998.

Holloway, T., Sakurai, T., Han, Z., Ehlers, S., Spak, S., Horowitz, L., Carmichael, G., Streets, D., Hozumi, Y., and Ueda, H.: MICS-Asia II: Impact of global emissions on regional air quality in Asia, Atmospheric Environment, 42, 3543-3561, 10.1016/j.atmosenv.2007.10.022, 2008.

Hong, C., Zhang, Q., He, K., Guan, D., Li, M., Liu, F., and Zheng, B.: Variations of China's emission estimates: response to uncertainties in energy statistics, Atmospheric Chemistry and Physics, 17, 1227-1239, 10.5194/acp-17-1227-2017, 2017.

Huang, K., Fu, J. S., Hsu, N. C., Gao, Y., Dong, X., Tsay, S.-C., and Lam, Y. F.: Impact assessment of biomass burning on air quality in Southeast and East Asia during BASE-ASIA, Atmospheric Environment, 78, 291-302, 10.1016/j.atmosenv.2012.03.048, 2013.

Huang, X., Song, Y., Li, M., Li, J., Huo, Q., Cai, X., Zhu, T., Hu, M., and Zhang, H.: A high-resolution ammonia emission inventory in China, Global Biogeochem. Cy., 26, GB1030, doi:10.1029/2011GB004161, 2012.

Huang, X., Song, Y., Zhao, C., Li, M., Zhu, T., Zhang, Q., and Zhang, X.: Pathways of sulfate enhancement by natural and anthropogenic mineral aerosols in China, J. Geophys. Res.-Atmos., 119, https://doi.org/10.1002/2014JD022301, 2014.

Huang, X., Wang, Z., and Ding, A.: Impact of Aerosol-PBL Interaction on Haze Pollution: Multiyear Observational Evidences in North China, Geophysical Research Letters, 10.1029/2018gl079239, 2018.

Ikeda, K., Yamaji, K., Kanaya, Y., Taketani, F., Pan, X., Komazaki, Y., Kurokawa, J.-i., and Ohara, T.: Sensitivity analysis of source regions to PM2.5 concentration at Fukue Island, Japan, Journal of the Air & Waste Management Association, 64, 445-452, 10.1080/10962247.2013.845618, 2013.

Itahashi, S., Uno, I., Irie, H., Kurokawa, J. I., and Ohara, T.: Regional modeling of tropospheric NO_2 vertical column density over East Asia during the period 2000–2010: comparison with multisatellite observations, Atmospheric Chemistry and Physics, 14, 3623-3635, 10.5194/acp-14-3623-2014, 2014.

Im, U.: Impact of sea-salt emissions on the model performance and aerosol chemical composition and deposition in the East Mediterranean coastal regions, Atmospheric Environment, 75, 329-340, 2013.

Jaeglé, L., Quinn, P. K., Bates, T. S., Alexander, B., and Lin, J.-T.: Global distribution of sea salt aerosols: new constraints from in situ and remote sensing observations, Atmos. Chem. Phys., 11, 3137-3157, https://doi.org/10.5194/acp-11-3137-2011, 2011.

Janssens-Maenhout, G., Crippa, M., Guizzardi, D., Dentener, F., Muntean, M., Pouliot, G., Keating, T., Zhang, Q., Kurokawa, J., Wankmüller, R., Denier van der Gon, H., Kuenen, J. J. P., Klimont, Z., Frost, G., Darras, S., Koffi, B., and Li, M.: HTAP_v2.2: a mosaic of regional and global emission grid maps for 2008 and 2010 to study hemispheric transport of air pollution, Atmospheric Chemistry and Physics, 15, 11411-11432, 10.5194/acp-15-11411-2015, 2015.

Jimenez, P., Baldasano, J. M., and Dabdub, D.: Comparison of photochemical mechanisms for air quality modeling, Atmos. Environ., 37, 4179–4194, 10.1016/S1352-2310(03)00567-3, 2003.

Kajino, M., Inomata, Y., Sato, K., Ueda, H., Han, Z., An, J., Katata, G., Deushi, M., Maki, T., Oshima, N., Kurokawa, J., Ohara, T., Takami, A., and Hatakeyama, S.: Development of the RAQM2 aerosol chemical transport model and predictions of the Northeast Asian aerosol mass, size, chemistry, and mixing type. Atmospheric Chemistry and Physics, 12(24), 11833, 10.5194/acp-12-11833-2012, 2012.

Kajino, M., Deushi, M., Sekiyama, T. T., Oshima, N., Yumimoto, K., Tanaka, T. Y., Ching, J., Hashimoto, A., Yamamoto, T., Ikegami, M., Kamada, A., Miyashita, M., Inomata, Y., Shima, S.-I., Adachi, K., Zaizen, Y., Igarashi, Y., Ueda, H., Maki,

28

T., and Mikami, M.: NHM-Chem, the Japan Meteorological Agency's regional meteorology – chemistry model (v1.0): model description and aerosol representations, Geosci. Model Dev. Discuss., 10.5194/gmd-2018-128, 2018.

Kang, J.Y., Yoon, S.C., Shao, Y., and Kim, S.W.: Comparison of vertical dust flux by implementing three dust emission schemes in WRF/Chem, J. Geophys. Res., 116, D09202, 10.1029/2010JD014649, 2011.

Kelly, J. T., Bhave, P. V., Nolte, C. G., Shankar, U., and Foley, K. M.: Simulating emission and chemical evolution of coarse sea-salt particles in the Community Multiscale Air Quality (CMAQ) model, Geoscientific Model Development, 3, 257-273, 2010.Kiley, C. M., Fuelberg, H. E., Palmer, P. I., Allen, D. J., Carmichael, G. R., Jacob, D. J., Mari, C., Pierce, R. B., Pickering, K. E., Tang, Y., Wild, O., Fairlie, T. D., Logan, J. A., Sachse, G. W., Shaack, T. K., and Streets, D. G.: An intercomparison and evaluation of aircraft-derived and simulated CO from seven chemical transport models during the TRACE-P experiment, Journal of Geophysical Research: Atmospheres, 108, 10.1029/2002jd003089, 2003.

Kim, S. W., Heckel, A., Frost, G. J., Richter, A., Gleason, J., Burrows, J. P., McKeen, S., Hsie, E. Y., Granier, C., and Trainer, M.: NO2 columns in the western United States observed from space and simulated by a regional chemistry model and their implications for NOx emissions, J. Geophys. Res.-Atmos., 114, D11301, 10.1029/2008JD011343, 2009.

Kim, Y., Couvidat, F., Sartelet, K., and Seigneur, C.: Comparison of different gas-phase mechanisms and aerosol modules for simulating particulate matter formation, J. Air Waste Manage. Assoc, 61, 1218–1226, 10.1080/10473289.2011.603999, 2011

Kong, X., Forkel, R., Sokhi, R. S., Suppan, P., Baklanov, A., Gauss, M., Brunner, D., Baro, R., Balzarini, A., Chemel, C., Curci, G., Jimenez-Guerrero, P., Hirtl, M., Honzak, L., Im, U., Perez, J. L., Pirovano, G., Jose, R. S., Schlunzen, K. H., Tsegas, G., Tuccella, P., Werhahn, J., Zabkar, R., and Galmarini, S.: Analysis of meteorology-chemistry interactions during air pollution episodes using online coupled models within AQMEII phase-2, 115, 527-540, doi: 10.1016/j.atmosenv.2014.09.020, 2015.

Kong, L., Tang, X., Zhu, J., Wang, Z., Fu, J. S., Wang, X., Itahashi, S., Yamaji, K., Nagashima, T., Lee, H.-J., Kim, C.-H., Lin, C.-Y., Chen, L., Zhang, M., Tao, Z., Li, J., Kajino, M., Liao, H., Sudo, K., Wang, Y., Pan, Y., Tang, G., Li, M., Wu, Q., Ge, B., and Carmichael, G. R.: Evaluation and uncertainty investigation of the NO2, CO and NH3 modeling over China under the framework of MICS-Asia III, Atmos. Chem. Phys. Discuss., 10.5194/acp-2018-1158, in review, 2019.

Kurokawa, J., Ohara, T., Morikawa, T., Hanayama, S., Janssens-Maenhout, G., Fukui, T., Kawashima, K., and Akimoto, H.: Emissions of air pollutants and greenhouse gases over Asian regions during 2000–2008: Regional Emission inventory in Asia (REAS) version 2, Atmos. Chem. Phys., 13, 11019–11058, doi:10.5194/acp-13-11019-2013, 2013.

Lai, S., Zhao, Y., Ding, A., Zhang, Y., Song, T., Zheng, J., Ho, K. F., Lee, S.-c., and Zhong, L.: Characterization of PM 2.5 and the major chemical components during a 1-year campaign in rural Guangzhou, Southern China, Atmospheric Research, 167, 208-215, 10.1016/j.atmosres.2015.08.007, 2016.

Lam, Y. F., Fu, J. S., Wu, S., and Mickley, L. J.: Impacts of future climate change and effects of biogenic emissions on surface ozone and particulate matter concentrations in the United States, Atmospheric Chemistry and Physics, 11, 4789-4806, 10.5194/acp-11-4789-2011, 2011.

Lee, D. G., Lee, Y. M., Jang, K. W., Yoo, C., Kang, K. H., Lee,J. H., Jung, S. W., Park, J. M., Lee, S. B., Han, J. S., Hong, J. H., and Lee, S. J.: Korean national emissions inventory system and 2007 air pollutant emissions, Asian J. Atmos. Environ., 5, 278–291, 2011.

Lee, H.-J., Jo, H.-Y., Nam, K.-P., Lee, K.-H., Kim, C.-H.: Measurement, simulation, and meteorological interpretation of medium-range transport of radionuclides to Korea during the Fukushima Dai-ichi nuclear accident, Annals of Nuclear Energy, 103, 412-423, doi: 10.1016/j.anucene.2017.01.037, 2017.

Li, J., Wang, Z., Zhuang, G., Luo, G., Sun, Y., and Wang, Q.: Mixing of Asian mineral dust with anthropogenic pollutants over East Asia: a model case study of a super-duststorm in March 2010, Atmospheric Chemistry and Physics, 12, 7591-7607, 10.5194/acp-12-7591-2012, 2012a.

Li, J.: Research on pollution characteristics of PM10 in Jinan and inversion of aerosol optical thickness, M.S. thesis, Shandong Normal University, China, 64 pp., 2012b.

Li, J.: Seasonal characteristics of air pollution and weekend effect in Shanghai, M.S. thesis, the University of Chinese Academy of Sciences, China, 77 pp., 2015.

Li, J., Du, H., Wang, Z., Sun, Y., Yang, W., Li, J., Tang, X., and Fu, P.: Rapid formation of a severe regional winter haze episode over a mega-city cluster on the North China Plain, Environ Pollut, 223, 605-615, 10.1016/j.envpol.2017.01.063, 2017a.

Li, J., Nagashima, T., Kong, L., Ge, B., Yamaji, K., Fu, J. S., Wang, X., Fan, Q., Itahashi, S., Lee, H.-J., Kim, C.-H., Lin, C.-Y., Zhang, M., Tao, Z., Kajino, M., Liao, H., Li, M., Woo, J.-H., Kurokawa, J.-I., Wu, Q., Akimoto, H., Carmichael, G. R., and Wang, Z.: Model evaluation and inter-comparison of surface-level ozone and relevant species in East Asia in the context of MICS-Asia phase III Part I: overview, Atmos. Chem. Phys. Discuss., 10.5194/acp-2018-1283, in review, 2019.Li, K., Liao, H., Zhu, J., and Moch, J. M.: Implications of RCP emissions on future PM$_{2.5}$ air quality and direct radiative forcing over China, Journal of Geophysical Research: Atmospheres, 121, 12,985-913,008, 10.1002/2016jd025623, 2016b.

Li, K., Liao, H., Mao, Y., and Ridley, D. A.: Source sector and region contributions to concentration and direct radiative forcing of black carbon in China, Atmospheric Environment, 124, 351-366, 10.1016/j.atmosenv.2015.06.014, 2016c.Li, M., Zhang, Q., Kurokawa, J.-i., Woo, J.-H., He, K., Lu, Z., Ohara, T., Song, Y., Streets, D. G., Carmichael, G. R., Cheng, Y., Hong, C., Huo, H., Jiang, X., Kang, S., Liu, F., Su, H., and Zheng, B.: MIX: a mosaic Asian anthropogenic emission inventory under the international collaboration framework of the MICS-Asia and HTAP, Atmospheric Chemistry and Physics, 17, 935-963, 10.5194/acp-17-935-2017, 2017b.

Li, Y., An, J., and Gultepe, I.: Effects of additional HONO sources on visibility over the North China Plain, Advances in Atmospheric Sciences, 31, 1221-1232, 10.1007/s00376-014-4019-1, 2014.

Li, Y., Tao, J., Zhang, L., Jia, X., and Wu, Y.: High Contributions of Secondary Inorganic Aerosols to PM$_{2.5}$ under Polluted Levels at a Regional Station in Northern China, International journal of environmental research and public health, 13, 10.3390/ijerph13121202, 2016a.

Liao, H., Chen, W.-T., and Seinfeld, J. H.: Role of climate change in global predictions of future tropospheric ozone and aerosols, Journal of Geophysical Research, 111, 10.1029/2005jd006852, 2006.

Lin, C. Y., Zhao, C., Liu, X., Lin, N. H., and Chen, W. N.: Modelling of long-range transport of Southeast Asia biomass-burning aerosols to Taiwan and their radiative forcings over East Asia. Tellus B: Chemical and Physical Meteorology, 66(1), 23733, 10.3402/tellusb.v66.23733, 2014.

Lin, Y., Zou, J., Yang, W., and Li, C.Q: A review of recent advances in research on PM2. 5 in China. International journal of environmental research and public health, 15(3), 438, 10.3390/ijerph15030438, 2018.

Liu, S.: Research of observations of haze and precursors in Tangshan industrial zone, M.S. thesis, Nanjing University of Information Science & Technology, China, 71 pp., 2012.

Liu, X. G., Li, J., Qu, Y., Han, T., Hou, L., Gu, J., Chen, C., Yang, Y., Liu, X., Yang, T., Zhang, Y., Tian, H., and Hu, M.: Formation and evolution mechanism of regional haze: a case study in the megacity Beijing, China, Atmos. Chem. Phys., 13, 4501–4514, doi:10.5194/acp-13-4501-2013, 2013.

Liu, Y. M., Zhang, S. T., Fan, Q., Wu, D., Chan, P. W., Wang, X. M., Fan, S. J., Feng, Y. R., and Hong, Y. Y.: Accessing the Impact of Sea-Salt Emissions on Aerosol Chemical Formation and Deposition over Pearl River Delta, China, Aerosol Air Qual Res, 15, 2232-2245, 2015.

Lohmann, U., and Diehl, K.: Sensitivity studies of the importance of dust ice nuclei for the indirect aerosol effect on stratiform mixed-phase clouds. Journal of the Atmospheric Sciences, 63(3), 968-982, 10.1175/JAS3662.1, 2006.

Lu, Z., Zhang, Q., and Streets, D. G.: Sulfur dioxide and primary carbonaceous aerosol emissions in China and India, 1996–2010, Atmos. Chem. Phys., 11, 9839–9864, 10.5194/acp-11-9839-2011, 2011.

Luecken, D. J., Phillips, S., Sarwar, G., and Jang, C.: Effects of using the CB05 vs. SAPRC99 vs. CB4 chemical mechanism on model predictions: ozone and gas-phase photochemical precursor concentrations, Atmos. Environ., 42, 5805–5820, 10.1016/j.atmosenv.2007.08.056, 2008.

Luo, G. andWang, Z. F.: A global environmental atmospheric transport model (GEATM): Model Description and validation (in Chinese), Chinese Journal of Atmospheric Sciences, 30, 504–518, doi:10.3878/j.issn.1006-9895.2006.03.13, 2006.

Makar, P. A., Moran, M. D., Zheng, Q., Cousineau, S., Sassi, M., Duhamel, A., Besner, M., Davignon, D., Crevier, L.-P., and Bouchet, V. S.: Modelling the impacts of ammonia emissions reductions on North American air quality, Atmos. Chem. Phys., 9, 7183-7212, https://doi.org/10.5194/acp-9-7183-2009, 2009.

Meng, Z., Jia, X., Zhang, R., Yu, X., and Ma, Q.: Characteristics of PM2.5 at Lin'an regional background station in the Yangtze River Delta Region, Journal of Applied Meteorological Science, 23(4), 424-432, 2012.

Monahan, E. C. and Muircheartaigh, I. O.: Optimal Power-Law Description of Oceanic Whitecap Coverage Dependence on Wind Speed, J. Phys. Oceanogr., 10, 2094–2099, doi:10.1175/1520-0485(1980)010<2094:OPLDOO>2.0.CO;2, 1980.

Murphy, B. N., and Pandis, S. N.: Simulating the Formation of Semivolatile Primary and Secondary Organic Aerosol in a

Regional Chemical Transport Model, Environmental science & technology, 43, 4722-4728, 2009.

Nagashima, T., Sudo, K., Akimoto, H., Kurokawa, J., and Ohara T.: Long-term change in the source contribution to surface ozone over Japan, Atmos. Chem. Phys., 17, 8231-8246, doi: 10.5194/acp-17-8231-2017, 2017.

Nenes, A., Pandis, S. N., and Pilinis, C.: ISORROPIA: A new thermodynamic equilibrium model for multiphase multicomponent inorganic aerosols. Aquatic geochemistry, 4(1), 123-152, 10.1023/A:1009604003981, 1998.

Nolte, C. G., Gilliland, A. B., Hogrefe, C., and Mickley, L. J.: Linking global to regional models to assess future climate impacts on surface ozone levels in the United States, Journal of Geophysical Research, 113, 10.1029/2007jd008497, 2008.

Pan, Y., Zhang, Y., and Sarwar, G.: Impact of gas-phase chemistry on WRF/CHEM predictions of O3 and PM2.5: Mechanism implementation and comparative evaluation, 7th annual CMAS conference, Chapel Hill, North Carolina, 2008.

Park, S.Y., Lee, H.J., Kang, J.E., Lee T. and Kim, C.H.: Aerosol radiative effects on mesoscale cloud precipitation variables over Northeast Asia during the MAPS-Seoul 2015 campaign, Atmos. Environ., 172, 109–123, 10.1016/j.atmosenv.2017.10.044, 2018.

Petaja, T., Jarvi, L., Kerminen, V. M., Ding, A. J., Sun, J. N., Nie, W., Kujansuu, J., Virkkula, A., Yang, X. Q., Fu, C. B., Zilitinkevich, S., and Kulmala, M.: Enhanced air pollution via aerosol-boundary layer feedback in China, Sci Rep, 6, 18998, 10.1038/srep18998, 2016.

Phadnis, M. J., Carmichael, G. R., Ichikawa, Y., and Hayami, H.: Evaluation of long-range transport models for acidic deposition in East Asia. Journal of Applied Meteorology, 37(10), 1127-1142, 10.1175/1520-0450(1998)037<1127:EOLRTM>2.0.CO;2, 1998.

Pope, C. A., and Dockery, D. W.: Health Effects of Fine Particulate Air Pollution: Lines that Connect, Journal of the Air & Waste Management Association, 56, 709-742, 10.1080/10473289.2006.10464485, 2006.

Qiu, Y., Liao, H., Zhang, R., and Hu, J.: Simulated impacts of direct radiative effects of scattering and absorbing aerosols on surface layer aerosol concentrations in China during a heavily polluted event in February 2014, Journal of Geophysical Research: Atmospheres, 122, 5955-5975, 10.1002/2016jd026309, 2017.

Tao, J., Zhang, L., Ho, K., Zhang, R., Lin, Z., Zhang, Z., Lin, M., Cao, J., Liu, S., and Wang, G.: Impact of PM2.5 chemical compositions on aerosol light scattering in Guangzhou — the largest megacity in South China, Atmospheric Research, 135-136, 48-58, 10.1016/j.atmosres.2013.08.015, 2014.

Reams, M. A., Lam, N. S., and Baker, A.: Measuring Capacity for Resilience among Coastal Counties of the US Northern Gulf of Mexico Region, Am J Clim Change, 1, 194-204, 10.4236/ajcc.2012.14016, 2012.

Reff, A., Bhave, P. V., Simon, H., Pace, T. G., Pouliot, G. A., Mobley, J. D., and Houyoux, M.: Emissions inventory of PM2.5 trace elements across the United States, Environ. Sci. Technol., 43, 5790–5796, 10.1021/es802930x, 2009.

Schell, B., Ackermann, I. J., Hass, H., Binkowski, F. S., and Ebel, A.: Modeling the formation of secondary organic aerosol within a comprehensive air quality model system, Journal of Geophysical Research: Atmospheres, 106, 28275-28293, 10.1029/2001jd000384, 2001.

Seinfeld, J.H. and Pandis, S.N.: Atmospheric Chemistry and Physics: From Air Pollution to Climate Change, second ed. John Willey & Sons, Inc., New York, 2006.

Shao, Y.,: A model for mineral dust emission, J. Geophys. Res., 106(D17), 20,239–20,254, 10.1029/2001JD900171, 2001.

Shao, Y.,: Simplification of a dust emission scheme and comparison with data, J. Geophys. Res., 109, D10202, 10.1029/2003JD004372, 2004.

Shao, P.: The network observation and research on air pollution in Zhangjiakou, Beijing and Langfang, M.S. thesis, Nanjing University of Information Science & Technology, China, 66 pp., 2012.

Shao, J., Chen, Q., Wang, Y., Lu, X., He, P., Sun, Y., Shah, V., Martin, R. V., Philip, S., Song, S., Zhao, Y., Xie, Z., Zhang, L., and Alexander, B.: Heterogeneous sulfate aerosol formation mechanisms during wintertime Chinese haze events: air quality model assessment using observations of sulfate oxygen isotopes in Beijing, Atmos. Chem. Phys., 19, 6107-6123, https://doi.org/10.5194/acp-19-6107-2019, 2019.

Singh, A., and Dey, S.: Influence of aerosol composition on visibility in megacity Delhi, Atmospheric Environment, 62, 367-373, 10.1016/j.atmosenv.2012.08.048, 2012.

Spence, M., Clarke, A., Buckley, R.M.: Urbanization and Growth; Commission on Growth and Development, World Bank Publications: Washington, DC, USA, 2008.

Stockwell, W. R., Middleton, P., Chang, J. S., and Tang, X.: The second generation regional acid deposition model chemical mechanism for regional air quality modeling. Journal of Geophysical Research: Atmospheres, 95(D10), 16343-16367, 10.1029/JD095iD10p16343, 1990.

Stockwell, W. R., Kirchner, F., Kuhn, M., and Seefeld, S.: A new mechanism for regional atmospheric chemistry modeling, Journal of Geophysical Research: Atmospheres, 102, 25847-25879, 10.1029/97jd00849, 1997.

Stuefer, M., Freitas, S. R., Grell, G., Webley, P., Peckham, S., McKeen, S. A., and Egan, S. D.: Inclusion of ash and SO 2 emissions from volcanic eruptions in WRF-Chem: development and some applications. Geoscientific Model Development, 6(2), 457-468, 10.5194/gmd-6-457-2013, 2013.

Su, L., and Fung, J.C.H.: Sensitivities of WRF-Chem to dust emission schemes and land surface properties in simulating dust cycles during springtime over East Asia, J. Geophys. Res. Atmos., 120, 11,215–11,230, 10.1002/2015JD023446, 2015.

Su, X., Tie, X., Li, G., Cao, J., Huang, R., Feng, T., Long, X., and Xu, R.: Effect of hydrolysis of N2O5 on nitrate and ammonium formation in Beijing China: WRF-Chem model simulation, The Science of the total environment, 579, 221-229, 10.1016/j.scitotenv.2016.11.125, 2017.

Sudo, K., Takahashi, M., Kurokawa, J., and Akimoto, H.: CHASER: A global chemical model of the troposphere-1. Model description, J. Geophys. Res.-Atmos., 107, 20, 10.1029/2001jd001113, 2002a.

Sudo, K., Takahashi, M., and Akimoto, H.: CHASER: A global chemical model of the troposphere-2. Model results and evaluation, J. Geophys. Res.-Atmos., 107, 39, 10.1029/2001jd001114, 2002b.

Sun, Y. L., Zhuang, G. S., Tang, A. H., Wang, Y., and An, Z. S.: Chemical characteristics of PM2:5 and PM10 in haze-fog episodes in Beijing, Environ. Sci. Technol., 40, 3148–3155, 10.1021/es051533g, 2006.

Sun, Y. L., Wang, Z. F., Du, W., Zhang, Q., Wang, Q. Q., Fu, P. Q., Pan, X. L., Li, J., Jayne, J., and Worsnop, D. R.: Long-term real-time measurements of aerosol particle composition in Beijing, China: seasonal variations, meteorological effects, and source analysis, Atmospheric Chemistry and Physics, 15, 10149-10165, 10.5194/acp-15-10149-2015, 2015.

Sun, Y. L., Du, W., Fu, P., Wang, Q., Li, J., Ge, X., Zhang, Q., Zhu, C., Ren, L., Xu, W., Zhao, J., Han, T., Worsnop, D. R., and Wang, Z.: Primary and secondary aerosols in Beijing in winter: sources, variations and process, Atmos. Chem. Phys., 16,8309-8329, 10.5194/acp-16-8309-2016, 2016a.

Sun, Y. L., Wang, Z., Wild, O., Xu, W., Chen, C., Fu, P., Du, W., Zhou, L., Zhang, Q., Han, T., Wang, Q., Pan, X., Zheng, H., Li, J., Guo, X., Liu, J., and Worsnop, D. R.: "APEC Blue": Secondary Aerosol Reductions from Emission Controls in Beijing, Sci. Rep., 6, 20668, 10.1038/srep20668, 2016b.

Tao, Z., Santanello, J. A., Chin, M., Zhou, S., Tan, Q., Kemp, E. M., and Peters-Lidard, C. D.: Effect of land cover on atmospheric processes and air quality over the continental United States – a NASA Unified WRF (NU-WRF) model study, Atmos. Chem. Phys., 13, 6207–6226, 10.5194/acp-13-6207-2013, 2013.

van der Werf, G. R., Randerson, J. T., Giglo, L., Collatz, G. J., Mu, M., Kasibhatla, P. S., Morton, D. C., DeFries, R. S., Jin, Y., and van Leeuwen, T. T.: Global fire emissions and the contribution of deforestation, savanna, forest, agricultural, and peat fires (1997-2009). Atmos. Chem. Phys., 10, 11707-11753, 10.5194/acp-10-11707-2010, 2010.

Walcek, C. J., and Taylor, G. R.: A theoretical method for computing vertical distributions of acidity and sulfate production within cumulus clouds. Journal of the Atmospheric Sciences, 43(4), 339-355, 10.1175/1520-0469(1986)043<0339:ATMFCV>2.0.CO;2, 1986.

Wang, C.: Impact of anthropogenic absorbing aerosols on clouds and precipitation: A review of recent progresses, Atmospheric Research, 122, 237-249, 10.1016/j.atmosres.2012.11.005, 2013a.

Wang, H., He, Q., Chen, Y., and Kang, Y.: Analysis of Characteristics of Black Carbon Concentration in Shanghai from 2008 to 2012, Environmental Science, 35(4), 1215-1222, 2014a.

Wang, H., Xie, S.-P., and Liu, Q.: Comparison of Climate Response to Anthropogenic Aerosol versus Greenhouse Gas Forcing: Distinct Patterns, Journal of Climate, 29, 5175-5188, 10.1175/jcli-d-16-0106.1, 2016a.

Wang, H. L., Qiao, L. P., Lou, S. R., Zhou, M., Ding, A. J., Huang, H. Y., Chen, J. M., Wang, Q., Tao, S. K., Chen, C. H., Li, L., and Huang, C.: Chemical composition of PM2.5 and meteorological impact among three years in urban Shanghai, China, Journal of Cleaner Production, 112, 1302-1311, 10.1016/j.jclepro.2015.04.099, 2016b.

Wang, J., Wang, X., Zhang, H., Lu, F., and Hou, P.: Comparison of PM2.5 concentration and elemental compositions in two typical sites in Beijing urban area, Acta Scientiae Circumstantiae, 32(1), 74-80, 2012a.

Wang, P., Cao, J.-j., Shen, Z.-x., Han, Y.-m., Lee, S.-c., Huang, Y., Zhu, C.-s., Wang, Q.-y., Xu, H.-m., and Huang, R.-j.:

Spatial and seasonal variations of PM 2.5 mass and species during 2010 in Xi'an, China, Science of The Total Environment, 508, 477-487, 10.1016/j.scitotenv.2014.11.007, 2015.

Wang, P., Wang, H., Wang, Y. Q., Zhang, X. Y., Gong, S. L., Xue, M., Zhou, C. H., Liu, H. L., An, X. Q., Niu, T., and Cheng, Y. L.: Inverse modeling of black carbon emissions over China using ensemble data assimilation, Atmospheric Chemistry and Physics, 16, 989-1002, 10.5194/acp-16-989-2016, 2016c.

Wang, X., Liao, J.B., Zhang, J., Shen, C., Chen, W.H., Xia, B.C. and Wang, T.J.: A Numeric Study of Regional Climate Change Induced by Urban Expansion in the Pearl River Delta, China, J. Appl. Meteor. Climatol., 53, 346-362, doi: 10.1175/JAMC-D-13-054.1, 2014b.

Wang, Y., Zhang, Q., He, K., Zhang, Q., and Chai, L.: Sulfate-nitrate-ammonium aerosols over China: response to 2000-2015 emission changes of sulfate dioxide, nitrogen oxides, and ammonia, Atmos. Chem. Phys., 13, 2635-2652, doi: 10.5194/acp-13-2635-2013, 2013b.

Wang, Y. S., Yao, L., Wang, L. L., Liu, Z. R., Ji, D. S., Tang, G. Q., Zhang, J. K., Sun, Y., Hu, B., and Xin, J. Y.: Mechanism for the formation of the January 2013 heavy haze pollution episode over central and eastern China, Sci. China Earth Sci., 57, 14–25, doi:10.1007/s11430-013-4773-4, 2014c.

Wang, Z. F., Ueda, H., and Huang, M. Y.: A deflation module for use in modeling long-range transport of yellow sand over East Asia, J. Geophys. Res.-Atmos., 105, 26947–26959, 2000.

Wang, Z., Maeda, T., Hayashi, M., Hsiao, L. F., and Liu, K. Y.: A nested air quality prediction modeling system for urban and regional scales: Application for high-ozone episode in Taiwan. Water, Air, & Soil Pollution, 130(1), 391-396, 10.1023/A:1013833217916, 2001.

Wang, Z. F., Akimoto, H., and Uno, I.: Neutralization of soil aerosol and its impact on the distribution of acid rain over east Asia: Observations and model results, J. Geophys. Res.-Atmos., 107, 4389, 10.1029/2001JD001040, 2002.

Wang, Z., Xie, F., Sakurai, T., Ueda, H., Han, Z., Carmichael, G., Streets, D., Engardt, M., Holloway, T., and Hayami, H.: MICS-Asia II: Model inter-comparison and evaluation of acid deposition, Atmospheric Environment, 42, 3528-3542, 10.1016/j.atmosenv.2007.12.071, 2008.

Wang, Z., Li, J., Wang, Z., Yang, W., Tang, X., Ge, B., Yan, P., Zhu, L., Chen, X., Chen, H., Wand, W., Li, J., Liu, B., Wang, X., Wand, W., Zhao, Y., Lu, N., and Su, D.: Modeling study of regional severe hazes over mid-eastern China in January 2013 and its implications on pollution prevention and control, Science China Earth Sciences, 57, 3-13, 10.1007/s11430-013-4793-0, 2013c.

Xie, H., Wu, D., Zhang, G., Li, M., Fang, H., Chen, Q., Li, X., and Zhai, G.: Characteristic analysis of fine particles PM2.5 in the ambient air in Dongguan, Air Pollution Control, doi:10.13205/j.hjgc.201406016, 2013.

Xu, Y.: The level of haze and PM2.5 in Zhengzhou and heat power plants' atmospheric environmental impact assessment, M.S. thesis, Zhengzhou University, China, 77 pp., 2012.

Yamaji, K., Ohara, T., Uno, I., Kurokawa, J.-i., Pochanart, P., and Akimoto, H.: Future prediction of surface ozone over east Asia using Models-3 Community Multiscale Air Quality Modeling System and Regional Emission Inventory in Asia, Journal of Geophysical Research, 113, 10.1029/2007jd008663, 2008.

Yan, Z.-W., Wang, J., Xia, J.-J., and Feng, J.-M.: Review of recent studies of the climatic effects of urbanization in China, Advances in Climate Change Research, 7, 154-168, 10.1016/j.accre.2016.09.003, 2016.

Yang, J.H., Kang, S.C., Ji, Z.M., and Chen, D.L.: Modeling the origin of anthropogenic black carbon and its climatic effect over the Tibetan Plateau and surrounding regions, J. Geophys. Res.-Atmos., 123, 671-692, 10.4209/aaqr.2017.05.0156, 2018.

Yang, Y., Russell, L. M., Lou, S., Lamjiri, M. A., Liu, Y., Singh, B., and Ghan, S. J.: Changes in Sea Salt Emissions Enhance ENSO Variability, J. Climate, 29, 8575–8588, 10.1175/JCLI-D-16-0237.1, 2016.

Yao, L., Yang, L., Yuan, Q., Yan, C., Dong, C., Meng, C., Sui, X., Yang, F., Lu, Y., and Wang, W.: Sources apportionment of PM2.5 in a background site in the North China Plain, The Science of the total environment, 541, 590-598, 10.1016/j.scitotenv.2015.09.123, 2016.

Yarwood, G., Rao, S., Yocke, M., and Whitten, G. Z.: Updates to the Carbon Bond Chemical Mechanism: CB05. Final Report to the US EPA, RT-0400675, 2005.

Yu, Y., Hu, B., and Wang, Y.: Changing characteristics of the main air pollutants of the Dongling Mountain in Beijing, Environmental Science, 34(7), doi:,10.13227/j.hjkx.2013.07.021, 2013.

Yue, X., Wang, H. J., Liao, H., and Fan, K.: Simulation of dust aerosol radiative feedback using the GMOD: 2. Dust climate

interactions, J. Geophys. Res.-Atmos., 115, D10202, 10.1029/2008JD010995, 2010.

Yue, X., Unger, N., Harper, K., Xia, X., Liao, H., Zhu, T., Xiao, J., Feng, Z., and Li, J.: Ozone and haze pollution weakens net primary productivity in China, Atmospheric Chemistry and Physics, 17, 6073-6089, 10.5194/acp-17-6073-2017, 2017.

5   Zaveri, R. A., and Peters, L. K.: A new lumped structure photochemical mechanism for large-scale applications, Journal of Geophysical Research: Atmospheres, 104, 30387-30415, 10.1029/1999jd900876, 1999.

Zhang, B., Wang, Y., and Hao, J.: Simulating aerosol–radiation–cloud feedbacks on meteorology and air quality over eastern China under severe haze condition in winter, Atmospheric Chemistry and Physics, 15, 2387-2404, 10.5194/acp-15-2387-2015, 2015a.

10 Zhang, M.: Numerical study of boundary layer ozone transport and photochemical production in east Asia in the wintertime, Geophysical Research Letters, 29, 10.1029/2001gl014368, 2002.

Zhang, M., Uno, I., Zhang, R., Han, Z., Wang, Z., and Pu, Y.: Evaluation of the Models-3 Community Multi-scale Air Quality (CMAQ) modeling system with observations obtained during the TRACE-P experiment: Comparison of ozone and its related species, Atmospheric Environment, 40, 4874-4882, 10.1016/j.atmosenv.2005.06.063, 2006.

15 Zhang, M., Han, Z., and Zhu, L.: Simulation of atmospheric aerosols in East Asia using modeling system RAMS-CMAQ: Model evaluation, China Particuology, 5, 321-327, 10.1016/j.cpart.2007.07.002, 2007.

Zhang, R., Sun, X. S., Shi, A. J., Huang, Y. H., Yan, J., Nie, T., Yan, X., and Li, X.: Secondary inorganic aerosols formation during haze episodes at an urban site in Beijing, China, Atmos. Environ., 177, 275–282, 10.1016/j.atmosenv.2017.12.031, 2018.

20 Zhang, X.: Study on long-term variation of Black Carbon aerosol over Peking and Hebei province during 2006-2012, M.S. thesis, Yunnan University, China, 116 pp., 2015b.

Zhao, C., Liu, X., Leung, L. R., Johnson, B., McFarlane, S. A., Gustafson Jr., W. I., Fast, J. D., and Easter, R.: The spatial distribution of mineral dust and its shortwave radiative forcing over North Africa: modeling sensitivities to dust emissions and aerosol size treatments, Atmos. Chem. Phys., 10, 8821-8838, https://doi.org/10.5194/acp-10-8821-2010, 25   2010.

Zhao, X. J., Zhao, P. S., Xu, J., Meng,, W., Pu, W. W., Dong, F., He, D., and Shi, Q. F.: Analysis of a winter regional haze event and its formation mechanism in the North China Plain, Atmos. Chem. Phys., 13, 5685-5696, https://doi.org/10.5194/acp-13-5685-2013, 2013.

Zheng, B., Zhang, Q., Zhang, Y., He, K. B.,Wang, K., Zheng, G. J., Duan, F. K., Ma, Y. L., and Kimoto, T.: Heterogeneous 30 chemistry: a mechanism missing in current models to explain secondary inorganic aerosol formation during the January 2013 haze episode in North China, Atmos. Chem. Phys., 15, 2031–2049, https://doi.org/10.5194/acp-15-2031-2015, 2015.

Zhu, J., Liao, H., Mao, Y., Yang, Y., and Jiang, H.: Interannual variation, decadal trend, and future change in ozone outflow from East Asia, Atmospheric Chemistry and Physics, 17, 3729-3747, 10.5194/acp-17-3729-2017, 2017.

35

Table 1. Basic configurations of participant models in MICS−Asia Phase III

Model Index	Model Version	Vertical Layers (1st height)	Horizontal advection	Vertical diffusion	Gas phase chemistry	Aerosol chemistry	Dry deposition	Wet scavenging	Dust scheme	Sea-salt scheme	Meteorology	Boundary Condition	Online/Offline	References
M1	WRFCMAQ5.0.2	40 (57 m)	Yamo	ACM2	SAPRC99	Aero6 ISORROPIA(v2)	Wesely	Henry's law	NA	Gong, Kelly	Standard[a]	GEOS-Chem	Online access	Fu et al., (2008a)
M2	WRFCMAQ5.0.2	40 (57 m)	Yamo	ACM2	SAPRC99	Aero6 ISORROPIA(v2)	Wesely	Henry's law	NA	Gong, Kelly	Standard[a]	Default	Online access	Wang et al., (2014b)
M3	WRFCMAQ5.0.1	40 (57 m)	Yamo	ACM2	CB05	Aero6 ISORROPIA(v2)	Wesely	Henry's law	NA	Gong, Kelly	Standard[a]	GEOS-Chem	Online access	Lam et al., (2011)
M4	WRFCMAQ4.7.1	40 (57 m)	Yamo	ACM2	SAPRC99	Aero5 ISORROPIA(v1.7)	Wesely	Henry's law	NA	Gong, Kelly	Standard[a]	CHASER	Offline	Itahashi et al., (2014)
M5	WRFCMAQ4.7.1	40 (57 m)	Yamo	ACM2	SAPRC99	Aero5 ISORROPIA(v1.7)	M3DRY	Henry's law	NA	Gong, Kelly	Standard[a]	CHASER	Offline	Yamaji et al., (2008)
M6	WRFCMAQ4.7.1	40 (57 m)	Yamo	ACM2	SAPRC99	Aero5 ISORROPIA(v1.7)	M3DRY	Henry's law	NA	Gong, Kelly	Standard[a]	CHASER	Offline	Nagashima et al., (2017)
M7	WRFChem3.7.1	40 (29 m)	5th order Monotonic	−	RACM−ESRL with KPP	MADE/SORGAM	Wesely	Henry's law	NA	NA	WRF/NCEP	Default	Online integrated	Park et al., (2018)
M8	WRFChem3.6.1	40 (57 m)	5th order Monotonic	MYJ	RACM with KPP	MADE/VBS	Wesely	Henry's law	NA	NA	WRF/NCEP	CHASER	Online integrated	Lin et al., (2014)
M9	WRFChem3.6	40 (16 m)	5th order Monotonic	YSU	RADM2	MADE/SORGAM	Wesely	Henry's law	Shao (2004)	Gong	WRF/NCEP	CHASER	Online integrated	Chen et al., (2017)
M10	NU-WRF v7lis7-3.5.1-p3	60 (44 m)	5th order Monotonic	YSU	RADM2	GOCART	Wesely	Grell	GOCART	Gong	WRF/MERRA2	MOZART+GOCART	Online integrated	Tao et al., (2013)
M11	NAQPMS	20 (50 m)	Walcek and Aleksic (1998)	K−theory	CBMZ	Aero5 ISORROPIA(v1.7)	Wesely	Henry's law	Wang (2000)	Gong	Standard[a]	CHASER	Online access	Wang et al., (2008)
M12	NHMChem	40 (54 m)	Walcek and Aleksic (1998)	FTCS	SAPRC99	ISORROPIA(v2)	Kajino	Kajino	Han (2004)	Clarke	JMA NHM	CHASER	Offline	Kajino et al., (2012)
M13	GEOS-Chem9.1.3	47 (60 m)	Lin and McElroy (2010)	Nox-Ox-HC-Br mechanism	ISORROPIA(v2)	Wesely	Liu	GOCART	Gong, Jaegle	Geos-5	NA	Offline	Zhu et al., (2017)
M14	RAMSCMAQ4.6	15 (100 m)	Yamo	ACM2	SAPRC99	Aero5 ISORROPIA(v1.7)	Wesely	Henry's law	Han (2004)	Gong	RAMS/NCEP	CHASER	Offline	Zhang et al., (2002)

[a]'Standard' represents the reference meteorological field provided by MICS−Asia III project.

5

Table 2. Statistics of BC, SO_4^{2-}, NO_3^-, NH_4^+, PM₂.₅, PM₁₀, and AOD. Best results are set to be bold with underline. Monthly mean observations and the number of stations (nstd) are listed with italic. In this table, monthly measurements except BC are taken from EANET, CNEMC, and AERONET. Monthly BC concentrations are collected from published literatures.

Species	Statistics	M1	M2	M4	M5	M6	M7	M8	M9	M11	M12	M13	M14	EM
BC	R	0.70	0.73	0.71	0.65	0.70	0.73	**0.80**	−	0.69	0.68	0.75	0.72	0.73
(5.0 μg m⁻³)	NMB(%)	**1.0**	12.7	−24.7	−54.9	−17.8	−11.7	−34.2	−	−17.5	−2.2	−26.8	−11.6	−17.0
(nstd=5)	RMSE	4.10	4.30	2.95	4.06	2.99	2.69	2.84	−	2.91	3.52	2.80	**2.64**	2.77
SO_4^{2-}	R	0.69	0.71	0.64	0.58	0.66	0.48	0.53	0.65	0.55	0.50	**0.76**	0.46	0.69
(3.8 μg m⁻³)	NMB(%)	−23.1	−13.0	−31.0	−26.4	−26.9	−67.7	**−1.6**	−67.0	−34.5	23.2	−31.9	69.3	−19.1
(nstd=31)	RMSE	3.21	**3.00**	3.46	3.57	3.35	4.64	3.62	4.45	3.78	4.01	3.24	5.51	3.22
NO_3^-	R	0.55	0.51	0.62	**0.65**	0.58	0.45	0.29	0.64	0.59	0.60	0.43	0.58	**0.65**
(1.7 μg m⁻³)	NMB(%)	9.0	−7.2	−42.7	**−1.7**	−11.8	−81.2	−80.6	125.7	46.5	54.0	22.7	35.4	4.9
(nstd=31)	RMSE	2.70	2.71	2.48	2.29	2.46	3.37	3.18	4.37	2.89	2.80	2.96	2.62	**2.27**
NH_4^+	R	0.67	0.64	0.68	0.66	0.69	0.55	0.34	**0.75**	0.66	0.62	0.64	0.68	0.71
(1.1 μg m⁻³)	NMB(%)	23.2	33.7	−10.6	**7.4**	14.6	−93.5	−34.2	45.3	35.0	49.9	34.9	56.3	14.0
(nstd=31)	RMSE	1.24	1.42	1.15	1.21	1.16	1.83	1.53	1.26	1.27	1.54	1.29	1.47	**1.11**
PM₂.₅	R	0.80	0.78	0.80	0.71	0.80	0.80	0.77	0.82	0.80	0.78	0.75	0.81	**0.83**
(51.4μg m⁻³)	NMB(%)	10.0	13.6	**−1.3**	−25.3	−5.8	−5.7	−15.3	26.2	5.2	31.4	−26.5	46.0	4.4
(nstd=14)	RMSE	27.56	34.88	23.03	28.00	21.80	23.54	24.83	28.52	22.06	34.87	27.10	35.85	**21.23**
PM₁₀	R	0.75	0.74	0.74	0.65	0.75	0.70	0.70	0.66	0.78	**0.82**	−	0.63	0.78
(80.7μg m⁻³)	NMB(%)	−40.7	−38.7	−35.7	−55.7	−46.6	−43.7	−43.4	−16.9	−25.4	−18.8	−	**7.1**	−32.6
(nstd=51)	RMSE	51.31	50.88	49.10	64.55	55.31	55.07	55.11	50.67	42.91	**37.28**	−	47.26	45.81
AOD	R	0.64	0.55	0.56	−	−	0.54	−	0.60	0.69	0.66	**0.71**	0.57	0.68
(0.2)	NMB(%)	**−2.0**	63.7	−28.5	−	−	−21.8	−	11.1	73.1	−6.2	47.1	36.7	18.7
(nstd=38)	RMSE	0.15	0.22	0.16	−	−	0.18	−	0.19	0.22	**0.13**	0.25	0.22	0.14

5

Table 3. The coefficient of variation (CV, standard deviation divided by the mean) of simulated coarse particles (subtract PM$_{2.5}$ from PM$_{10}$) in each defined sub-region.

CV	Normal[a]	Without_SS_Dust[b]	Without_Dust[c]	With_SS_Dust[d]
Region_1	1.3	0.29	0.37	0.97
Region_2	1.39	0.3	0.65	1.04
Region_3	1.43	0.33	0.48	1.27
Region_4	1.21	0.19	0.59	0.95
Region_5	0.85	0.09	0.65	0.88

5   [a]"Normal" means that simulation results from all participant models are considered.
[b]"Without_SS_Dust" means that the impacts of sea salt and dust aerosols are not considered, i.e., only simulation results from M7 and M8 are used to calculate the CV.
[c]"Without_Dust" means that the impacts of dust aerosols are not considered, i.e., only simulation results from M1, M2, M4, M5 and M6 are used to calculate the CV.
10   [d]"With_SS_Dust" means that both the impacts of sea salt and dust aerosols are considered, i.e., simulation results from M9, M11, M12 and M14 are used to calculate the CV.
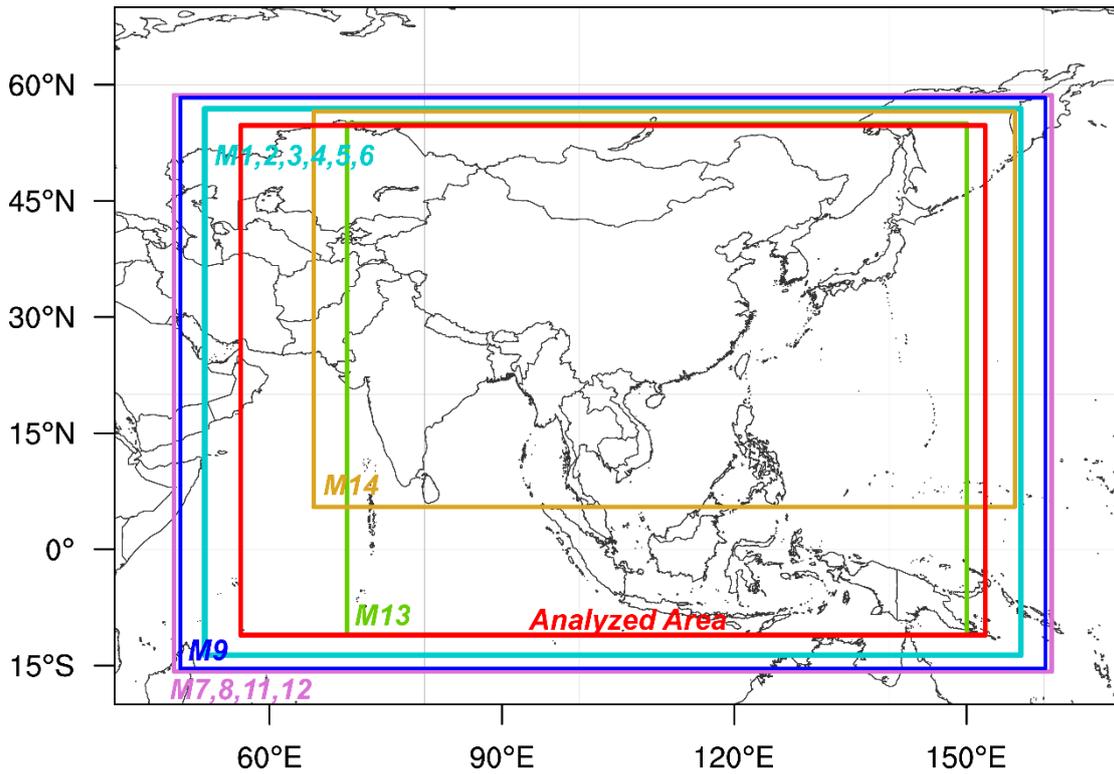
Figure 1. Simulation domain for each participant model. The final analyzed region is also shown.

5

Figure 2. The geographical locations of observation stations: EANET (shown in black circles, the number of stations is 39), CNEMC (shown in red triangles, the number of stations is 32), Others (observations collected from published literatures, shown in purple stars, the number of stations is 32), and AERONET (shown in black boxs, the number of stations is 33). Five defined sub-regions (Region_1 to Region_5) are also shown.

Figure 3. Comparison of observed and simulated concentrations of (a) BC, (b) SO_4^{2-}, (c) NO_3^-, (d) NH_4^+, (e) PM$_{2.5}$, and (f) PM$_{10}$. In each panel, the grey bars represent observations, the colored dots represent simulations, and the black solid lines represent the MMEM (multi–model ensemble mean). The x axis presents the monitoring sites (the information of these sites is listed in Table S1). Normalized mean biases (NMBs) between observations and MMEM in each defined sub-region (shown in black) and the entire analyzed region (shown in red) are also shown. In this figure, the annual mean observations are taken from EANET, CNEMC, and published literatures.

Figure 4. Time series of the monthly observed and simulated aerosol compositions: (a1) BC, (b1)-(b3) $PM_{2.5}$, (c1)-(c4) PM_{10}. The thin grey lines represent simulation results, and the grey shaded areas indicate the spread. The thick black lines are the ensemble mean. The red solid lines mean the observations, and the dashed red lines represent one standard deviation. Correlation coefficients (Rs, shown in black) for the whole year and normalized mean biases (NMBs, shown in blue) for each season between observations and MMEM are shown in each panel. The number of monitoring sites used to calculate the statistics in each sub-region is also listed above each panel. In this figure, the monthly observations except BC are taken from EANET and CNEMC; the monthly BC concentrations are collected from published literatures.
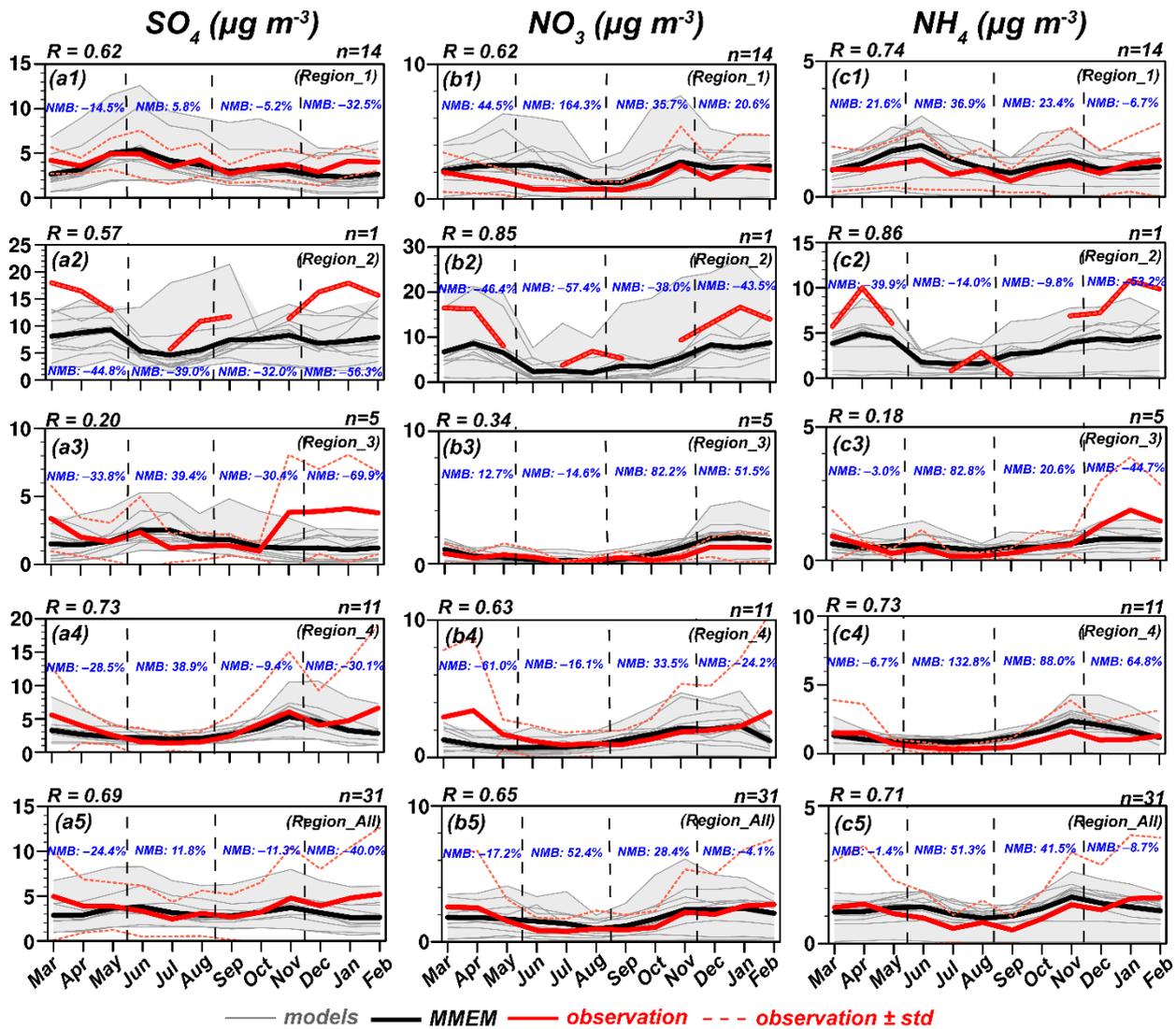
Figure 5. The same as Fig. 4, but for (a1-a5) SO_4^{2-}, (b1-b5) NO_3^-, and (c1-c5) NH_4^+. In this figure, the monthly measurements are taken from EANET.

5
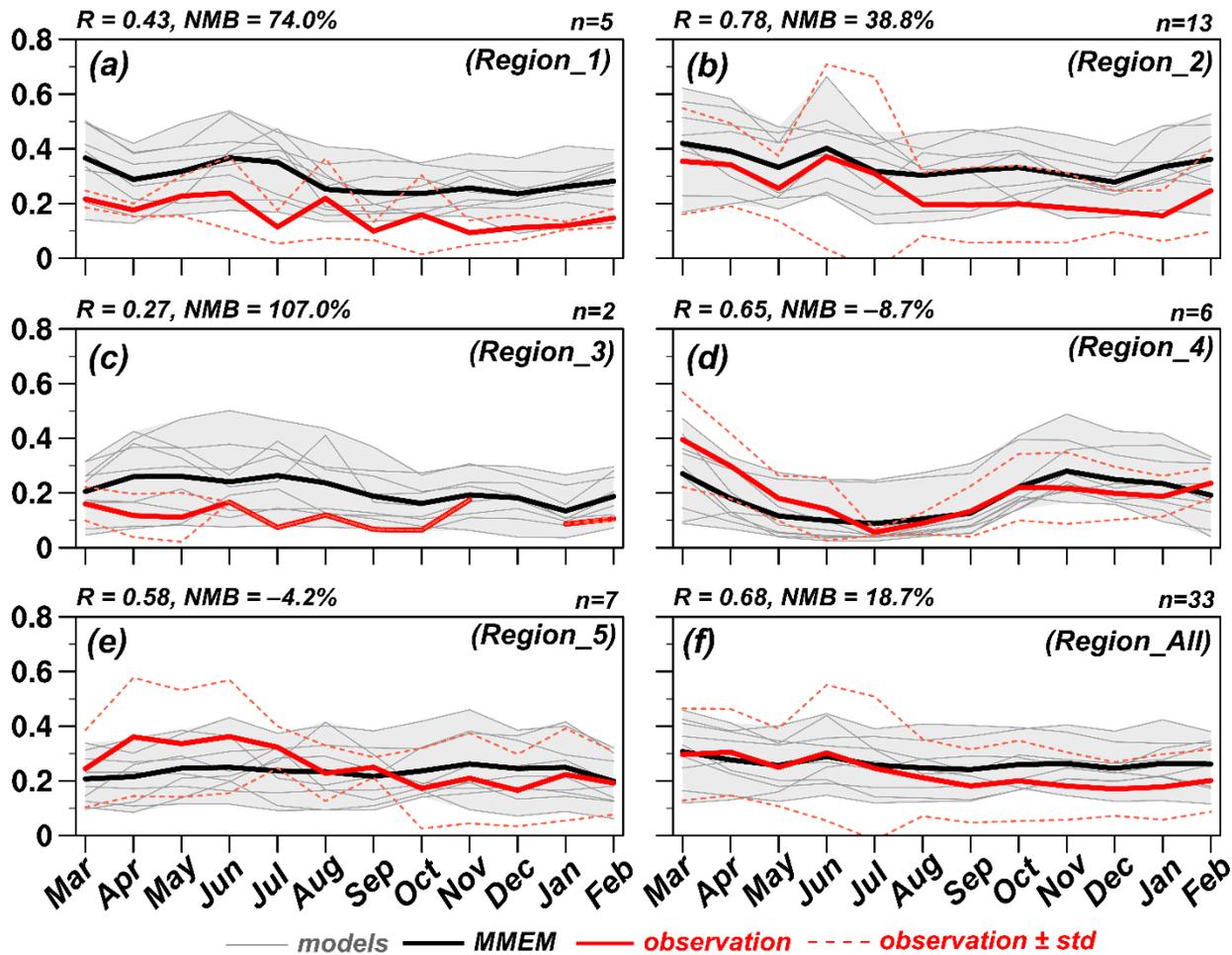
Figure 6. Similar as Fig, 4, but for seasonal cycles of aerosol optical depth (AOD) at 550 nm. In this figure, the monthly measurements are taken from AERONET.

5

Figure 7. Spatial distributions of observed and simulated aerosol optical depth (AOD) at 550 nm. The observed AOD values are retrieved from MODIS. Spatial correlation coefficients are given in the bottom left corner of each panel. Observed AOD from AERONET are also shown in circles.

Figure 8. Inter-comparison of model performance between MICS-Asia Phase II (blue) and Phase III (red) for SO_4^{2-}, NO_3^-, and NH_4^+. Detailed information about the observations and simulations used in Phase II can be obtained from Hayami et al. (2008). Each boxplot exhibits the full range, the interquartile, and the median for (a) RMSE and (b) correlation coefficient. Detailed values of the median (the 25th percentile, the 75th percentile) are also listed above each panel.

Figure 9. Spatial distributions of simulated PM₂.₅ concentrations from each participant model and the MMEM. The calculated coefficient of variation (CV, standard deviation divided by the mean) is also shown. The values listed in the bottom right corner of the figure represent the averaged CV (the minimum CV, the maximum CV) in each defined sub-region. The ratio of SNA (sulfate, nitrate, and ammonium) to PM₂.₅, the SOR (sulfur oxidation ratio), the NOR (nitric oxidation ratio), and the PNR (particle neutralization ratio) are also given at the bottom of each panel.

46

Figure 10. The same as Fig. 9, but for PM_coarse (coarse particles, subtract PM$_{2.5}$ from PM$_{10}$).

5

Figure 11. (a) The spatial distributions of PM_{10} concentrations for MMEM. (a1-a6) Simulated aerosol chemical compositions for participant models and the MMEM in the six metropolitans (Beijing, Tokyo, Seoul, Shanghai, Guangzhou, and Delhi). (b1-b6) The ratios of each composition to $PM_{2.5}$ for MMEM. (c1-c6) The seasonal $PM_{2.5}$ concentrations for MMEM. It is noted that $PM_{10}=SNA+OTHER1+PM_{coarse}$, $SNA=SO_4^{2-}+NO_3^-+NH_4^+$, and $OTHER1=BC+OC+OTHER2$.

48